
Doctoral Dissertations

Student Theses and Dissertations

Spring 2018

Effects of milling methods, cooling strategies and end-mill coatings on machinability in high speed end-milling of Inconel-718 using carbide end-mills

Paras Mohan Jasra

Follow this and additional works at: https://scholarsmine.mst.edu/doctoral_dissertations



Part of the [Mechanical Engineering Commons](#)

Department: Mechanical and Aerospace Engineering

Recommended Citation

Jasra, Paras Mohan, "Effects of milling methods, cooling strategies and end-mill coatings on machinability in high speed end-milling of Inconel- 718 using carbide end-mills" (2018). *Doctoral Dissertations*. 3130.

https://scholarsmine.mst.edu/doctoral_dissertations/3130

This thesis is brought to you by Scholars' Mine, a service of the Missouri S&T Library and Learning Resources. This work is protected by U. S. Copyright Law. Unauthorized use including reproduction for redistribution requires the permission of the copyright holder. For more information, please contact scholarsmine@mst.edu.

EFFECTS OF MILLING METHODS, COOLING STRATEGIES AND END-MILL
COATINGS ON MACHINABILITY IN HIGH SPEED END-MILLING OF INCONEL-
718 USING CARBIDE END-MILLS

by

PARAS MOHAN JASRA

A DISSERTATION

Presented to the Faculty of the Graduate School of the
MISSOURI UNIVERSITY OF SCIENCE AND TECHNOLOGY

In Partial Fulfillment of the Requirements for the Degree

DOCTOR OF PHILOSOPHY

in

MECHANICAL ENGINEERING

2018

Approved by

Dr. Anthony C. Okafor (Advisor)
Dr. K. Chandrashekhara
Dr. Lokesh Dharani
Dr. Lianyi Chen
Dr. V. A. Samaranayake

© 2018

Paras Mohan Jasra

All Rights Reserved

PUBLICATION DISSERTATION OPTION

This dissertation is presented in publication format and is divided into four separate papers: Paper I, comprising pages 5 through 60 is under review for publication in the *Journal of Machining Science and Technology*, under the title, “Effects of Up-milling and Down-Milling Methods, and Cooling Strategies on Cutting Forces and Tooth Frequency in High Speed End-Milling of Inconel 718 Using Uncoated Solid Carbide End-Mills”. Paper II, comprising pages 61 through 100 is under review for publication in the *International Journal of Advanced Manufacturing Technology*, under the title, “Effects of Cooling Strategies and Tool Coatings on Cutting Forces and Tooth Frequency in High Speed Down-milling of Inconel-718 using Helical Bull-nose Solid Carbide End-mills”. Paper III, comprising pages 101 through 153 is under review for publication in the *International Journal of Machining and Machinability of Materials*, under the title, “Effects of Up-Milling and Down-Milling Methods, and Cooling Strategies on Tool Wear, Chip Morphology and Surface Roughness in High Speed End-Milling of Inconel-718 using Uncoated Solid Carbide End-Mills”. Paper IV, comprising pages 154 through 191 has been submitted for publication in the *Journal of Machining Science and Technology*, under the title, “Effects of Cooling Strategies and Tool Coatings on Tool Wear, Chip Morphology and Surface Roughness in High Speed Down-milling of Inconel 718 using Helical Bull Nose Solid Carbide End-mills”. The balance of the dissertation follows the standard dissertation format.

ABSTRACT

Inconel-718 superalloy is used extensively in aerospace and nuclear industries due to its excellent properties such as: high strength-to-weight ratio, ability to retain its properties at high temperature, high corrosion and creep resistance. However, Inconel-718 is characterized as a “difficult-to-cut metal”, because it poses severe problems during machining such as: high temperature at the cutting zone due to low thermal conductivity, hardening tendency at elevated temperature, high cutting forces, rapid tool wear and high chemical affinity with many cutting tools. Appropriate cooling strategies, milling methods, tool coatings and cutting speeds play important roles in addressing these problems. This research presents the results of the effects of end-milling methods (Up and down-milling), cooling strategies (Conventional emulsion cooling, Minimum Quantity Lubrication (MQL), Liquid Nitrogen (LN₂) and (MQL+LN₂)) and tool coatings (Uncoated, AlTiN and GMS²) on cutting forces, cutter tooth frequency, tool wear, chip morphology and surface roughness in high-speed end-milling of Inconel-718 to improve its machinability and reduce cost. Firstly, a comparative investigation of milling methods and cooling strategies using uncoated tools was conducted and analyzed to find better milling method and three best cooling strategies to perform further experiments using coated tools. Results show that down-milling improves machinability. Then, the performance of three tool coatings and three best cooling strategies (MQL, LN₂ and (MQL+LN₂)), determined from first set of experiments was analyzed. Finally, the best cooling strategy and tool coating were determined for machining Inconel-718 at given parameters. Results show that MQL, an environmentally friendly cooling strategy, improves machinability and can successfully replace conventional emulsion cooling.

ACKNOWLEDGMENTS

Firstly, I would like to express my sincere gratitude to my advisor Dr. A. C. Okafor for his generous advice, inspiring guidance, and encouragement throughout my four years of research. His guidance helped me in all the time of research and writing of this thesis.

I would also like to thank the rest of my dissertation committee members: Dr. K. Chandrashekhara, Dr. Lokesh Dharani, Dr. Lianyi Chen and Dr. V. A. Samaranayake, who checked my work and enriched it with their valuable recommendations and advice.

The financial support from the Intelligent System Centre (ISC) of the Missouri University of Science and Technology is greatly acknowledged. The financial assistance provided in the form of Graduate Teaching Assistantship by the Department of Mechanical and Aerospace Engineering is also greatly acknowledged.

Special thanks are extended to the members of my research group Mahmood Ameen, Chukwujekwu Nnadi and Abdulhakim Ali Sultan, for their help and encouragements. I would like to thank Mr. Mitchell Cottrell for technical assistance he provided during experimental work whenever needed and Mr. Randall S. Lewis for providing assistance in measuring emulsion concentration.

I would also like to thank my uncle Dr. Rakshvir Jasra for his help and encouragement to pursue PhD.

I would like to dedicate my dissertation to my beloved parents for their continuous support that has made every opportunity available to me throughout my life. Last but not least, I am thankful to my brother, wife and my little daughter “Suhasi” for their love, understanding and continuous support to complete this research work.

TABLE OF CONTENTS

	Page
PUBLICATION DISSERTATION OPTION	iii
ABSTRACT	iv
ACKNOWLEDGMENTS	v
LIST OF ILLUSTRATIONS	xii
LIST OF TABLES	xx
 SECTION	
1. INTRODUCTION	1
 PAPER	
I. EFFECTS OF UP-MILLING AND DOWN-MILLING METHODS, AND COOLING STRATEGIES ON CUTTING FORCES AND TOOTH FREQUENCY IN HIGH SPEED END-MILLING OF INCONEL 718 USING UNCOATED SOLID CARBIDE END-MILLS	5
ABSTRACT	5
1. INTRODUCTION	6
2. EXPERIMENTAL DESIGN	16
2.1. EXPERIMENTAL PARAMETERS AND CUTTING CONDITIONS	16
2.2. COOLING STRATEGIES SETUP	19
2.2.1. Emulsion Cooling Setup.	19
2.2.2. Minimum Quantity Lubrication Setup.	20
2.2.3. Cryogenic Liquid Nitrogen Setup.	21
2.2.3.1. Calibration of liquid nitrogen set up.....	22
3. EXPERIMENTAL SETUP AND PROCEDURE	26
3.1. WORKPIECE PREPARATION	26
3.2. EXPERIMENTAL SET UP	29
3.3. CUTTING FORCE AND FFT ACQUISITION	29

3.4. CUTTING FORCE AND FFT DATA PROCESSING	30
3.5. PROCEDURE	31
4. RESULT ANALYSIS.....	35
4.1. SAMPLE PLOTS FOR MAXIMUM CUTTING FORCE COMPONENTS AND FAST FOURIER TRANSFORMS (FFT) VERSUS MACHINED LENGTH (PASS NUMBER)	35
4.2. MAXIMUM CUTTING FORCE COMPONENTS AND RESULTANT CUTTING FORCE AND, AMPLITUDE OF FAST FOURIER TRANSFORMS (FFT) AT TOOTH FREQUENCY	38
4.2.1. Emulsion Cooling.....	38
4.2.2. MQL Cooling	42
4.2.3. LN2 Cooling.....	45
4.2.4. Combined (MQL + LN ₂) Cooling.....	48
4.3. COMPARATIVE INVESTIGATION OF RESULTANT CUTTING FORCES FOR ALL FOUR COOLING STRATEGIES UNDER UP AND DOWN- MILLING METHODS	51
5. CONCLUSIONS.....	54
ACKNOWLEDGEMENTS	56
REFERENCES	56
II. EFFECTS OF COOLING STRATEGIES AND TOOL COATINGS ON CUTTING FORCES AND TOOTH FREQUENCY IN HIGH SPEED DOWN-MILLING OF INCONEL-718 USING HELICAL BULL-NOSE SOLID CARBIDE END-MILLS	61
ABSTRACT.....	61
1. INTRODUCTION	62
2. EXPERIMENTAL PLAN AND PROCEDURE.....	70
2.1. COOLING STRATEGIES SET-UP	73
2.2. WORKPIECE PREPARATION	74
2.3. EXPERIMENTAL SET-UP AND PROCEDURE	75

2.3.1. Approach Distance Calculation.....	76
3. RESULT ANALYSIS.....	77
3.1. SAMPLE PLOTS FOR MAXIMUM CUTTING FORCE COMPONENTS AND FAST FOURIER TRANSFORM (FFT) VERSUS MACHINED LENGTH (PASS NUMBER)	77
3.2. MAXIMUM CUTTING FORCE COMPONENTS, RESULTANT CUTTING FORCE, AND FAST FOURIER TRANSFORMS (FFT) USING UNCOATED CARBIDE END-MILLS	80
3.2.1. MQL Cooling Strategy.....	80
3.2.2. LN ₂ Cooling Strategy.	82
3.2.3. Combined (MQL + LN ₂) Cooling Strategy.	84
3.3. MAXIMUM CUTTING FORCE COMPONENTS, RESULTANT CUTTING FORCE, AND FAST FOURIER TRANSFORMS (FFT) USING ALTIN COATED CARBIDE END-MILLS	86
3.3.1. MQL Cooling Strategy.....	86
3.3.2. LN ₂ Cooling Strategy.	87
3.3.3. Combined (MQL + LN ₂) Cooling Strategy.	89
3.4. MAXIMUM CUTTING FORCE COMPONENTS, RESULTANT CUTTING FORCE, AND FAST FOURIER TRANSFORMS (FFT) USING GMS ² COATED CARBIDE END-MILLS	90
3.4.1. MQL Cooling Strategy.....	90
3.4.2. LN ₂ Cooling Strategy.	91
3.4.3. Combined (MQL + LN ₂) Cooling Strategy.	93
3.5. COMPARATIVE INVESTIGATION OF RESULTANT CUTTING FORCES UNDER MQL, LN ₂ AND COMBINED (MQL + LN ₂) COOLING STRATEGIES, USING UNCOATED, ALTIN COATED AND GMS ² COATED END-MILLS	94
4. CONCLUSIONS.....	96
ACKNOWLEDGEMENTS	97
REFERENCES	97

III. EFFECTS OF UP AND DOWN-MILLING, AND COOLING STRATEGIES ON TOOL WEAR, CHIP MORPHOLOGY AND SURFACE ROUGHNESS IN HIGH SPEED END-MILLING OF INCONEL-718.....	101
ABSTRACT.....	101
1. INTRODUCTION	102
2. EXPERIMENTAL PLAN AND PROCEDURE.....	110
2.1. COOLING STRATEGIES SETUP.....	113
2.2. WORKPIECE PREPARATION	114
2.3. EXPERIMENTAL SETUP AND PROCEDURE.....	114
2.3.1. Tool Wear Measurement.....	115
2.3.2. Chip Analysis.....	115
2.3.3. Surface Roughness Measurement.....	115
2.3.4. Cutter Entry and Exit Angle during Up and Down-Milling, Chip Length and Approach Distance Calculations.....	116
3. RESULT ANALYSIS.....	122
3.1. MAXIMUM FLANK WEAR AND CHIP MORPHOLOGY FOR UP-MILLING AND DOWN-MILLING METHOD UNDER EMULSION COOLING STRATEGY.....	122
3.1.1. Maximum Flank Wear.....	122
3.1.2. Chip Morphology.....	125
3.2. MAXIMUM FLANK WEAR AND CHIP MORPHOLOGY FOR UP-MILLING AND DOWN-MILLING METHOD UNDER MQL COOLING STRATEGY.....	130
3.2.1. Maximum Flank Wear.....	130
3.2.2. Chip Morphology.....	132
3.3. MAXIMUM FLANK WEAR AND CHIP MORPHOLOGY FOR UP-MILLING AND DOWN-MILLING METHOD USING LN ₂ COOLING STRATEGY.....	135
3.3.1. Maximum Flank Wear.....	135

3.3.2. Chip Morphology	138
3.4. MAXIMUM FLANK WEAR AND CHIP MORPHOLOGY FOR UP AND DOWN-MILLING METHOD USING COMBINED (MQL + LN ₂) STRATEGY	140
3.4.1. Maximum Flank Wear.	140
3.4.2. Chip Morphology	142
3.5. COMPARITIVE EVALUATION OF AVERAGE SURFACE ROUGHNESS UNDER FOUR COOLING STRATEGIES FOR UP AND DOWN-MILLING METHODS	144
3.6. COMPARATIVE INVESTIGATION OF MAXIMUM FLANK WEAR UNDER FOUR COOLING STRATEGIES FOR UP AND DOWN METHODS	145
3.7. COMPARATIVE INVESTIGATION OF CALCULATED AND MEASURED CHIP LENGTHS FOR LAST PASS UNDER FOUR COOLING STRATEGIES FOR UP-MILLING AND DOWN-MILLING METHODS	148
4. CONCLUSIONS.....	149
ACKNOWLEDGEMENTS	150
REFERENCES	150
IV. EFFECTS OF TOOL COATINGS AND COOLING STRATEGIES ON TOOL WEAR, CHIP MORPHOLOGY AND SURFACE ROUGHNESS IN HIGH SPEED DOWN-MILLING OF INCONEL 718	154
ABSTRACT.....	154
1. INTRODUCTION	155
2. EXPERIMENTAL PLAN AND PROCEDURE.....	161
3. RESULTS AND DISCUSSIONS.....	170
3.1. MAXIMUM FLANK WEAR AND CHIP MORPHOLOGY FOR ALTIN COATED END-MILLS.....	170
3.1.1. Maximum Flank Wear.	170
3.1.2. Chip Morphology	174

3.2. MAXIMUM FLANK WEAR AND CHIP MORPHOLOGY FOR GMS ² COATED END-MILLS	178
3.2.1. Maximum Flank Wear.	178
3.2.2. Chip Morphology.	181
3.3. COMPARITIVE INVESTIGATION OF MAXIMUM FLANK WEAR UNDER ALL COOLING STRATEGIES AND TOOL COATINGS	184
3.4. COMPARITIVE EVALUATION OF END-MILL COATINGS AND COOLING STRATEGIES ON AVERAGE SURFACE ROUGHNESS.....	186
4. CONCLUSIONS.....	187
ACKNOWLEDGEMENTS	188
REFERENCES	189
SECTION	
2. CONCLUSIONS.....	192
2.1. CONCLUSIONS FROM EFFECTS OF UP-MILLING AND DOWN- MILLING METHODS, AND COOLING STRATEGIES ON CUTTING FORCES AND TOOTH FREQUENCY IN HIGH SPEED END-MILLING OF INCONEL 718 USING UNCOATED SOLID CARBIDE END-MILLS	192
2.2. CONCLUSIONS FROM EFFECTS OF COOLING STRATEGIES AND TOOL COATINGS ON CUTTING FORCES AND TOOTH FREQUENCY IN HIGH SPEED DOWN-MILLING OF INCONEL-718 USING HELICAL BULL-NOSE SOLID CARBIDE END-MILLS	193
2.3. CONCLUSIONS FROM EFFECTS OF UP AND DOWN-MILLING METHODS, AND COOLING STRATEGIES ON TOOL WEAR, CHIP MORPHOLOGY AND SURFACE ROUGHNESS IN HIGH SPEED END- MILLING OF INCONEL-718.....	195
2.4. CONCLUSIONS FROM EFFECTS OF TOOL COATINGS AND COOLING STRATEGIES ON TOOL WEAR, CHIP MORPHOLOGY AND SURFACE ROUGHNESS IN HIGH SPEED DOWN-MILLING OF INCONEL-718	196
VITA	198

LIST OF ILLUSTRATIONS

PAPER I	Page
Figure 1: High-speed cutting ranges in machining of various materials (redrawn) (Fallböhmer et al., 2000)	15
Figure 2: Initial shape of prepared work-piece, with holes for clamping on Cutting Force Dynamometer	17
Figure 3: Schematic of experiments performed on workpieces. (a) Workpiece 1 for experiment 1,2,5 and 6 and (b) Workpiece 2 for experiment 3,4,7 and 8.....	18
Figure 4: Experimental set-up with cryogenic and MQL flow lines and data acquisition system. (a) Schematic and (b) actual picture	28
Figure 5: Cutter entry and exit angle, and approach distance. (a) Cutter entry angle during down-milling and cutter exit angle during up-milling, (b) approach distance during down-milling and up-milling	32
Figure 6: Cutting force and FFT signals at 3 rd pass (255.81 mm machined length) for emulsion up-milling at 1127 rpm and 114.5 mm/min. (a) F_x , (b) F_y , (c) F_z , (d) FFT_x , (e) FFT_y and (f) FFT_z	36
Figure 7: Maximum cutting force components, resultant cutting force and FFT amplitudes of cutting force components vs pass numbers (machined length) in x, y and z-directions under emulsion, up-milling. (a) Maximum cutting force components and resultant cutting force, (b) FFT amplitudes	38
Figure 8: 3-D Material removal process (chip profile). (a) Up-milling and (b) Down-milling	40
Figure 9: Maximum cutting force components, resultant cutting force and FFT amplitudes of cutting force components vs pass numbers (machined length) in x, y and z-directions under emulsion, down-milling. (a) Maximum cutting force components and resultant cutting force, (b) FFT amplitudes	41
Figure 10: Maximum cutting force components, resultant cutting force and FFT amplitudes of cutting force components vs pass numbers (machined length) in x, y and z-directions under MQL, up-milling. (a) Maximum cutting force components and resultant cutting force, (b) FFT amplitudes.....	43
Figure 11: Maximum cutting force components, resultant cutting force and FFT amplitudes of cutting force components vs pass numbers (machined length) in x, y and z-directions under MQL, down-milling. (a) Maximum cutting force components and resultant cutting force, (b) FFT amplitudes	44

Figure 12: Maximum cutting force components, resultant cutting force and FFT amplitudes of cutting force components vs pass numbers (machined length) in x, y and z-directions under LN2, up-milling. (a) Maximum cutting force components and resultant cutting force, (b) FFT amplitudes.....	46
Figure 13: Maximum cutting force components, resultant cutting force and FFT amplitudes of cutting force components vs pass numbers (machined length) in x, y and z-directions under LN2, down-milling. (a) Maximum cutting force components and resultant cutting force, (b) FFT amplitudes	48
Figure 14: Maximum cutting force components, resultant cutting force and FFT amplitudes of cutting force components vs pass numbers (machined length) in x, y and z-directions under MQL + LN2, up-milling. (a) Maximum cutting force components and resultant cutting force, (b) FFT amplitudes	49
Figure 15: Maximum cutting force components, resultant cutting force and FFT amplitudes of cutting force components vs pass numbers (machined length) in x, y and z-directions under MQL + LN2, down-milling. (a) Maximum cutting force components and resultant cutting force, (b) FFT amplitudes	50
Figure 16: Resultant cutting forces against pass numbers (machined length) for all four cooling strategies under up-milling method.....	52
Figure 17: Resultant cutting forces against pass numbers (machined length) for all four cooling strategies under down-milling method.....	53
PAPER II	
Figure 1: High-speed cutting ranges in machining of various materials (redrawn) [25] ..	69
Figure 2: Initial shape of prepared work-piece, with drilled, counter-bored and tapped holes for clamping.....	71
Figure 3: Work-piece with schematic of experiments performed under three cooling strategies.....	72
Figure 4: Experimental set-up with cryogenic and MQL flow lines and data acquisition system.	74
Figure 5: Approach distance during down-milling operation	76
Figure 6: Cutting force and FFT signals for the 3 rd pass (255.81 mm machined length) for MQL down-milling using uncoated solid carbide tool at spindle speed of 1127 rpm and feedrate of 114.5 mm/min. (a) F_x , (b) F_y , (c) F_z , (d) FFT_x , (e) FFT_y and (f) FFT_z	78

Figure 7: Maximum cutting force components, resultant cutting force and FFT amplitudes of cutting force components vs pass numbers (machined length) in x, y and z-directions under MQL cooling strategy using uncoated end-mill. (a) Maximum cutting force components and resultant cutting force, (b) FFT amplitudes.....	81
Figure 8: 3-D Material removal process (chip profile) during down-milling method	82
Figure 9: Maximum cutting force components, resultant cutting force and FFT amplitudes of cutting force components vs pass numbers (machined length) in x, y and z-directions under LN ₂ cooling strategy using uncoated end-mill. (a) Maximum cutting force components and resultant cutting force, (b) FFT amplitudes	83
Figure 10: Maximum cutting force components, resultant cutting force and FFT amplitudes of cutting force components vs pass numbers (machined length) in x, y and z-directions under combined (MQL + LN ₂) cooling strategy using uncoated end-mill. (a) Maximum cutting force components and resultant cutting force, (b) FFT amplitudes.....	85
Figure 11: Maximum cutting force components, resultant cutting force and FFT amplitudes of cutting force components vs pass numbers (machined length) in x, y and z-directions under MQL cooling strategy using AlTiN coated end-mill. (a) Maximum cutting force components and resultant cutting force, (b) FFT amplitudes.....	86
Figure 12: Maximum cutting force components, resultant cutting force and FFT amplitudes of cutting force components vs pass numbers (machined length) in x, y and z-directions under LN ₂ cooling strategy using AlTiN coated end-mill. (a) Maximum cutting force components and resultant cutting force, (b) FFT amplitudes.....	88
Figure 13: Maximum cutting force components, resultant cutting force and FFT amplitudes of cutting force components vs pass numbers (machined length) in x, y and z-directions under combined (MQL + LN ₂) cooling strategy using AlTiN coated end-mill. (a) Maximum cutting force components and resultant force, (b) FFT amplitudes.....	89
Figure 14: Maximum cutting force components, resultant cutting force and FFT amplitudes of cutting force components vs pass numbers (machined length) in x, y and z-directions under MQL cooling strategy using GMS ² coated end-mill. (a) Maximum cutting force components and resultant cutting force, (b) FFT amplitudes.....	91

Figure 15: Maximum cutting force components, resultant cutting force and FFT amplitudes of cutting force components vs pass numbers (machined length) in x, y and z-directions under LN ₂ cooling strategy using GMS ² coated end-mill. (a) Maximum cutting force components and resultant cutting force, (b) FFT amplitudes.....	92
Figure 16: Maximum cutting force components, resultant cutting force and FFT amplitudes of cutting force components vs pass numbers (machined length) in x, y and z-directions under combined (MQL + LN ₂) cooling strategy using GMS ² coated end-mill. (a) Maximum cutting force components and resultant cutting force, (b) FFT amplitudes.....	93
Figure 17: Resultant cutting forces vs pass numbers (machined length) under all cooling strategies and end-mill coatings	95
 PAPER III	
Figure 1: High-speed cutting ranges in machining of various materials (redrawn) (Fallböhmer et al., 2000)	109
Figure 2: Initial shape of prepared work-piece, with drilled, counter-bored and tapped holes for clamping	111
Figure 3: Schematic of experiments performed on workpieces. (a) Workpiece 1 for experiment #1,2,5 and 6 and (b) Workpiece 2 for experiment #3,4,7 and 8...112	
Figure 4: Workpiece with surface roughness measurement locations	116
Figure 5: Cutter entry angle during down-milling and cutter exit angle during up-milling	117
Figure 6: Chip morphology with blown-up images showing maximum chip thickness and chip length. (a) Chip morphology, (b) maximum chip thickness and (c) chip length	119
Figure 7: Approach distance during down-milling and up-milling operation.....	121
Figure 8: Maximum flank wear vs number of passes (machined length) for up and down-milling under emulsion cooling strategy	122
Figure 9: Initial flank land and progressive flank wear for up and down-milling under emulsion cooling strategy. Emulsion up-milling at (a) pass 0, (b) pass 1, (c) pass 5 and (d) pass 8 and, emulsion down-milling at (e) pass 0, (f) pass 1, (g) pass 5 and (h) pass 8	123
Figure 10: 3-D Chip formation during up-milling and down-milling operations. (a) Up-milling and (b) down-milling operation	124

Figure 11: Free and Back surfaces of the chip. (a) Free Surface and (b) back surface	125
Figure 12: Free surface of chips for up and down-milling under emulsion cooling strategy. Emulsion up-milling at (a) pass 1, (b) pass 5 and (c) pass 8 and, emulsion down-milling at (d) pass 1, (e) pass 5 and (f) pass 8	126
Figure 13: Images of chips for up and down-milling under emulsion cooling strategy. Emulsion up-milling at (a) pass 1, (b) pass 5 and (c) pass 8 and, emulsion down-milling at (d) pass 1, (e) pass 5 and (f) pass 8	127
Figure 14: 3-D chip morphology during up and down-milling operations. (a) Up-milling and (b) down-milling operation	128
Figure 15: Segmented chips with typical saw-tooth obtained in emulsion up-milling. (a) pass 1 (b) pass 5 and (c) pass 8	129
Figure 16: Calculated and measured chip lengths vs number of passes (machined length) and milling methods under emulsion cooling strategy	130
Figure 17: Maximum flank wear vs number of passes (machined length) for up and down-milling under MQL cooling strategy	131
Figure 18: Measured maximum flank wear for up and down-milling under MQL cooling strategy. MQL up-milling at (a) pass 0, (b) pass 1, (c) pass 2 and (c) pass 4 and, MQL down-milling at (e) pass 0, (f) pass 1, (g) pass 4 and (h) pass 8	132
Figure 19: Images of chips for up and down-milling under MQL cooling strategy. MQL up-milling at (a) pass 1, (b) pass 2 and (c) pass 4 and, MQL down-milling at (d) pass 1, (e) pass 4 and (f) pass 8	133
Figure 20: Free surface of chips for up and down-milling under MQL cooling strategy. MQL up-milling at (a) pass 1, (b) pass 2 and (c) pass 4 and MQL down-milling at (d) pass 1, (e) pass 4 and (f) pass 8	134
Figure 21: Calculated and measured chip lengths vs number of passes (machined length) and milling methods under MQL cooling strategy	135
Figure 22: Maximum flank wear vs number of passes (machined length) for up and down-milling under LN ₂ cooling strategy	136
Figure 23: Maximum flank wear for up and down-milling under LN ₂ cooling strategy. LN ₂ up-milling at (a) pass 0 and (b) pass 1 and, LN ₂ down-milling at (c) pass 0, (d) pass 1, (e) pass 6 and (f) pass 8	137

Figure 24: Images of chips for up and down-milling under LN ₂ cooling strategy. LN ₂ up-milling at (a) pass 1 and LN ₂ down-milling at (d) pass 1, (e) pass 6 and (f) pass 8	138
Figure 25: Free and back surface of chips for up-milling and free surface of chips for down-milling under LN ₂ cooling strategy. (a) Free and back surface of chips for LN ₂ up-milling at pass 1 and, free surface of chips for LN ₂ down-milling at (d) pass 1, (e) pass 6 and (f) pass 8	139
Figure 26: Calculated and measured chip lengths vs number of passes (machined length) and milling methods under LN ₂ cooling strategy.....	140
Figure 27: Maximum flank wear vs number of passes (machined length) for up and down-milling under combined (MQL + LN ₂) cooling strategy.....	140
Figure 28: Measured maximum flank wear for up and down-milling under MQL + LN ₂ cooling strategy. MQL + LN ₂ up-milling at (a) pass 0, (b) pass 1, (c) pass 2 and (c) pass 3 and, MQL + LN ₂ down-milling at (e) pass 0, (f) pass 1, (g) pass 4 and (h) pass 8.....	141
Figure 29: Images of chips for up and down-milling under MQL + LN ₂ cooling strategy. MQL + LN ₂ up-milling at (a) pass 1, (b) pass 2 and (c) pass 3 and MQL + LN ₂ down-milling at (d) pass 1, (e) pass 3 and (f) pass 8	142
Figure 30: Free surface of chips for up and down-milling under combined (MQL + LN ₂) cooling strategy. Combined (MQL + LN ₂) up-milling at (a) pass 1, (b) pass 2 and (c) pass 3 and, (MQL + LN ₂) down-milling at (d) pass 1, (e) pass 3 and (f) pass 8	143
Figure 31: Calculated and measured chip lengths vs number of passes (machined length) and milling methods under MQL + LN ₂ cooling strategy	144
Figure 32: Surface roughness vs cooling strategies and milling methods	145
Figure 33: Maximum flank wear vs machining passes (machined length) for up-milling method under four cooling strategies	146
Figure 34: Maximum flank wear vs machining passes (machined length) for down-milling method under four cooling strategies.....	147
Figure 35: Calculated chip length and measured chip lengths vs milling methods and cooling strategies for for last passes.....	148
 PAPER IV	
Figure 1: Initial shape of prepared work-piece, with drilled, counter-bored and tapped holes for clamping	163

Figure 2: Schematic of experiments performed on workpiece.....	165
Figure 3: Workpiece with surface roughness measurement locations	166
Figure 4: Cutter entry angle during down-milling operation and blown-up image showing chip length and maximum chip thickness. (a) Cutter entry angle during down-milling and (b) Chip length, L_c	167
Figure 5: Approach distance during down-milling operation	170
Figure 6: Maximum flank wear vs number of passes (Machined length) for AlTiN coated end-mills using four cooling strategies	171
Figure 7: 3-D Chip formation during down-milling operation	172
Figure 8: Initial flank land and progressive flank wear for AlTiN coated end-mills under four cooling strategies. MQL cooling (a) Pass 0, (b) Pass 1, (c) Pass 4 and (d) Pass 8, LN ₂ cooling (e) Pass 0, (f) Pass 1, (g) Pass 4 and (h) Pass 8 and, Combined (MQL + LN ₂) cooling (i) Pass 0, (j) Pass 1, (k) Pass 4 and (l) Pass 8	173
Figure 9: Free and Back surfaces of the chip. (a) Free surface and (b) Back surface	174
Figure 10: Schematic and actual chip morphology showing lamella structure during down-milling operation. (a) Schematic of 3-D chip and (b) Actual chip showing lamella structure.....	175
Figure 11: Free surface of chips for AlTiN coated end-mills under four cooling strategies. MQL cooling (a) Pass 1, (b) Pass 4 and (c) Pass 8, LN ₂ cooling (d) Pass 1, (e) Pass 4 and (f) Pass 8 and, Combined (MQL + LN ₂) cooling (g) Pass 1, (h) Pass 4 and (i) Pass 8.....	176
Figure 12: Images of chips for AlTiN coated end-mills under four cooling strategies. MQL cooling (a) Pass 1, (b) Pass 4 and (c) Pass 8, LN ₂ cooling (d) Pass 1, (e) Pass 4 and (f) Pass 8 and, Combined (MQL + LN ₂) cooling (g) Pass 1, (h) Pass 4 and (i) Pass 8.....	177
Figure 13: Calculated and measured chip lengths vs number of passes (Machined length) and cooling strategies for AlTiN coated end-mills	178
Figure 14: Maximum flank wear vs number of passes (Machined length) for GMS ² Coated end-mills under four cooling strategies.....	179

- Figure 15: Initial flank land and progressive flank wear for GMS²coated end-mills under four cooling strategies. MQL cooling (a) Pass 0, (b) Pass 1, (c) Pass 4 and (d) Pass 8, LN₂ cooling (e) Pass 0, (f) Pass 1, (g) Pass 4 and (h) Pass 8 and, Combined (MQL + LN₂) cooling (i) Pass 0, (j) Pass 1, (k) Pass 4 and (l) Pass 8180
- Figure 16: Free surface of chips for GMS² coated end-mills under four cooling strategies. MQL cooling (a) Pass 1, (b) Pass 4 and (c) Pass 8, LN₂ cooling (d) Pass 1, (e) Pass 4 and (f) Pass 7 and, Combined (MQL + LN₂) cooling (g) Pass 1, (h) Pass 4 and (i) Pass 8.....181
- Figure 17: Images of chips for GMS² coated end-mills under four cooling strategies. MQL cooling (a) Pass 1, (b) Pass 4 and (c) Pass 8, LN₂ cooling (d) Pass 1, (e) Pass 4 and (f) Pass 7 and, Combined (MQL + LN₂) cooling (g) Pass 1, (h) Pass 4 and (i) Pass 8.....183
- Figure 18: Calculated and measured chip lengths vs number of passes (Machined length) and cooling strategies for GMS² coated end-mills.....184
- Figure 19: Maximum flank wear vs end-mill coatings and cooling strategies after 1st pass185
- Figure 20: Average surface roughness vs cooling strategies and end-mill coatings186

LIST OF TABLES

PAPER I	Page
Table 1: Experiment plan for investigation of end-milling methods, cooling strategies and machining parameters using uncoated helical bull-nose solid carbide end-mills	19
Table 2: Calibration data for cryogenic temperature.....	24
Table 3: ANOVA for Calibration of Cryogenic set-up.....	24
Table 4: Results of multiple regression model for calibration data.....	25
Table 5: Pressure predicted values from calibration equation.....	26
Table 6: Physical and Mechanical properties of Inconel 718 (A. Shokrani et al., 2012).....	26
Table 7: Chemical composition of Inconel 718 given by manufacturer	27
PAPER II	
Table 1: Experiment plan for investigation of cooling strategies, tool coatings and machining parameters under down-milling operation using helical bull-nose solid carbide end-mills	70
PAPER III	
Table1: Experiment plan for investigation of end-milling methods, cooling strategies and machining parameters using uncoated helical bull-nose solid carbide end-mills	110
PAPER IV	
Table 1: Experiment plan for investigation of cooling strategies, tool coatings and machining parameters under down-milling operation using helical bull-nose solid carbide end-mills	162

SECTION

1. INTRODUCTION

Inconel 718 super alloy is used extensively in aerospace and nuclear industries for components such as turbine blades, low and high-pressure disc compressors used in high temperature, high load and corrosion resistance compartments of jet and gas turbine engines, due to its excellent properties such as: high strength-to-weight ratio, ability to retain its properties at high temperatures, high corrosion and creep resistance. However, Inconel 718 is characterized as a very “difficult-to-cut” material, because it poses problems during machining. Enormous amount of heat is generated in the cutting zone due to high friction between the tool-chip interface and tool-workpiece interface and is not removed as quickly as it is generated due to its low thermal conductivity. Therefore, the heat is mostly concentrated on the tool cutting edges, causing severe tool wear. Also, due to high temperature and pressure at the cutting zone, some fragments of chips from the workpiece get welded on the cutting edges of the tool, which further exacerbates tool wear. Its good mechanical strength and ability to work harden at elevated temperatures leads to high cutting forces and its high chemical affinity with many cutting tool materials leads to welding of the tool to form built-up edge (BUE). End milling is a widely used machining operation due to its versatility. Its applications may range from aerospace and automotive industries to small tool and die shops, as it can be used for milling many features like peripheral, slot or face milling. Some problems encountered while machining using end-milling operations are high cutting forces, high cutting temperature, rapid tool wear, tool breakage, and chatter. These problems associated with

end-milling are further exacerbated while machining difficult-to-cut metals such as Inconel 718 because the desired properties of this difficult-to-cut metal become disadvantage while machining them. Due to the problems mentioned above, care must be taken to select appropriate machining parameters when machining difficult-to-cut metals. Also, it is pertinent to decrease the cutting zone temperature so as to reduce tool wear and cutting forces. Application of coolants and lubricants play an important role in addressing these problems, as they reduce cutting temperature, friction and tool wear, cutting force/power consumed, improve surface roughness, and hence, improve machinability. Mineral-based conventional cutting fluids commonly used in most industries are expensive, environmentally unfriendly and difficult to dispose and, cause health hazards. Thus, there is a need to find sustainable environmentally friendly cooling strategies to replace expensive, difficult-to-dispose conventional emulsion cooling strategy with sustainable, cost-effective, environmentally friendly and more efficient cooling strategy to reduce cost and improve performance. From literature, it has been seen that the other parameters, which have potential to improve the machinability of Inconel-718, are: milling methods, end-mill coatings and machining at elevated cutting speeds. Also, it has been seen that there is a lack of comprehensive study summarizing the effects of milling methods, sustainable cooling strategies and end-mill coatings on machinability parameters: cutting forces, amplitude of tooth frequency, tool wear, chip morphology and surface roughness in end-milling of Inconel-718 at a cutting speed higher than currently being used in industry.

The current research is focused on the investigation of different cooling strategies and end-mill coatings with up and down-milling to improve machinability of Inconel 718 and is accomplished under two objectives.

The first objective of the current research is to investigate the results of the effects of four cooling strategies (Conventional emulsion flood cooling, Minimum Quantity Lubrication (MQL), Liquid Nitrogen (LN₂) and Combined (MQL+LN₂)) on cutting force components in the x, y and z directions (F_x , F_y , F_z), calculated resulting cutting force (F_r), Fast Fourier Transforms (FFT) of cutting force components in the x, y and z directions, maximum flank wear, chip morphology and surface roughness (R_a) in peripheral end-milling of Inconel-718 under high speed machining, during up and down-milling operations, using 4-flute uncoated solid carbide bull-nose helical end-mills. Results from the first objective are analyzed to find the better milling method among up-milling and down-milling and to identify three (3) best cooling strategies among the four (4), which were used to perform further experiments under second objective using coated carbide end-mills.

The second objective is to investigate the effects of three best cooling strategies determined from the first objective and three tool coatings (Uncoated, AlTiN coated, GMS² coated) on cutting force components in the x, y and z directions (F_x , F_y , F_z), calculated resulting cutting force (F_r), FFT of cutting force components in the x, y and z directions (FFT_x , FFT_y , FFT_z), maximum flank wear, chip morphology and surface roughness (R_a) in peripheral end-milling of Inconel 718 under high speed machining, using best milling method among up-milling and down-milling determined from first objective, with multi-flute solid carbide bull-nose helical end-mills.

Finally, a better milling method among up and down-milling, cooling strategy among four (Conventional emulsion flood cooling, Minimum Quantity Lubrication (MQL), Liquid Nitrogen (LN₂) and Combined (MQL+LN₂)) and end-mill coating among the three (Uncoated, AlTiN coated, GMS² coated) are determined for high-speed machining of Inconel 718.

PAPER**I. EFFECTS OF UP-MILLING AND DOWN-MILLING METHODS, AND COOLING STRATEGIES ON CUTTING FORCES AND TOOTH FREQUENCY IN HIGH SPEED END-MILLING OF INCONEL 718 USING UNCOATED SOLID CARBIDE END-MILLS**

A. Chukwujekwu Okafor, Paras Mohan Jasra
Computer Numeric Control and Virtual Manufacturing Laboratory
Department of Mechanical and Aerospace Engineering
Missouri University of Science and Technology
327 Toomey Hall, Rolla MO. 65409-005, USA
E-mail: okafor@mst.edu

ABSTRACT

This paper presents the results of experimental investigation of the effects of milling methods (up-milling and down-milling) and four cooling strategies (Emulsion flood, Minimum Quantity Lubrication (MQL), Cryogenic cooling using Liquid Nitrogen (LN₂) and Combined (MQL+LN₂)) on cutting force components (F_x , F_y , F_z), the resultant cutting force, F_r , and cutter tooth frequency in peripheral high speed end-milling of Inconel 718. All the experiments were conducted on a Cincinnati Milacron Sabre 750 Vertical Machining Centre (VMC), equipped with Acramatic 2100 CNC controller using 4-flute uncoated solid carbide bull-nose helical end-mills. The three cutting force components and their Fast Fourier Transforms (FFT) were acquired using a Kistler 9272 4-component dynamometer. Resultant cutting forces, F_r , were calculated from acquired cutting force components, as well as the amplitudes of the FFTs. The experimental results show that down-milling generated lower cutting forces than up-milling under all

cooling strategies. Also, MQL cooling generated the lowest cutting forces, followed by combined (MQL+LN₂) cooling using down-milling operation. The amplitude of FFT of the cutting force components at 75.13 Hz tooth frequency versus machined length follows the same trend as cutting force components and thus, can be used to perform a comparative evaluation of cutting forces.

Keywords: Up-milling and Down-milling; Inconel 718; Cutting force components; Fast Fourier Transforms; Minimum Quantity Lubrication; Cryogenic cooling

1. INTRODUCTION

Inconel 718 is one of the Nickel-based superalloys used extensively in aerospace and automotive industries for applications in high temperature media such as in jet engines, gas turbines, spacecraft, and nuclear reactor. They are suitable for hostile environments due to their excellent combination of peculiar properties such as: high strength-to-weight ratio, ability to retain their properties at high temperatures, high corrosion and creep resistance (Ezugwu & Wang, 1997). Inconel 718 is among the most “difficult-to-cut materials”, due to its high strength even at elevated temperatures and the problems it poses during machining such as: low thermal conductivity (Shokrani et al., 2017), ability to work harden at elevated temperatures, high chemical affinity with many cutting tool materials (Hadi et al., 2013), high cutting forces and rapid tool wear (Liao et al., 2008). Inconel 718 has specifically low thermal conductivity. Thus, the high heat generated during its machining is not removed as quickly as it is generated which increases the temperature at the cutting zone. This extreme heat generated in the cutting zone adversely affects the cutting tool flutes and increases tool wear and hence, cutting forces. End-milling operations are performed widely in aerospace and automotive

industries due to its versatility. Applications may range from aerospace to small tool and die shop, as it can be used for milling many features like peripheral, slot or face milling. Some problems encountered in end-milling operations are high cutting forces, high cutting temperature, rapid tool wear, tool breakage, and chatter. These problems are exacerbated while machining difficult-to-cut metals because the desired properties of difficult-to-cut metals become disadvantage while machining them.

Application of coolants and lubricants play important roles in addressing these problems, as they reduce cutting temperature, decrease tool wear, improve surface roughness, reduce cutting force/power consumed and hence, improve machinability. The conventional emulsion cutting fluids commonly used in most industries are expensive, environmentally unfriendly and difficult to dispose, and cause health hazards (Kamata and Obikawa, 2007).

The use of Minimum Quantity Lubrication (MQL) eliminates the problem of disposal of conventional coolants. MQL sprays tiny particles of oil in mist form on the cutting zone in very less quantity which acts as a lubricant, thereby solving the problem of disposal. Moreover, MQL does not have any health hazard and is considered to be environmentally friendly. There is a vast literature showing efficient use of MQL in improving machinability. Zhao et al. (2007) investigated the effect of dry and MQL machining on cutting forces, surface roughness, tool wear and tool life using uncoated cemented carbide inserts in high speed peripheral milling of Ti-6Al-4V. They reported that MQL reduced the cutting forces and surface roughness, and increased tool life. Dhar et al. (2007) compared the performance of MQL to dry lubrication in turning of AISI-1040 steel based on the measurements of cutting temperature, chip reduction coefficient,

cutting forces, tool wears, surface finish, and dimensional deviation. They reported that MQL lubrication reduced the cutting temperature and cutting forces, improved tool-chip interaction and, reduced tool wears, surface roughness and dimensional deviation.

Ahmad Yasir et al. (2009) investigated the machinability of Ti-6Al-4V at two different flow rates of MQL (50 and 100 mL/H) and three levels of cutting speed (120, 135 and 150 m/min) in down-milling under dry and MQL cutting conditions using Physical Vapour Deposition (PVD) coated cemented carbide tools. They concluded that the application of MQL was more effective at a cutting speed of 135 m/min and longer tool life was achieved when higher MQL flow rate was applied. They also concluded that higher MQL flow rate was less effective than lower MQL flow rate at high cutting speed due to difficulty of penetration of larger MQL particles into cutting zone. It was shown that the surface roughness was more sensitive to the feed-rate and the depth of cut compared to the cutting speed and that coolant flow rate were not sensitive to surface roughness. Also, they reported that MQL was more effective with worn out tools.

Kamata and Obikawa (2007) applied MQL to finish-turning of Inconel 718 with three different coated carbide tools and compared the performance of MQL with dry and wet cooling. They found that varying the air pressure and flow rate of MQL affects tool life in finish-turning of Inconel 718. It was also concluded that argon plays an important role as a carrier gas of oil mist in MQL. Boubekri and Shaikh (2012) emphasized the need to install the mist collector and filtering equipment in the work area where MQL is used as MQL generates quite a large amount of mist which can be detrimental to operators.

Liquid Nitrogen (LN₂) cooling, commonly called cryogenic cooling is applied to the cutting zone to reduce temperature at the cutting zone. It evaporates as nitrogen gas

after reducing the cutting zone temperature which does not cause greenhouse effect, hence causing no problem of disposal unlike conventional coolants. Kaynak (2014) investigated the machining performance of cryogenic machining of Inconel 718 and compared it with dry and MQL machining. He concluded that MQL resulted in lower cutting forces at a cutting speed of 60 m/min than dry and cryogenic machining whereas, cryogenic machining yielded lower cutting forces than dry and MQL machining at a cutting speed of 120 m/min. He also concluded that at higher cutting speed, cryogenic cooling performed better whereas MQL is recommended at lower cutting speed. Hong et al. (2001) proposed a new approach of cryogenic cooling to improve tool life in machining Ti-6Al-4V. They reported that the combination of two specially designed nozzles provides most effective way of cooling while using lowest flow rate of liquid nitrogen. The nitrogen was provided through micro nozzles into tool chip interface at the point of highest temperature. When nitrogen evaporated, the evaporating nitrogen provided the cushion at tool chip interface which reduced the coefficient of friction between the chip and the tool. Aramcharoen and Chuan (2014) investigated the effects of dry, wet and cryogenic cooling on cutting force, machining temperature, tool wear, machined surface quality, chip formation and energy consumption in milling of Inconel 718. They reported improvement in machinability in terms of tool wear reduction and improved machined surface quality. They reported that the application of cryogenic increased the cutting forces as compared to conventional oil based coolant. Also, they reported that cryogenic cooling reduced the contact friction between the tool-chip interface and thus, enhanced the efficiency of lubricating action. Dhananchezian and Kumar (2011) investigated the effects of cryogenic cooling and wet cooling on cutting

temperature, cutting forces, surface roughness and tool wear in turning Ti-6Al-4V using coated carbide inserts. They reported that cryogenic cooling caused significant reduction in cutting temperature, cutting force, surface roughness and tool wear as compared to wet machining. Ravi and Kumar (2011) presented the results on the effects of dry, wet and LN₂ cooling on machinability in end-milling of hardened steel using PVD coated carbide inserts. They reported that LN₂ lowered the cutting forces, cutting temperature, tool flank wear and surface roughness as compared with dry and wet machining. Kim et al. (2001) investigated the effects of dry, flood and compressed chilly-air coolants on tool life in machining difficult-to-cut materials having hardness varying from HRc28 to HRc60 using various coated tools. They reported improvement in tool life when machining using compressed chilly-air coolant. Su et al. (2007) investigated the effects of dry cutting, cooling air at -20°C and cooling air and minimum quantity lubrication (CAMQL) cooling at -20°C in finish turning of Inconel 718 and the effects of dry cutting, MQL cooling and cooling air at -20°C in high speed milling of AISI D2 cold work tool steel on tool wear, surface finish and chip shape. They reported improvement in tool wear, surface finish and chip shape using cooling air and CAMQL in finish turning of Inconel 718, whereas in high speed milling of AISI D2, cooling air cutting provided long tool life and slightly higher surface roughness than dry cutting and MQL. Shokrani et al. (2012) investigated the effects of dry and cryogenic machining on surface roughness and power consumption in end-milling of Inconel 718. They reported that cryogenic improved the surface roughness without noticeable increase in power consumption. They also reported that the use of cryogenic cooling reduced the tool life of coated solid carbide end-mills. Hong et al. (2001) while investigating the effects of cryogenic cooling machining on

friction and cutting forces in machining of Ti-6Al-4V proposed a new economical cryogenic cooling approach. In this approach, they used a minimum amount of LN₂ which was injected through micro-nozzle between tool rake and chip breaker and also assisted by auxiliary mini-nozzle on flank face for cooling flank. In this way, the LN₂ is not wasted by cooling the unnecessary areas which reduces the negative impact of increase of cutting forces and abrasion of pre-cooling of workpiece. Shokrani et al. (2016) conducted several experiments at various combinations of cutting parameters to investigate the effects of dry, flood and cryogenic cooling on surface integrity in the end-milling of Ti-6Al-4V titanium alloy using TiN-TiAlN coated solid carbide tool and reported that cryogenic cooling improved the surface roughness and reduced the surface roughness defect as compared to dry and flood cooling. Musfirah et al. (2017) reported that cryogenic cooling reduced tool wear, cutting forces, surface roughness and deformation of microstructure changes at the cut surface level than dry machining in high speed machining of Inconel 718 using PVD TiAlN/AlCrN coated tungsten carbide inserts.

MQL cooling combined with LN₂ cooling helps in reduction of cutting zone temperature and provides lubrication between tool and workpiece during machining. Su et al. (2010) investigated the effect of cryogenic minimum quantity lubrication (CMQL) at a temperature of -10 and -20°C on cutting temperature and tool wear in high-speed end-milling of titanium alloys and compared the performance of CMQL with dry milling and refrigerated air cutting at -10 and -20°C. They reported that CMQL at -20°C resulted in reduction in cutting temperature and tool wear when machining Ti-6Al-4V at high speed. Zhang et al. (2012) investigated tool wear and cutting forces in end-milling

of Inconel 718 under dry and Minimum Quantity Cooling Lubrication (MQCL) cooling strategies using cemented coated carbide insert. They concluded that tool life under MQCL cutting condition is 1.57 times better than dry cutting condition due to less tool wear. Also, they reported lower cutting forces under MQCL cutting condition as compared to dry cutting condition. Su et al. (2006) investigated the effect of different cooling strategies on tool life in high speed end-milling of Ti-6Al-4V. The cooling strategies used were dry, flood coolant, nitrogen-oil-mist cooling, compressed cold nitrogen gas (CCNG) at 0 and -10°C and, compressed cold nitrogen gas and oil mist (CCNGOM) at -10°C. They concluded that CCNGOM at -10°C yielded the best tool life among all cooling strategies. They also reported that flank wear was responsible for tool failure while machining using dry, nitrogen-oil-mist cooling, CCNG and CCNGOM cooling, whereas, excessive chipping at cutting edge and fracture on the flank face were responsible for tool failure when machining using flood cooling. Yuan et al. (2011) investigated the influence of dry, wet, MQL and MQL with cooling air at different temperatures of 0, -15°C, -30°C and -45°C on cutting force, tool wear, surface roughness and chip morphology in milling of Ti-6Al-4V with uncoated cemented carbide inserts having two teeth. They found that MQL cooling with cooling air significantly reduced the cutting force, tool wear and surface roughness. Also, MQL with cooling air at -15°C provided more favourable effects than MQL with cooling air at other temperatures. They found that MQL with cooling air produced shorter chips because high velocity of cooling air increased the chip brittleness which helped the chips to break easily and also helped the lubricant to penetrate to the chip-tool interface to reduce friction. Shokrani et al. (2017) investigated the effects of MQL, cryogenic cooling and a novel hybrid cryogenic

and MQL (CryoMQL) cooling on tool life and surface roughness in milling of age hardened Inconel 718 and reported that hybrid CryoMQL increased the tool life due to reduction in tool wear growth rate and average surface roughness of the bottom surface of milled workpiece reduced by 18% as compared to MQL. Iturbe et al. (2016) further reported that the benefits of cryogenic + MQL machining over conventional machining are not evident where machining time is longer and cutting conditions are close to that used in industry and thus, the cryogenic + MQL has tool life even shorter than the tool life requirements established by industry.

Tool wear and vibrations/chatter in machining have been shown to be correlated with cutter tooth frequency. Cutter tooth frequency and their higher harmonics are obtained by FFT of the cutting force signals or acceleration signals and used for indirect monitoring of tool wear and vibrations. As stated by Lee et al. (2017), signal features which are usually considered in frequency domain are signal energy in specific frequency range and the amplitude of the dominant spectral peaks. Huang et al.(2013) stated that when chatter occurs, milling forces increase dramatically as compared to stable cutting condition.

High Speed Machining (HSM), considered among the most efficient and effective modern manufacturing technologies, is employed to increase productivity, improve product quality and reduce manufacturing costs (Fang and Wu, 2009). Figure 1 shows the commonly accepted cutting speed ranges in high-speed machining of various materials (Fallböhmer et al., 2000). The figure shows that high cutting speed range depends on the strength and machinability of the material. The higher the strength and the more difficult-to cut of the material, the lower the high cutting speed range. Thus high

cutting speed range for Aluminium is higher than high cutting speed range for Nickel alloys. Safari et al. (2014) investigated the effects of 3 cutting speeds (200, 250 and 300 mm/min) on cutting force and surface roughness in cryogenic high speed end-milling of Ti-6Al-4V using coated and uncoated tools. They reported lowest cutting forces at highest cutting speed of 300 mm/min. Liao et al. (2008) studied the behaviour of side and slot-milling in high speed machining of Inconel 718. They concluded that cutting temperature and chip flow condition are the two most important factors affecting high speed milling of Inconel 718. They recommended appropriate cutting speed range of 55-135 m/min for side milling. Abele and Fröhlich (2008) reviewed several published research and concluded that high speed milling of Ti-6Al-4V reduces cutting forces as compared to conventional machining and improves performance by increasing material removal rate.

Another factor that can also help increase the efficiency in machining of Inconel 718 alloy and other difficult-of-cut metals is milling method. The kinematics of milling process (up-milling or down-milling) has significant effect on cutting performance and stress distribution during the material removal (Bouzakis et al., 2008). Tian et al. (2013) conducted series of experiments to identify the effects of cutting speed on cutting force and tool wear in high speed face milling of Inconel 718 using up-milling and down-milling methods. They reported that at a cutting speed range of 600 – 1400 m/min, the resultant cutting forces under down-milling were higher than up-milling whereas at a cutting speed range of 1800 – 3000 m/min, resultant cutting forces under up-milling were higher. Li et al. (2006) concluded that tool flank wear propagation in down-milling was

less rapid than in up-milling during end-milling of Inconel 718 using coated carbide inserts.

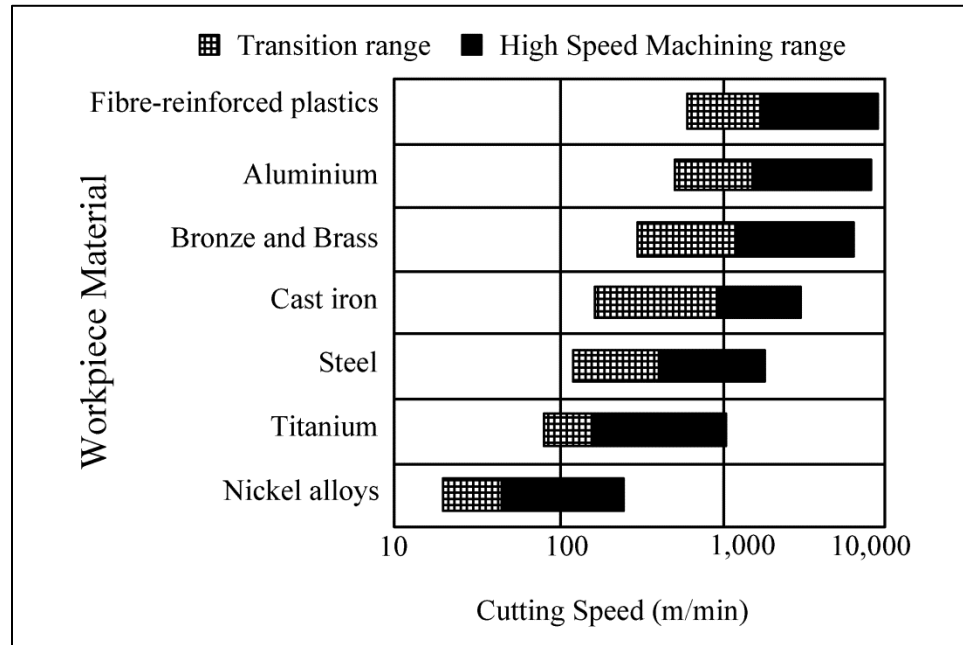


Figure 1: High-speed cutting ranges in machining of various materials (redrawn) (Fallböhmer et al., 2000)

From the above literature, it can be seen that there is a lack of comprehensive study summarizing the effects of milling methods and cooling strategies on cutting force and amplitude of tooth frequency in high-speed end-milling of Inconel-718. Furthermore, the potential of combining two different cooling strategies using carbide end-mills at machining speed higher than current industry standards (Ulutan et al., 2015) for milling nickel-based superalloy using uncoated carbide end-mills has not been investigated. Most of the published research on machinability of Inconel-718 alloy focused on dry machining or on one individual cooling strategy and mostly in turning, but the mechanics of milling is different from that of turning. Only a few studies have been performed comparing different cooling strategies using one of the milling methods

on some of the difficult-to-cut metals at claimed high cutting speeds but at very low material removal rate and total material removed, which are too low to be implemented in actual industry for machining nickel alloys like Inconel 718, which is a highly difficult-to-cut metal. Although limited literature is available to understand the cutting force of some of the materials at high cutting speed ranges like cast iron, steel or titanium as shown in Figure 1, but it is difficult to apply the research findings of one material to other as published literature on HSM of two materials often involves different machining setups (Fang & Wu, 2009). Therefore, there is a strong need to investigate the effects of different cooling strategies under up-milling and down-milling methods to improve machinability of Inconel-718.

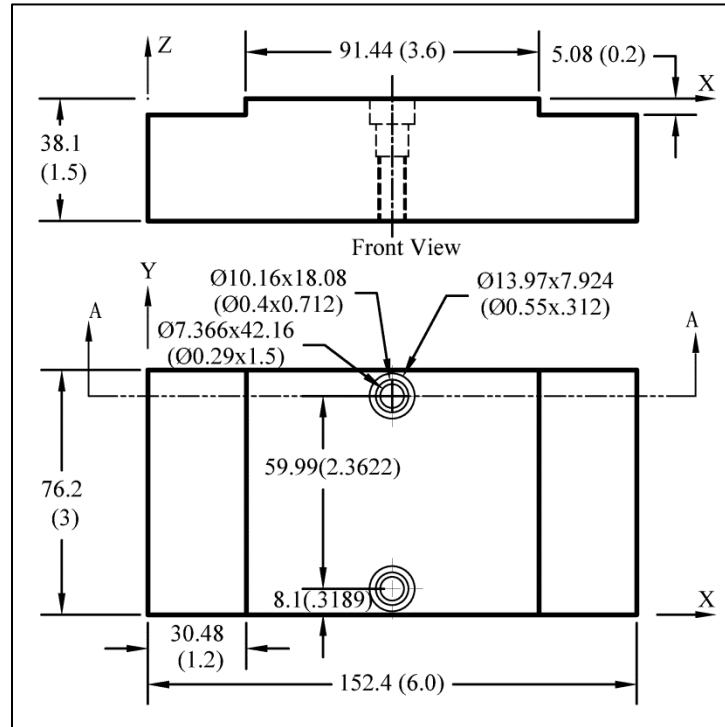
2. EXPERIMENTAL DESIGN

Peripheral high-speed end-milling tests were conducted on Cincinnati Milacron Sabre 750 Vertical Machining Centre (VMC), equipped with Acramatic 2100 CNC controller, using four-flute uncoated solid carbide end-mills of diameter 12.7 mm (0.5 inches).

2.1. EXPERIMENTAL PARAMETERS AND CUTTING CONDITIONS

Peripheral high-speed end-milling tests were conducted on two (2) workpiece blocks, each having two steps on each of the two sides, using 12.7 mm (0.5 in) diameter, uncoated 4-flute carbide end-mills for both up-milling and down-milling. Four (4) cooling strategies (Emulsion, MQL, LN₂ and combined (MQL+LN₂)) were investigated under each of the up-milling and down-milling methods. Each experiment was replicated

once, thus the total number of experiments was sixteen (16). The initial shape of the workpiece is given in Figure 2.

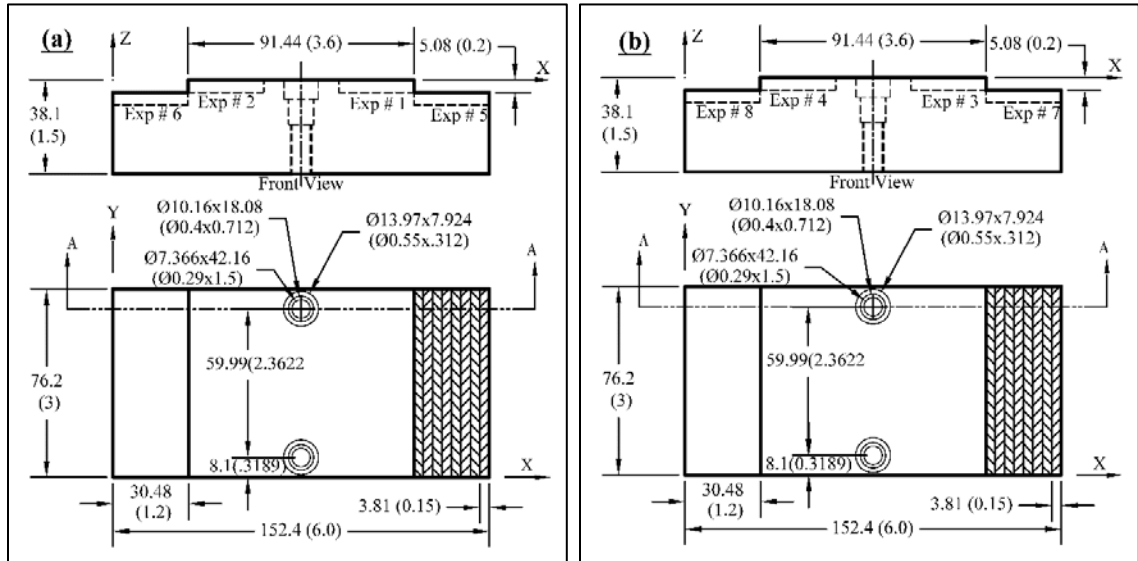


All dimensions in mm (inches)

Figure 2: Initial shape of prepared work-piece, with holes for clamping on Cutting Force Dynamometer

All the experiments were performed at same cutting speed of 1127 rpm (45 m/min), feed-rate of 114.5 mm/min (4.510 ipm), axial depth of cut (a_a) of 5.08 mm (0.2 in) and radial depth of cut (a_r) of 3.81 mm (0.15 in) which were selected based on literature review and preliminary investigation. Axial depth of cut (a_a), radial depth of cut (a_r) and feed per revolution (f_r) were kept constant and were selected to improve productivity without adversely sacrificing tool life (performance). For one set of experiments, the total number of tools used was eight (8) uncoated carbide end-mills, and workpieces used were two (2). Figure 3 (a) Shows workpiece 1 with the sequence of

experiments performed. Figure 3 (b) shows workpiece 2 and the sequence of experiments performed.



All dimensions in mm (inches)

Figure 3: Schematic of experiments performed on workpieces. (a) Workpiece 1 for experiment 1,2,5 and 6 and (b) Workpiece 2 for experiment 3,4,7 and 8

As shown in Figure 3 (a), block 1 was used to conduct peripheral end-milling test under emulsion cooling strategy for up-milling (Experiment #1) and down-milling (Experiment #2) and, peripheral milling test under LN₂ cooling strategy for up-milling (Experiment #5) and down-milling (Experiment #6). Similarly block 2 was used to conduct peripheral milling test under MQL cooling strategy for up-milling (Experiment #3) and down-milling (Experiment #4) and, peripheral milling test under combined (MQL+LN₂) cooling strategy for up-milling (Experiment #7) and down-milling (Experiment #8). The detailed experimental plan for the investigation of the effects of cooling strategies, end-milling methods and machining parameters using uncoated carbide bull-nose end-mills is summarized in Table 1.

Table 1: Experiment plan for investigation of end-milling methods, cooling strategies and machining parameters using uncoated helical bull-nose solid carbide end-mills

Cooling Strategy	Milling method		Block No.	Cutting Speed m/min	Feed per revolution mm/rev	Depths of cut		MRR (mm ³ /min)
	Up-milling	Down-milling				Axial (a _a) mm	Radial (a _r) mm	
Emulsion	Exp # 1	Exp # 2	1	45	0.1016	5.08	3.81	2216.2
MQL	Exp # 3	Exp # 4	2	45	0.1016	5.08	3.81	2216.2
LN ₂ (-15 °C)	Exp# 5	Exp# 6	1	45	0.1016	5.08	3.81	2216.2
MQL + LN ₂ (-15 °C)	Exp# 7	Exp# 8	2	45	0.1016	5.08	3.81	2216.2

2.2. COOLING STRATEGIES SETUP

The main objective of this experiment is to investigate the effects of cooling strategies on cutting forces and FFT. The cooling strategies that were investigated were: Emulsion, MQL, LN₂ and the combination of MQL+LN₂. Each of the above-mentioned cooling strategies was set independently for this experiment.

2.2.1. Emulsion Cooling Setup. The application of emulsion lowers down the temperature of the cutting zone and removes the chips away from the cutting zone. In addition to that, it lubricates the tool flutes and cutting zone. A semi-synthetic emulsion coolant named VPTECH, manufactured by Walter tools was used for this purpose. The emulsion coolant was mixed with water to achieve the desired concentration of coolant in water. The concentration of the coolant in water was kept within the recommended concentration of 6-10%, given by the manufacturer. A refractometer was used to measure the concentration of the coolant.

2.2.2. Minimum Quantity Lubrication Setup. The Accu-Lube LB-2000 biodegradable mineral oil was used as a lubricant for this experiment. MQL that was sprayed on the cutting zone in the mist form was a mixture of mineral oil and air. Accu-Lube MQL precision pump applicator was used to mix the oil and air which uses a positive displacement system and pressurized air to spray the lubricant on the cutting zone and on the tool. The applicator system can be regulated to control the pressure and amount of air and, the amount of lubricant. The shop air supplied to CNC at a pressure of 5.86 bar (85 psi) was stepped down to 5.17 bar (75 psi) to precision pump applicator for this experiment. It also has an air valve that is used to control the volume of air that is mixed with the lubricant. Sufficient volume of air was provided to atomize and transport the lubricant to the cutting zone and flush the chips away from the cutting zone. The Accu-Lube precision pump applicator has also a valve graduated from 0 to 7, which are controlled to regulate the volume of the oil that gets mixed with the air to form the lubricant depending on the type of operation involved. For milling experiment, the valve was set at a value of 7, between 0 and 6 as recommended in Accu-Lube precision pump applicator manual. The precision pump has also a frequency generator to regulate the number of times the lubricant is provided to cutting zone per second, which is the pump cycle. For this experiment, various pump cycles were investigated to see the effectiveness of pump cycles in milling Inconel 718 without wasting so much lubricant. For this experiment, the pump cycle of 3 strokes per seconds was chosen, which is also within the manufacturer's recommendation for milling. Lastly, a lock-line adjustable nozzle was connected at the end of MQL precision pump applicator to spray the MQL to the cutting zone from applicator.

2.2.3. Cryogenic Liquid Nitrogen Setup. To remove the enormous amount of heat from the cutting zone generated during machining of Inconel 718, cryogenic liquid nitrogen (LN₂) was applied at sub-zero temperature to the cutting zone. This method is very effective in heat removal from the cutting zone. For this purpose, a 160 litres cryogenic Dewar with a pressure relief valve of 15.9 bar (230 psi) was used to store liquid nitrogen for this experiment. Pipe couplings, valve and a flexible cryogenic flow line were connected to the Dewar containing liquid nitrogen and used to transport liquid nitrogen from the Dewar through a nozzle to cutting zone. To measure the pressure of liquid nitrogen flowing through cryogenic flow line, a pressure gauge was fitted to it. To prevent the liquid nitrogen from getting in contact with the pressure gauge so as not to damage the pressure gauge, it had a 6.35 mm (0.25 inches) Swagelok pipe fitted to it, which was also connected to a 6.35 mm (0.25 inches) Tee, and in turn linked up to a 6.35 mm (0.25 inches) pig tail pipe. The temperature of liquid nitrogen in the Dewar was at -196°C, which was so extreme that if liquid nitrogen is sprayed to the cutting zone this way, it would negatively affect the milling of Inconel 718. The extremely cold temperatures have the tendency to increase the hardness of difficult-to-cut metals. This increase in hardness of difficult-to-cut metals would increase the cutting forces and this increase in cutting forces would lead to tool breakage. Thus, it was important to increase the temperature of liquid nitrogen to a more acceptable working temperature to avoid work-hardening of the workpiece before applying it to cutting zone. For this purpose, a 38.1 mm (1.5 inches) outer diameter and 34.9 mm (1.375 inches) inner diameter nozzle with an orifice of 1.59 mm (0.0625 inches) was designed to increase the liquid nitrogen temperature from -196°C to -15°C by mixing the shop air with liquid nitrogen. The

temperature of -15°C was chosen for the mixture of LN_2 and shop air. To decide the temperature of -15°C for machining, first the published literature was reviewed. Yuan et al. (2011) in their paper have reported that MQL with cooling air at -15°C has more favourable effects in milling of Ti-6Al-4V. Su et al. (2010) have reported that -20°C temperature yielded better results than -10°C in high-speed end-milling of titanium alloys. Su et al. (2006) in another paper reported better tool life and tool wear using -10°C temperature in high-speed end-milling of Ti-6Al-4V. Zhang et al. (2012) used a temperature of -30°C for minimum quantity cooling lubrication in end-milling of Inconel 718. Due to difference in temperatures used in the literature by different authors, preliminary set of experiments were performed and -15°C temperature was selected for LN_2 and MQL + LN_2 cooling strategies for up-milling and down-milling operations.

2.2.3.1. Calibration of liquid nitrogen set up. To ensure the repeatability in getting a fixed temperature of 15°C at the nozzle outlet, the calibration of liquid nitrogen was setup. Thus, it was important to determine a fixed amount of liquid nitrogen pressure and air pressure combination that would yield a fixed temperature of 15°C at nozzle outlet. To calibrate the temperature, different temperatures at nozzle outlet were recorded using different combinations of LN_2 pressure and air pressure. A total of 11 different temperatures were recorded using different combinations of LN_2 pressure and air pressure. Finally, a regression model was developed using Statistica software 7 from Stat Soft to perform the calibration. The multiple regression model has 2 factors: LN_2 pressure and shop air pressure and, dependent variable was the temperature at the nozzle outlet. The purpose of regression model was to establish the relationship between LN_2 pressure and shop air pressure and, dependent variable temperature at the nozzle outlet.

To record the temperature of nozzle outlet, a 3.175 mm (0.125 inches) diameter ungrounded K-type thermocouple was taped around the nozzle outlet. The multiple regression model performed using a significance level of 0.05 is shown as:

$$Y = B_0 + B_1X_1 + B_2X_2 + C \quad (1)$$

Where Y is the dependent variable which is the temperature at the nozzle outlet, X_1 represents LN₂ pressure, X_2 represents shop air pressure, B_0 represents the intercept of equation, B_1 is coefficient of LN₂ pressure, B_2 represents coefficient of shop air pressure and C represents error. To begin calibration, the cryogenic flow line was turned on for the LN₂ to gush out of nozzle outlet for about 20 minutes to ensure the pressure of LN₂ in the flow line was steady and not fluctuating as seen from the gauge. This made the whole length of the flow line completely frozen and ice became visible throughout the length of flow line.

After the LN₂ pressure became steady, different values of LN₂ pressure and air pressure were chosen and their respective outputs were recorded. The LN₂ pressure was varied from 2.76 bars (40 psi) to 5.17 bar (75 psi) and air pressure range chosen from 1.03 to 3.1 bar (15 to 45 psi). A total of 11 readings were captured using different combinations of air pressure and LN₂ pressures. The temperature calibration data for 11 readings is given in the Table 2. The input and output values were then entered into Statistica Software 7 and Analysis of Variance (ANOVA) was conducted on the observations given in Table 2 to see if the treatment combination mean was significantly different from zero. Table 3 presents the results obtained from Statistica to see if the results were significant.

Table 2: Calibration data for cryogenic temperature

LN ₂ Pressure (Psi)	Air Pressure (Psi)	Temperature (°C)
40	15	2.41268
50	20	1.02068
55	30	-0.33645
60	15	-25.9122
60	30	-13.7055
60	25	-15.8007
65	30	-17.3153
65	35	-15.1913
70	35	-24.6755
70	40	-20.2317
75	45	-24.6572

Table 3: ANOVA for Calibration of Cryogenic set-up

Effect	Analysis of Variance; Dependent Variable: Temperature				
	Sum of Squares	df	Mean Squares	F	P-level
Regression	1023.510	2	511.7551	49.81684	0.000031
Residual	82.182	8	10.2727		
Total	1105.692				

The p-value shown gives the probability that the observations were due to random chance and due to effects of actual variation. Since the p-value is very less than significance level ($\alpha = 0.05$), it gives the sufficient evidence to conclude that the calibration is significant at a significance level of 0.05. The next task was to fit a multiple regression model to observations, to generate an equation to best approximate relation between LN₂ pressure and air pressure (independent variables) and temperature (dependent variable). Table 4 gives the results from multiple regression model results for calibration data.

Table 4: Results of multiple regression model for calibration data

Regression Summary for Dependent Variable: Temperature						
R = 0.96211945 R ² = 0.92567383 Adjusted R ² = 0.90709228						
F (2,8) = 49.817 P<0.00003 Std. Error of estimate: 3.2051						
	Beta	Standard Error of Beta	B	Standard Error of Beta	T(8)	p-level
Intercept			59.01976	7.417012	7.95735	0.000045
LN ₂ Pressure	-1.52675	0.176607	-1.61276	0.186555	-8.64493	0.000025
Air Pressure	0.79834	0.176607	0.86543	0.191448	4.52045	0.001949

As can be seen from Table 4, the p-values for intercept, LN₂ pressure and air pressure are less than the significance level of 0.05, which means they are significant and are not due to just random chance. Also, the R² value of the model is given as 0.92567383. This value measures the validity of the model and it means that model will account for 95.57% of observed values. From Table 4, the multiple regression equation becomes:

$$Y = 59.01976 - 1.61276 X_1 + 0.86543 X_2 \quad (2)$$

In the above equation, Y represents the temperature which is dependent variable, X₁ represents LN₂ pressure and X₂ represents air pressure, both independent variables. From the equation (2), the value of one independent value can be calculated, if value of another independent variable and dependent variable is known. In other words, if shop air pressure and output temperature are known, the value of LN₂ pressure can be calculated using this equation or if LN₂ pressure and temperature are known, the value of shop air pressure can be calculated. The air pressure values were predicted by fixing the values of LN₂ pressure and temperature for this experiment and are given in Table 5. For this experiment, LN₂ pressure of 3.79 bar (55 psi) was used so as to consume LN₂ at slower

rate and the corresponding air pressure used was 1.17 bar (16.99 psi) to achieve output temperature of -15°C .

Table 5: Pressure predicted values from calibration equation

Temperature ($^{\circ}\text{C}$)	LN ₂ Pressure (psi)	Air Pressure (psi)
-10°C	55	22.77
	60	32.09
	65	41.42
-15°C	55	16.99
	60	26.31
	65	35.64
-20°C	55	11.21
	60	20.53
	65	29.86

3. EXPERIMENTAL SETUP AND PROCEDURE

3.1. WORKPIECE PREPARATION

The physical and mechanical properties of Inconel 718 are shown in Table 6.

Table 7 shows the chemical composition of Inconel 718 as given by manufacturer.

Table 6: Physical and Mechanical properties of Inconel 718 (A. Shokrani et al., 2012)

Property	Unit	
Density	Kg/m ³	8190
Young's Modulus	GPa	200
Ultimate Tensile Strength	MPa (min)	1375
Yield Tensile Strength	MPa	1100
Thermal conductivity	w/m ⁰ K	11.4
Specific Heat Capacity	J/Kg ⁰ C	435
Melting Point	$^{\circ}\text{C}$	1260-1336

Table 7: Chemical composition of Inconel 718 given by manufacturer

Content	Ni	Cr	Fe	Nb	Mo	Ti	Al	Co	Cu	Mn
Weight %	53.58	18.63	17.31	5.17	2.91	0.96	0.58	0.27	0.21	0.13
Content	Si	C	P	Ta	B	S	Bi	Pb	Se	
Weight %	0.09	0.03	0.01	0.004	0.002	0.001	$<10^{-6}$	$<10^{-6}$	$<10^{-6}$	

To prepare the initial shape of workpiece, 2 holes 38.1 mm (1.5 in) deep and 60 mm (2.3622 in) apart were drilled on the rectangular workpiece. These holes were used for clamping the workpiece on a Kistler 4-component dynamometer (used for measuring three components of the cutting force F_x , F_y , F_z , and Moment M_z). Then, two counter bores of \varnothing 10.16 mm (0.4 in) \times 18.1 mm (0.712 in) and 13.97 mm (0.55 in) \times 7.92 mm (0.312 in) were machined on each of the two drilled holes to accommodate the dimensions of the clamping bolts. Lastly, these two drilled and holes were tapped to fasten the workpiece on dynamometer using bolts. Two steps were made on the both sides of the workpiece, each having a width of 30.48 mm (1.2 in) and height 5.08 mm (0.2 in). Each step was used to perform one experiment and thus, four experiments were performed on one workpiece. CNC codes were written and used for drilling, counter boring and tapping the two holes and for milling the steps on the workpiece.

Figure 4 shows schematic and actual picture of the experimental setup with cryogenic and MQL flow lines and data acquisition system.

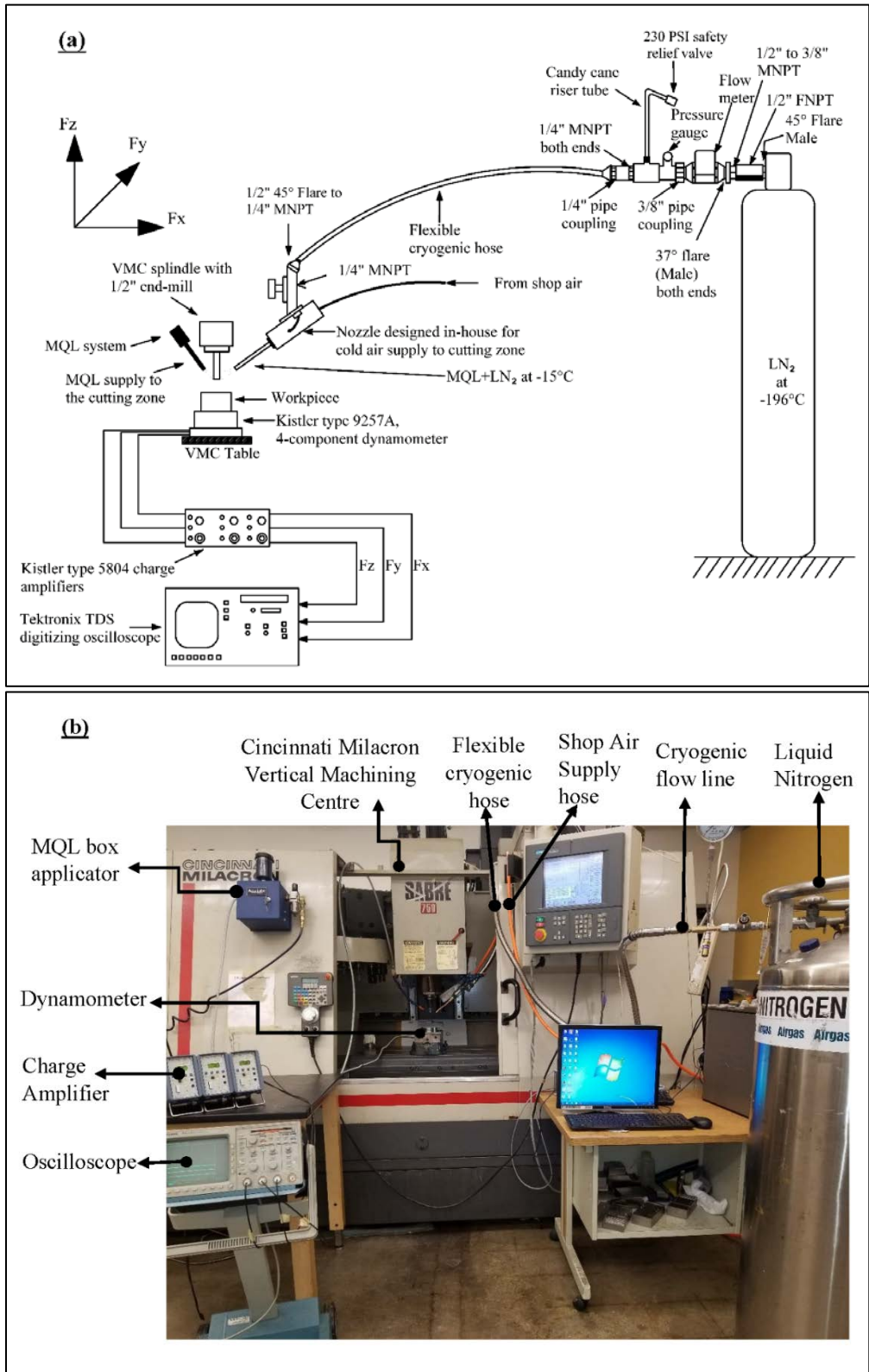


Figure 4: Experimental set-up with cryogenic and MQL flow lines and data acquisition system. (a) Schematic and (b) actual picture

3.2. EXPERIMENTAL SET UP

The prepared workpiece was fastened on the Kistler 9272 4-component dynamometer by screwing the bolts through the holes made on the workpiece. The cutting force and FFT signals were then acquired during machining and separated into their respective components.

3.3. CUTTING FORCE AND FFT ACQUISITION

The prepared workpiece was clamped on a Kistler 9272 4-component dynamometer using two (2) fastening bolts. The dynamometer was then tightened on the vice of the Cincinnati VMC table. A silver cable was attached to the dynamometer whose other end was connected to a Kistler 5405 A signal breakout junction box, which splits the force and FFT signals generated during machining and sensed by the dynamometer into 3 components in the x, y and z directions. To acquire components of the cutting force and FFT in the x, y and z directions, 3 black cables were used to connect to junction output. The other ends of these cables were connected to 3 separate channels of Kistler type 5010 B dual mode amplifiers, where the acquired signals were amplified. These amplified signals were then passed through low pass filter having a set frequency of 680 Hz to remove the unwanted noise and vibrations from the signals. The filtered signals were then passed to Tektronics TDS 420A digitizing oscilloscope where the cutting force components and Fast Fourier Transform (FFT) signals were saved in spreadsheet format. In the oscilloscope, the signals were digitized at a sampling frequency of 1 Ks/s and 5000 sampling points per signal, which resulted in a record length of 5 seconds. It is the total length of time it took to acquire signals of cutting force. In the frequency domain (FFT), 2500 sampling points per signal were acquired.

The digitized saved signals were then saved to floppy drive and transferred to a computer for further processing.

3.4. CUTTING FORCE AND FFT DATA PROCESSING

For each experiment, the cutting force components (F_x , F_y and F_z) and Fast Fourier Transforms of cutting force components (FFT_x , FFT_y and FFT_z) in the x, y and z directions were acquired after each pass. The plots were processed using 8-point moving average to remove noise and vibrations from the actual signal. For cutting force components, the value of maximum cutting force components in the x, y and z directions was also determined from the processed signals. These maximum values of cutting force components from the plot of each pass were selected by enlarging the plot and looking in both positive and negative directions. Then the modulus of the maximum values was chosen as the maximum cutting force component for that pass in the given direction. These maximum cutting forces components in the x, y and z directions were then plotted against machined length. The resultant cutting force for each pass was also determined and plotted against machined length using maximum cutting force components. The resultant cutting force was calculated from maximum cutting force components in the x, y and z directions using the formula:

$$F_r = \sqrt{F_{xmax}^2 + F_{ymax}^2 + F_{zmax}^2} \quad (3)$$

Where: F_r is resultant cutting force components, F_x is maximum cutting force component in x direction, F_y is maximum cutting force component in the y direction and F_z is maximum cutting force component in the z direction. For FFT cutting force components, the calculated tooth frequency of 4-flute end-mill at 1127 rpm spindle

rotation is 75.13 Hz. Thus, the amplitude of FFT of cutting force in the x, y and z directions at 75.13 Hz tooth frequency was determined from the processed FFT signal after each pass and plotted against the machined length.

3.5. PROCEDURE

Peripheral end-milling experiments were conducted on Cincinnati Milacron Vertical Machining Centre (VMC), Sabre 750 equipped with Acramatic 2100 controller. Rectangular workpieces of Inconel 718, each measuring 76.2 mm (3 inches) \times 152.4 mm (6 inches) \times 38.1 mm (1.5 inches), were used for the peripheral end-milling experiments. Four-flute uncoated solid carbide bullnose helical end-mills of 12.7 mm (0.5 inch) shank diameter, 76.2 mm overall length (3 inches) and 25.4 mm (1 inch) flute length with a corner radius of 0.762 mm (0.03 inches) were used for all experiment runs. End-mills with corner radius are used in aerospace manufacturing to reduce the stress concentration on machined parts. The workpiece length (L) along the feed direction was 76.2 mm (3.0 in). For each workpiece block, each experiment consisted of eight (8) radial passes. Each radial pass consisted of radial depth of cut (a_r) of 3.81 mm (0.15 in), thus making the total radial depth of cut of 30.48 mm (1.2 inches). Figure 5a shows the cutter entry angle during down-milling operation and cutter exit angle during up-milling.

Figure 5b shows the approach distance during up-milling and down-milling. It is the distance when the cutter starts cutting the workpiece. This distance is taken between centre of cutter and nearest edge of the workpiece, perpendicular to the feed direction as shown in Figure 5(a).

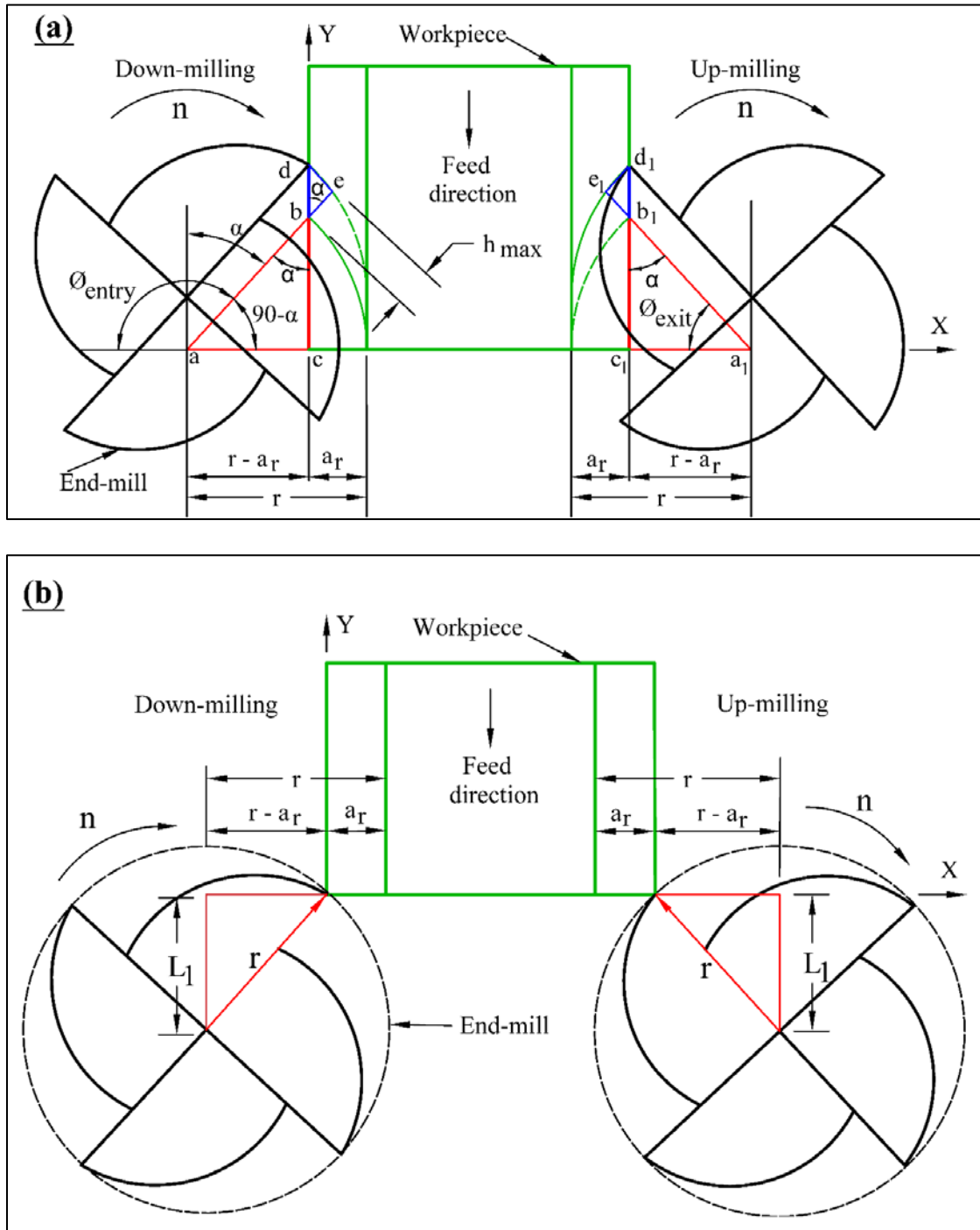


Figure 5: Cutter entry and exit angle, and approach distance. (a) Cutter entry angle during down-milling and cutter exit angle during up-milling, (b) approach distance during down-milling and up-milling

The cutter entry and exit angles for both up and down-milling are calculated below:

For down-milling

The tool always come out of the workpiece at an angle of 180° with negative x-axis. Thus,

$$\phi_{\text{exit}} = 180^\circ \quad (4)$$

The entry angle is calculated using Figure 5a as follows:

$$\phi_{\text{entry}} = 180 - (90 - \alpha) \quad (5a)$$

From Δabc

$$\text{Cos}(90 - \alpha) = \frac{ac}{ab} = \frac{r - a_r}{r} \quad (5b)$$

where, r is the radius of tool and a_r is the radial depth of cut.

$$90 - \alpha = \arccos\left(\frac{r - a_r}{r}\right) \quad (5c)$$

$$90 - \alpha = \arccos\left(\frac{6.35 - 3.81}{6.35}\right) = \arccos(0.4) = 66.42^\circ$$

Substituting the value of $90 - \alpha$ in (5a)

$$\phi_{\text{entry}} = 180 - \arccos\left(\frac{r - a_r}{r}\right) \quad (5d)$$

$$\phi_{\text{entry}} = 180 - 66.42 = 113.58^\circ$$

For up-milling

From Figure 5a, it can be seen that the tool penetrates into the workpiece at an angle of 0° with negative x-axis. So,

$$\phi_{\text{entry}} = 0^\circ \quad (6)$$

Exit angle can be found using from $\Delta a_1b_1c_1$

$$\cos \phi_{\text{exit}} = \frac{a_1 c_1}{a_1 b_1} = \left(\frac{r - a_r}{r} \right) \quad (7a)$$

$$\phi_{\text{exit}} = \arccos \left(\frac{r - a_r}{r} \right) \quad (7b)$$

$$\phi_{\text{exit}} = \arccos \left(\frac{6.35 - 3.81}{6.35} \right) = 66.42^\circ$$

The tool starts cutting during up and down-milling when the center of the tool is at a distance of L_1 (approach distance) from the workpiece edge perpendicular to feed direction as shown in Figure 5b. The L_1 distance is given as follows.

$$L_1 = \sqrt{r^2 - (r - a_r)^2} \quad (8)$$

$$L_1 = \sqrt{6.35^2 - (6.35 - 3.81)^2} = 5.82 \text{ mm}$$

As the workpiece length (L) along the feed direction was 76.2 mm (3 inches), the total machined length for each machining pass becomes:

$$ML \text{ (Machined Length of single pass)} = L + L_1 = 76.2 + 5.82 = 82.02 \text{ mm} \quad (9)$$

All the 8 passes resulted to a total length of cut of 656.16 mm (25.83 in). Each experiment requires eight (8) radial passes which resulted to a total machined width of 30.48 mm (1.2 in). The corresponding machined lengths for each of the eight (8) passes after adding the additional cutter approach (L_1) length in each pass are 82.02 mm, 164.04 mm, 246.06 mm, 328.08 mm, 410.1 mm, 492.12 mm, 574.14 mm and 656.16 mm respectively. A new tool was used for each cooling strategy to eliminate the effect of tool wear. The results of the eight (8) experiments with uncoated carbide end-mills were analyzed to find the best cooling strategy among the four cooling strategies investigated, and better milling method among up-milling and down-milling.

4. RESULT ANALYSIS

4.1. SAMPLE PLOTS FOR MAXIMUM CUTTING FORCE COMPONENTS AND FAST FOURIER TRANSFORMS (FFT) VERSUS MACHINED LENGTH (PASS NUMBER)

Figure 6 (a), (b) and (c) show the sample plots of the acquired signals of the cutting force components (F_x , F_y and F_z) in the x, y and z directions for the 3rd pass at a spindle speed of 1127 rpm (45 m/min cutting speed), feed-rate of 114.5 mm/min (4.510 ipm), axial and radial depth of cut of 5.08 mm (0.2 inches) and 3.81 mm (0.15 inches) respectively using emulsion down-milling cooling strategy. The value of maximum cutting force components in the x, y and z directions for each pass were determined from the processed signals. These maximum cutting force components were plotted against machined length. The resultant cutting forces were also determined using maximum cutting force components and plotted against machined length. Figure 6 (d), (e) and (f) show the sample plot of FFT's of cutting force components (FFT_x , FFT_y and FFT_z) in the x, y and z directions for 3rd pass at a spindle speed of 1127 rpm (at 45 m/min cutting speed), feed-rate of 114.5 mm/min (4.510 ipm), axial and radial depth of cut of 5.08 mm (0.2 inches) and 3.81 mm (0.15 inches) respectively using emulsion down-milling cooling strategy. As can be seen from the Figures, the amplitude of FFT is highest at a tooth frequency of 75.13 Hz. This gives the amplitude of vibrations at the tooth frequency. The values of amplitude of FFT in the x, y and z directions at a tooth frequency of 75.13 Hz were determined for each pass from the processed signals and plotted against machined length.

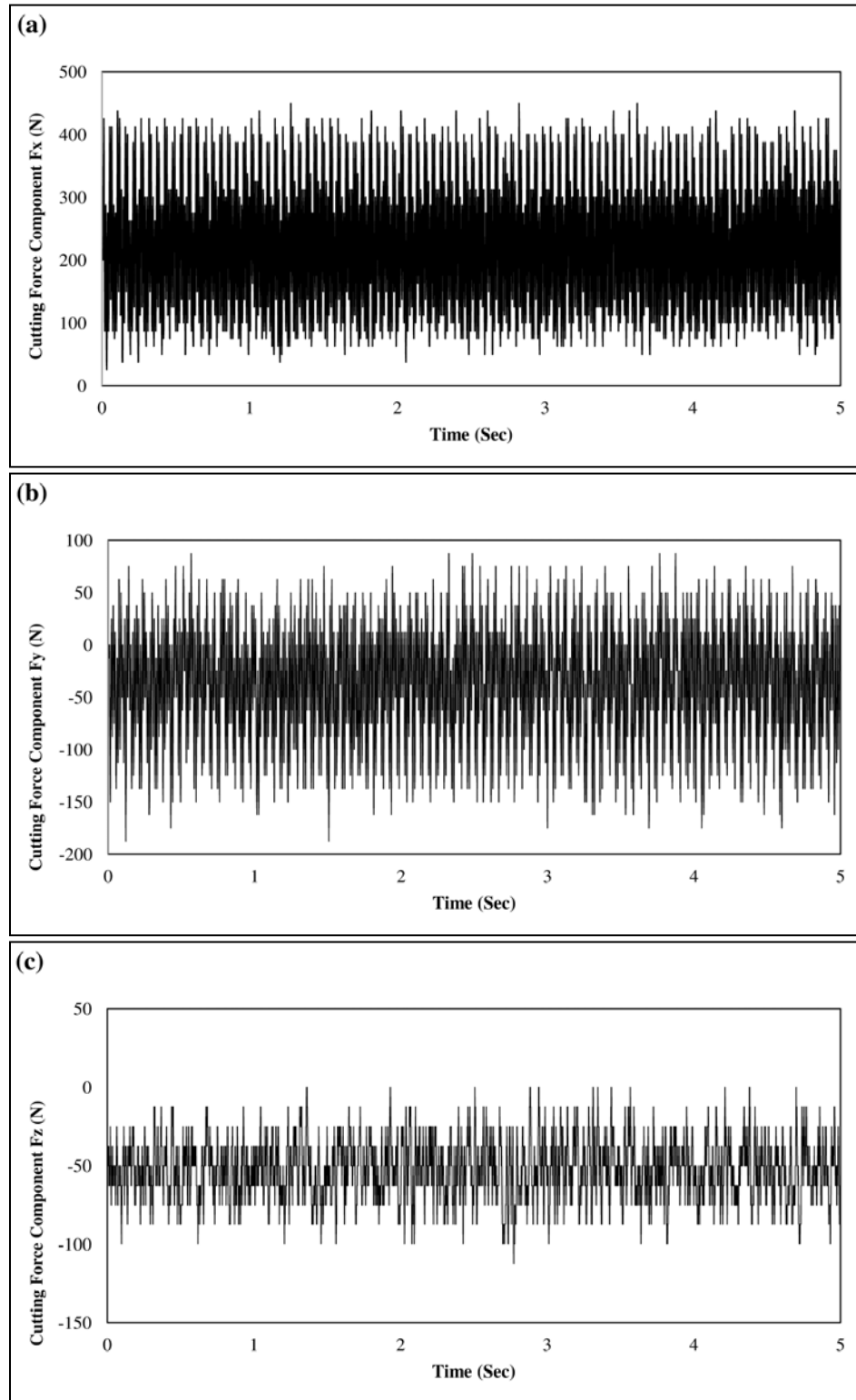


Figure 6: Cutting force and FFT signals at 3rd pass (255.81 mm machined length) for emulsion up-milling at 1127 rpm and 114.5 mm/min. (a) F_x , (b) F_y , (c) F_z , (d) FFT_x , (e) FFT_y and (f) FFT_z

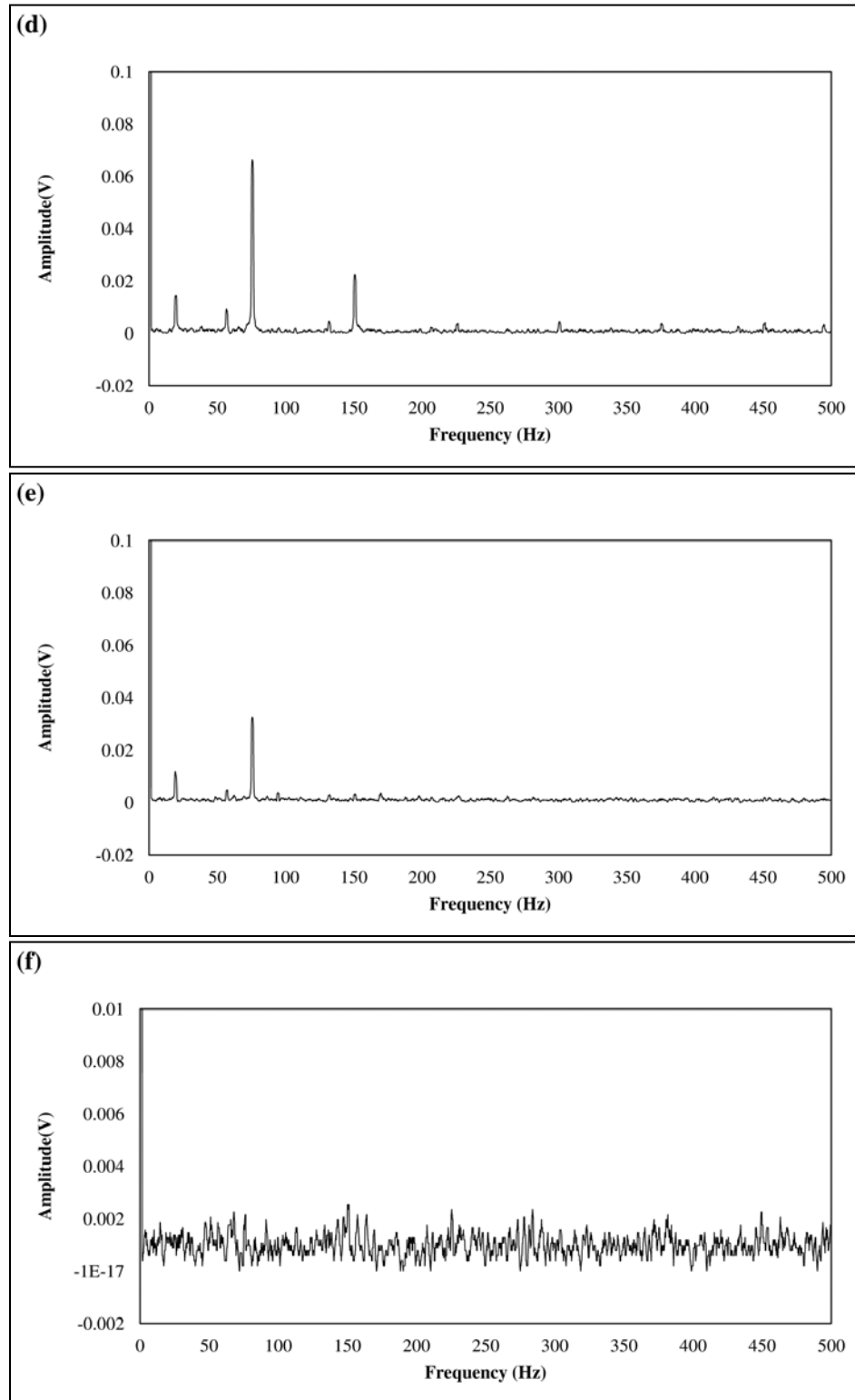


Figure 6: Cutting force and FFT signals at 3rd pass (255.81 mm machined length) for emulsion up-milling at 1127 rpm and 114.5 mm/min. (a) F_x , (b) F_y , (c) F_z , (d) FFT $_x$, (e) FFT $_y$ and (f) FFT $_z$ (Contd.)

4.2. MAXIMUM CUTTING FORCE COMPONENTS AND RESULTANT CUTTING FORCE AND, AMPLITUDE OF FAST FOURIER TRANSFORMS (FFT) AT TOOTH FREQUENCY

4.2.1. Emulsion Cooling. Figure 7 shows the plots of maximum cutting force components (F_x , F_y , F_z) and resultant cutting force (F_r) and, the amplitude of FFT of cutting force components F_x , F_y and F_z at 75.13 Hz tooth frequency under emulsion cooling, up-milling method, at a cutting speed of 45 m/min (1127 rpm) and a federate of 114.5 mm/min (4.510 ipm). While plotting the cutting force components against machined length, two wild points were detected for cutting force component F_y at pass numbers 6 and 7 and were removed according to Chauvenet's Criteria for rejection of a reading (Coleman & Steele, 1989). Additional 2 passes were machined to get the accurate trend and thus, the total number of machined passes was 10 instead of 8 for emulsion up-milling method.

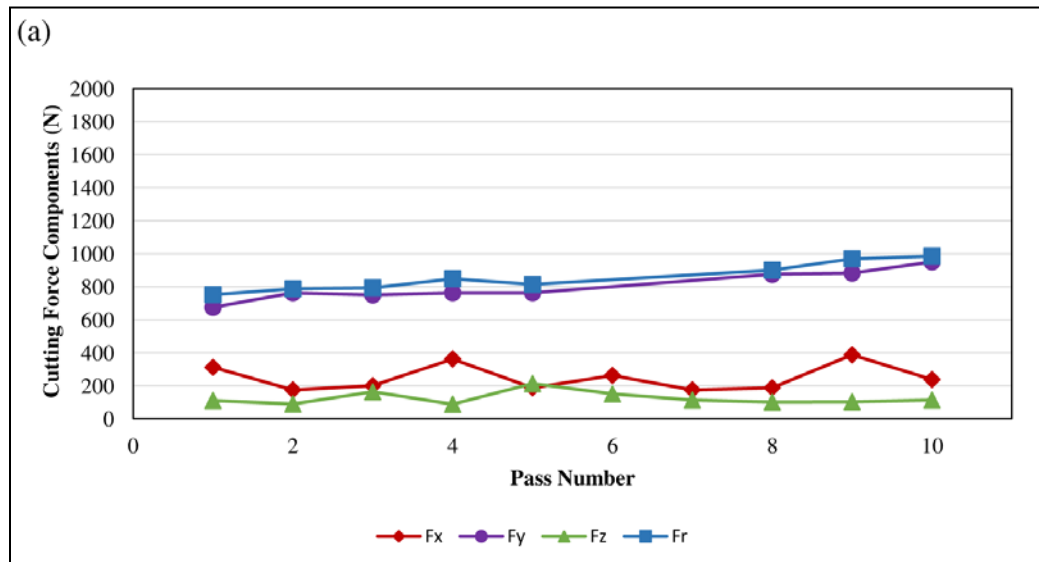


Figure 7: Maximum cutting force components, resultant cutting force and FFT amplitudes of cutting force components vs pass numbers (machined length) in x, y and z-directions under emulsion, up-milling. (a) Maximum cutting force components and resultant cutting force, (b) FFT amplitudes

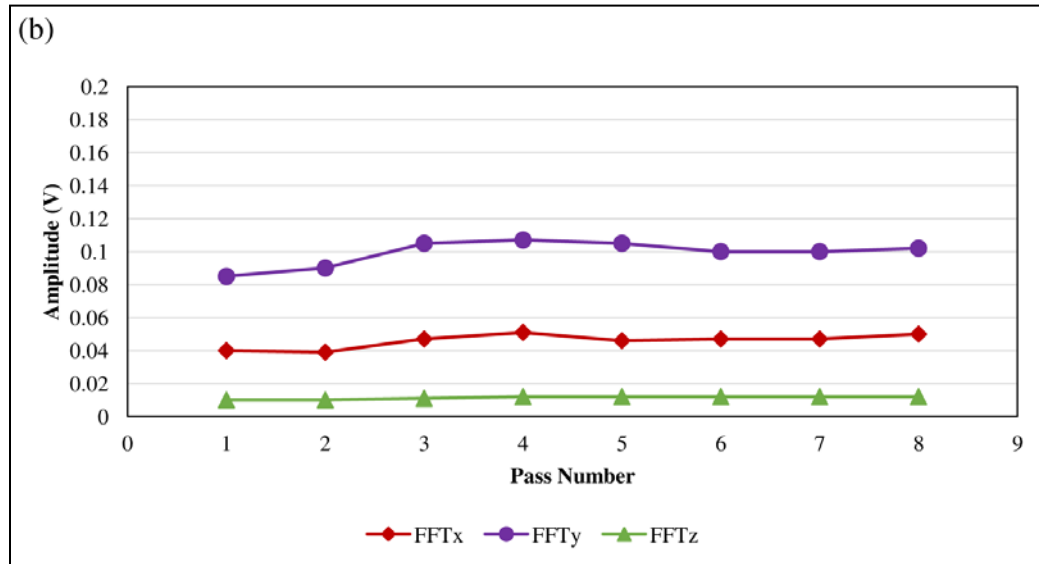


Figure 7: Maximum cutting force components, resultant cutting force and FFT amplitudes of cutting force components vs pass numbers (machined length) in x, y and z-directions under emulsion, up-milling. (a) Maximum cutting force components and resultant cutting force, (b) FFT amplitudes (Contd.)

The plots show that the cutting force component F_y (Feed force) to be the highest throughout the machining. During up-milling operation, the cutting tool enters the workpiece along the y-axis. In a single rotation of one tooth of the tool, the chip thickness is least when it enters the workpiece and increases to maximum when the tooth comes out of the workpiece in up-milling method. The material removal process in up-milling method is illustrated in Figure 8a. The rubbing in the beginning of cut causes an excessive work hardening layer on the newly exposed surface of the workpiece (Hadi et al., 2013). During the rotation of the tool, when the successive tooth starts entering the workpiece, it has to enter in the workpiece along the y-axis through the work hardened layer created by the previous tooth. The layer kept on hardening with the successive rotations of the tool. Due to this continuous hardening of the surface, the impact force kept on increasing, which in turn increases the cutting force component F_y . Figure 7 (a)

also shows that the cutting force components F_x and F_z kept on fluctuating throughout the machining. This might happen as during machining, the segmented chip kept on entangling with the tool, causing the fluctuation of these cutting force components. The FFT plot shows the amplitude of FFT_y to be the highest, followed by the amplitude of FFT_x and, FFT_z amplitude being the least throughout the machining. FFT_x and FFT_y amplitudes follow almost similar trends as their respective cutting force components. The magnitude of FFT_z was almost constant throughout the machining.

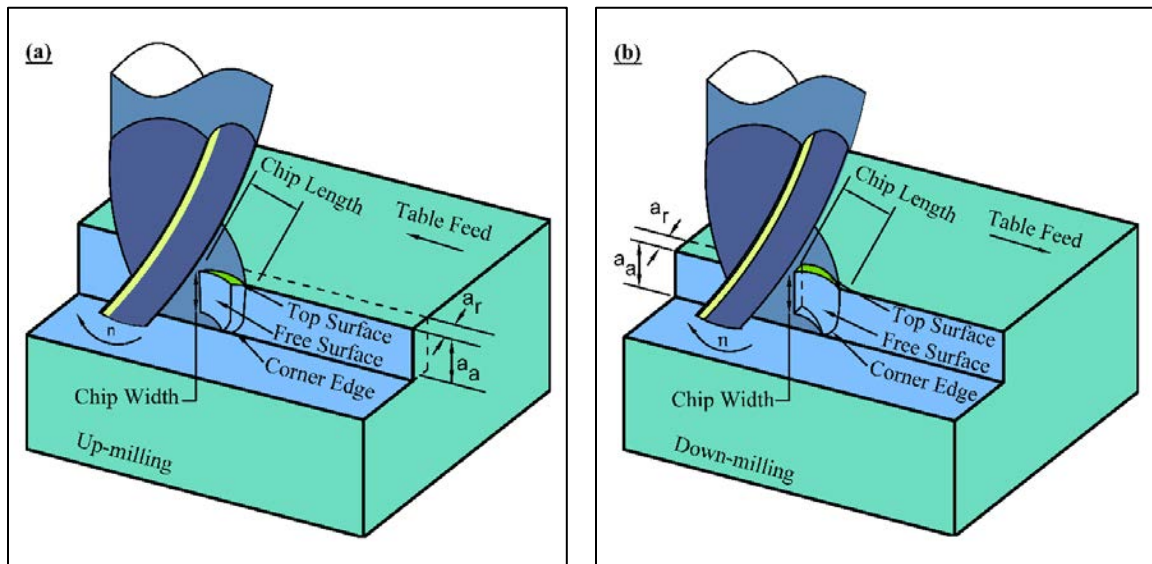


Figure 8: 3-D Material removal process (chip profile). (a) Up-milling and (b) Down-milling

Figure 9 shows the plots under emulsion cooling, down-milling method. As 10 passes were machined for emulsion up-milling method due to lack of data, additional 2 passes were machined for emulsion down-milling as well so as to maintain the consistency in number of passes for emulsion cooling strategy. The plot shows that the cutting force component F_x which is perpendicular to feed-direction, is the highest throughout the machining.

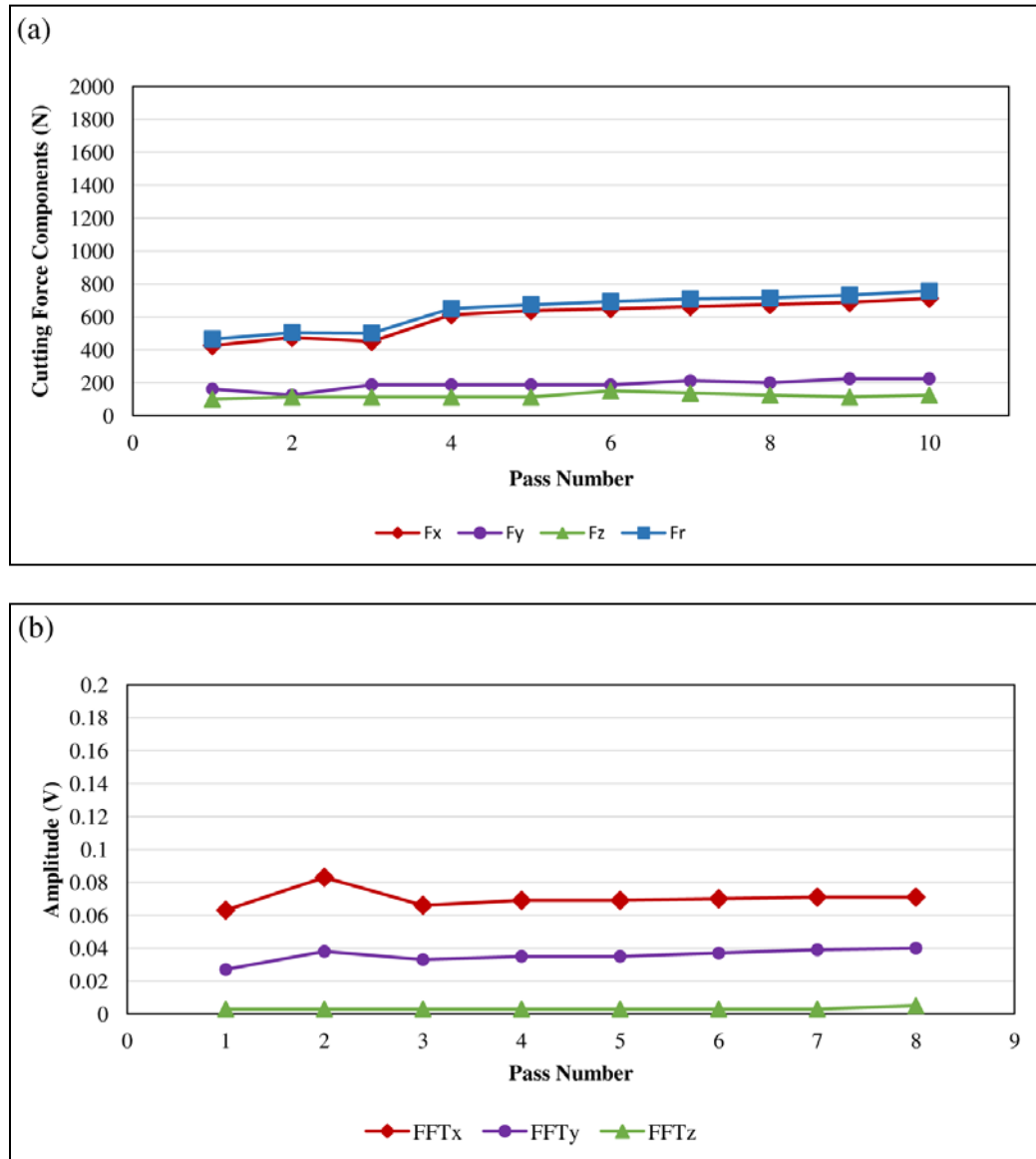


Figure 9: Maximum cutting force components, resultant cutting force and FFT amplitudes of cutting force components vs pass numbers (machined length) in x, y and z-directions under emulsion, down-milling. (a) Maximum cutting force components and resultant cutting force, (b) FFT amplitudes

The chip removal process in down-milling is shown in Figure 8b. The cutter encounters maximum chip thickness when it enters the workpiece along the x-direction and the chip thickness is minimum when it comes out along the y-direction. This makes cutting force component F_x highest among the three components during down-milling

operation. Also, during the rotation of the tool, the successive tooth penetrates into the fresh surface of the workpiece and not into the work hardened surface created by the previous tooth. Thus, there is no impact of surface hardening on successive tooth, created by the previous tooth, which makes the cutting force components in down-milling lower than those in emulsion up-milling. The FFT plot of emulsion down-milling is shown in Figure 9 (b). The amplitude of FFT at tooth frequency of 75.13 Hz in emulsion down-milling is less than in emulsion up-milling. The FFT plots followed almost the same trend as cutting force components. In x-direction, there was an increase in the vibrations in 2nd pass and hence, the cutting force component F_x also increased due to increase in the vibration during 2nd pass. The cutting force component in the 3rd pass decreased, as the vibration amplitude decreased. The vibrations increased gradually after 3rd pass due to the fact that there was increase in tool wear with progression of time. The amplitude of FFT_z was least and almost constant throughout the machining length.

4.2.2. MQL Cooling. Figure 10 shows the plots under MQL cooling, up-milling method. The plot shows that the cutting force component F_y is the highest, with F_z being the least throughout the machining and contributed least towards resultant cutting force. Even though MQL cooling provides very good lubrication, the rate of heat generated at the cutting zone was much higher than the rate at which the heat was removed by MQL cooling during up-milling. Also, there was an excessive work hardening of surface of Inconel 718 workpiece during up-milling as discussed earlier. Due to excessive work hardening of workpiece, cutting forces increased drastically during 4th pass. The MQL up-milling strategy was not able to remove heat from the cutting zone as quickly as it was generated and hence, red hot cutting zone was observed. High cutting forces increased

the vibrations drastically as seen from the FFT plot. As there was excessive chipping on the flutes of the tool, further machining was terminated. The chips produced were segmented which were difficult to be removed by MQL cooling.

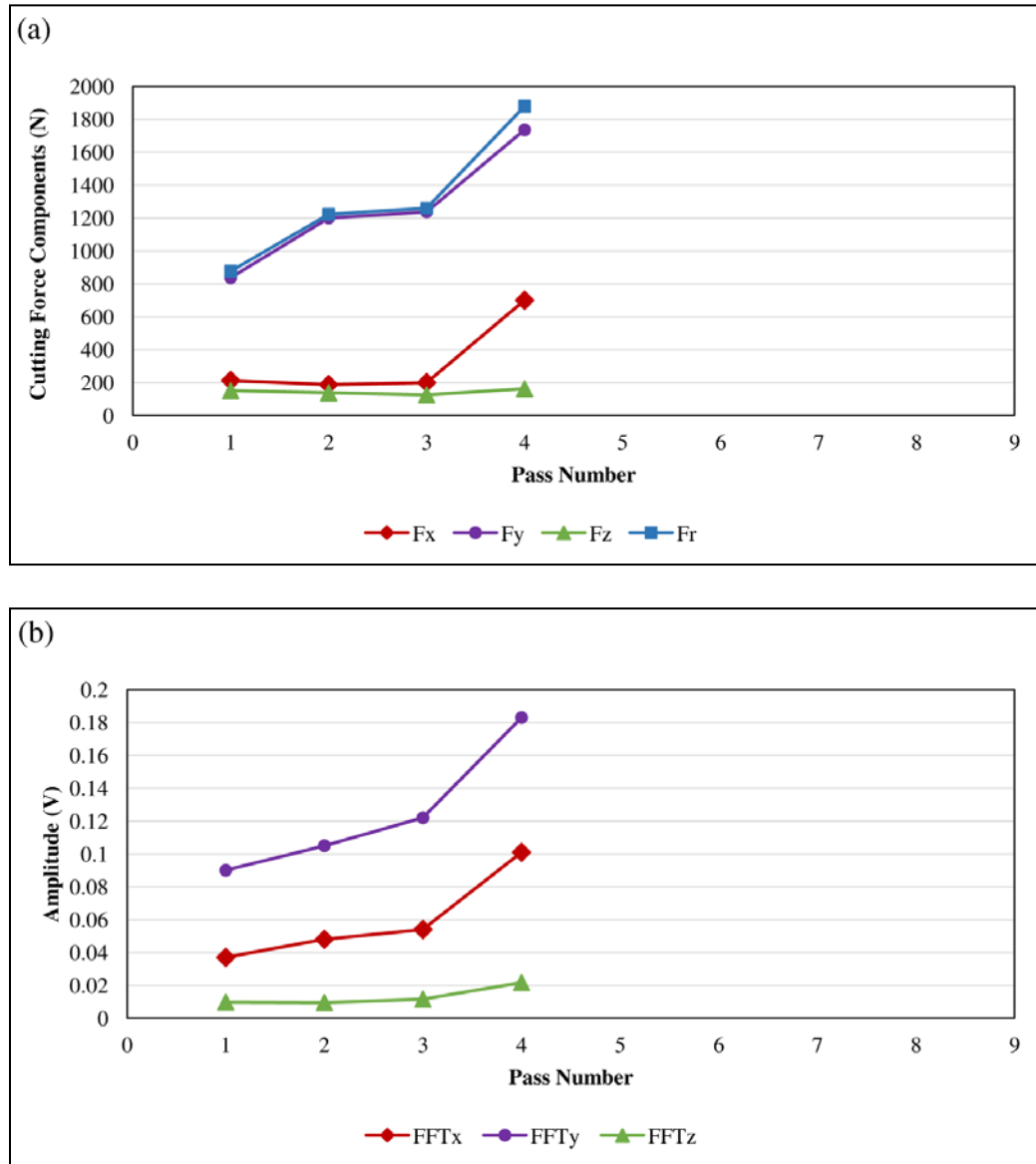


Figure 10: Maximum cutting force components, resultant cutting force and FFT amplitudes of cutting force components vs pass numbers (machined length) in x, y and z-directions under MQL, up-milling. (a) Maximum cutting force components and resultant cutting force, (b) FFT amplitudes

Although, MQL provides a better lubrication to the cutting zone, it was not very effective in lowering the cutting forces, decreasing the cutting zone temperature and flushing the hot chips away from the cutting zone effectively, when machining using up-milling. Figure 11 shows the plots under MQL cooling, down-milling method.

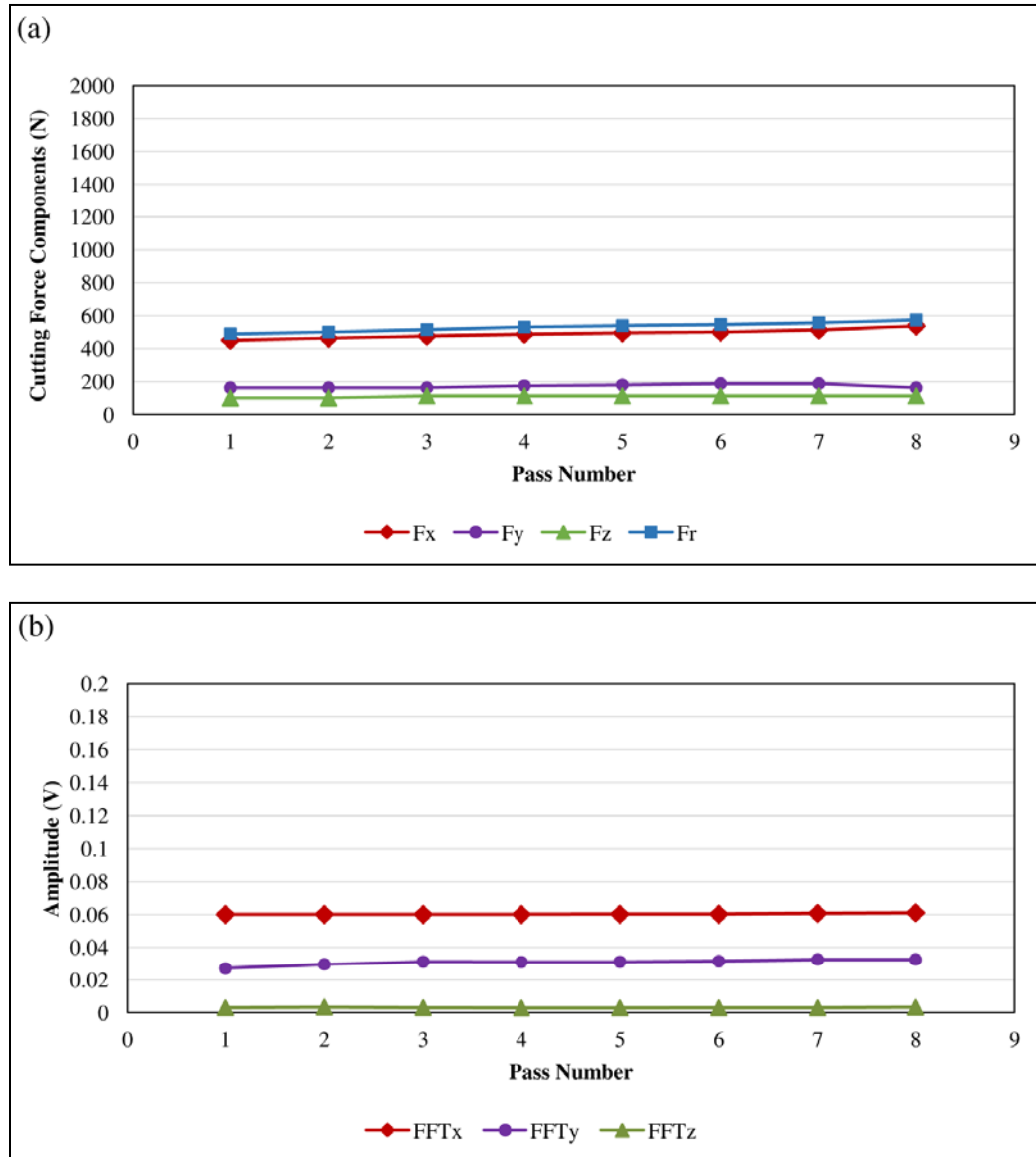


Figure 11: Maximum cutting force components, resultant cutting force and FFT amplitudes of cutting force components vs pass numbers (machined length) in x, y and z-directions under MQL, down-milling. (a) Maximum cutting force components and resultant cutting force, (b) FFT amplitudes

The plot shows that the cutting force component perpendicular to the feed direction (F_x) is highest among all three cutting force components throughout the machining length. The increase in cutting force components with machining pass was very gradual and smooth. The MQL cooling strategy in combination with down-milling method provided the better lubrication at the cutting zone which decreased the cutting force components. Also, discontinuous serrated chips were produced which were easily removed by MQL. The increase in cutting force components with machining pass was very gradual and smooth. The MQL cooling strategy in combination with down-milling method provided the better lubrication at the cutting zone which decreased the cutting force components. Also, discontinuous serrated chips were produced which were easy to be removed by MQL cooling. The amplitude of FFT in the x-direction (perpendicular to the feed direction) is almost constant throughout the machining length (number of passes), which signifies lower or absence of vibrations during down milling operation. This combination of MQL with down-milling provided the lowest resultant cutting force among all 8 combinations of 4 cooling strategies and 2 milling methods.

4.2.3. LN₂ Cooling. Figure 12 shows the plots under LN₂ cooling, up-milling method. The plot shows that the cutting force component in the feed direction (F_y) is the highest among all three cutting force components. The cutting forces under LN₂ up-milling increased so rapidly during the 1st pass that the tool could not last after that. The reason for the drastic increase of cutting forces can be explained as follows. The application of LN₂ cooling strategy increased the hardness of the workpiece at sub-zero temperature (Park et al., 2017). Due to the increase in hardness, it became more difficult for the tool to penetrate through the material which increased the vibrations drastically.

Moreover, LN_2 does not provide enough lubrication to the cutting zone. Although, LN_2 provides cooling to cutting zone, the absence of lubrication further increased the cutting forces. Due to this increase in hardness of workpiece and tool, absence of sufficient lubrication, the increase of thermal shock due to the intermittent cutting action and cryogenic cooling, the cutting forces increased drastically and the red hot cutting zone was seen which led to massive chipping of the cutting edges of the tool. The tool started rubbing against the workpiece instead of cutting thereby generating thick curly peel of burnt metal. All the cutting flutes were burnt completely and the tool had gone under plastic deformation. Further machining was terminated after first pass as the tool had exceeded its life.

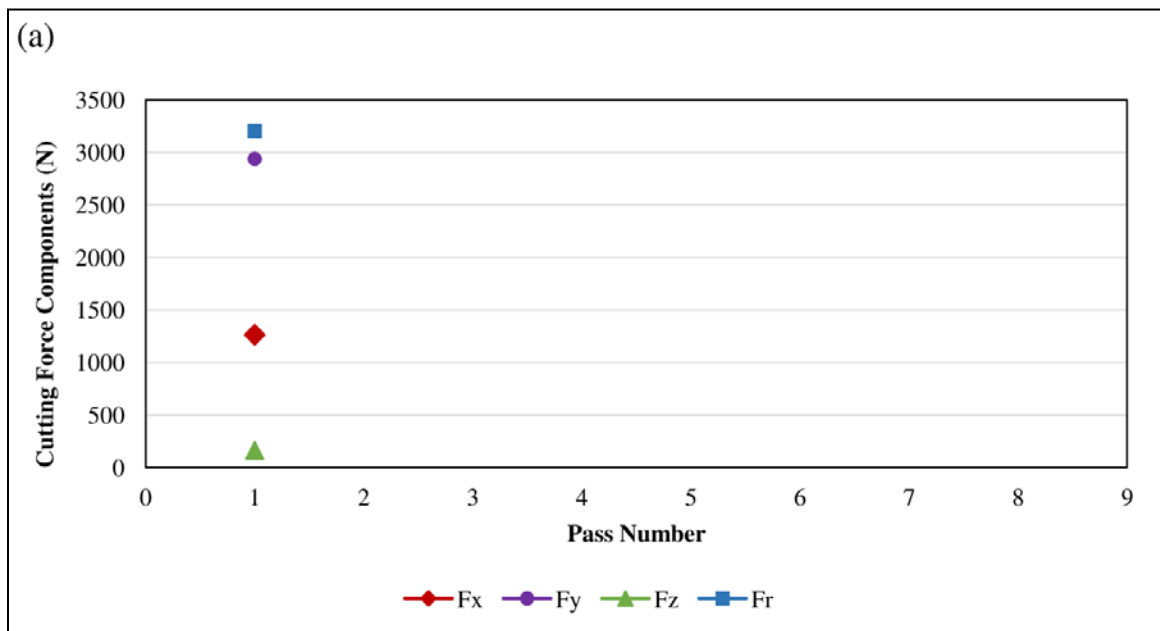


Figure 12: Maximum cutting force components, resultant cutting force and FFT amplitudes of cutting force components vs pass numbers (machined length) in x, y and z-directions under LN_2 , up-milling. (a) Maximum cutting force components and resultant cutting force, (b) FFT amplitudes

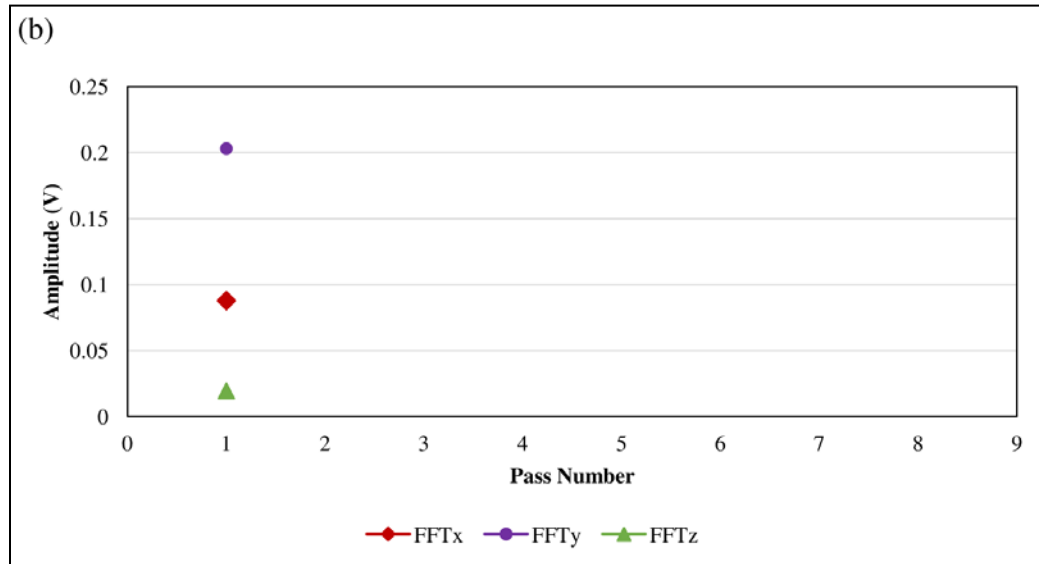


Figure 12: Maximum cutting force components, resultant cutting force and FFT amplitudes of cutting force components vs pass numbers (machined length) in x, y and z-directions under LN₂, up-milling. (a) Maximum cutting force components and resultant cutting force, (b) FFT amplitudes (Contd.)

Figure 13 shows the plots under LN₂ cooling, down-milling. As shown earlier under emulsion and MQL cooling strategies, the cutting force components under LN₂ down-milling are lower than LN₂ up-milling. LN₂ cooling reduces the cutting zone temperature but due to absence of sufficient lubrication, the rate of increase of cutting forces in successive passes is higher than emulsion and MQL down-milling operations. LN₂ cooling generated highest resultant cutting force components than other cooling strategies during down-milling operation. This is because of increased hardness of material by application of LN₂ at sub-zero temperature in the primary shear zone (Hong et al., 2001). The amplitude of FFT under LN₂ cooling also followed the same trend as their cutting force components. Again, the cutting force component perpendicular to the feed direction (F_x) is the highest among all three cutting force components throughout the machining length.

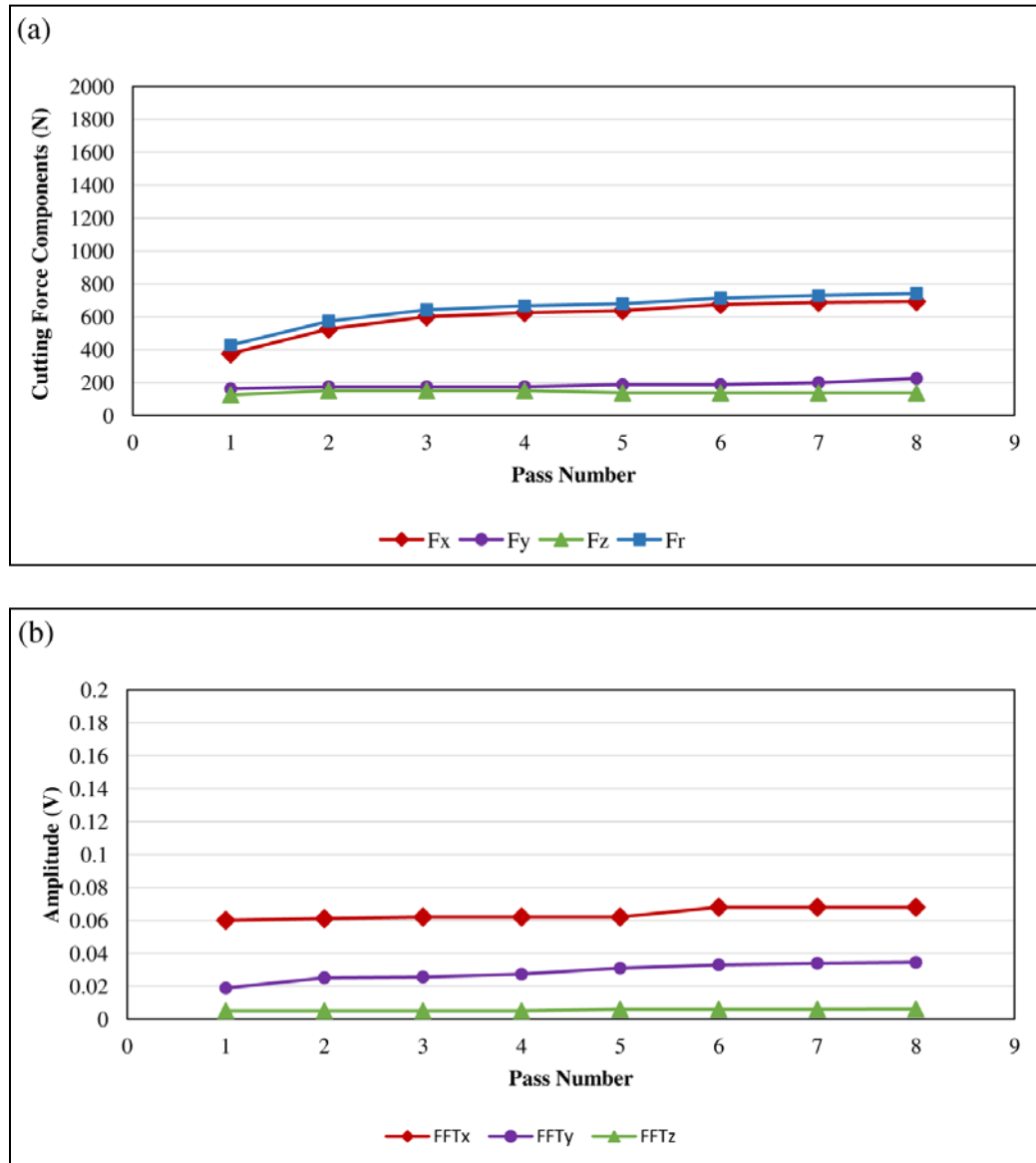


Figure 13: Maximum cutting force components, resultant cutting force and FFT amplitudes of cutting force components vs pass numbers (machined length) in x, y and z-directions under LN₂, down-milling. (a) Maximum cutting force components and resultant cutting force, (b) FFT amplitudes

4.2.4. Combined (MQL + LN₂) Cooling. Figure 14 shows the plots under combined (MQL + LN₂) cooling, up-milling method. The plots show that the cutting force components are higher in (MQL + LN₂) up-milling than in emulsion and MQL up-milling but lower than LN₂ up-milling.

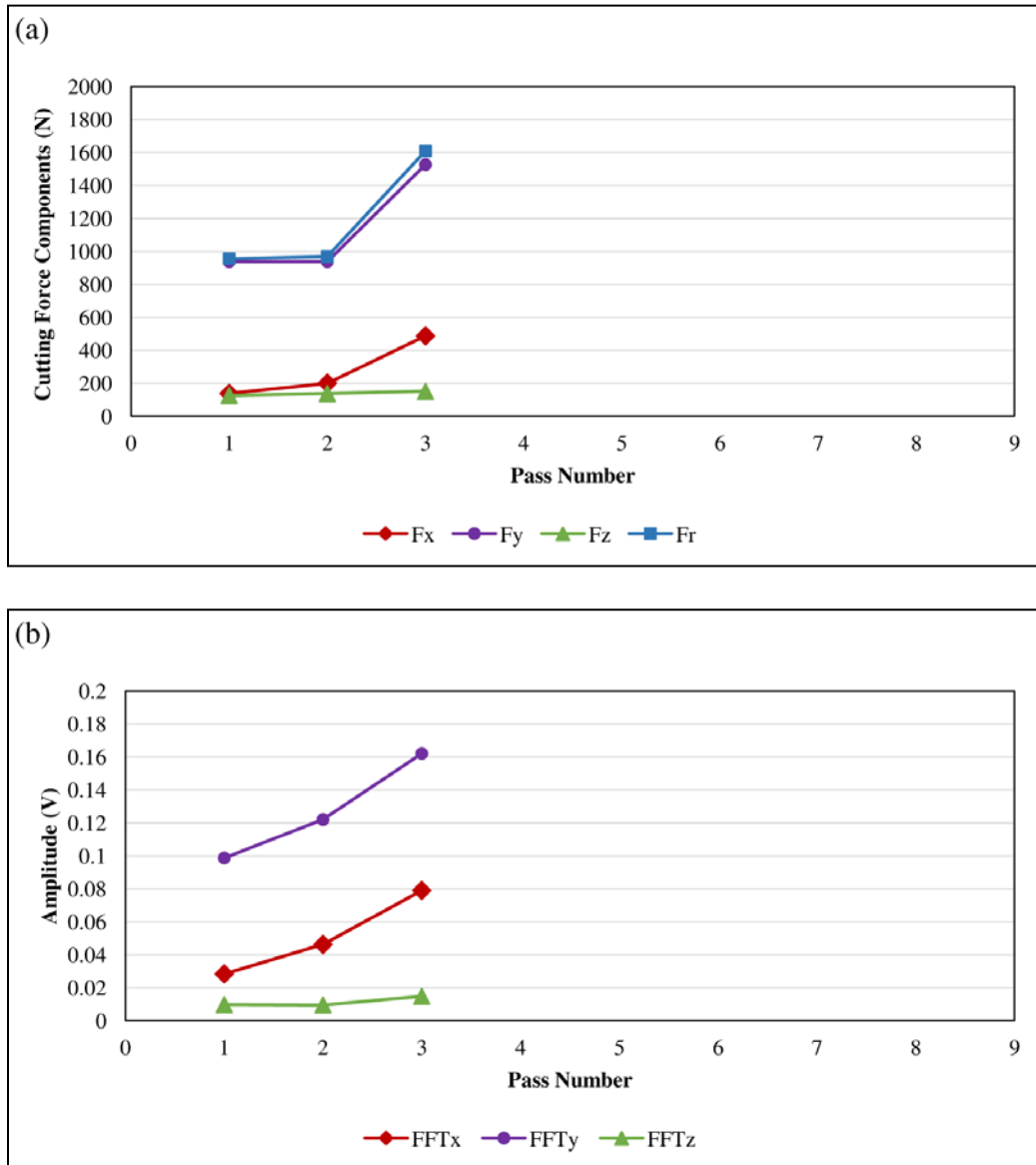


Figure 14: Maximum cutting force components, resultant cutting force and FFT amplitudes of cutting force components vs pass numbers (machined length) in x, y and z-directions under MQL + LN₂, up-milling. (a) Maximum cutting force components and resultant cutting force, (b) FFT amplitudes

The presence of LN₂ cooling lowered down the temperature of cutting zone whereas; MQL provided the lubrication to the cutting zone. This addition of MQL in LN₂ increased the tool life to 3 passes under MQL + LN₂ up-milling as compared to single pass under LN₂ up-milling. Due to the nature of up-milling method and production

of segmented chips during up-milling, the cutting forces were very high from the 1st pass. The application of LN₂ further increased the tool wear due to the increased hardness of workpiece which in turn, increased the cutting forces. The tool worn out completely after 3 passes due to high cutting forces and hence, the machining was terminated thereafter. Figure 15 shows the plots under combined (MQL + LN₂) down-milling. The combination of MQL lubrication and LN₂ cooling, along with down-milling, provided a favorable environment for machining Inconel-718. The force component F_z is lowest among all and hence, contributes least towards resultant cutting force. The FFT plot shows the F_x cutting force component to be the highest among all. Also, FFT_x and FFT_y increased after 6th pass and surpassed the FFT amplitude for LN₂ cooling, which was not expected. The reasonable explanation for this increase is that some chips might have been left in the cutting zone and interfered in cutting process, causing increase in vibrations.

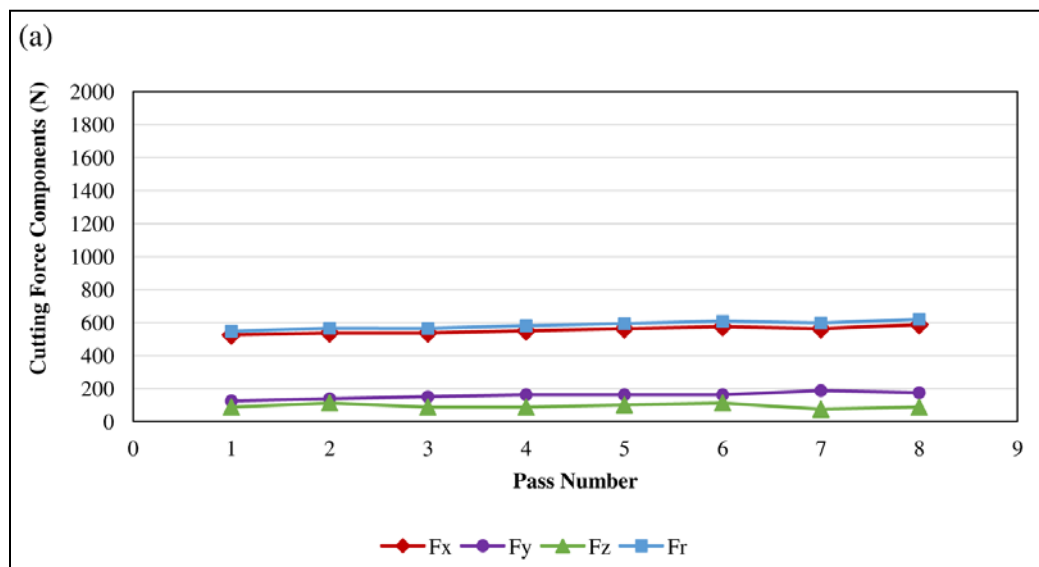


Figure 15: Maximum cutting force components, resultant cutting force and FFT amplitudes of cutting force components vs pass numbers (machined length) in x, y and z-directions under MQL + LN₂, down-milling. (a) Maximum cutting force components and resultant cutting force, (b) FFT amplitudes

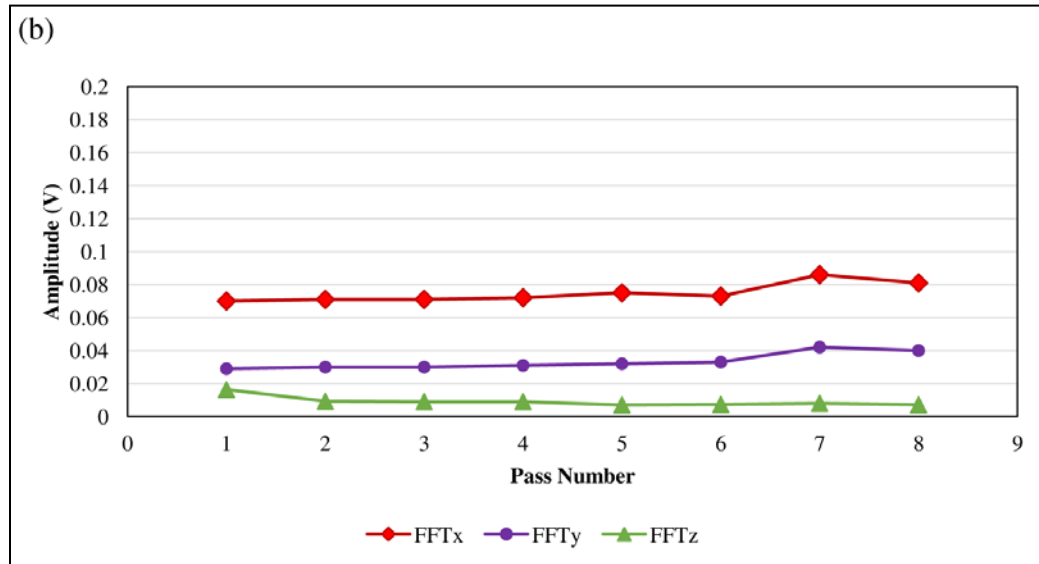


Figure 15: Maximum cutting force components, resultant cutting force and FFT amplitudes of cutting force components vs pass numbers (machined length) in x, y and z-directions under MQL + LN2, down-milling. (a) Maximum cutting force components and resultant cutting force, (b) FFT amplitudes (Contd.)

4.3. COMPARATIVE INVESTIGATION OF RESULTANT CUTTING FORCES FOR ALL FOUR COOLING STRATEGIES UNDER UP AND DOWN-MILLING METHODS

Figure 16 shows the plot of resultant cutting forces for all four cooling strategies plotted against machined length under up-milling method. As can be seen from the plot, emulsion gives the lowest resultant cutting forces throughout the machining length when machining using up-milling method. This is because of the increase in temperature at the cutting zone under emulsion cooling, heat is not removed as quickly as it is generated at the cutting zone, which increases the temperature at the cutting zone and results in material softening and more plastic deformation of the workpiece, which decreases the cutting forces (Aramcharoen and Chuan, 2014). Also, emulsion cooling provided lubrication to the cutting zone, and chip removal under emulsion cooling was more

effective than other cooling strategies in up-milling. The other cooling strategies under up-milling operation were not that much effective in chip removal and/or lowering the temperature of cutting zone as compared to emulsion cooling, leading to high cutting forces and hence, the tool did not last up to 8 passes under any cooling strategy other than emulsion. The cutting tool did not last more than 1st pass under LN₂ cooling because of high cutting forces and severe plastic deformation of the tool. Though, LN₂ provided effective cooling to the cutting zone, it did not provide enough lubrication to the cutting zone, increased tool and material hardness at -15°C temperature and was not very much effective in flushing the chips away from the cutting zone. The tool survived 4 passes under MQL cooling in up-milling method due to the lubrication provided by MQL cooling. When MQL was combined with LN₂ cooling, it increased the life of the tool as compared to LN₂ alone due to lubrication provided by MQL, but could not go beyond 3rd pass due to increase in the hardness of the tool and workpiece by the application of LN₂.

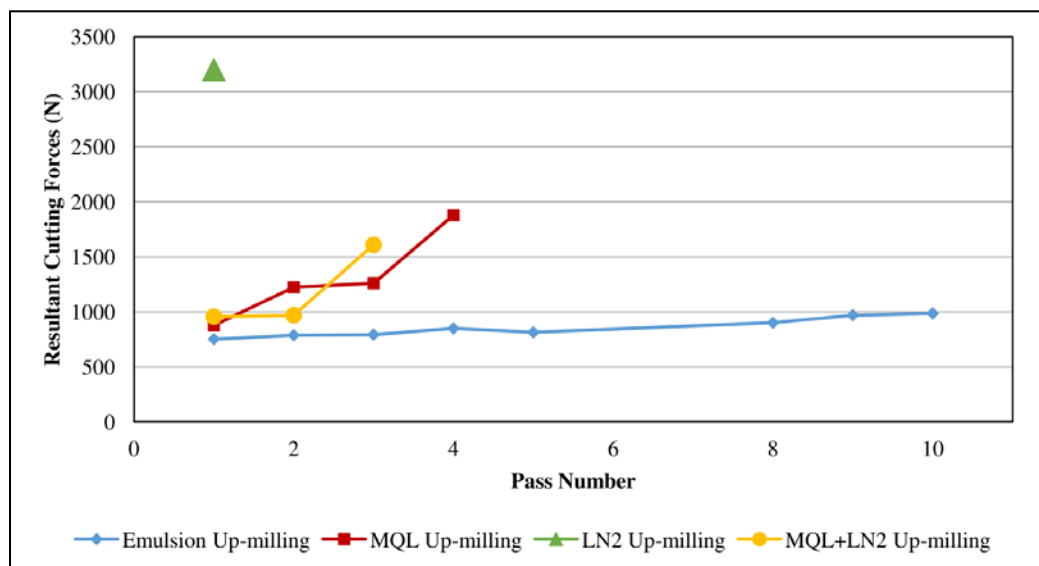


Figure 16: Resultant cutting forces against pass numbers (machined length) for all four cooling strategies under up-milling method

Figure 17 shows the plot of resultant cutting forces for all four cooling strategies plotted against machined length under down-milling method. The plot shows that down-milling method generated lowest resultant cutting force than up-milling method under all four cooling strategies. Under down-milling operation, the chip removal was much effective as compared to up-milling operation, which made all the cooling strategies to complete 8 passes.

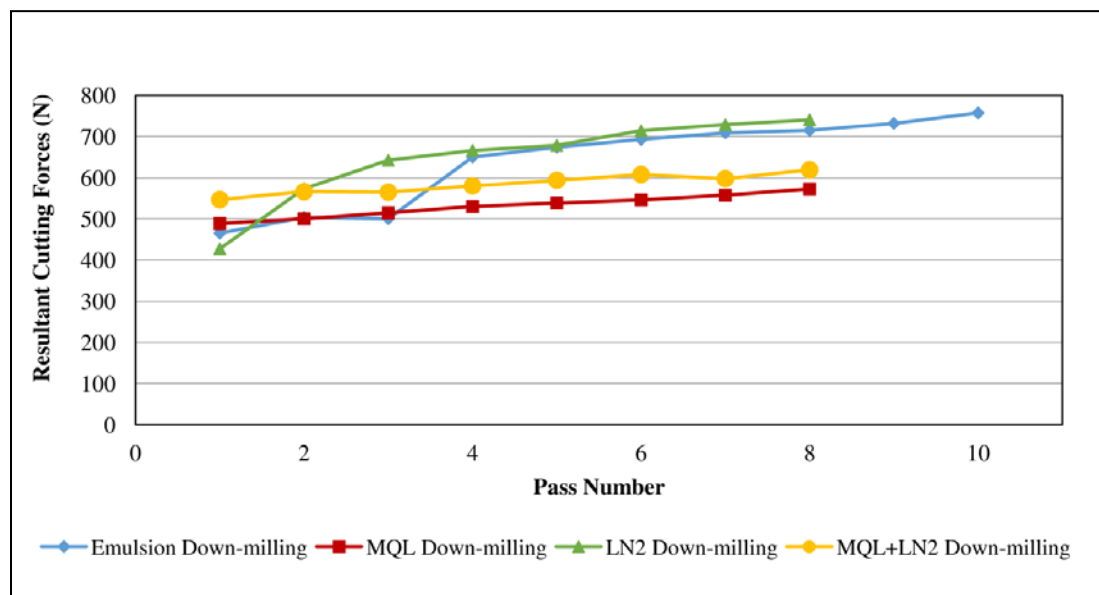


Figure 17: Resultant cutting forces against pass numbers (machined length) for all four cooling strategies under down-milling method

During the 1st pass, the resultant cutting force was least under LN₂ cooling, followed by emulsion cooling, whereas combined (MQL+LN₂) cooling generated the highest resultant cutting force. During the 8th pass, MQL cooling generated lowest resultant cutting force, followed by combined (MQL+LN₂), whereas LN₂ cooling generated the highest resultant cutting force. As can be seen from Figures 16 and 17, LN₂ cooling strategy generates the highest cutting forces than other cooling strategies in both up and down-milling operations. This is because LN₂ provides cooling to the cutting

zone without providing sufficient lubrication, which increases the coefficient of friction between tool and workpiece. Also, application of LN₂ at the cutting zone increases the hardness of both the tool and the workpiece. This increase in hardness and coefficient of friction by the application of LN₂ increases the cutting force components as compared to other cooling strategies in both up and down-milling operations. On the other hand, the MQL cooling provides sufficient lubrication at the cutting zone, which decreases the coefficient of friction between the tool and workpiece. This decrease in coefficient of friction lowers the cutting force components under MQL cooling. Although, emulsion cooling generated lowest resultant cutting force throughout the machining in up-milling, it generated second highest resultant force after LN₂ cooling in down-milling because emulsion cooling in down-milling was not as effective in lowering the coefficient of friction as the application of MQL in both MQL and combined (MQL+LN₂) cooling strategies, thus generated higher resultant cutting force than MQL and combined (MQL+LN₂) cooling strategies.

5. CONCLUSIONS

This research investigated the effects of four cooling strategies (Emulsion, MQL, LN₂ and combined (MQL+LN₂)) and milling methods (Up-milling and Down-milling) on cutting force components (F_x , F_y , F_z) and their Fast Fourier Transforms (FFT's) and, the resultant cutting force during peripheral end-milling of Inconel 718 alloy using uncoated 4-flutes bull nose helical end-mills. From the results obtained, the following conclusions can be made:

1. Cutting force component F_y (along the feed direction) is the highest as compared to F_x and F_z in up-milling and increases rapidly with machining passes (tool wear).

2. Cutting force component F_x (perpendicular to the feed direction) is highest as compared to F_y and F_z in down-milling and increases with machining passes (tool wear).
3. Down-milling generates lower cutting force than up-milling and thus improves machinability.
4. The resultant cutting force follows the similar trend and magnitude as the feed force in up-milling or perpendicular to feed force in down-milling.
5. The resultant cutting force F_r is highest in up-milling as compare to down-milling.
6. The amplitude of FFT of cutting force in the x, y and z directions at 75.13 Hz tooth frequency follows almost the same trend as cutting force components.
7. The amplitudes of FFT for all cutting force components versus machining length under down-milling operation are almost flat with machined length (Number of passes) which indicates the lower vibrations and smoother operation in down-milling as compared to up-milling, while in up-milling the amplitude of FFT increases rapidly which indicates higher vibrations and tendency for rapid tool wear and breakage.
8. A comparative evaluation of four cooling strategies using up-milling method shows that emulsion cooling strategy generates the least resultant cutting force with LN_2 cooling strategy generating the highest resultant cutting force.
9. A comparative evaluation of four cooling strategies using down-milling method shows that MQL cooling strategy generates the least resultant cutting force, followed by combined MQL+ LN_2 with emulsion generating the highest resultant cutting force.

10. Using LN₂ cooling strategy alone is not recommended for machining Inconel-718 due to high cutting forces and vibrations.
11. Down-milling with MQL cooling strategy is recommended for improving the machinability of Inconel 718 alloy at given machining parameters.

ACKNOWLEDGEMENTS

The financial support from the Intelligent System Centre (ISC) of the Missouri University of Science and Technology is greatly acknowledged. The financial assistance provided in the form of Graduate Teaching Assistantship by the Department of Mechanical and Aerospace Engineering at Missouri University of Science and Technology is also greatly acknowledged.

REFERENCES

- Abele, E. and Fröhlich, B. (2008) 'High Speed Milling of Titanium Alloys', *Journal of Advances in Production Engineering & Management* 3, pp. 131–140.
- Ahmad Yasir, M. S. et al. (2009) 'Machinability of Ti-6Al-4V Under Dry and Near Dry Condition Using Carbide Tools', *The Open Industrial and Manufacturing Engineering Journal*, 2(April), pp. 1–9. doi: 10.2174/1874152500902010001.
- Aramcharoen, A. and Chuan, S. K. (2014) 'An experimental investigation on cryogenic milling of inconel 718 and its sustainability assessment', in *Procedia CIRP*, pp. 529–534. doi: 10.1016/j.procir.2014.03.076.
- Boubekri, N. and Shaikh, V. (2012) 'Machining Using Minimum Quantity Lubrication: A Technology for Sustainability', *International Journal of Applied Science and Technology*, 2(1), pp. 111–115.
- Bouzakis, K. D., Gerardis, S., Katirtzoglou, G., Makrimalakis, S., Michailidis, N., & Lili, E. (2008). Increasing tool life by adjusting the milling cutting conditions according to PVD films' properties. *CIRP Annals - Manufacturing Technology*, 57(1), 105–108. <https://doi.org/10.1016/j.cirp.2008.03.070>

- Coleman, H. W. and Steele, W. G. (1989) Experimentation and uncertainty analysis for engineers. Wiley (A Wiley-interscience publication). Available at: <https://books.google.com/books?id=H25RAAAAMAAJ>.
- Dhananchezian, M. and Pradeep Kumar, M. (2011) 'Cryogenic turning of the Ti-6Al-4V alloy with modified cutting tool inserts', *Cryogenics*, 51(1), pp. 34–40. doi: 10.1016/j.cryogenics.2010.10.011.
- Dhar, N. R., Ahmed, M. T. and Islam, S. (2007) 'An experimental investigation on effect of minimum quantity lubrication in machining AISI 1040 steel', *International Journal of Machine Tools and Manufacture*, 47(5 SPEC. ISS.), pp. 748–753. doi: 10.1016/j.ijmachtools.2006.09.017.
- Ezugwu, E. O. and Wang, Z. M. (1997) 'Titanium alloys and their machinability—a review', *Journal of Materials Processing Technology*, 68(3), pp. 262–274. doi: 10.1016/S0924-0136(96)00030-1.
- Fallböhmer, P. et al. (2000) 'High-speed machining of cast iron and alloy steels for die and mold manufacturing', *Journal of Materials Processing Technology*, 98(1), pp. 104–115. doi: 10.1016/S0924-0136(99)00311-8.
- Fang, N. and Wu, Q. (2009) 'A comparative study of the cutting forces in high speed machining of Ti-6Al-4V and Inconel 718 with a round cutting edge tool', *Journal of Materials Processing Technology*, 209(9), pp. 4385–4389. doi: 10.1016/j.jmatprotec.2008.10.013.
- Hadi, M. A., Ghani, J. A., Che Haron, C. H., & Kasim, M. S. (2013) 'Comparison between up-milling and down-milling operations on tool wear in milling Inconel 718', *Procedia Engineering*. Elsevier B.V., 68, pp. 647–653. doi: 10.1016/j.proeng.2013.12.234.
- Hong, S. Y., Ding, Y. and Jeong, W. cheol (2001) 'Friction and cutting forces in cryogenic machining of Ti-6Al-4V', *International Journal of Machine Tools and Manufacture*, 41(15), pp. 2271–2285. doi: 10.1016/S0890-6955(01)00029-3.
- Hong, S. Y., Markus, I. and Jeong, W. cheol (2001) 'New cooling approach and tool life improvement in cryogenic machining of titanium alloy Ti-6Al-4V', *International Journal of Machine Tools and Manufacture*, 41(15), pp. 2245–2260. doi: 10.1016/S0890-6955(01)00041-4.
- Huang, P., Li, J., Sun, J., & Zhou, J. (2013). Vibration analysis in milling titanium alloy based on signal processing of cutting force. *The International Journal of Advanced Manufacturing Technology*, 64(5–8), 613–621. <https://doi.org/10.1007/s00170-012-4039-x>

- Iturbe, A., Hormaetxe, E., Garay, A., & Arrazola, P. J. (2016). Surface Integrity Analysis when Machining Inconel 718 with Conventional and Cryogenic Cooling. In *Procedia CIRP* (Vol. 45, pp. 67–70). <https://doi.org/10.1016/j.procir.2016.02.095>
- Kamata, Y. and Obikawa, T. (2007) ‘High speed MQL finish-turning of Inconel 718 with different coated tools’, *Journal of Materials Processing Technology*, 192–193, pp. 281–286. doi: 10.1016/j.jmatprotec.2007.04.052.
- Kaynak, Y. (2014) ‘Evaluation of machining performance in cryogenic machining of Inconel 718 and comparison with dry and MQL machining’, *International Journal of Advanced Manufacturing Technology*, 72(5–8), pp. 919–933. doi: 10.1007/s00170-014-5683-0.
- Kim, S. W., Lee, D. W., Kang, M. C., & Kim, J. S. (2001) ‘Evaluation of machinability by cutting environments in high-speed milling of difficult-to-cut materials’, *Journal of Materials Processing Technology*, 111(1–3), pp. 256–260. doi: 10.1016/S0924-0136(01)00529-5.
- Lee, W. K., Ratnam, M. M., & Ahmad, Z. A. (2017). Detection of chipping in ceramic cutting inserts from workpiece profile during turning using fast Fourier transform (FFT) and continuous wavelet transform (CWT). *Precision Engineering*, 47, 406–423. <https://doi.org/10.1016/j.precisioneng.2016.09.014>
- Li, H. Z., Zeng, H. and Chen, X. Q. (2006) ‘An experimental study of tool wear and cutting force variation in the end milling of Inconel 718 with coated carbide inserts’, *Journal of Materials Processing Technology*, 180(1–3), pp. 296–304. doi: 10.1016/j.jmatprotec.2006.07.009.
- Liao, Y. S., Lin, H. M. and Wang, J. H. (2008) ‘Behaviors of end milling Inconel 718 superalloy by cemented carbide tools’, *Journal of Materials Processing Technology*, 201(1–3), pp. 460–465. doi: <http://dx.doi.org/10.1016/j.jmatprotec.2007.11.176>.
- Musfirah, A. H., Ghani, J. A., & Haron, C. H. C. (2017). Tool wear and surface integrity of inconel 718 in dry and cryogenic coolant at high cutting speed. *Wear*, 376–377, 125–133. <https://doi.org/10.1016/j.wear.2017.01.031>
- Park, K.-H., Suhaimi, M. A., Yang, G.-D., Lee, D.-Y., Lee, S.-W., & Kwon, P. (2017) ‘Milling of titanium alloy with cryogenic cooling and minimum quantity lubrication (MQL)’, *International Journal of Precision Engineering and Manufacturing*, 18(1), pp. 5–14. doi: 10.1007/s12541-017-0001-z.
- Ravi, S. and Pradeep Kumar, M. (2011) ‘Experimental investigations on cryogenic cooling by liquid nitrogen in the end milling of hardened steel’, *Cryogenics*, 51(9), pp. 509–515. doi: 10.1016/j.cryogenics.2011.06.006.

- Safari, H. et al. (2014) 'Cutting Force and Surface Roughness Characterization in Cryogenic High-Speed End Milling of Ti-6Al-4V ELI', *Materials and Manufacturing Processes*, 29(3), pp. 350–356. doi: 10.1080/10426914.2013.872257.
- Shokrani, A., Dhokia, V., & Newman, S. T. (2016). Investigation of the effects of cryogenic machining on surface integrity in CNC end milling of Ti-6Al-4V titanium alloy. *Journal of Manufacturing Processes*, 21, 172–179. <https://doi.org/10.1016/j.jmapro.2015.12.002>
- Shokrani, A., Dhokia, V., & Newman, S. T. (2017). Hybrid Cooling and Lubricating Technology for CNC Milling of Inconel 718 Nickel Alloy. *Procedia Manufacturing*, 11, 625–632. <https://doi.org/10.1016/j.promfg.2017.07.160>
- Shokrani, A., Dhokia, V., Newman, S. T., & Imani-Asrai, R. (2012) 'An initial study of the effect of using liquid nitrogen coolant on the surface roughness of inconel 718 nickel-based alloy in CNC milling', *Procedia CIRP*, 3(1), pp. 121–125. doi: 10.1016/j.procir.2012.07.022.
- Su, Y., He, N. and Li, L. (2010) 'Effect of Cryogenic Minimum Quantity Lubrication (CMQL) on Cutting Temperature and Tool Wear in High-Speed End Milling of Titanium Alloys', *Applied Mechanics and Materials*, 34–35, pp. 1816–1821. doi: 10.4028/www.scientific.net/AMM.34-35.1816.
- Su, Y., He, N., Li, L., Iqbal, A., Xiao, M. H., Xu, S., & Qiu, B. G. (2007) 'Refrigerated cooling air cutting of difficult-to-cut materials', *International Journal of Machine Tools and Manufacture*, 47(6), pp. 927–933. doi: 10.1016/j.ijmachtools.2006.07.005.
- Su, Y., He, N., Li, L., & Li, X. L. (2006) 'An experimental investigation of effects of cooling/lubrication conditions on tool wear in high-speed end milling of Ti-6Al-4V', *Wear*, 261(7–8), pp. 760–766. doi: 10.1016/j.wear.2006.01.013.
- Tian, X., Zhao, J., Zhao, J., Gong, Z., & Dong, Y. (2013) 'Effect of cutting speed on cutting forces and wear mechanisms in high-speed face milling of Inconel 718 with Sialon ceramic tools', *International Journal of Advanced Manufacturing Technology*, 69(9–12), pp. 2669–2678. doi: 10.1007/s00170-013-5206-4.
- Ulutun, D., Pleta, A., Henderson, A., & Mears, L. (2015). Comparison and Cost Optimization of Solid Tool Life in End Milling Nickel-Based Superalloy. *Procedia Manufacturing*, 1, 522–533. <https://doi.org/10.1016/j.promfg.2015.09.024>
- Yuan, S. M., Yan, L. T., Liu, W. D., & Liu, Q. (2011). Effects of cooling air temperature on cryogenic machining of Ti-6Al-4V alloy. *Journal of Materials Processing Technology*, 211(3), 356–362. <https://doi.org/10.1016/j.jmatprotec.2010.10.009>

Zhang, S., Li, J. F., & Wang, Y. W. (2012). Tool life and cutting forces in end milling Inconel 718 under dry and minimum quantity cooling lubrication cutting conditions. *Journal of Cleaner Production*, 32, 81–87.

<https://doi.org/10.1016/j.jclepro.2012.03.014>

Zhao, W., He, N., & Li, L. (2007). High Speed Milling of Ti6Al4V Alloy with Minimal Quantity Lubrication. *Key Engineering Materials*, 375–376, 435–439.

<https://doi.org/10.4028/www.scientific.net/KEM.329.663>

II. EFFECTS OF COOLING STRATEGIES AND TOOL COATINGS ON CUTTING FORCES AND TOOTH FREQUENCY IN HIGH SPEED DOWN-MILLING OF INCONEL-718 USING HELICAL BULL-NOSE SOLID CARBIDE END-MILLS

A. Chukwujekwu Okafor*, Paras Mohan Jasra
Computer Numeric Control and Virtual Manufacturing Laboratory
Department of Mechanical and Aerospace Engineering
Missouri University of Science and Technology
327 Toomey Hall, Rolla, MO-65409-0050, USA
Email: okafor@mst.edu

ABSTRACT

This paper presents the results of experimental investigation of the effects of three (3) cooling strategies (Minimum Quantity Lubrication (MQL), Cryogenic cooling using Liquid Nitrogen (LN₂) and Combined (MQL+LN₂)) and three (3) tool coatings (uncoated, AlTiN coated and GMS² coated) on cutting force components (F_x , F_y , F_z), the resultant cutting force, F_r , and cutter tooth frequency in peripheral high speed end-milling of Inconel-718 to improve machinability and reduce cost. All the experiments were conducted on a Cincinnati Milacron Sabre 750 Vertical Machining Centre (VMC), equipped with Acramatic 2100 CNC controller using uncoated, AlTiN coated and GMS² coated solid helical bull-nose solid carbide end-mills of 12.7 mm (0.5 inches) diameter, and 0.762 mm (0.03 inches) corner radius. Each experiment consists of 8 passes, each pass of 76.2 mm (3 inches) cutting length. Axial and radial depths of cut, cutting speed, and material removal rate were kept constant for all experiments. Three cutting force components (F_x , F_y , F_z) and their Fast Fourier Transforms (FFT) were acquired using a

Kistler 9272 4-component dynamometer, a Kistler 5010B dual mode amplifier, and a Tektronix TDS 420A digitizing oscilloscope for data acquisition, analysis and visualization. Resultant cutting forces, F_r , for all cooling strategies and end-mill coatings under down-milling operation were calculated from the acquired cutting force components, as well as the amplitudes of the FFTs. The experimental results show that uncoated end-mills generate lowest resultant cutting forces, whereas GMS^2 coated end-mills generate highest resultant cutting forces under all cooling strategies. MQL cooling strategy generates lowest resultant cutting forces, whereas LN_2 cooling strategy generates highest resultant cutting forces with all end-mill coatings. Using LN_2 cooling strategy alone is not recommended for machining Inconel-718 due to high cutting forces and vibrations. Uncoated end-mills under MQL cooling strategy generate the lowest cutting forces and are recommended for machining Inconel-718, whereas GMS^2 coated end-mills under LN_2 cooling strategy generated highest cutting forces.

Keywords: Cutting force components, Inconel-718, Tool coatings, Minimum Quantity Lubrication, Cryogenic cooling, High speed down-milling

1. INTRODUCTION

Inconel-718 super-alloy is used extensively in aerospace and nuclear industries due to its excellent properties such as: high strength-to-weight ratio, ability to retain its properties at high temperatures, high corrosion and creep resistance [1]. However, Inconel-718 is characterized as a very “difficult-to-cut” material, because it poses severe problems during machining. One of the problems posed by Inconel-718 is that enormous amount of heat is generated in the cutting zone due to high friction between the tool-chip interface and tool-workpiece interface and is not removed as quickly as it is generated

due to its low thermal conductivity. Therefore the heat is mostly concentrated on the tool cutting edges, causing severe tool wear. Due to high temperature and pressure at the cutting zone, and its high chemical affinity with many cutting tool materials, some chip fragments from the workpiece get welded on the cutting edges of the tool to form built-up edge (BUE), which further exacerbates tool wear and cutting forces. Moreover, its good mechanical strength and ability to work harden at elevated temperatures leads to high cutting forces which further leads to high tool wear. End milling is a widely used machining operation due to its versatility and applications may range from aerospace and automotive industries to small tool and die shops, as it can be used for milling many features like peripheral, slot or face milling. Some problems encountered while machining using end-milling operations are high cutting forces, high cutting temperature, rapid tool wear, tool breakage, and chatter. These problems associated with end-milling are further exacerbated while machining difficult-to-cut metals such as Inconel-718 because the desired properties of this difficult-to-cut metal become disadvantage while machining them.

Coolants and lubricants play an important role in addressing these problems, as they reduce cutting temperature, friction and tool wear, cutting force/power consumed, improve surface roughness, and hence, improve machinability. Mineral-based conventional cutting fluids commonly used in most industries are expensive, environmentally unfriendly and difficult to dispose and, cause health hazards.

Minimum Quantity Lubrication (MQL) refers to a technique that minimizes the use of coolant by mixing a small amount of lubricant and compressed air to form aerosol, which is sprayed in mist form to the cutting zone with the help of a nozzle, which acts as

a lubricant and coolant instead of flooding the workpiece and the cutting tool. MQL technique eliminates the problems caused by conventional cutting fluids. There is no problem of disposal of MQL. Also, MQL is less expensive as compared to conventional fluids and does not cause health hazards and hence, considered as environmentally friendly. It also helps to flush the chips away from the cutting zone. Zhao et al. [2] reported that MQL improved machinability in terms of cutting forces, surface roughness and tool life as compared to dry machining in high speed peripheral milling of Ti-6Al-4V using uncoated cemented carbide inserts. Dhar et al. [3] reported improvement in machinability in terms of cutting temperature, chip-tool interaction, cutting forces, tool wear, surface finish, and dimensional deviation with MQL cooling over dry machining in turning of AISI-1040 steel. Ahmad Yasir et al. [4] reported that higher quantity of MQL sprayed on the cutting zone is less efficient than spraying less quantity due to difficulty of large MQL particles to effectively penetrate into the cutting zone in machining of Ti-6Al-4V using Physical Vapor Deposition (PVD) coated cemented carbide tools. Obikawa et al. [5] used a small amount of lubrication, called micro-liter lubrication, to spray on the cutting zone using a specially designed nozzle to concentrate the small amounts of oil mist onto the cutting interface in the machining of Inconel-718 and reported that micro-liter spraying with specially designed nozzle was quite effective in increasing tool life than ordinary MQL spray. Boubekri and Shaikh [6] mentioned the need to collect the mist generated by MQL which can be detrimental to operators.

The application of Liquid Nitrogen (LN_2), commonly called cryogenic cooling helps in reducing the cutting zone temperature and hence, improves the machinability. Liquid nitrogen when sprayed on the red hot cutting zone evaporates into the

environment. Thus, there is no health hazard and no problem of disposal using liquid nitrogen as a coolant unlike conventional coolants. Kaynak [7] reported that MQL performed better at a lower cutting speed of 60 m/min whereas the performance of liquid nitrogen was better than MQL at a higher cutting speed of 120 m/min in machining of Inconel-718. He also emphasized that the number of nozzles in cryogenic machining plays a vital role in controlling cutting forces and power consumption. Aramcharoen and Chuan [8] reported that cryogenic cooling reduced tool wear, improved machined surface quality, reduced contact friction between tool-chip interface but increased cutting forces than dry and conventional oil based coolant in milling of Inconel-718. Dhananchezian and Kumar [9] reported improvement in machinability in turning of Ti-6Al-4V with application of cryogenic cooling in terms of temperature, cutting forces, surface roughness and tool wear when compared with wet cooling using coated carbide inserts. Kim et al. [10] also reported improvement in tool life in machining of difficult-to-cut metals having hardness varying from HRc28 to HRc60 using compressed chilly-air coolants as compared to dry and flood coolants. Ravi and Kumar [11] reported that LN₂ cooling improved cutting forces, cutting temperature, tool flank wear and surface roughness than dry and wet end-milling of hardened steel using PVD coated carbide inserts. Hong et al. [12] investigated the effects of cryogenic cooling on friction and cutting forces in machining of Ti-6Al-4V using a minimum amount of LN₂ injected through micro-nozzle between tool rake and chip breaker and by auxiliary mini-nozzle on the flank face for cooling the flank, so that the LN₂ is not wasted by cooling the unnecessary areas which reduces the negative impact of increase of cutting forces and abrasion of pre-cooling of workpiece.

Combined (MQL + LN₂) cooling strategy provides the benefits of both cooling strategies. MQL provides the enough lubrication while LN₂ cools down the cutting zone temperature and hence, the combination of both provides an ideal environment for cutting difficult-to-metals. Su et al. [13] compared the performance of Cryogenic Minimum Quantity Lubrication (CMQL) at two different temperatures (-10 and -20⁰C) with dry milling and refrigerated air cutting at -10 and -20⁰C in high-speed end-milling of titanium alloys. They reported improvement in performance in terms of temperature and tool wear when using CMQL at -20⁰C. Su et al. [14] also compared the performance of dry, flood coolant, nitrogen-oil-mist cooling, compressed cold nitrogen gas (CCNG) at 0 and -10⁰C and, compressed cold nitrogen gas and oil mist (CCNGOM) at -10⁰C on tool life in high speed end-milling of Ti-6Al-4V and concluded that CCNGOM yielded the best tool life among all cooling strategies. Zhang et al. [15] reported improvement in tool life and cutting forces with Minimum Quantity Cooling Lubrication (MQCL) cutting than dry cutting in machining using cemented coated carbide insert. Yuan et al. [16] compared the performance of MQL with cooling air at different temperatures of 0, -15⁰C, -30⁰C and -45⁰C with dry, wet and MQL cooling. They reported that MQL cooling with cooling air improved the performance in terms of cutting force, tool wear and surface roughness and MQL with cooling air at -15⁰C provided more favourable effects than MQL with cooling air at other temperatures. Park et al. [17] reported that combined (MQL + LN₂) cooling provided the least cutting forces and tool wear than dry, wet, MQL and LN₂ cooling strategies in machining Ti-6Al-4V. They further reported that MQL when mixed with a small amount (~0.1%) of graphite nano-platelets (xGnPs), generated least tool wear than

MQL and combined (MQL + LN₂) at both cutting speeds investigated (100 m/min and 120 m/min).

End-mill coatings provide additional strength to the end-mill which helps in machining of difficult-to-cut metals. Researchers have investigated different tool coatings and their effect on machinability of difficult-to-cut metals. Wang et al. [18] investigated the performance of two PVD coated (TiAlN and TiSiN) carbide tools in high speed machining of hardened steel (SKD11/HRC 62, S136/HRC 51). They reported that the tools coated with TiSiN yielded higher life than the tools coated with TiAlN due to reduced abrasive wear. Jawaid et al. [19] investigated the performance of PVD-TiN coated and CVD – TiCN + Al₂O₃ coated tools in face milling of Ti-6Al-4V. They reported that CVD coated tools yielded better performance in terms of volume of material removed and tool life. Jawaid et al. [20] further investigated the performance of PVD TiN coated carbide tools in face milling of Inconel-718 and compared it with uncoated tools. They reported that uncoated tools performed better at low speeds whereas coated tools performed slightly better while the speed was raised. Ozel et al. [21] investigated the effect of uncoated, cBN, TiAlN, and TiAlN + cBN coated, single and multi-layer coated tungsten carbide inserts on cutting forces and tool wear in turning Ti-6Al-4V alloy. They concluded that the cBN and TiAlN+cBN coated tungsten carbide inserts generated lowest cutting forces at cutting speed of 50 m/min, whereas they generated largest cutting force at higher cutting speed of 100 m/min but yielded the favorable wear development. Kamata and Obikawa [22] applied MQL to finish-turning of Inconel-718 with three different coated carbide tools (TiCN/Al₂O₃/TiN (CVD), TiN/AlN superlattice (PVD) and TiAlN (PVD)). The performance of MQL cutting with three coatings was

evaluated in terms of tool life and surface finish and compared with those in dry and wet coating. Cutting speeds used were 1.0 m/s and 1.5 m/s. At a cutting speed of 1.0 m/s, TiCN/Al₂O₃/TiN (CVD) coating yielded best performance in MQL and coating TiN/AlN super lattice (PVD) exhibited second best performance in MQL cutting. TiCN/Al₂O₃/TiN (CVD) coating in wet cutting yielded the longest tool life but surface finish was second worst.

High Speed Machining (HSM) is employed to increase productivity, improve product quality and reduce manufacturing costs and thus, it is considered as the most efficient manufacturing technology [23]. Safari et al. [24] reported the lowest cutting forces at highest cutting speed of 300 mm/min during the investigation of the effects of 3 cutting speeds (200, 250 and 300 mm/min) in cryogenic high speed end-milling of Ti-6AL-4V using coated and uncoated tools.

Figure 1 shows the commonly accepted high-speed cutting ranges in machining of various materials [25], which depends on the strength and machinability of the material. The higher the strength and the more difficult-to cut of the material, the lower the high cutting speed range. Thus high cutting speed range for Aluminium is higher than high cutting speed range for Nickel alloys. Abele and Fröhlich [26] concluded that high speed milling of Ti-6AL-4V reduces cutting forces and improves performance as compared to conventional machining by increasing the material removal rate. Liao et al. [27] recommended the appropriate speed ranges of 55-135 m/min for side milling in high speed machining of Inconel-718. From the above literature, it can be seen that there is a lack of total comprehensive study summarizing the effects of cooling strategies and tool coatings on machinability in high speed end-milling of Inconel-718.

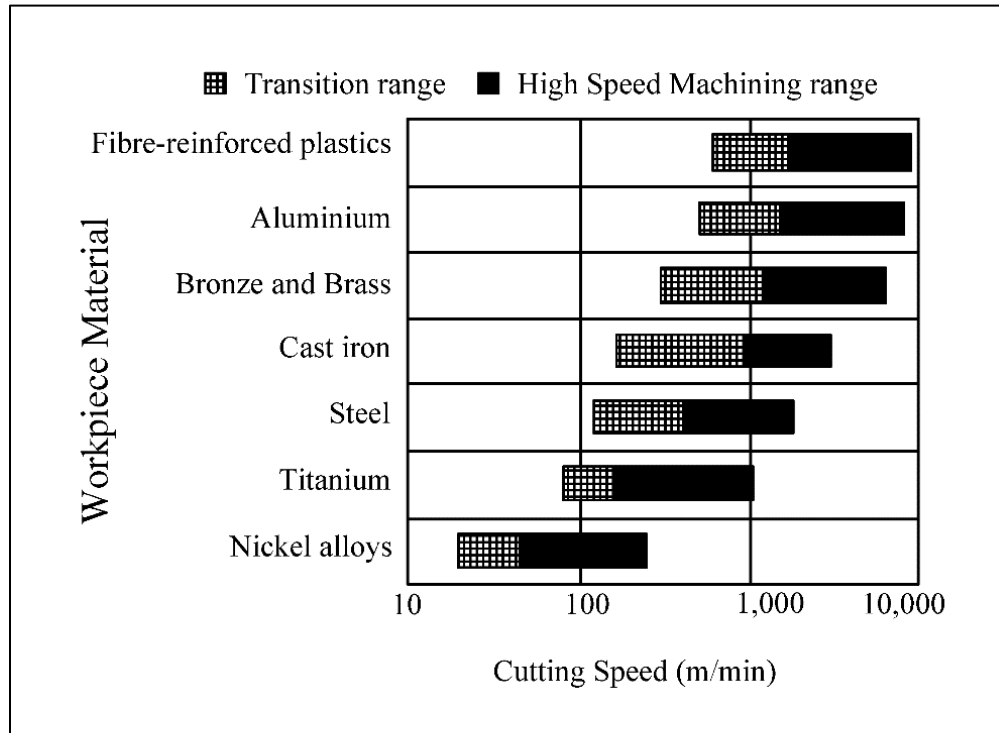


Figure 1: High-speed cutting ranges in machining of various materials (redrawn) [25]

Most of the published research on machinability of Inconel-718 alloy focused on dry machining or on one individual cooling strategy, conventional tool coatings and mostly in turning. There is a need to explore the potential of combining two different cooling strategies and to investigate their effects on machinability in end-milling of Inconel-718 alloy. Although, limited literature is present in combining two different cooling strategies for some other materials having high cutting speed ranges titanium alloys as shown in Figure 1, but the research findings of one material cannot be applied to other as published literature on HSM of two materials often involves different machining set-ups [23]. The current research investigates the effect of different cooling strategies and end-mill coatings to improve the machinability of Inconel-718 alloy.

2. EXPERIMENTAL PLAN AND PROCEDURE

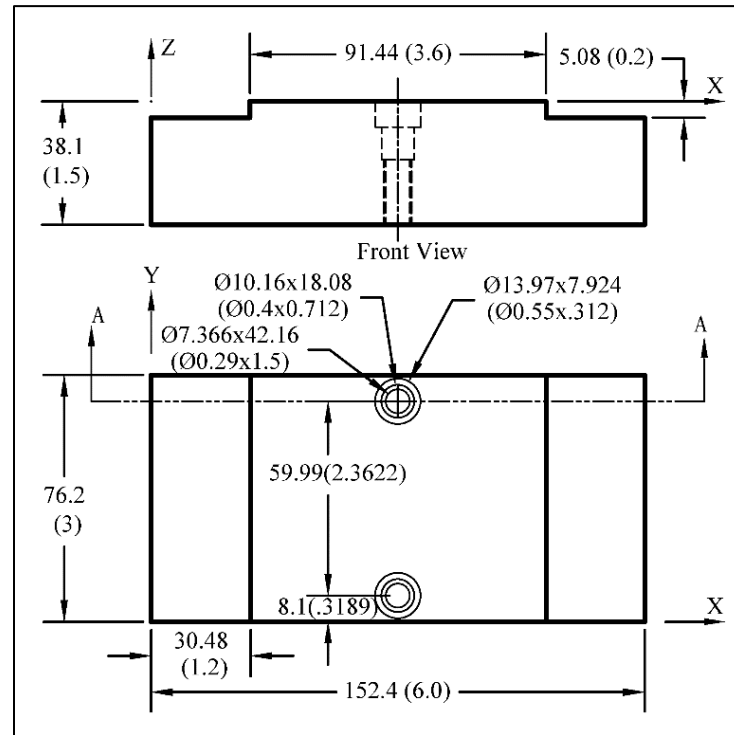
Peripheral high-speed end-milling tests were conducted on Cincinnati Milacron Sabre 750 Vertical Machining Centre (VMC), equipped with Acramatic 2100 CNC controller, using 4-flutes uncoated and AlTiN coated and, 7-flute GMS² coated solid carbide end-mills of diameter 12.7 mm (0.5 inches). The detailed experimental plan for the investigation of the effects of cooling strategies, tool coatings and machining parameters using uncoated and coated carbide helical bull-nose solid carbide end-mills is summarized in Table 1.

Table 1: Experiment plan for investigation of cooling strategies, tool coatings and machining parameters under down-milling operation using helical bull-nose solid carbide end-mills

Ex. No	Block No.	Tool Coatings	Cooling Strategy	Cutting Speed m/min	Feed per revolution mm/rev	Depths of cut		MRR mm ³ /m in
						Axial (a _a) mm	Radial (a _r) mm	
1	1	Uncoated	MQL	45	0.1016	5.08	3.81	2216.2
2			LN ₂ (-15 °C)	45	0.1016	5.08	3.81	2216.2
3			MQL + LN ₂ (-15 °C)	45	0.1016	5.08	3.81	2216.2
4	2	AlTiN	MQL	45	0.1016	5.08	3.81	2216.2
5			LN ₂ (-15 °C)	45	0.1016	5.08	3.81	2216.2
6			MQL + LN ₂ (-15 °C)	45	0.1016	5.08	3.81	2216.2
7	3	GMS ²	MQL	45	0.1016	5.08	3.81	2216.2
8			LN ₂ (-15 °C)	45	0.1016	5.08	3.81	2216.2
9			MQL + LN ₂ (-15 °C)	45	0.1016	5.08	3.81	2216.2

All the experiments were performed at constant cutting speed of 1127 rpm (45 m/min), feed-rate of 114.5 mm/min (4.510 ipm), axial depth of cut (a_a) of 5.08 mm (0.2 in) and radial depth of cut (a_r) of 3.81 mm (0.15 in) and were selected based on literature

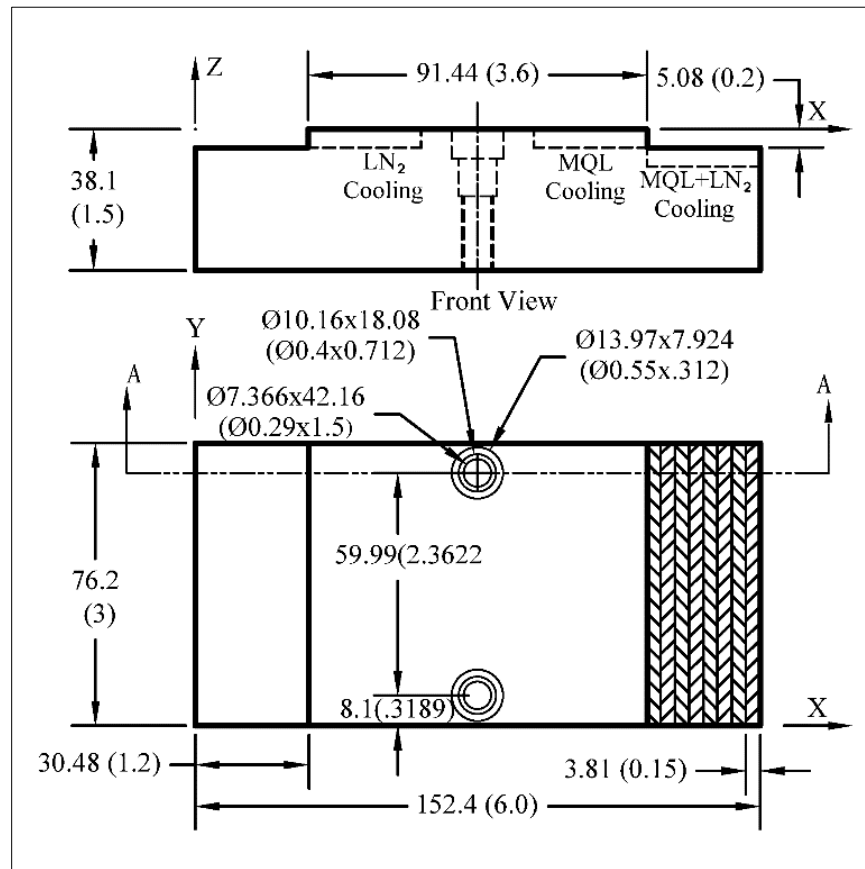
review and preliminary research investigation. Axial depth of cut (a_a), radial depth of cut (a_r) and feed per revolution (f_r) were kept constant and were selected to improve productivity without adversely sacrificing tool life (performance). Each experiment consisted of 8 passes, each pass of 76.2 mm (3 inches) cutting length. Three (3) cooling strategies (MQL, LN₂ and combined (MQL+LN₂)) were investigated for each of uncoated, AlTiN coated and GMS² coated end-mills under down-milling operation. For each set of experiments, the total number of tools used was nine (9) carbide end-mills (three for each of the uncoated and coated end-mills) and Inconel-718 workpieces used were three (3), one for each coating. Each experiment was replicated once, thus the total number of experiments was eighteen (18). The initial shape of prepared work-piece, with drilled, counter-bored and tapped holes for clamping is given in Figure 2.



All dimensions in mm (inches)

Figure 2: Initial shape of prepared work-piece, with drilled, counter-bored and tapped holes for clamping

Peripheral high-speed end-milling tests were conducted on three (3) work-piece blocks, each having two steps on each of the two sides, using 12.7 mm (0.5 in) diameter, 4-flute uncoated, 4-flute AlTiN coated and 7-flute GMS² coated carbide end-mills for down-milling operation. Figure 3 shows workpiece with the sequence of experiments performed using three cooling strategies.



All dimensions are in mm (inches)

Figure 3: Work-piece with schematic of experiments performed under three cooling strategies

Machining experiment under MQL cooling was conducted before machining experiment under LN₂ cooling or combined (MQL + LN₂) cooling because if LN₂ or (MQL + LN₂) cooling strategy was applied first, it would have affected the hardness of

the workpiece steps and hence, the results of experiments following that machining experiment. Also, neither of the two cooling strategies, LN₂ or combined (MQL + LN₂) was applied on the same side because they might affect the results of the subsequent cooling experiment by increasing the hardness of workpiece. A new tool was used for each cooling strategy to eliminate the effect of tool wear. The results of the nine (9) experiments were analyzed to find the best cooling strategy among MQL, LN₂ and combined (MQL + LN₂) cooling and better tool coating among uncoated, AlTiN coated and GMS² coated end-mill.

2.1. COOLING STRATEGIES SET-UP

The main objective of these experiments is to investigate the effects of cooling strategies and end-mill coatings on cutting force components (F_x , F_y and F_z), the resultant cutting force F_r and amplitude of FFT of cutting force components (FFT_x , FFT_y , FFT_z) at cutter tooth frequency in down-milling of Inconel-718 alloy. Each of the cooling strategies investigated (MQL, LN₂ and the combined MQL+LN₂) were set independently for each set of experiment reported in Table 1. The experimental set-up with cryogenic and MQL flow lines and data acquisition system is shown in Figure 4. The Accu-Lube LB-2000 biodegradable mineral oil, used as a lubricant for MQL experiments, is investigated as a possible environmentally friendly replacement of conventional emulsion coolant. For experiments involving nitrogen, cryogenic liquid nitrogen (LN₂) was applied at -15°C temperature to the cutting zone. The temperature of -15°C was chosen for the mixture of LN₂ and shop air as ideal temperature for Inconel 178 based on published literature [16].

2.2. WORKPIECE PREPARATION

The initial shape of the work-piece was machined from rectangular blocks of Inconel-718 of dimensions 152.4 mm x 76.2 mm x 38.1 mm (6 in x 3 in x 1.5 in) on Cincinnati Milacron Sabre 750 Vertical Machining Center (VMC). Two steps were machined on both sides of the workpiece, each having a width of 30.48 mm (1.2 in) and height 5.08 mm (0.2”). Each step was used to perform one experiment and thus, four experiments could be performed on one workpiece. Two counter-bored holes of diameter 7.366 (0.29 in.), 38.1 mm (1.5 in.) deep and 60 mm (2.3622 in.) apart were drilled and tapped for clamping the workpiece on a dynamometer.

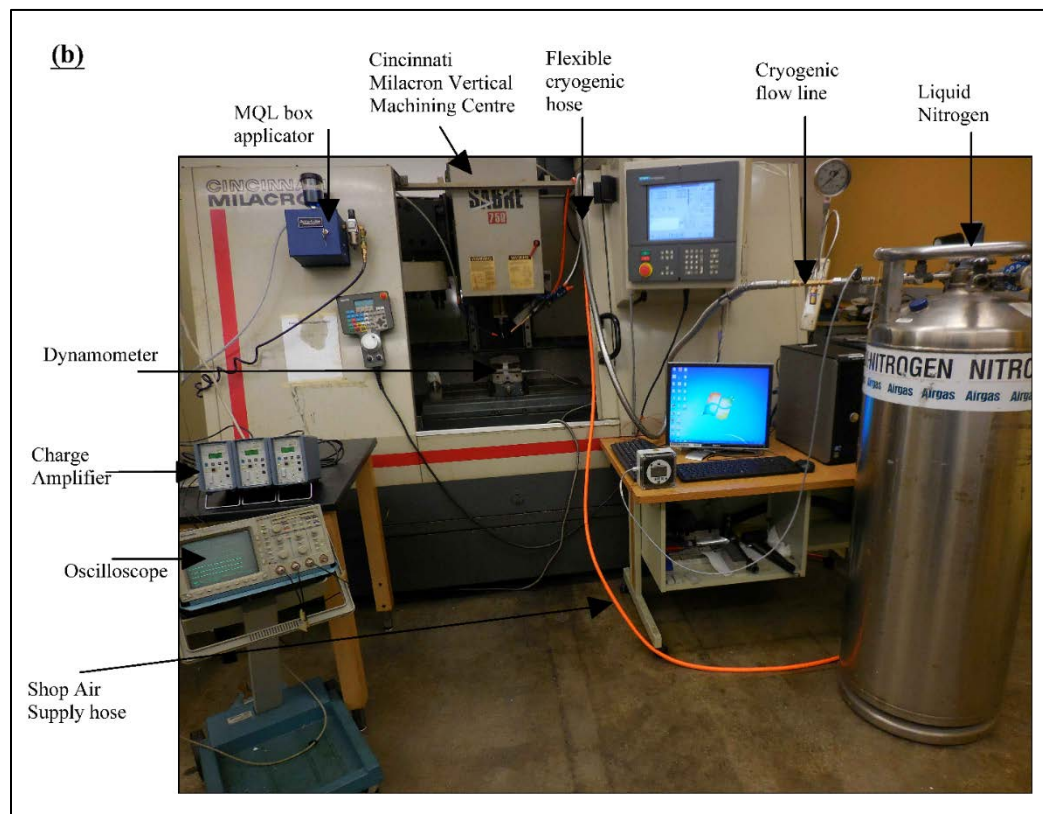


Figure 4: Experimental set-up with cryogenic and MQL flow lines and data acquisition system.

2.3. EXPERIMENTAL SET-UP AND PROCEDURE

The prepared workpiece was clamped on Cincinnati Milacron Sabre 750 Vertical Machining Centre (VMC), equipped with Acramatic 2100 CNC controller and 8 machining passes were made for each experimental condition shown in Table 1 using CNC program written for each experiment.

For each experiment, the cutting force components (F_x , F_y and F_z) and Fast Fourier Transforms of cutting force components (FFT_x , FFT_y and FFT_z) in the x, y and z directions were acquired and plotted after each pass. These plots were processed using 8-point moving average to remove noise and vibrations from the actual signal. For cutting force components, the value of maximum cutting force components in the x, y and z directions was determined from the processed signals. These maximum cutting forces components in the x, y and z directions were then plotted against machined length. The resultant cutting force was calculated from maximum cutting force components in the x, y and z directions using the formula:

$$F_r = \sqrt{(F_{x_{\max}}^2 + F_{y_{\max}}^2 + F_{z_{\max}}^2)} \quad (1)$$

Where: F_r is Resultant cutting force components, F_x is maximum cutting force component in x direction, F_y is maximum cutting force component in y direction and F_z is maximum cutting force component in z direction. For FFT cutting force components, the calculated tooth frequency of 4-flute end-mill at 1127 rpm spindle rotation was 75.13 Hz. Thus, the amplitude of FFT of cutting force in the x, y and z directions at 75.13 Hz tooth frequency was determined from the processed FFT signal after each pass and plotted against the machined length.

2.3.1. Approach Distance Calculation. Figure 5 shows the approach distance (L_1) during and down-milling operation. Tool starts cutting the workpiece during down-milling when the center of the tool is at a distance of L_1 (approach distance) from the workpiece edge perpendicular to feed direction as shown in Figure 4.

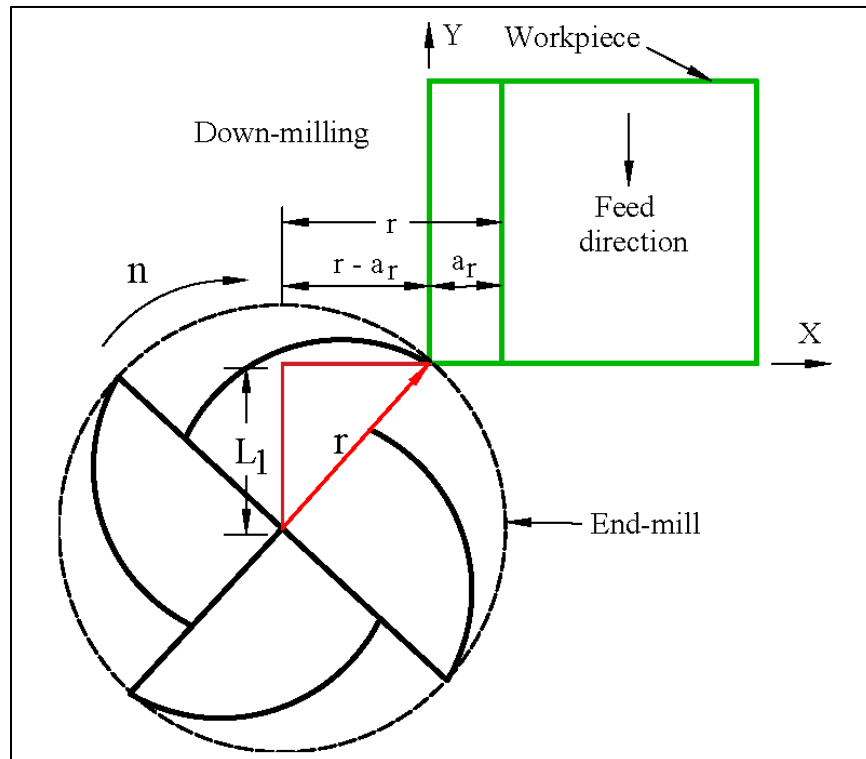


Figure 5: Approach distance during down-milling operation

The L_1 distance is given as follows:

$$L_1 = \sqrt{r^2 - (r - a_r)^2} \quad (2)$$

$$L_1 = \sqrt{6.35^2 - (6.35 - 3.81)^2} = 5.82 \text{ mm}$$

As the workpiece machined length (L) along the feed direction was 76.2 mm (3 inches), the total machined length for each machining pass becomes:

$$\text{ML (Machined Length of single pass)} = L + L_1 = 76.2 + 5.82 = 82.02 \text{ mm} \quad (3)$$

All the 8 passes resulted to a total length of cut of 656.16 mm (25.83 in). Each experiment consisted of eight (8) radial passes resulted to a total machined width of 30.48 mm (1.2 in). The corresponding machined lengths for 8 passes after adding additional approach length L_1 length to each pass, is 82.02 mm, 164.04 mm, 246.06 mm, 328.08 mm, 410.1 mm, 492.12 mm, 574.14 mm and 656.16 mm respectively.

3. RESULT ANALYSIS

3.1. SAMPLE PLOTS FOR MAXIMUM CUTTING FORCE COMPONENTS AND FAST FOURIER TRANSFORM (FFT) VERSUS MACHINED LENGTH (PASS NUMBER)

Figure 6 (a), (b) and (c) show the sample plots of acquired signal of cutting force components (F_x , F_y and F_z) in the x, y and z directions for the 3rd pass at a spindle speed of 1127 rpm (45 m/min cutting speed), feed-rate of 114.5 mm/min (4.510 ipm), axial and radial depths of cut of 5.08 mm (0.2 inches) and 3.81 mm (0.15 inches) respectively, using MQL down-milling strategy, with uncoated bull-nose tool. The value of maximum cutting force components in the x, y and z directions for each pass were determined from the processed signals. These maximum cutting force components were plotted against machined length (number of passes). The resultant cutting forces were also determined using maximum cutting force components and plotted against machined length. Figure 6 (d), (e) and (f) show the sample plot of FFT's of cutting force components (FFT_x , FFT_y and FFT_z) in the x, y and z directions for the 3rd pass at a spindle speed of 1127 rpm, feed-rate of 114.5 mm/min, axial and radial depth of cut of 5.08 mm and 3.81 mm respectively using MQL down-milling, with uncoated solid carbide tool.

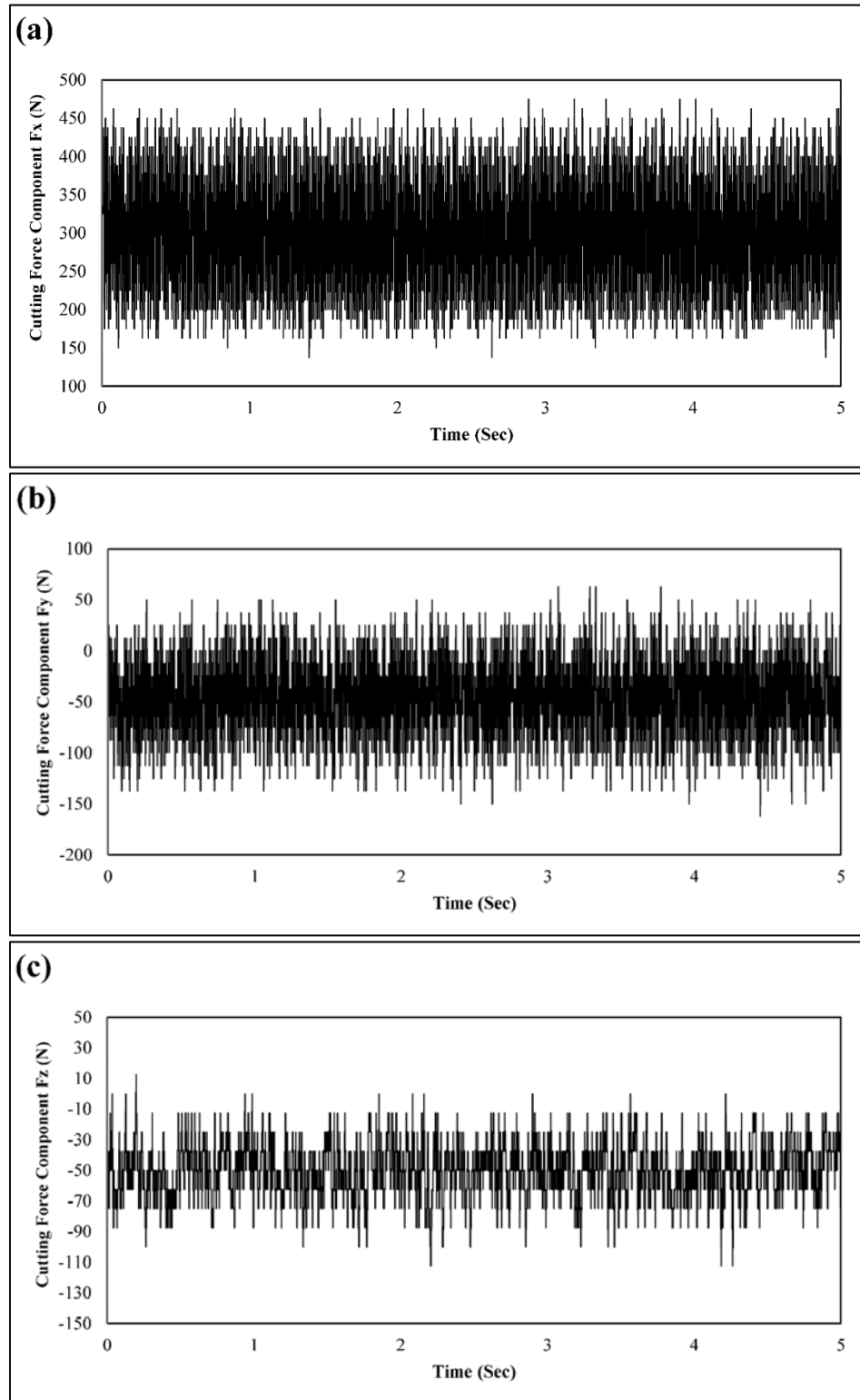


Figure 6: Cutting force and FFT signals for the 3rd pass (255.81 mm machined length) for MQL down-milling using uncoated solid carbide tool at spindle speed of 1127 rpm and feedrate of 114.5 mm/min. (a) F_x , (b) F_y , (c) F_z , (d) FFT_x , (e) FFT_y and (f) FFT_z

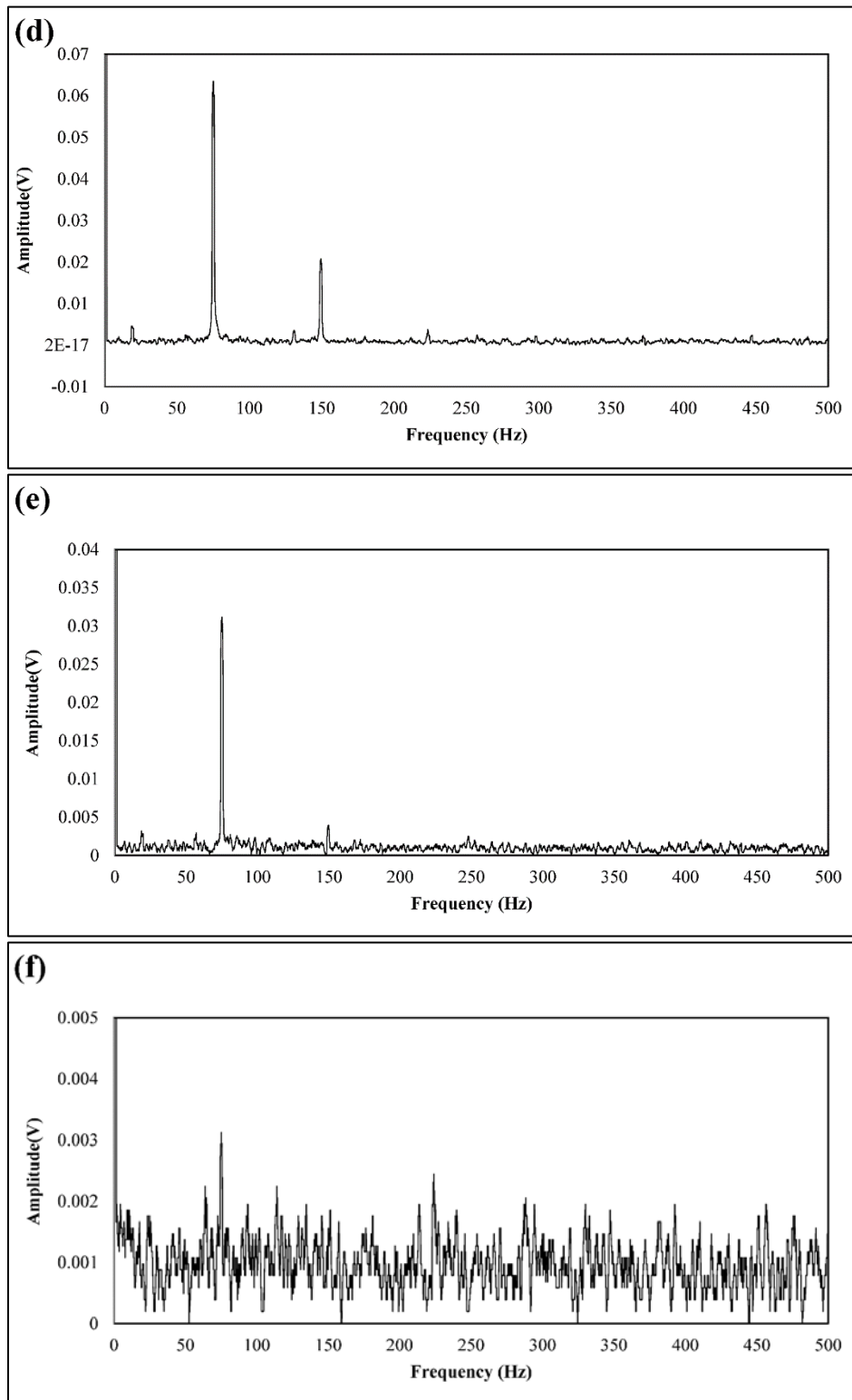


Figure 6: Cutting force and FFT signals for the 3rd pass (255.81 mm machined length) for MQL down-milling using uncoated solid carbide tool at spindle speed of 1127 rpm and feedrate of 114.5 mm/min. (a) F_x , (b) F_y , (c) F_z , (d) FFT_x , (e) FFT_y and (f) FFT_z (Contd.)

As can be seen from the Figures, the amplitude of FFT is highest at a tooth frequency of 75.13 Hz. This gives the amplitude of vibrations at the end-mill (cutter) tooth frequency. The values of the amplitude of FFT in the x, y and z directions at tooth frequency of 75.13 Hz were determined for each pass from the processed signals and plotted against machined length (number of passes). The number of flutes in GMS² coated end-mills was 7, thus the tooth frequency of the GMS² coated end-mills came out to be 131.5 Hz at which the amplitude of FFT of cutting forces were determined.

3.2. MAXIMUM CUTTING FORCE COMPONENTS, RESULTANT CUTTING FORCE, AND FAST FOURIER TRANSFORMS (FFT) USING UNCOATED CARBIDE END-MILLS

3.2.1. MQL Cooling Strategy. Figure 7 shows the plots of maximum cutting force components (F_x , F_y , F_z), resultant cutting force (F_r) and, amplitude of FFT of cutting force components F_x , F_y and F_z at 75.13 Hz tooth frequency under MQL cooling strategy using uncoated end-mill at a cutting speed of 45 m/min (1127 rpm) and a federate of 114.5 mm/min (4.510 ipm). The reason for high value of cutting force component F_x can be explained as follows: During down-milling operation, each cutting flute enters the workpiece at an angle with x-axis and starts scooping the metal. Figure 8 shows the 3-D chip profile during down-milling operation. As can be seen from figure 8, the chip thickness is highest when tool enters into the workpiece and decreases to zero the exit of tool from the workpiece. This provides the maximum impact to cutting flutes at the entry of the tool along x-direction. Due to this maximum impact, the cutting force component F_x is highest among all three components. Figure 7 (a) shows that there is a gradual increase in the cutting force components with progression of machining passes

(tool wear). Also, the resultant cutting force followed the same trend as dominant cutting force component F_x .

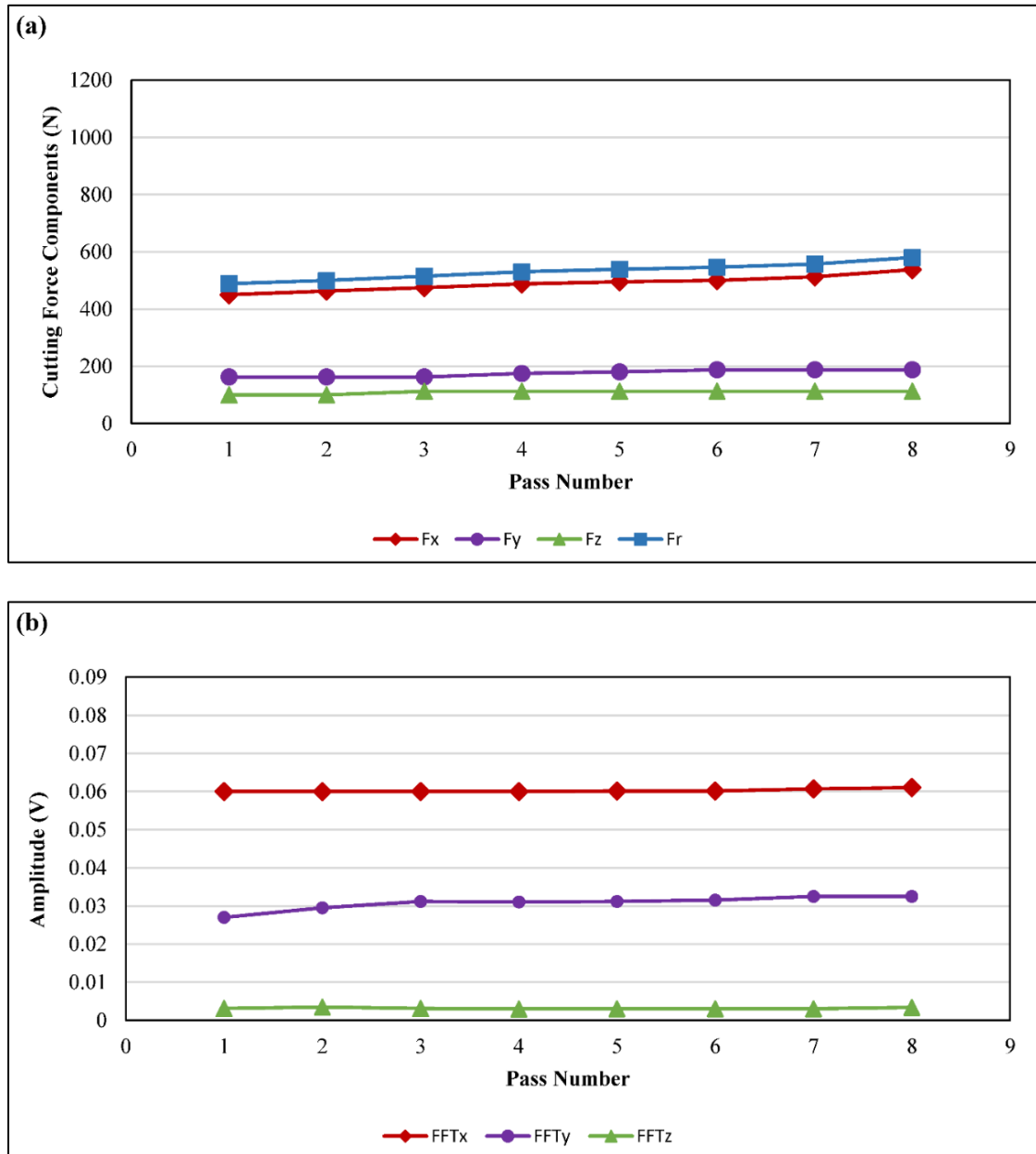


Figure 7: Maximum cutting force components, resultant cutting force and FFT amplitudes of cutting force components vs pass numbers (machined length) in x, y and z-directions under MQL cooling strategy using uncoated end-mill. (a) Maximum cutting force components and resultant cutting force, (b) FFT amplitudes

The plot shows that cutting force component F_x , perpendicular to feed direction, is the most dominant among all three cutting force components throughout the machining. From Figure 7 (b), it can be seen that the amplitude of FFT at tooth frequency is constant, which means that the vibrations did not increase much through the machining. Amplitude of FFT of cutting forces at tooth frequency followed the same trend as their respective cutting force components. MQL cooling provided least resultant cutting force using uncoated end-mill.

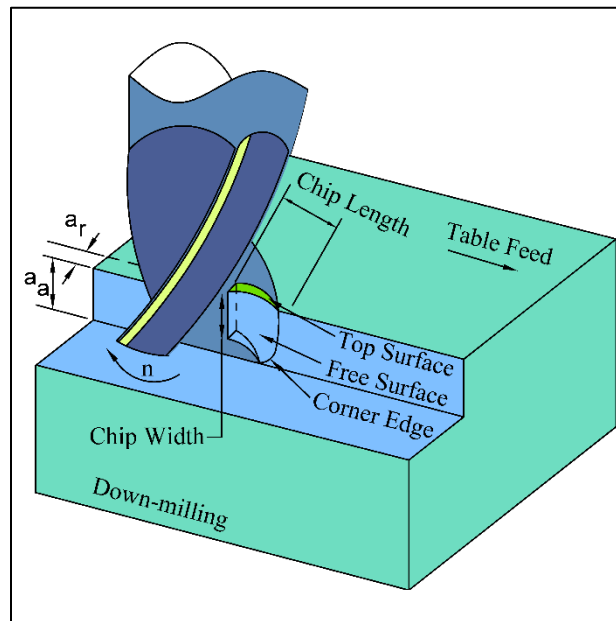


Figure 8: 3-D Material removal process (chip profile) during down-milling method

3.2.2. LN₂ Cooling Strategy. Figure 9 shows the plots of maximum cutting force components (F_x , F_y , F_z), resultant cutting force (F_r) and, amplitude of FFT of cutting force components F_x , F_y and F_z at 75.13 Hz tooth frequency under LN₂ cooling strategy using uncoated end-mill at a cutting speed of 45 m/min (1127 rpm) and a federate of 114.5 mm/min (4.510 ipm).

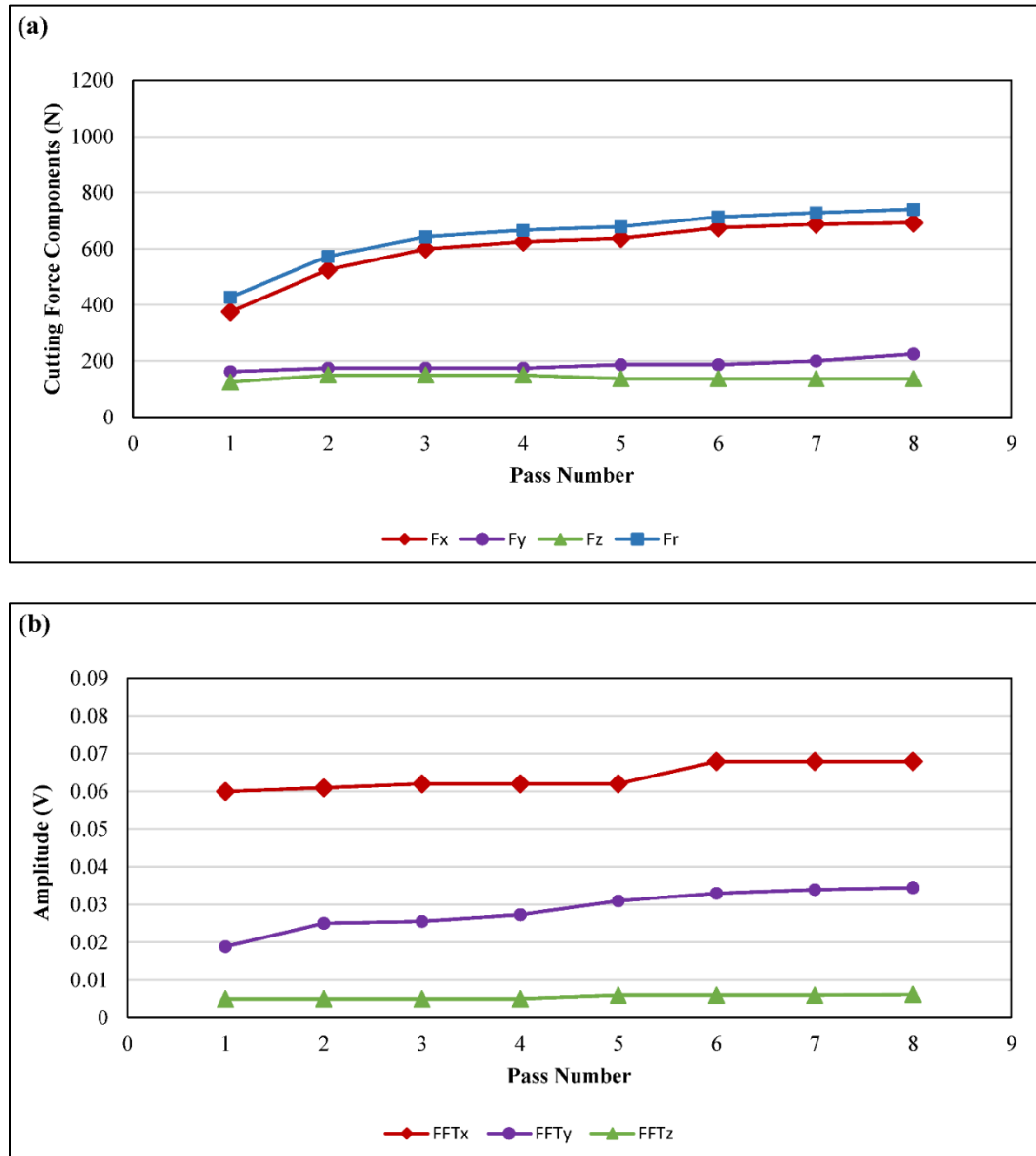


Figure 9: Maximum cutting force components, resultant cutting force and FFT amplitudes of cutting force components vs pass numbers (machined length) in x, y and z-directions under LN₂ cooling strategy using uncoated end-mill. (a) Maximum cutting force components and resultant cutting force, (b) FFT amplitudes

Although, the application of liquid nitrogen (LN₂) on the cutting zone decreases the cutting zone temperature, it also increases the hardness of workpiece and the tool as well, which may affect the machinability negatively [17]. LN₂ does even provide

sufficient lubrication which increases the coefficient of friction between tool and workpiece, which in turn increases the cutting forces drastically. Dominant cutting force component F_x , perpendicular to feed direction, increased rapidly than MQL cooling due to absence of sufficient lubrication and increase in the hardness of the workpiece and cutting tool. Vibrations during machining also increased due to increase in cutting forces under LN_2 cooling than MQL, which can be verified from the plot of amplitude of FFT of cutting forces.

3.2.3. Combined (MQL + LN_2) Cooling Strategy. Figure 10 shows the plots of maximum cutting force components (F_x , F_y , F_z), resultant cutting force (F_r) and, amplitude of FFT of cutting force components F_x , F_y and F_z at 75.13 Hz tooth frequency under combined (MQL + LN_2) cooling strategy using uncoated end-mill at a cutting speed of 45 m/min (1127 rpm) and a federate of 114.5 mm/min (4.510 ipm). Application of MQL provides the lubrication to cutting zone and using LN_2 cooling helps to lower down the temperature of the cutting zone. Both cooling strategies provided a favorable environment for machining Inconel-718, when applied to the cutting zone. Plot shows that the cutting force components did not increase drastically but gradually with increase in number of passes (machined length). The dominant cutting force component perpendicular to feed direction (F_x) was slightly higher than that of MQL. This is because the application of LN_2 might have increased the hardness of Inconel-718 which in turn increased cutting forces. FFT plot also shows that the vibrations in the x and y directions increased unexpectedly during 7th pass. This might have happened as all the chips were not removed completely by (MQL + LN_2) cooling strategy. These chip might

have interfered with the cutting tool and increased the tool wear and hence, cutting forces.

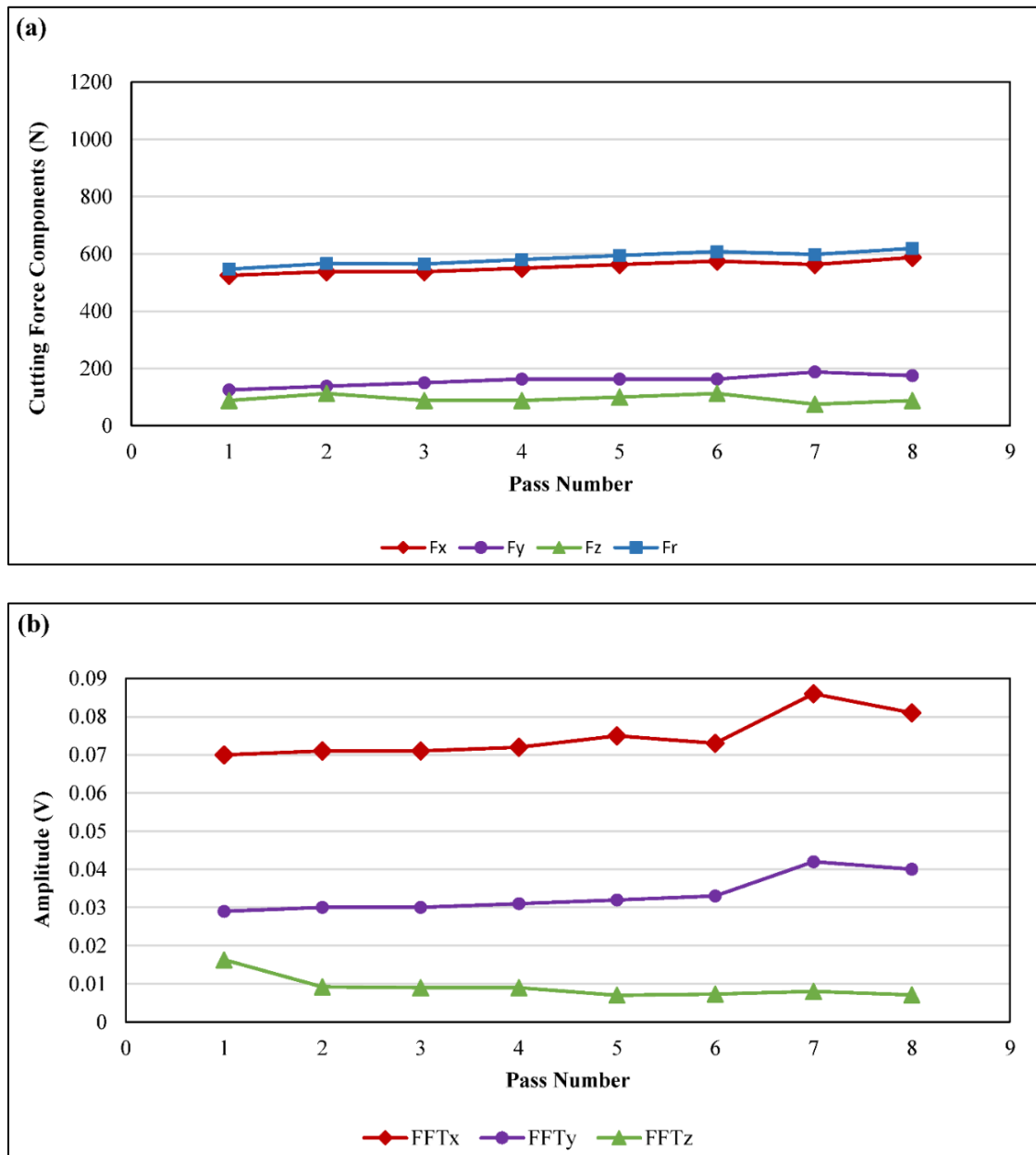


Figure 10: Maximum cutting force components, resultant cutting force and FFT amplitudes of cutting force components vs pass numbers (machined length) in x, y and z-directions under combined (MQL + LN₂) cooling strategy using uncoated end-mill. (a) Maximum cutting force components and resultant cutting force, (b) FFT amplitudes

3.3. MAXIMUM CUTTING FORCE COMPONENTS, RESULTANT CUTTING FORCE, AND FAST FOURIER TRANSFORMS (FFT) USING ALTiN COATED CARBIDE END-MILLS

3.3.1. MQL Cooling Strategy. Figure 11 shows the plots under MQL cooling strategy using ALTiN coated end-mill. MQL provides sufficient lubrication to the cutting zone and removes chips away from the cutting zone, which gives the most favorable environment while machining the Inconel-718. As can be seen from figure, a gradual increase has been seen in the cutting force component with number of passes (machined length). Resultant cutting force followed the same trend as dominant cutting force component F_x . FFT plots followed the same trend as their respective cutting force components and gradually increased with number of passes which shows fewer vibrations during machining.

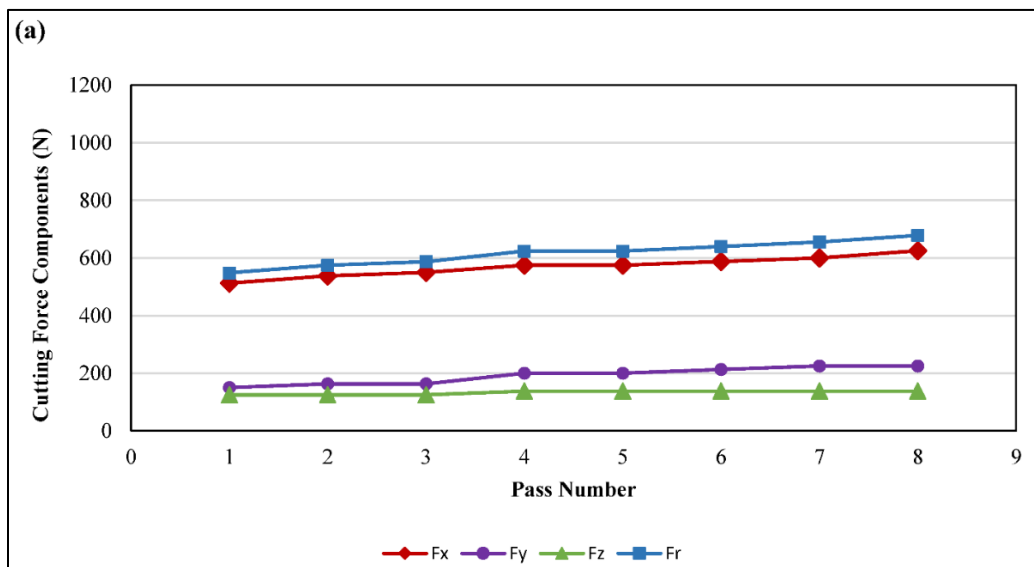


Figure 11: Maximum cutting force components, resultant cutting force and FFT amplitudes of cutting force components vs pass numbers (machined length) in x, y and z-directions under MQL cooling strategy using ALTiN coated end-mill. (a) Maximum cutting force components and resultant cutting force, (b) FFT amplitudes

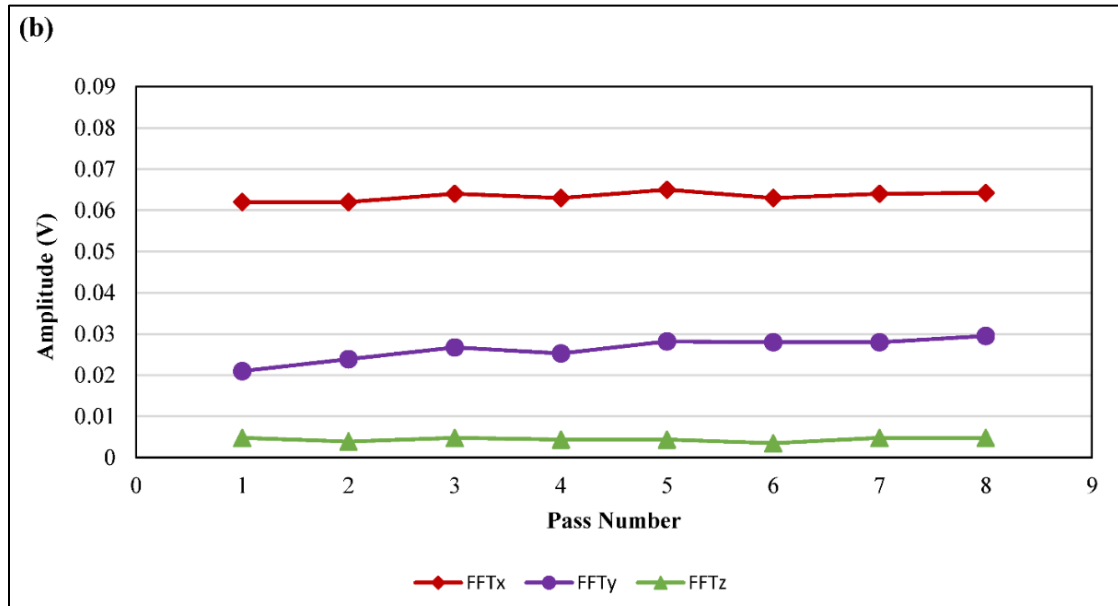


Figure 11: Maximum cutting force components, resultant cutting force and FFT amplitudes of cutting force components vs pass numbers (machined length) in x, y and z-directions under MQL cooling strategy using AlTiN coated end-mill. (a) Maximum cutting force components and resultant cutting force, (b) FFT amplitudes (Contd.)

MQL provides sufficient lubrication to the cutting zone and removes chips away from the cutting zone, which gives the most favorable environment while machining the Inconel-718. As can be seen from figure, a gradual increase has been seen in the cutting force component with number of passes (machined length). Resultant cutting force followed the same trend as dominant cutting force component F_x , perpendicular to the direction of feed. FFT plots followed the same trend as their respective cutting force components and gradually increased with number of passes which shows fewer vibrations during machining.

3.3.2. LN₂ Cooling Strategy. Figure 12 shows the plots under LN₂ cooling using AlTiN coated end-mills. Application of LN₂ lowered down the cutting zone temperature, but in the absence of lubrication, cutting forces increased rapidly.

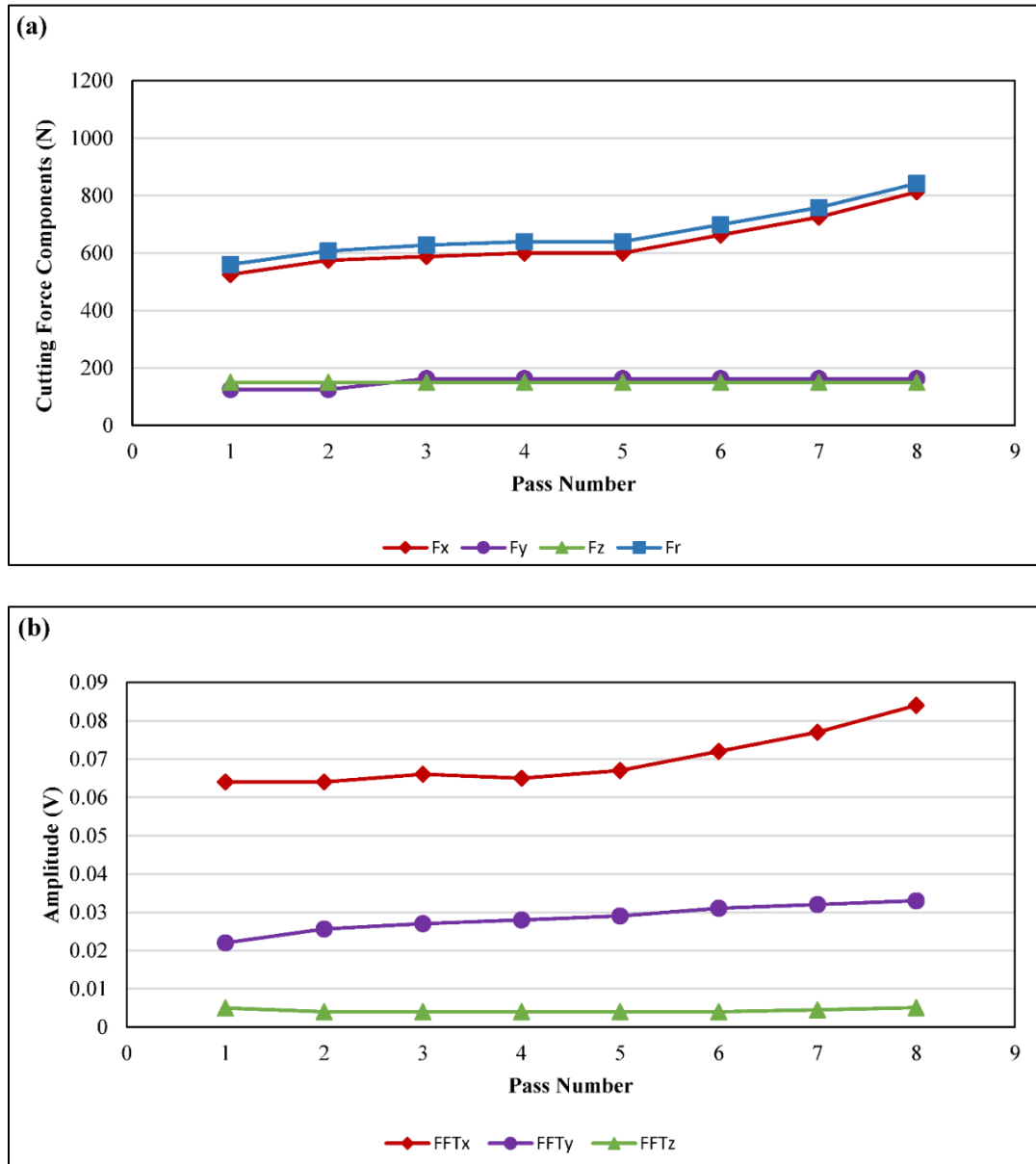


Figure 12: Maximum cutting force components, resultant cutting force and FFT amplitudes of cutting force components vs pass numbers (machined length) in x, y and z-directions under LN₂ cooling strategy using AlTiN coated end-mill. (a) Maximum cutting force components and resultant cutting force, (b) FFT amplitudes

Dominant cutting force component (F_x) increased slowly until 5th pass but after 5th pass, it increased rapidly due to increase in the tool wear. Also, application of liquid nitrogen increased the hardness of Inconel-718, which further exacerbated cutting forces.

Also, amplitude of FFT followed the same trend as cutting force components and showed increase in vibrations after 5th pass. Most of the vibrations occurred along the feed direction (FFT_y) or perpendicular to feed (FFT_x), whereas there were fewer vibrations along z direction and hence, the amplitude of FFT_z was least among all three in all combinations of cooling strategies and tool coatings.

3.3.3. Combined (MQL + LN₂) Cooling Strategy. Figure 13 shows the plots under combined (MQL + LN₂) cooling strategy using AlTiN coated end-mill. LN₂ when combined with MQL, an improvement in cutting force components and vibrations is seen as compared to LN₂ cooling alone. As LN₂ cools down the cutting zone temperature and MQL provides sufficient lubrication to the tool and workpiece, the machining generated very few vibrations as can be seen from Figure 13 (b). Also, cutting force component and vibrations along z direction remained almost constant throughout the machining.

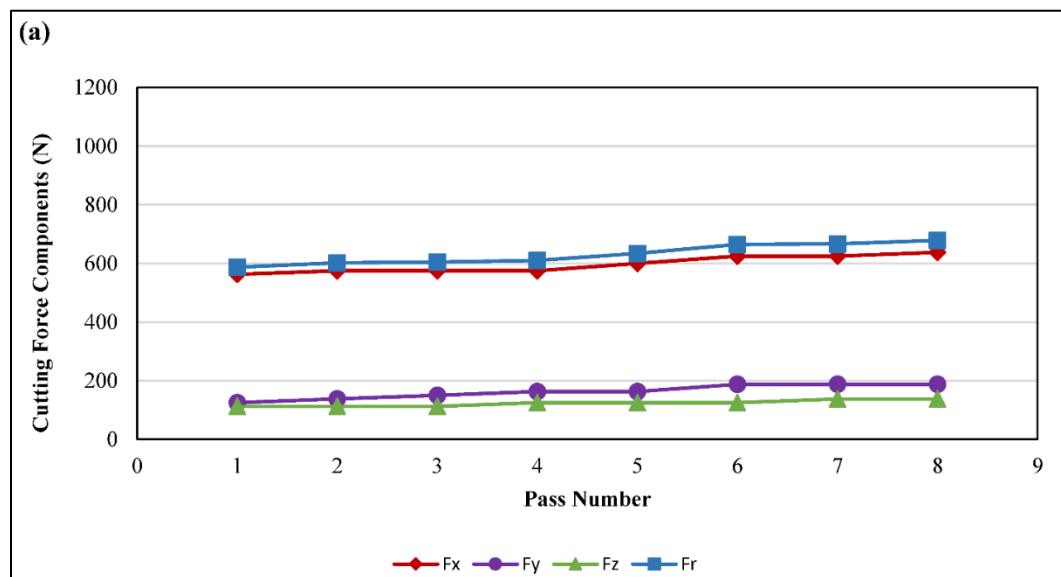


Figure 13: Maximum cutting force components, resultant cutting force and FFT amplitudes of cutting force components vs pass numbers (machined length) in x, y and z-directions under combined (MQL + LN₂) cooling strategy using AlTiN coated end-mill.
(a) Maximum cutting force components and resultant force, (b) FFT amplitudes

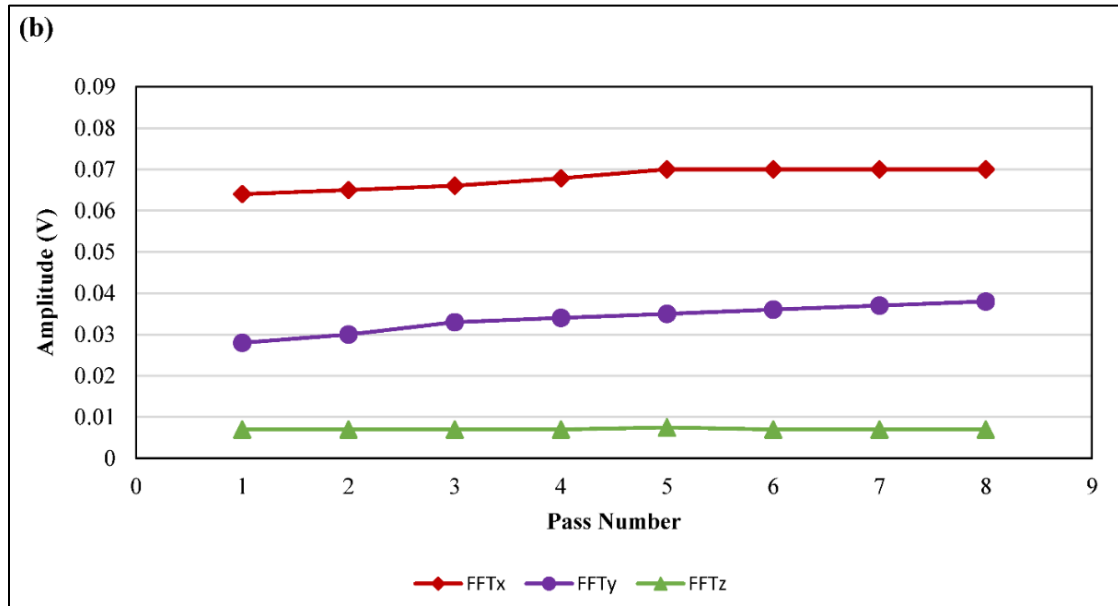


Figure 13: Maximum cutting force components, resultant cutting force and FFT amplitudes of cutting force components vs pass numbers (machined length) in x, y and z-directions under combined (MQL + LN₂) cooling strategy using AlTiN coated end-mill. (a) Maximum cutting force components and resultant force, (b) FFT amplitudes (Contd.)

3.4. MAXIMUM CUTTING FORCE COMPONENTS, RESULTANT CUTTING FORCE, AND FAST FOURIER TRANSFORMS (FFT) USING GMS² COATED CARBIDE END-MILLS

3.4.1. MQL Cooling Strategy. Figure 14 shows the plots under MQL cooling strategy using GMS² coated end-mill. Plot shows a gradual increase in cutting force components throughout the machining. GMS² coated end-mill had lower chip load due to more number of cutting flutes than uncoated and AlTiN coated tools even though the feed per revolution in all three kind of tools was same. In other words, the material scooped by each tooth of GMS² coated seven-flute tool was less than that of uncoated and AlTiN coated end-mills. Thus, the vibrations generated during machining using GMS² were less than uncoated and AlTiN coated end-mills. Even though, material scooped by each tooth

of GMS^2 coated end-mills was less than that of uncoated and AlTiN coated end-mills, cutting force components were higher.

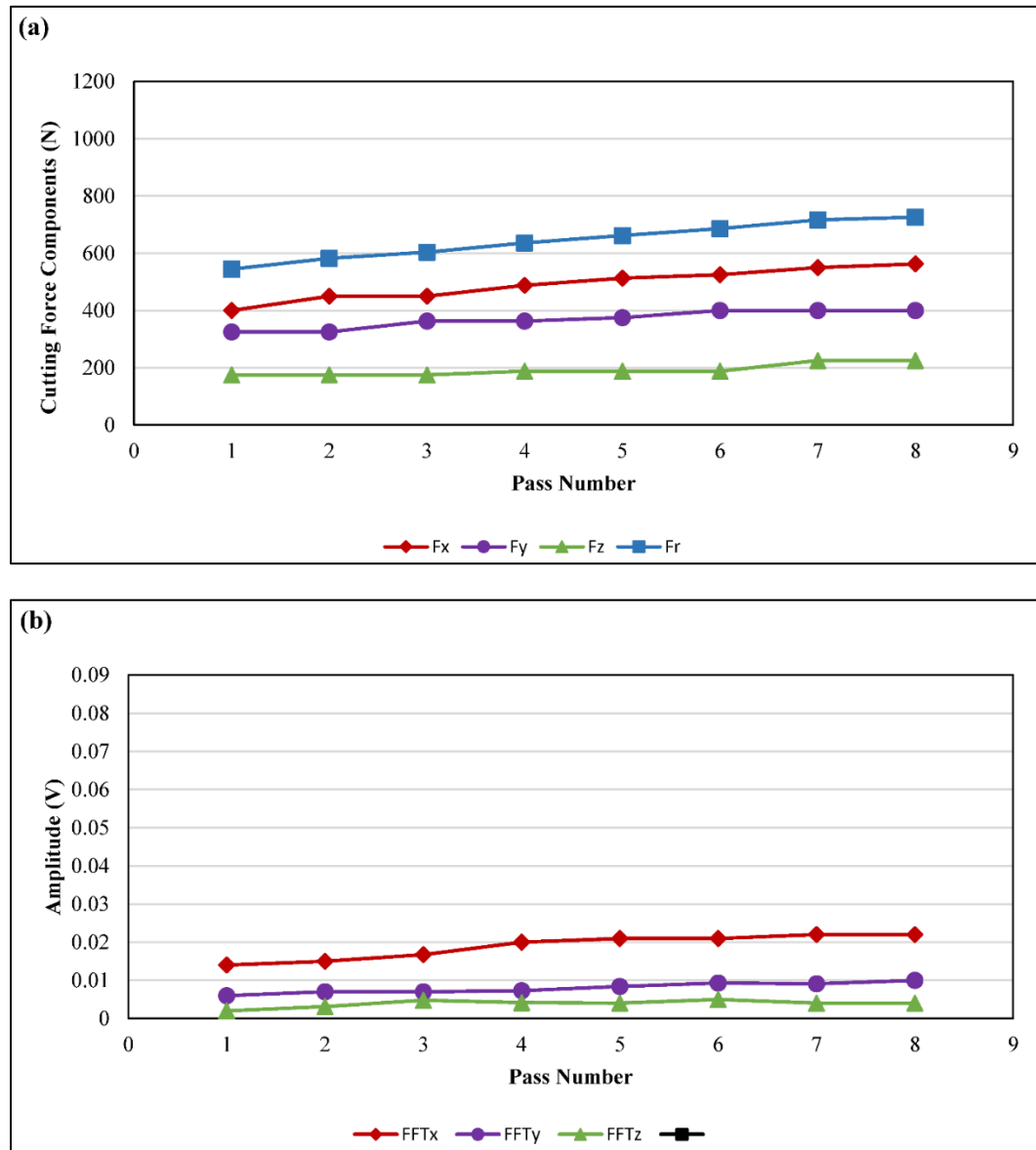


Figure 14: Maximum cutting force components, resultant cutting force and FFT amplitudes of cutting force components vs pass numbers (machined length) in x, y and z-directions under MQL cooling strategy using GMS^2 coated end-mill. (a) Maximum cutting force components and resultant cutting force, (b) FFT amplitudes

3.4.2. LN_2 Cooling Strategy. Figure 15 shows the cutting force components, the resultant cutting force and FFT plots under LN_2 cooling using GMS^2 coated end-mill.

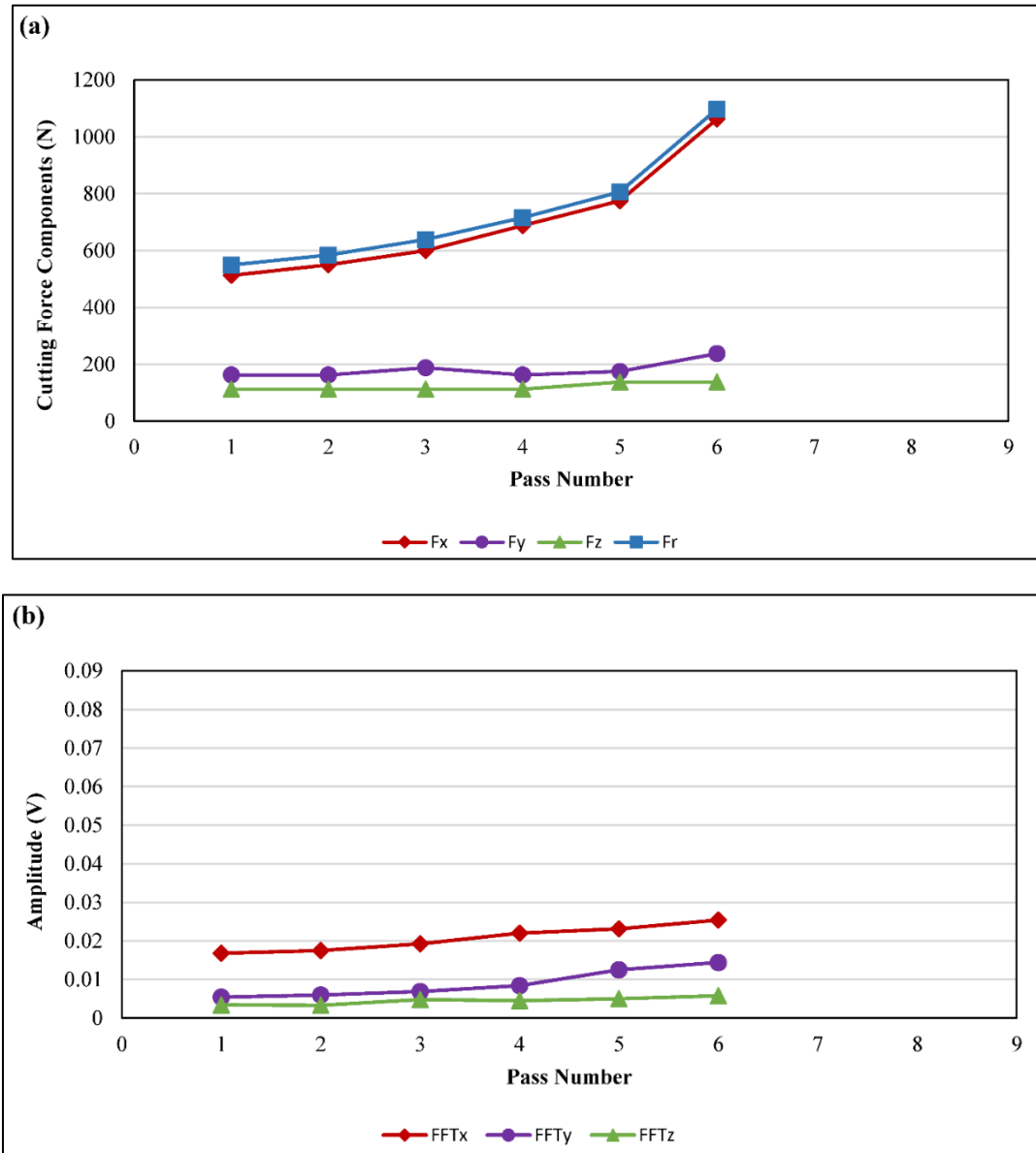


Figure 15: Maximum cutting force components, resultant cutting force and FFT amplitudes of cutting force components vs pass numbers (machined length) in x, y and z-directions under LN₂ cooling strategy using GMS² coated end-mill. (a) Maximum cutting force components and resultant cutting force, (b) FFT amplitudes

Application of LN₂ on GMS² coated end-mills caused the tool to generate highest cutting forces among all tool coatings and cooling strategies. Dominant cutting force component F_x was very high from beginning and increased rapidly until 7th pass. The

tool broke when the 7th pass before acquiring the force components and their FFTs.

Cutting force F_z did not increase much and contribute least towards resultant force.

3.4.3. Combined (MQL + LN₂) Cooling Strategy. Figure 16 shows the plots under combined (MQL + LN₂) cooling strategy using GMS² coated end-mill. Due to application of lubrication on the cutting zone along with cryogenic cooling, the tool was able to machine all 8 passes. A gradual increase in cutting force components F_x and F_y has been seen, whereas the magnitude of cutting force component F_z kept on fluctuating till 5th pass and remained almost flat after that. Although, combined (MQL + LN₂) cooling improved the machinability of Inconel-718 as compared to LN₂ machining alone, the forces were quite higher as compared to those in MQL cooling.

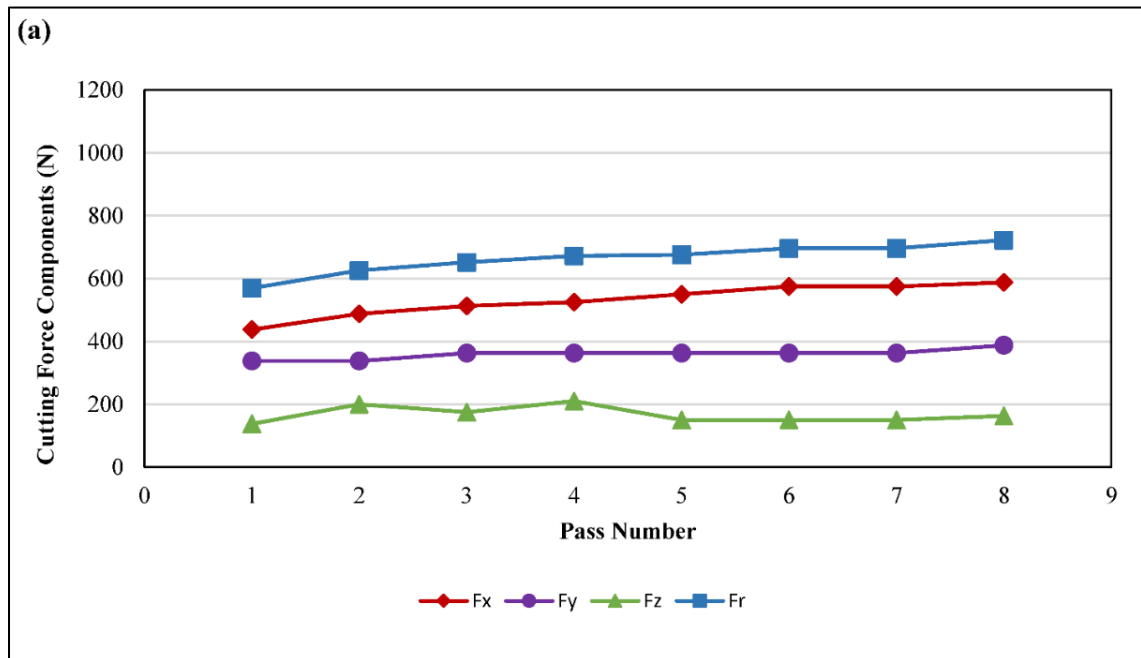


Figure 16: Maximum cutting force components, resultant cutting force and FFT amplitudes of cutting force components vs pass numbers (machined length) in x, y and z-directions under combined (MQL + LN₂) cooling strategy using GMS² coated end-mill. (a) Maximum cutting force components and resultant cutting force, (b) FFT amplitudes

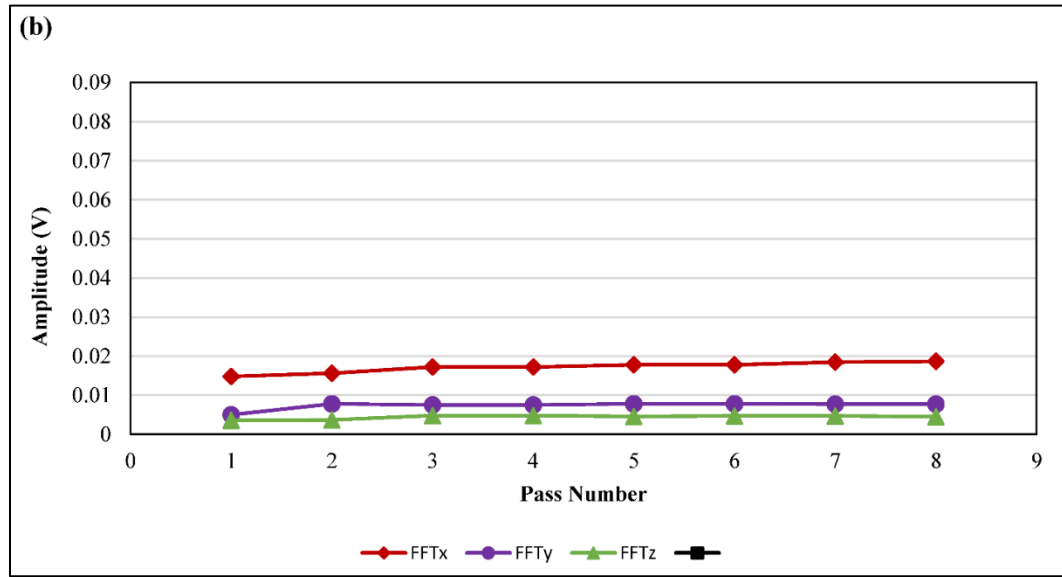


Figure 16: Maximum cutting force components, resultant cutting force and FFT amplitudes of cutting force components vs pass numbers (machined length) in x, y and z-directions under combined (MQL + LN₂) cooling strategy using GMS² coated end-mill. (a) Maximum cutting force components and resultant cutting force, (b) FFT amplitudes (Contd.)

3.5. COMPARATIVE INVESTIGATION OF RESULTANT CUTTING FORCES UNDER MQL, LN₂ AND COMBINED (MQL + LN₂) COOLING STRATEGIES, USING UNCOATED, ALTiN COATED AND GMS² COATED END-MILLS

Figure 17 shows the resultant cutting forces vs end-mill coatings and cooling strategies using uncoated, ALTiN coated and GMS² coated end-mills under MQL, LN₂ and combined (MQL + LN₂) cooling strategies. Plot shows that uncoated end-mills generated lower resultant cutting forces than ALTiN coated and GMS² coated end-mills under same cooling strategy, followed by ALTiN coated end-mills. GMS² coated end-mills generated the highest resultant cutting forces under all three cooling strategies. From literature, it has already been seen that the tool coatings are not always effective in terms of cutting forces [20]. Plot also shows that the MQL cooling strategy generated

lower resultant cutting forces using same end-mill coatings, followed by combined (MQL + LN₂) cooling strategy, whereas LN₂ cooling generated highest resultant cutting forces. Uncoated end-mill under MQL cooling strategy generated the least resultant cutting force. When GMS² coated end-mill used with LN₂ cooling strategy, the machining could only last until 6th pass before the tool broke and generated the highest resultant cutting force than other cooling strategies and end-mill coatings. It is evident that LN₂ cooling alone generates highest cutting forces and should be avoided while machining Inconel-718.

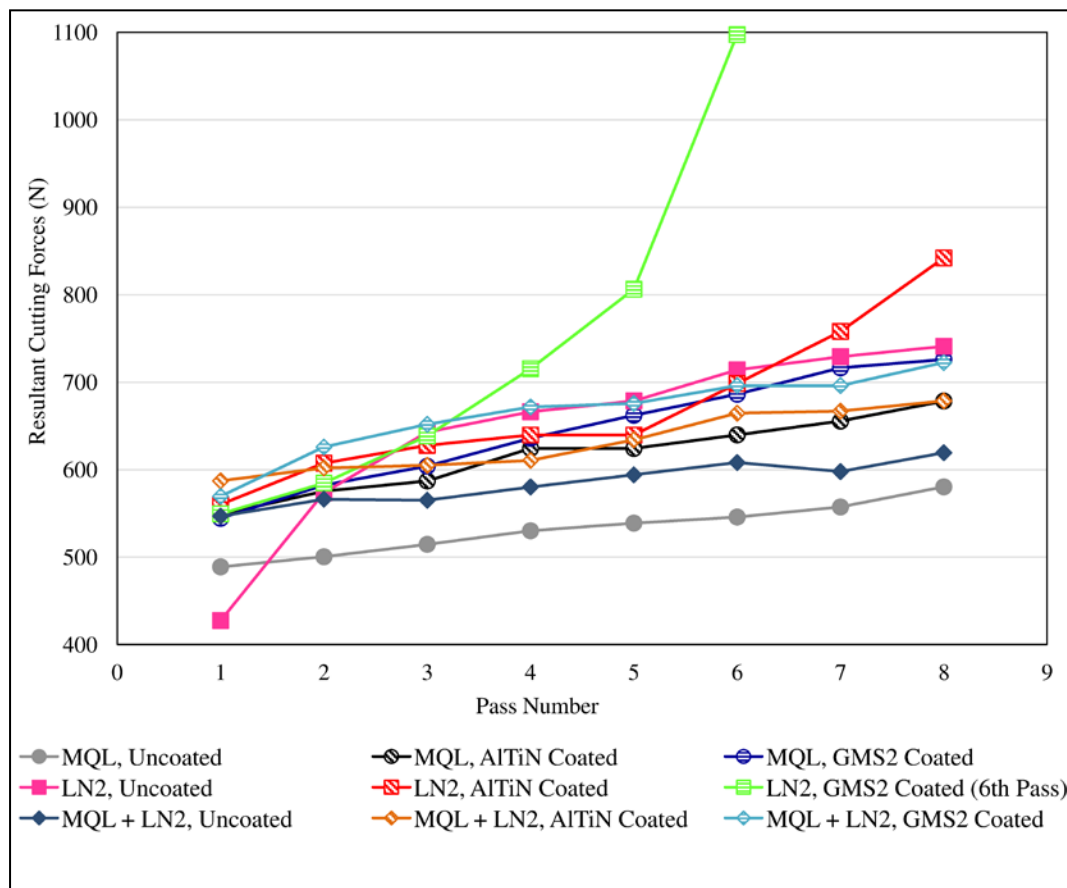


Figure 17: Resultant cutting forces vs pass numbers (machined length) under all cooling strategies and end-mill coatings

4. CONCLUSIONS

This research investigated the effects of three cooling strategies (MQL, LN₂ and MQL+LN₂) and three tool coatings (Uncoated, AlTiN coated and GMS² coated) on cutting force components (F_x , F_y , F_z) and their Fast Fourier Transforms (FFT's) and, the resultant cutting force during peripheral down-milling of Inconel-718 alloy using solid carbide bull-nose helical end-mills. From the results obtained, the following conclusions can be made:

1. Cutting force component F_x , perpendicular to the feed direction, is always dominant among all three cutting force components and increases with number of passes (machined length).
2. Resultant cutting force always follows similar trend and magnitude as the dominant cutting force component F_x , perpendicular to the feed direction.
3. Amplitudes of FFT of cutting forces in the x, y and z directions at tooth frequency almost follow similar trend as their respective cutting force components.
4. The amplitudes of FFT for all cutting force components versus machining length for MQL and combined (MQL + LN₂) cooling strategies are almost flat, which indicates the lower vibrations and smoother operation as compared LN₂ cooling strategy, where the amplitude of FFT increases rapidly which indicates higher vibrations and hence, cutting forces.
5. Due to increase in number of teeth, GMS² coated end-mills generates the least amplitude of FFT of cutting force components which indicates the lower vibrations, as GMS² coated end-mills scoop less material than uncoated and AlTiN coated end-mills.

6. Comparative evaluation of resultant cutting forces shows that uncoated end-mills generate lowest resultant cutting forces, followed by AlTiN coated end-mills, whereas GMS² coated end-mills generate highest resultant forces under all cooling strategies.
7. Comparative evaluation of resultant cutting forces shows that the MQL cooling strategy generates lowest resultant cutting forces, followed by combined (MQL + LN₂) cooling, whereas LN₂ cooling strategy generates highest resultant cutting forces with all end-mill coatings.
8. Using LN₂ cooling strategy alone is not recommended for machining Inconel-718 due to high cutting forces and vibrations.
9. Uncoated end-mills under MQL cooling strategy are recommended for machining Inconel-718 based on cutting forces.

ACKNOWLEDGEMENTS

The financial support from the Intelligent System Centre (ISC) of the Missouri University of Science and Technology is greatly acknowledged. The financial assistance provided in the form of Graduate Teaching Assistantship by the Department of Mechanical and Aerospace Engineering at Missouri University of Science and Technology is also greatly acknowledged.

REFERENCES

1. Ezugwu EO, Wang ZM (1997) Titanium alloys and their machinability—a review. *J Mater Process Technol* 68:262–274 . doi: 10.1016/S0924-0136(96)00030-1
2. Zhao W, He N, Li L (2007) High Speed Milling of Ti6Al4V Alloy with Minimal Quantity Lubrication. *Key Eng Mater* 375–376:435–439 . doi: 10.4028/www.scientific.net/KEM.329.663

3. Dhar NR, Ahmed MT, Islam S (2007) An experimental investigation on effect of minimum quantity lubrication in machining AISI 1040 steel. *Int J Mach Tools Manuf* 47:748–753 . doi: 10.1016/j.ijmachtools.2006.09.017
4. Ahmad Yasir MS, Che Hassan CH, Jaharah AG, et al (2009) Machinability of Ti-6Al-4V Under Dry and Near Dry Condition Using Carbide Tools. *Open Ind Manuf Eng J* 2:1–9 . doi: 10.2174/1874152500902010001
5. Kamata Y, Obikawa T (2007) High speed MQL finish-turning of Inconel 718 with different coated tools. *J Mater Process Technol* 192–193:281–286 . doi: 10.1016/j.jmatprotec.2007.04.052
6. Boubekri N, Shaikh V (2012) Machining Using Minimum Quantity Lubrication: A Technology for Sustainability. *Int J Appl Sci Technol* 2:111–115
7. Kaynak Y (2014) Evaluation of machining performance in cryogenic machining of Inconel 718 and comparison with dry and MQL machining. *Int J Adv Manuf Technol* 72:919–933 . doi: 10.1007/s00170-014-5683-0
8. Aramcharoen A, Chuan SK (2014) An experimental investigation on cryogenic milling of inconel 718 and its sustainability assessment. In: *Procedia CIRP*. pp 529–534
9. Dhananchezian M, Pradeep Kumar M (2011) Cryogenic turning of the Ti-6Al-4V alloy with modified cutting tool inserts. *Cryogenics (Guildf)* 51:34–40 . doi: 10.1016/j.cryogenics.2010.10.011
10. Kim SW, Lee DW, Kang MC, Kim JS (2001) Evaluation of machinability by cutting environments in high-speed milling of difficult-to-cut materials. *J Mater Process Technol* 111:256–260 . doi: 10.1016/S0924-0136(01)00529-5
11. Ravi S, Pradeep Kumar M (2011) Experimental investigations on cryogenic cooling by liquid nitrogen in the end milling of hardened steel. *Cryogenics (Guildf)* 51:509–515 . doi: 10.1016/j.cryogenics.2011.06.006
12. Hong SY, Markus I, Jeong W cheol (2001) New cooling approach and tool life improvement in cryogenic machining of titanium alloy Ti-6Al-4V. *Int J Mach Tools Manuf* 41:2245–2260 . doi: 10.1016/S0890-6955(01)00041-4
13. Su Y, He N, Li L (2010) Effect of Cryogenic Minimum Quantity Lubrication (CMQL) on Cutting Temperature and Tool Wear in High-Speed End Milling of Titanium Alloys. *Appl Mech Mater* 34–35:1816–1821 . doi: 10.4028/www.scientific.net/AMM.34-35.1816
14. Su Y, He N, Li L, Li XL (2006) An experimental investigation of effects of cooling/lubrication conditions on tool wear in high-speed end milling of Ti-6Al-4V. *Wear* 261:760–766 . doi: 10.1016/j.wear.2006.01.013

15. Zhang S, Li JF, Wang YW (2012) Tool life and cutting forces in end milling Inconel 718 under dry and minimum quantity cooling lubrication cutting conditions. *J Clean Prod* 32:81–87 . doi: 10.1016/j.jclepro.2012.03.014
16. Yuan SM, Yan LT, Liu WD, Liu Q (2011) Effects of cooling air temperature on cryogenic machining of Ti-6Al-4V alloy. *J Mater Process Technol* 211:356–362 . doi: 10.1016/j.jmatprotec.2010.10.009
17. Park K-H, Suhaimi MA, Yang G-D, et al (2017) Milling of titanium alloy with cryogenic cooling and minimum quantity lubrication (MQL). *Int J Precis Eng Manuf* 18:5–14 . doi: 10.1007/s12541-017-0001-z
18. Wang CY, Xie YX, Qin Z, et al (2015) Wear and breakage of TiAlN- and TiSiN-coated carbide tools during high-speed milling of hardened steel. *Wear* 336–337:29–42 . doi: <http://dx.doi.org/10.1016/j.wear.2015.04.018>
19. Jawaid A, Sharif S, Koksai S (2000) Evaluation of wear mechanisms of coated carbide tools when face milling titanium alloy. *J Mater Process Technol* 99:266–274 . doi: [http://dx.doi.org/10.1016/S0924-0136\(99\)00438-0](http://dx.doi.org/10.1016/S0924-0136(99)00438-0)
20. Jawaid A, Koksai S, Sharif S (2001) Cutting performance and wear characteristics of {PVD} coated and uncoated carbide tools in face milling Inconel 718 aerospace alloy. *J Mater Process Technol* 116:2–9 . doi: [http://dx.doi.org/10.1016/S0924-0136\(01\)00850-0](http://dx.doi.org/10.1016/S0924-0136(01)00850-0)
21. Özel T, Sima M, Srivastava AK, Kaftanoglu B (2010) Investigations on the effects of multi-layered coated inserts in machining Ti-6Al-4V alloy with experiments and finite element simulations. *CIRP Ann - Manuf Technol* 59:77–82 . doi: 10.1016/j.cirp.2010.03.055
22. Kamata Y, Obikawa T (2007) High speed MQL finish-turning of Inconel 718 with different coated tools. *Journal of Materials Processing Technology* 192–193:281–286 . doi: 10.1016/j.jmatprotec.2007.04.052
23. Fang N, Wu Q (2009) A comparative study of the cutting forces in high speed machining of Ti-6Al-4V and Inconel 718 with a round cutting edge tool. *J Mater Process Technol* 209:4385–4389 . doi: 10.1016/j.jmatprotec.2008.10.013
24. Safari H, Sharif S, Izman S, et al (2014) Cutting Force and Surface Roughness Characterization in Cryogenic High-Speed End Milling of Ti-6Al-4V ELI. *Mater Manuf Process* 29:350–356 . doi: 10.1080/10426914.2013.872257
25. Fallböhmer P, Rodríguez CA, Özel T, Altan T (2000) High-speed machining of cast iron and alloy steels for die and mold manufacturing. *J Mater Process Technol* 98:104–115 . doi: 10.1016/S0924-0136(99)00311-8

26. Abele E, Fröhlich B (2008) High Speed Milling of Titanium Alloys. *J Adv Prod Eng Manag* 3 131–140
27. Liao YS, Lin HM, Wang JH (2008) Behaviors of end milling Inconel 718 superalloy by cemented carbide tools. *J Mater Process Technol* 201:460–465 . doi: <http://dx.doi.org/10.1016/j.jmatprotec.2007.11.176>

III.EFFECTS OF UP AND DOWN-MILLING, AND COOLING STRATEGIES ON TOOL WEAR, CHIP MORPHOLOGY AND SURFACE ROUGHNESS IN HIGH SPEED END-MILLING OF INCONEL-718

A. Chukwujekwu Okafor*, Paras Mohan Jasra
Computer Numeric Control and Virtual Manufacturing Laboratory
Department of Mechanical and Aerospace Engineering
Missouri University of Science and Technology
327 Toomey Hall, Rolla, MO-65409-0050, USA
Email: okafor@mst.edu

ABSTRACT

This paper presents the results of experimental investigation of the effects of milling methods (up-milling and down-milling) and cooling strategies [Emulsion cooling, Minimum Quantity Lubrication (MQL), Cryogenic cooling using Liquid Nitrogen (LN₂) and Combined (MQL+LN₂)] on flank wear, chip morphology and surface roughness in peripheral high speed end-milling of Inconel-718. The experimental results show that down-milling generated lower maximum flank wear than up-milling for all cooling strategies, thus improves machinability. MQL cooling with down-milling generated lowest maximum flank wear and is recommended for machining Inconel-718, whereas LN₂ with up-milling generated highest flank wear. Tool wear mechanism in up-milling is adhesion and failure modes are chipping and plastic deformation, causing rapid tool wear, while abrasion is the tool wear mechanism under down-milling causing progressive tool wear. Also, emulsion up-milling operation generated lowest surface roughness whereas, emulsion, MQL and combined (MQL + LN₂) strategies with down-milling generated

equal and second lowest surface roughness. Results show that using MQL cooling with down-milling operation for machining Inconel-718 can lead to significant cost saving and sustainable machining.

Keywords: High Speed Up-milling and Down-milling; Inconel 718; Flank wear; Chip morphology; Minimum Quantity Lubrication; Cryogenic machining.

1. INTRODUCTION

Inconel 718 superalloy is used extensively in aerospace and nuclear industries for components such as turbine blades, low and high-pressure disc compressors used in high temperature, high load and corrosion resistance compartments of jet and gas turbine engines, due to its excellent properties such as: high strength-to-weight ratio, ability to retain its properties at high temperatures, high corrosion and creep resistance Inconel 718 superalloy, made up mainly of nickel, chromium and molybdenum, is suitable for use in aggressive environments due to its excellent properties like high strength to weight ratio which is maintained at elevated temperatures also, corrosion and fracture resistance (Ezugwu & Wang, 1997). That is why they are used extensively in turbines, nuclear reactors, space craft, automotive and aerospace industries. However, Inconel 718 is characterized as a very “difficult-to-cut” material, because it poses severe problems during machining. E like enormous amount of heat is generated in the cutting zone due to high friction between the tool-chip interface and tool-workpiece interface and is not removed as quickly as it is generated due to its low thermal conductivity and mostly concentrated on the tool cutting edges, causing severe tool wear. Therefore the heat is mostly concentrated on the tool cutting edges, causing severe tool wear. Also, due to high temperature and pressure at the cutting zone, some particles from the workpiece get

welded on the cutting edges of the tool, which further exacerbates tool wear. Its good mechanical strength and ability to work harden at elevated temperatures and pressures leads to high cutting forces and its high chemical affinity with many cutting tool materials leads to welding of the tool to form built-up edge (BUE). End-milling is a widely used machining operation due to its versatility. Its applications may range from aerospace and automotive industries to small tool and die shops, as it can be used for milling many features like peripheral, slot or face milling. Some problems encountered while machining using end-milling operations are high cutting forces, high cutting temperature, rapid tool wear, tool breakage, and chatter. These problems associated with end-milling are further exacerbated while machining difficult-to-cut metals such as Inconel 718 because the desired properties of this difficult-to-cut metal become disadvantage while machining them.

Due to the problems mentioned above, care must be taken to select appropriate machining parameters when machining difficult-to-cut metals. Tool wear is an important factor affecting machinability of Inconel 718, as it cannot be avoided during machining, improvement in tool wear helps to reduce the cutting zone temperature, cutting forces and improving surface roughness. Su et al. (2010) compared the performance of Cryogenic Minimum Quantity Lubrication (CMQL) at two different temperatures with dry machining and refrigerated air cutting at two different temperatures in high speed end-milling of titanium alloys. They reported improvement in temperature and tool wear using CMQL at -20°C . Su et al., (2006) also investigated the effects of cooling/lubrications on tool life in high speed end-milling of Ti-6Al-4V. They concluded that compressed cold nitrogen gas and oil mist (CCNGOM) at -10°C yielded the best tool

life among all cooling strategies. They also discussed various failure modes and wear mechanisms under different cooling conditions. Özel et al. (2010) investigated the effects of uncoated, cBN, TiAlN, and TiAlN+cBN coated single and multi-layer coated tungsten carbide inserts in turning Ti-6Al-4V on cutting forces and tool wear and concluded that the cBN coated tungsten carbide inserts generated least tool wear. Zhang et al. (2012) investigated the effects of dry and Minimum Quantity Cooling Lubrication (MQCL) on cutting forces and tool wear in end-milling of Inconel 718. They reported that MQCL achieved lower cutting forces and tool wear compared to dry machining. Kim et al. (2001) investigated the effect dry and compressed chilly-air coolant on flank wear in high-speed milling of different difficult-to-cut metals having hardness varying from HRc28 to HRc60 using different coated tools. They reported improvement in flank wear using compressed chilly-air coolants compared to dry and flood coolants. Musfirah et al. (2017) reported that the application of cryogenic cooling reduced the tool wear and surface roughness as compared to dry machining in high speed machining of Inconel 718 coated tungsten carbide inserts. Along with tool wear, surface roughness is another factor used to analyze the performance of difficult-to-cut metals. Zhao et al. (2007) reported some improvement in cutting forces, surface roughness and tool life when using MQL over dry machining in high speed milling of Ti-6Al-4V using uncoated cemented carbide inserts. Dhananchezian and Kumar (2011) reported improvement in tool wear, surface roughness, temperature and cutting forces using cryogenic cooling as compared to wet cooling in turning of Ti-6Al-4V using modified coated carbide inserts. Shokrani et al. (2016) conducted several experiments to investigate the effects of dry, flood and cryogenic cooling on surface integrity in the end-milling of Ti-6Al-4V titanium alloy

using coated carbide tools. They reported improvement in surface roughness and surface roughness defects using cryogenic cooling over dry and flood cooling. Ravi and Kumar (2011) reported improvement in tool wear with cryogenic cooling by 29-34 % and 10-12% than dry and wet cooling respectively in end-milling of hardened steel using PVD coated carbide inserts. The surface roughness with cryogenic cooling was improved by 33-40% and 25-29% over dry and wet cooling respectively. Ahmad Yasir et al. (2009) investigated the effects of dry and MQL cooling with different MQL flow rates on flank wear and surface roughness during machining of Ti-6Al-4V using PVD coated cemented carbide tools at three cutting speeds. They reported that MQL was more effective when applied on worn out tools. Also, they reported that the effect of feed-rate on surface roughness is more significant than other parameters. Shokrani et al. (2017) reported that a novel hybrid cryogenic and MQL (CryoMQL) cooling increased the tool life in milling of age hardened Inconel 718 due to reduction in tool wear growth rate. Also, they reported that the average surface roughness of the bottom surface of milled workpiece reduced by 18% by the application of hybrid cryogenic and MQL (cryoMQL) cooling as compared to MQL. Wang et al. (2017) investigated the effects of cutting speed and feed-rate on surface roughness and fatigue life in face milling of Inconel 718. They concluded that surface roughness increased with increase in feed-rate, whereas surface roughness was barely affected by cutting speed within chosen parameters.

It has been seen that using different combinations of machining parameters, cooling strategies and milling methods produce different chip morphologies. Thus, it becomes pertinent to analyze chip morphology while investigating tool wear, to understand the effects of specific cutting conditions on machinability of Inconel 718.

These chips if not removed quickly, can increase the cutting zone temperature drastically and also interrupt the machining process, which may increase tool wear and hence, lead to tool failure and breakage. Liao et al. (2008) reported that cutting temperature and chip disposal are two main problems encountered in high-speed end-milling of Inconel 718. Dhar et al. (2007) reported improvement in tool-chip interface temperature, chip reduction coefficient, average principle and auxiliary flank wear and surface roughness using MQL over dry machining in turning AISI-1040 steel. Su et al. (2007) reported improvement in tool wear, surface finish and chip shape using cooling air and CAMQL in finish turning of Inconel 718. Yuan et al. (2011) reported that MQL with cooling air - 15°C yielded the most favorable environment for machining Ti-6Al-4V alloy in terms of cutting force, tool wear, surface roughness and chip morphology. They further reported that MQL with cooling air produced the shorter chips, which helped the lubricant to effectively penetrate into tool-chip interface. Aramcharoen and Chuan (2014) reported that cryogenic cooling helped chip breakability in milling of Inconel 718. Cryogenic cooling was very effective in tool wear reduction, improving the machined surface quality and also reduced the contact friction between tool-chip interface which further improved the efficiency of lubricating action. Obikawa et al. (2008) reported that by spraying small amount of lubrication, called micro-liter lubrication, on cutting zone using specially designed nozzle increased the tool life as compared to ordinary MQL spraying in machining of Inconel 718. Cui et al. (2016) reported that the degree of chip serration increased and tool-chip contact length decreased with increase in cutting speed in high and ultra-high speed milling of AISI H13 hardened steel. They reported that the main tool wear pattern was flank wear. Zhu et al. (2016) investigated the mechanism under

which the degree of segmentation of chip becomes more and more with progression of tool wear in the end-milling of Ti-6Al-4V.

Hadi et al. (2013) reported improvement in tool wear using down-milling operation than up-milling in ball nose end-milling of Inconel 718 using MQL. They reported that the tool wear increased with increase in depth of cut, feed-rate and cutting speed. The pitting and notch wear on the edge of the tool were predominant failure modes. Segmented chips with typically saw-tooth shape were produced using up-milling, whereas discontinuous serrated chips were produced using down-milling operation. Sun and Guo (2008) presented a new multi-view approach to characterize the chip morphology including top, free, back and cross section surfaces of the chips in end-milling of Ti-6Al-4V using flood coolant. Patwari et al. (2010) identified primary and secondary saw/serrated teeth appeared at the free edge of the chip as the instabilities of periodic nature using a mathematical model in machining of medium carbon steel (S45C). They also studied the mechanism of the formation of teeth and their frequency of formation and, verified using ANOVA. Milling method also plays a vital role in improving tool wear and overall machinability. Bouzakis et al. (2008) reported that the kinematics of milling process has significant effect in cutting performance and distribution of stress. Li et al. (2006) reported that the flank wear, the predominant failure mode, propagated more in up-milling than down-milling in end-milling of Inconel 718 with coated carbide inserts under dry cutting. Also, the mean peak cutting force propagation increased with the propagation of tool wear. Tian et al. (2013) reported improvement in tool wear using down-milling over up-milling in high speed milling of

Inconel 718 using cemented coated carbide inserts. They also obtained and showed the correlations of the chips from FEM model with the actually produced chips.

Krain et al. (2007) reported the highest tool life at a chip thickness of 0.07 mm and 12.5% radial immersion in the end-milling of Inconel 718. Also, the tool life decreased with increased in chip thickness and radial immersion. The tool wear mechanisms were adhesion and attrition and modes of tool failure were average flank wear, notching and localized wear. High speed machining has the advantage to increase material removal rate, lower cutting forces and improve surface roughness, and has been successfully applied in machining aluminum alloys of aircraft parts and die steels in die and mold industry. Figure 1 shows the commonly accepted high-speed cutting ranges in machining of various materials (Fallböhmer et al., 2000). The figure shows that high cutting speed range depends on the strength and machinability of the material. The higher the strength and the more difficult-to cut of the material, the lower the high cutting speed range. Thus, high cutting speed range for Aluminium is higher than high cutting speed range for Nickel alloys. From above literature, it is clear that there has been no comprehensive study to investigate the combined effects of milling methods (up-milling and down-milling) with different cooling strategies (Emulsion, MQL, LN2 and combined MQL + LN2) on tool wear, surface roughness and chip morphology in high-speed cutting range for Inconel 718 alloy. The potential of combining two different cooling strategies using carbide end-mills at machining speed higher than current industry standards (Ulutan, Pleta, Henderson, & Mears, 2015) for milling nickel-based superalloy using uncoated carbide end-mills has not been investigated. as reported by Iturbe et al. (2016) that the benefits of cryogenic + MQL machining over conventional machining are not

evident over long machining time and at industrial cutting conditions and the cryogenic + MQL has shorter tool life than the tool life requirements established by industry. Only a few studies have been performed in combining different cooling strategies using one of the milling methods on some of the difficult-to-cut metals at claimed high cutting speeds but at very low material removal rate and total material removed, which are too low to be implemented in actual industry for machining nickel alloys like Inconel 718, which is a highly difficult-to-cut metal.

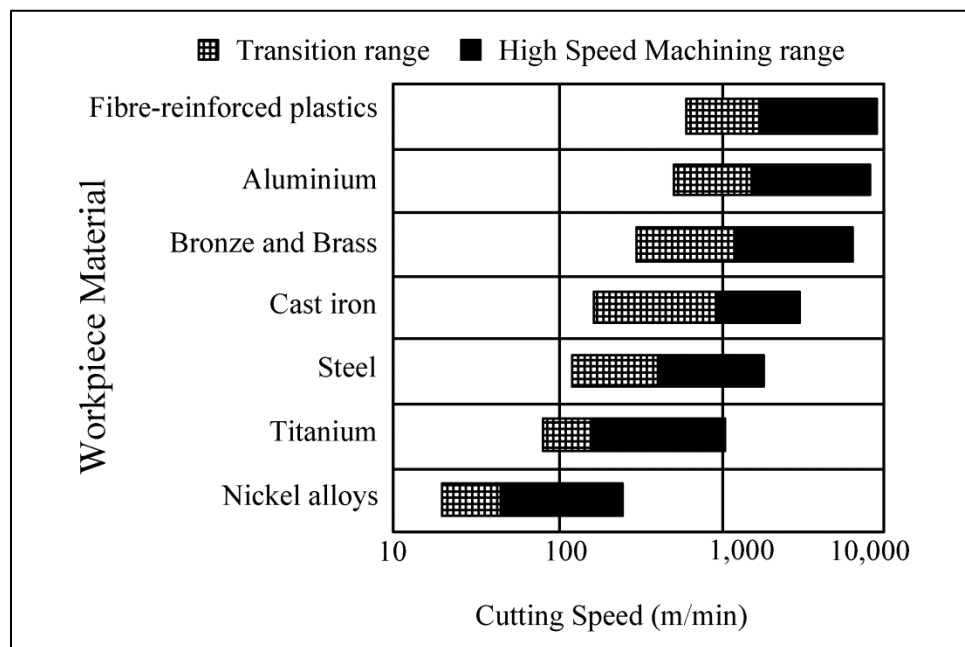


Figure 1: High-speed cutting ranges in machining of various materials (redrawn) (Fallböhmer et al., 2000)

Although, limited literature is available to understand the wear mechanism, failure modes and chip morphology of some of the materials having higher high cutting speed ranges like cast iron, steel or titanium as shown in Figure 1, it is difficult to predict the machinability of one material by studying the research findings of other material. Fang and Wu (Fang & Wu, 2009) also reported that the research findings of one material are

difficult to apply on other as high speed machining of two different materials involves completely different machining setups. The current work focuses on investigation of different cooling strategies with up and down-milling to improve machinability of Inconel 718.

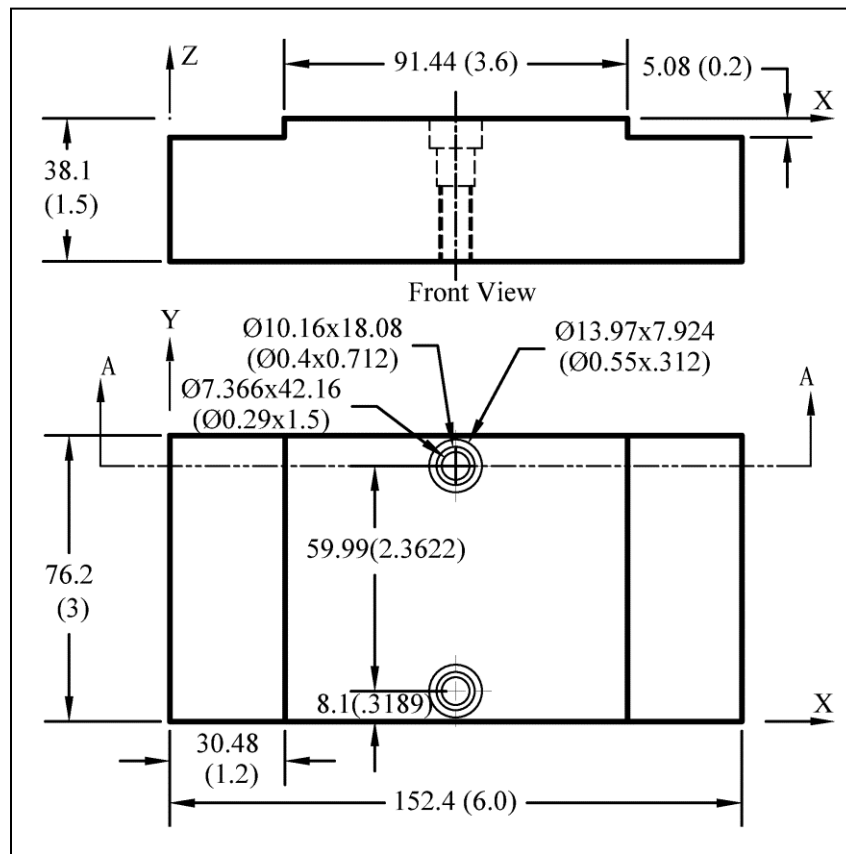
2. EXPERIMENTAL PLAN AND PROCEDURE

Peripheral high-speed end-milling tests were conducted on Cincinnati Milacron Sabre 750 Vertical Machining Centre (VMC), equipped with Acramatic 2100 CNC controller, using 4-flutes uncoated helical bull-nose solid carbide end-mills of diameter 12.7 mm (0.5 inches). The detailed experimental plan for the investigation of the effects of end-milling methods, cooling strategies and machining parameters using uncoated helical bull-nose solid carbide end-mills is summarized in Table 1.

Table1: Experiment plan for investigation of end-milling methods, cooling strategies and machining parameters using uncoated helical bull-nose solid carbide end-mills

Cooling Strategy	Milling method		Block No.	Cutting Speed m/min	Feed per revolution mm/rev	Depths of cut		MRR (mm ³ /min)
	Up-milling	Down-milling				Axial (a _a) mm	Radial (a _r) mm	
Emulsion	Exp # 1	Exp # 2	1	45	0.1016	5.08	3.81	2216.2
MQL	Exp # 3	Exp # 4	2	45	0.1016	5.08	3.81	2216.2
LN ₂ (-15°C)	Exp# 5	Exp# 6	1	45	0.1016	5.08	3.81	2216.2
MQL + LN ₂ (-15°C)	Exp# 7	Exp# 8	2	45	0.1016	5.08	3.81	2216.2

All the experiments were conducted at constant cutting speed of 1127 rpm (45 m/min), feed-rate of 114.5 mm/min (4.510 ipm), axial depth of cut (a_a) of 5.08 mm (0.2 in) and radial depth of cut (a_r) of 3.81 mm (0.15 in), these were selected based on literature review and preliminary research investigation. Axial depth of cut (a_a), radial depth of cut (a_r) and feed per revolution (f_r) were kept constant and were selected to improve productivity without adversely sacrificing tool life (performance). Each experiment consists of 8 passes, each pass of 76.2 mm (3 inches) cutting length. Four (4) cooling strategies (Emulsion, MQL, LN₂ and combined (MQL+LN₂)) were investigated under each of the up-milling and down-milling methods.



All dimensions in mm (inches)

Figure 2: Initial shape of prepared work-piece, with drilled, counter-bored and tapped holes for clamping

For each set of experiments, the total number of tools used was eight (8) uncoated carbide end-mills and Inconel 718 workpiece blocks used were two (2). Each experiment was replicated once, thus the total number of experiments was sixteen (16). The initial shape of prepared workpiece, with drilled, counter-bored and tapped holes for clamping is given in Figure 2. Peripheral high-speed end-milling tests were conducted on three (3) workpiece blocks, each having two steps on each of the two sides, using 12.7 mm (0.5 in) diameter, 4-flute uncoated carbide end-mills for up-milling and down-milling operations. Figure 3 (a) Shows workpiece 1 with the sequence of experiments performed (Experiments #1, 2, 5 and 6). Figure 3 (b) shows workpiece 2 and the sequence of experiments performed (Experiments # 3, 4, 7 and 8).

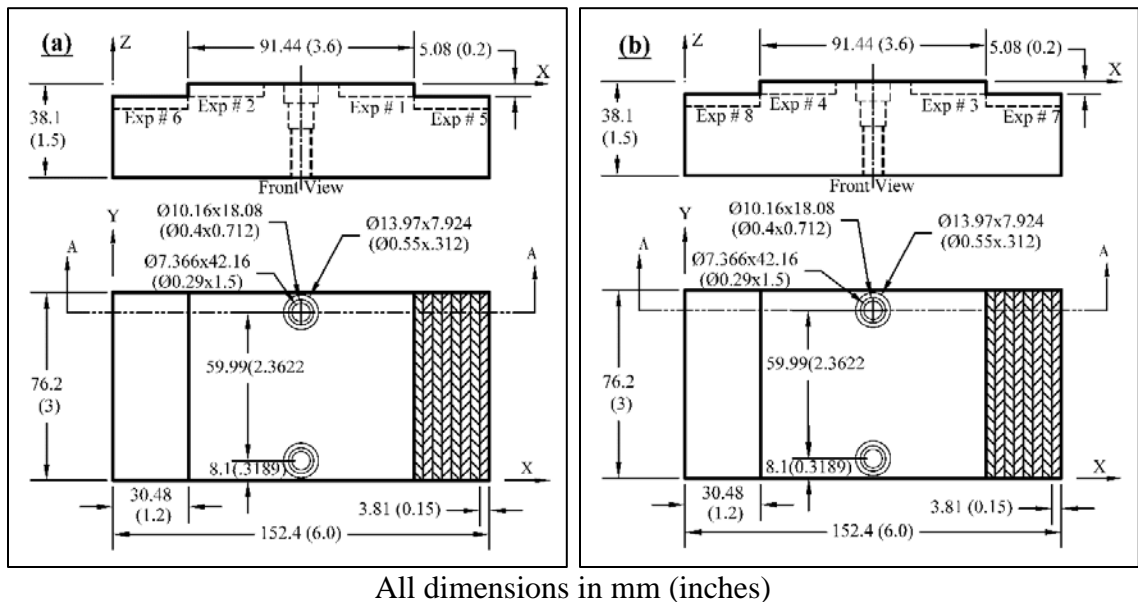


Figure 3: Schematic of experiments performed on workpieces. (a) Workpiece 1 for experiment #1,2,5 and 6 and (b) Workpiece 2 for experiment #3,4,7 and 8

Machining experiment under emulsion and MQL cooling strategies were conducted before machining experiment under LN₂ cooling or combined (MQL + LN₂)

cooling because if LN₂ or (MQL + LN₂) cooling strategy was applied first, it would have affected the hardness of the workpiece steps and hence, the results of the experiments following that machining experiment. Also, neither of the two cooling strategies, LN₂ or combined (MQL + LN₂) was applied on the same side because they might affect the results of the subsequent cooling experiment by increasing the hardness of workpiece. A new tool was used for each cooling strategy to eliminate the effect of tool wear. The results of the eight (8) experiments were analyzed to find the best milling method among up-milling and down-milling, and better cooling strategy among conventional emulsion, MQL, LN₂ and combined (MQL + LN₂) cooling.

2.1. COOLING STRATEGIES SETUP

The main objective of these experiments is to investigate the effects of milling methods and cooling strategies on maximum flank wear, chip morphology and surface roughness. Each of the cooling strategies investigated (Emulsion, MQL, LN₂ and combination of (MQL+LN₂)) were set independently for each set of experiment reported in Table 1. The application of conventional emulsion reduces the temperature at the cutting zone and washes the chips away from the cutting zone. In addition to that, it reduces friction between the chip and tool rake face, the tool flank and workpiece machined surface. A semi-synthetic emulsion coolant, type VPTECH, manufactured by Walter Tools was used for this purpose as a conventional emulsion cutting fluid. The emulsion coolant was mixed with water to achieve the recommended concentration of 6-10%, given by the manufacturer for machining nickel alloys. A refractometer was used to measure the concentration of the coolant. The Accu-Lube LB-2000 biodegradable mineral oil, used as a lubricant for performing experiments involving MQL, is

investigated as a possible environmentally friendly replacement of conventional emulsion coolant.

A 160 liters liquid nitrogen cylinder with an operating pressure of 15.9 bar (230 psi) containing liquid nitrogen was used for the experiments involving liquid nitrogen (LN₂) at -15°C to cool down the cutting zone temperature. The temperature of -15°C was chosen for the mixture of LN₂ and shop air as ideal temperature for Inconel 178 based on published literature (Yuan et al., 2011).

2.2. WORKPIECE PREPARATION

The initial shape of the workpiece was machined from rectangular blocks of Inconel 718 of dimensions 152.4 mm x 76.2 mm x 38.1 mm (6 in. x 3 in. x 1.5 in.) on Cincinnati Milacron Sabre 750 vertical machining center (VMC). Two steps were machined on both sides of the workpiece, each having a width of 30.48 mm (1.2 in.) and height 5.08 mm (0.2 in.). Each step was used to perform one experiment and thus, four experiments were performed on one workpiece. Two counter-bored holes of diameter 7.366 (0.29 in.), 38.1 mm (1.5 in.) deep and 60 mm (2.3622 in.) apart were drilled and tapped for clamping the workpiece on a dynamometer.

2.3. EXPERIMENTAL SETUP AND PROCEDURE

The prepared workpiece was clamped on Cincinnati Milacron Sabre 750 Vertical Machining Centre (VMC), equipped with Acramatic 2100 CNC controller and 8 machining passes were made for each experimental condition shown in Table 1 using CNC program written for each experiment. Cutting forces were acquired during each pass and analyzed later. The operation was stopped after each pass, chip samples were

collected for analysis, and the tool was taken out from the CNC machine to measure maximum flank wear. Surface roughness of machined surfaces were also measured after the end of each experiment. Cutting force analysis are not reported in this paper.

2.3.1. Tool Wear Measurement. After completion of each machining pass, the operation was stopped and the tool was taken out from the machine tool drum and the maximum flank wear was measured using Keyence VHX – 5000 digital microscope. To measure the maximum flank wear, a reference line along the tool cutting edge above the axial depth of cut was drawn, from which the measurements of flank wear land were made in the beginning and after each cutting pass. This procedure was repeated after each pass.

2.3.2. Chip Analysis. After each pass, the machining was stopped and samples of chips were collected and analyzed. The individual chips were analyzed under VHX – 5000 digital microscope. Chips images were captured using a digital camera. Also, the chip length were measured using VHX – 5000 digital microscope.

2.3.3. Surface Roughness Measurement. Surface roughness was measured on the machined surface using a portable Brown and Sharpe pocket surf profilometer. The measurements were made on the surface perpendicular to feed direction. For each experiment, the arithmetic average surface roughness (R_a) of the machined workpiece was measured at three different locations which were 25.4 mm (1 in.) apart from each other. Measurements were made using a traverse length of 5 mm (0.195 in.) at a speed of 5.08 mm/sec. The cut-off of tracing length was 0.8 mm (0.03 in.) and the number of cut-offs used was 5 which made a total evaluation length of 4.0 mm (0.15 in.). Figure 4

cutting tool is rotating in clockwise direction in both up and down-milling operation. During up-milling operation, the cutting tool is rotating up-against the workpiece feed direction and the tool flutes enter the workpiece along y direction with an angle of -180° with negative x-axis and comes out of the workpiece at an angle of ϕ_{exit} with negative x-axis. Also, the chip thickness at the entry of the cutting tool into workpiece is zero and it increases to maximum when the tool comes out of the workpiece. In case of down-milling operation, the cutting tool rotates along the feed direction and the tool flutes enter into the workpiece at an angle of ϕ_{entry} with negative x-axis and comes out of the workpiece at an angle of 0° with x-axis. The chip thickness is maximum when the cutting tool enters into the workpiece in down-milling and it reduces to zero when the tool comes out of the workpiece.

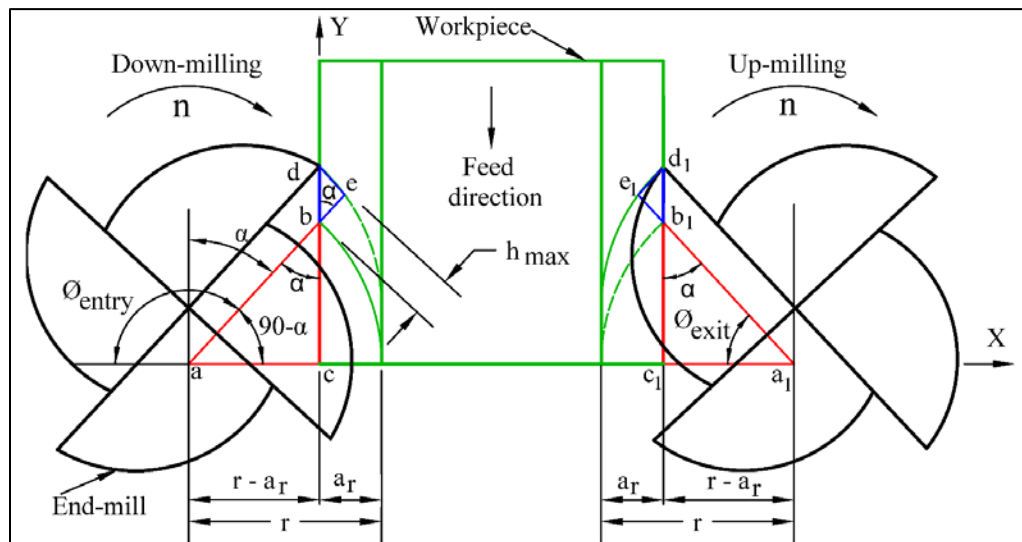


Figure 5: Cutter entry angle during down-milling and cutter exit angle during up-milling

The cutter entry and exit angles for both up and down-milling are calculated below:

For down-milling. The tool always comes out of the workpiece at an angle of 180° with negative x-axis. Thus,

$$\phi_{\text{exit}} = 180^\circ \quad (2)$$

The entry angle is calculated using Figure 5 as follows:

$$\phi_{\text{entry}} = 180 - (90 - \alpha) \quad (3a)$$

From Δabc

$$\text{Cos } (90 - \alpha) = \frac{ac}{ab} = \frac{r - a_r}{r} \quad (3b)$$

where, r is the radius of tool and a_r is the radial depth of cut.

$$90 - \alpha = \arccos \left(\frac{r - a_r}{r} \right) \quad (3c)$$

$$90 - \alpha = \arccos \left(\frac{6.35 - 3.81}{6.35} \right) = \arccos (0.4) = 66.42^\circ$$

Substituting the value of $90 - \alpha$ in (3a)

$$\phi_{\text{entry}} = 180 - \arccos \left(\frac{r - a_r}{r} \right) \quad (3d)$$

$$\phi_{\text{entry}} = 180 - 66.42 = 113.58^\circ$$

For up-milling. From Figure 5, the tool penetrates into the workpiece at an angle of 0°

with negative x-axis. Thus,

$$\phi_{\text{entry}} = 0^\circ \quad (4)$$

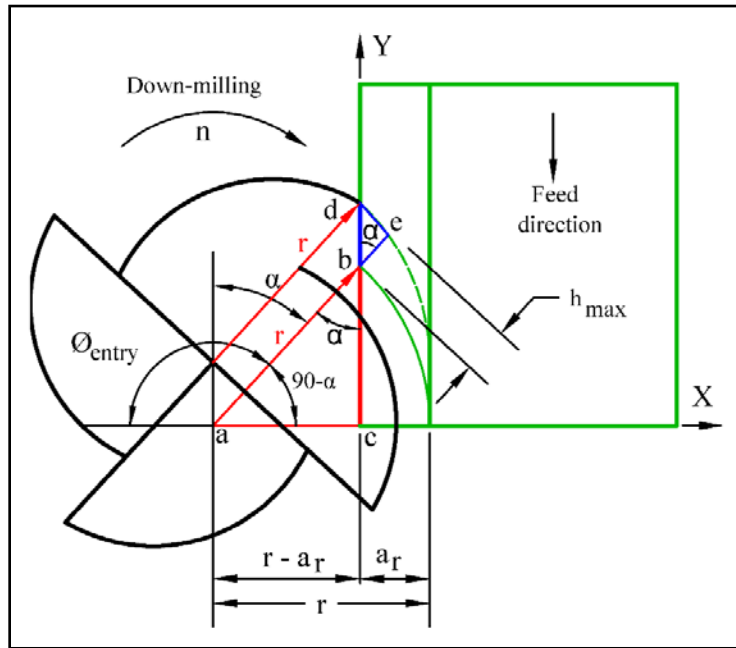
Exit angle can be found using from $\Delta a_1b_1c_1$

$$\text{Cos } \phi_{\text{exit}} = \frac{a_1c_1}{a_1b_1} = \left(\frac{r - a_r}{r} \right) \quad (5a)$$

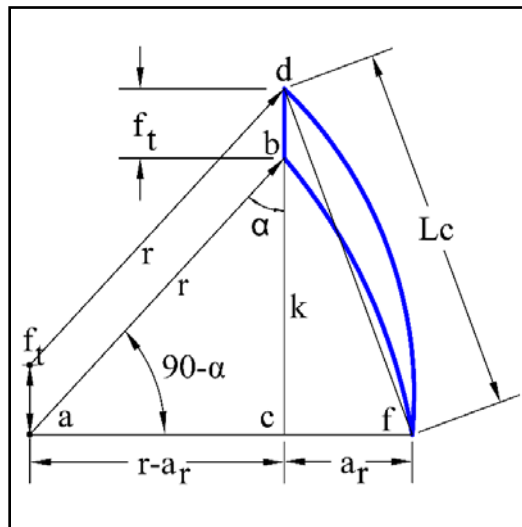
$$\phi_{\text{exit}} = \arccos \left(\frac{r - a_r}{r} \right) \quad (5b)$$

$$\phi_{\text{exit}} = \arccos\left(\frac{6.35 - 3.81}{6.35}\right) = 66.42^\circ \text{ T}$$

The shear action of the tool while machining creates the chips of specific length depending upon the feed per tooth and radial depth of cut as shown in Figure 6.



(a) Chip formation during down-milling operation



(c) Chip length, L_c

Figure 6: Chip morphology with blown-up images showing maximum chip thickness and chip length. (a) Chip morphology, (b) maximum chip thickness and (c) chip length

Chip Length

The chip length is calculated from Figure 6b as follows:

From Δ cdf:

$$L_c^2 = a_r^2 + (k + f_t)^2 \quad (6)$$

From Δ abc:

$$\text{Cos}(\alpha) = \frac{k}{r} \Rightarrow k = r \text{Cos}(\alpha) \quad (7)$$

Substituting the value of k in (6)

$$L_c^2 = a_r^2 + (k + f_t)^2 = a_r^2 + (r \text{Cos}(\alpha) + f_t)^2 \quad (8a)$$

$$L_c = \sqrt{a_r^2 + (r \text{Cos}(\alpha) + f_t)^2} \quad (8b)$$

From Δ abc:

$$k^2 + (r - a_r)^2 = r^2 \quad (9a)$$

$$k^2 = r^2 - (r - a_r)^2 = [r + (r - a_r)] [r - (r - a_r)] = [2r - a_r] [a_r] \quad (9b)$$

$$k = \sqrt{2r a_r - a_r^2} \quad (9c)$$

$$\text{As we know, } \text{Cos}(\alpha) = \frac{k}{r} = \frac{\sqrt{2r a_r - a_r^2}}{r} \quad [\text{From (7) and (9c)}] \quad (10)$$

Substituting the value of $\text{Cos}(\alpha)$ in (8b)

$$L_c = \sqrt{a_r^2 + (r \text{Cos}(\alpha) + f_t)^2} = \sqrt{a_r^2 + \left(r \frac{\sqrt{2r a_r - a_r^2}}{r} + f_t\right)^2} = \sqrt{a_r^2 + (\sqrt{2r a_r - a_r^2} + f_t)^2} \quad (11)$$

Expanding (11), we get

$$L_c = \sqrt{2r a_r + 2f_t \sqrt{2r a_r - a_r^2} + f_t^2} \quad (12)$$

$$L_c = \sqrt{2 \times 6.35 \times 3.81 + 2 \times 0.0254 \sqrt{2 \times 6.35 \times 3.81 - 3.81^2}} + 0.0254^2 = 6.977 \text{ mm}$$

Chip length after each pass was also measured using digital microscope. The measured chip length was compared with calculated chip length under all cooling strategies and milling methods.

The tool starts cutting during up and down-milling when the center of the end-mill is at a distance of L_1 (approach distance) from the workpiece edge perpendicular to feed direction as shown in Figure 7. The distance L_1 is given as follows.

$$L_1 = \sqrt{r^2 - (r - a_r)^2} \quad (13)$$

$$L_1 = \sqrt{6.35^2 - (6.35 - 3.81)^2} = 5.82 \text{ mm}$$

As the workpiece machined length (L) along the feed direction was 76.2 mm (3 inches), the total machined length for each machining pass becomes:

$$ML \text{ (Machined Length of single pass)} = L + L_1 = 76.2 + 5.82 = 82.02 \text{ mm} \quad (14)$$

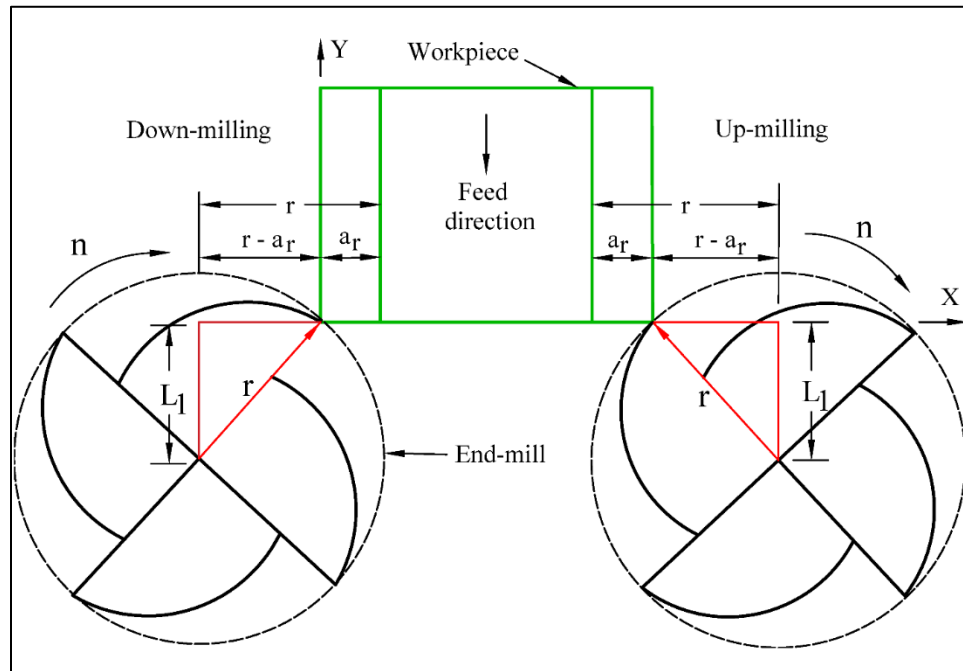


Figure 7: Approach distance during down-milling and up-milling operation

3. RESULT ANALYSIS

3.1. MAXIMUM FLANK WEAR AND CHIP MORPHOLOGY FOR UP-MILLING AND DOWN-MILLING METHOD UNDER EMULSION COOLING STRATEGY

3.1.1. Maximum Flank Wear. Figure 8 shows the plot for maximum flank wear vs number of passes (machined length) for up and down-milling methods under emulsion cooling strategy at a cutting speed of 45 m/min (1127 rpm) and 114.5 mm/min (4.510 ipm) feed-rate.

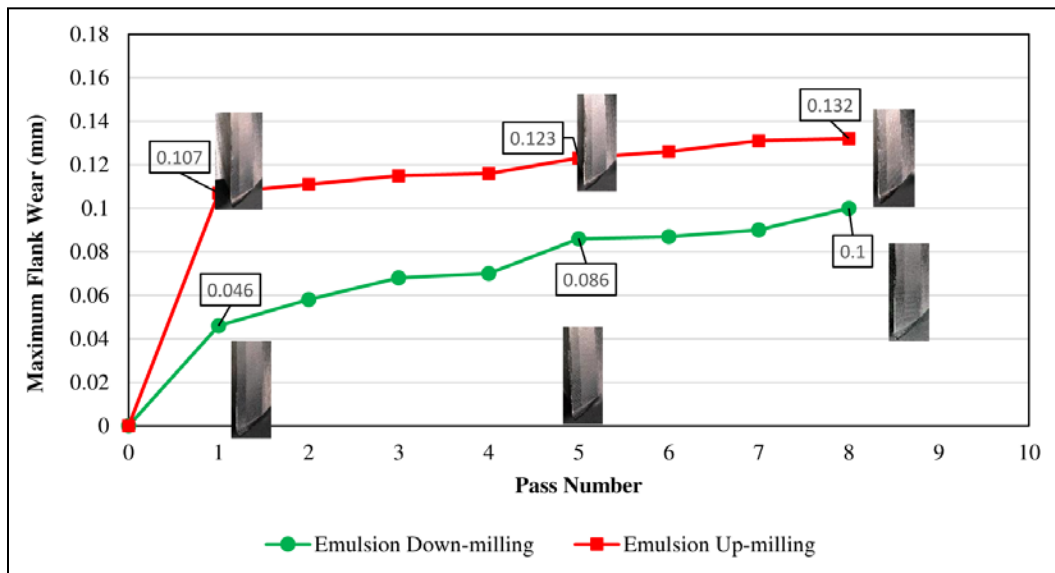


Figure 8: Maximum flank wear vs number of passes (machined length) for up and down-milling under emulsion cooling strategy

The plot shows that the maximum flank wear in emulsion down-milling method is less than that in up-milling throughout the machining length and increases gradually with number of passes (machined length). The initial flank land and progressive flank wear after 1st, 5th and 8th passes under emulsion cooling strategy for up and down-milling methods are shown in Figure 9.

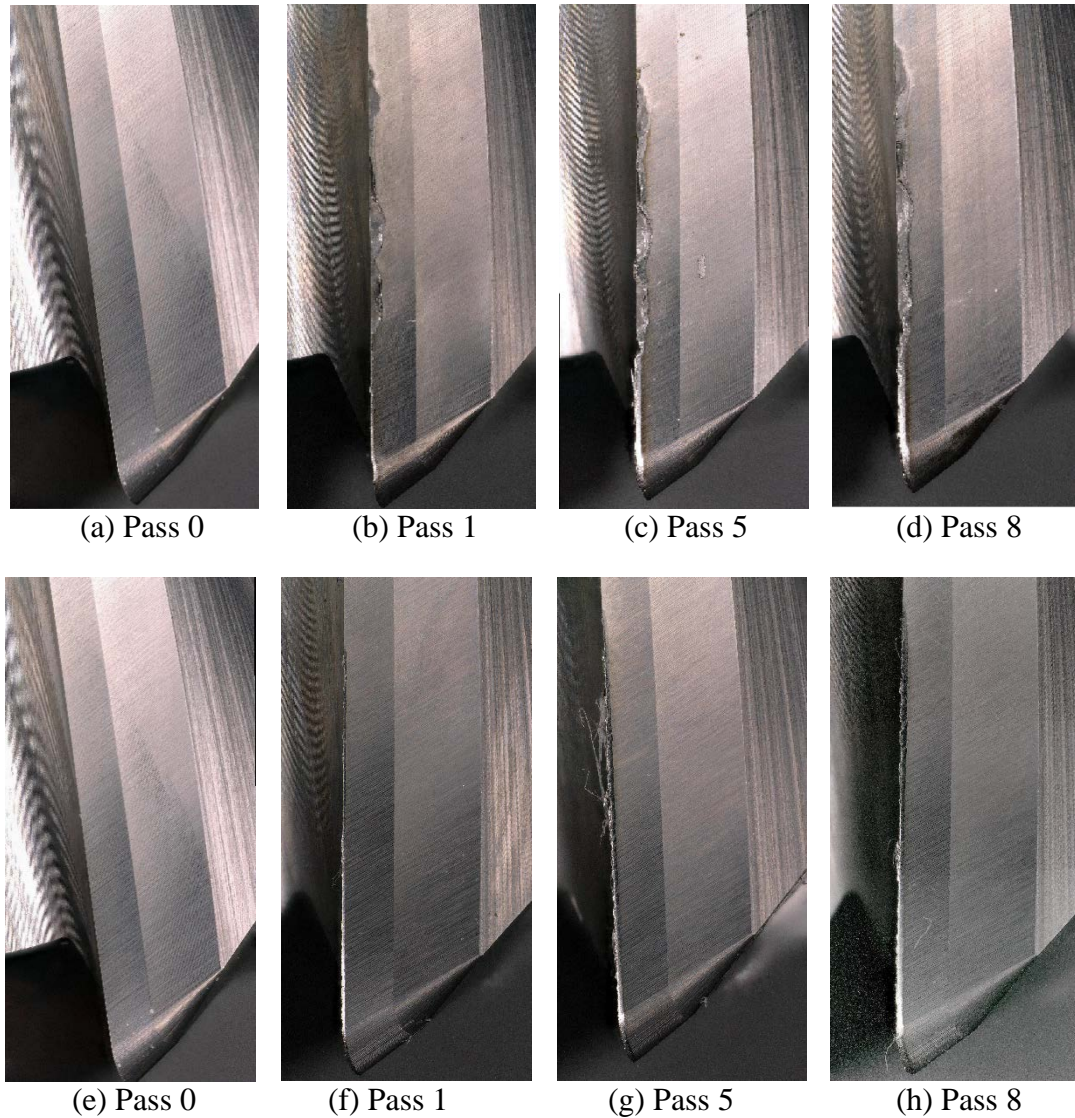


Figure 9: Initial flank land and progressive flank wear for up and down-milling under emulsion cooling strategy. Emulsion up-milling at (a) pass 0, (b) pass 1, (c) pass 5 and (d) pass 8 and, emulsion down-milling at (e) pass 0, (f) pass 1, (g) pass 5 and (h) pass 8

As can be seen from figure, tool wear under emulsion up-milling operation is very high as compared to emulsion down-milling method. The formation of notch wear can also be seen from the 1st pass of up-milling operation. The mode of tool wear in up-milling is chipping of tool edge and notching which increase the area of contact between tool edge and chips. This further increased tool wear in successive passes. During

emulsion down-milling, the tool wear increased gradually due to increase in tool edge and chip contact area with progression of time. Also, no chipping or notch wear was seen throughout the machining in down-milling operation and the mode of tool wear in down-milling is abrasion. The reason of high flank wear in up-milling can be explained with help of chip formation during up and down-milling operation as shown in Figure 10.

During up-milling operation, the chip thickness at the entry of the tooth into the workpiece is zero and keeps on increasing till the tooth comes out of the workpiece. This rubbing of the tool against the workpiece causes excessive adhesive tool wear during up-milling operation. Also, a work hardening layer is produced on the newly exposed surface of the workpiece. During the next rotation, the tooth penetrates into the work hardened layer created by previous rotation of the tooth, further exacerbates the tool wear.

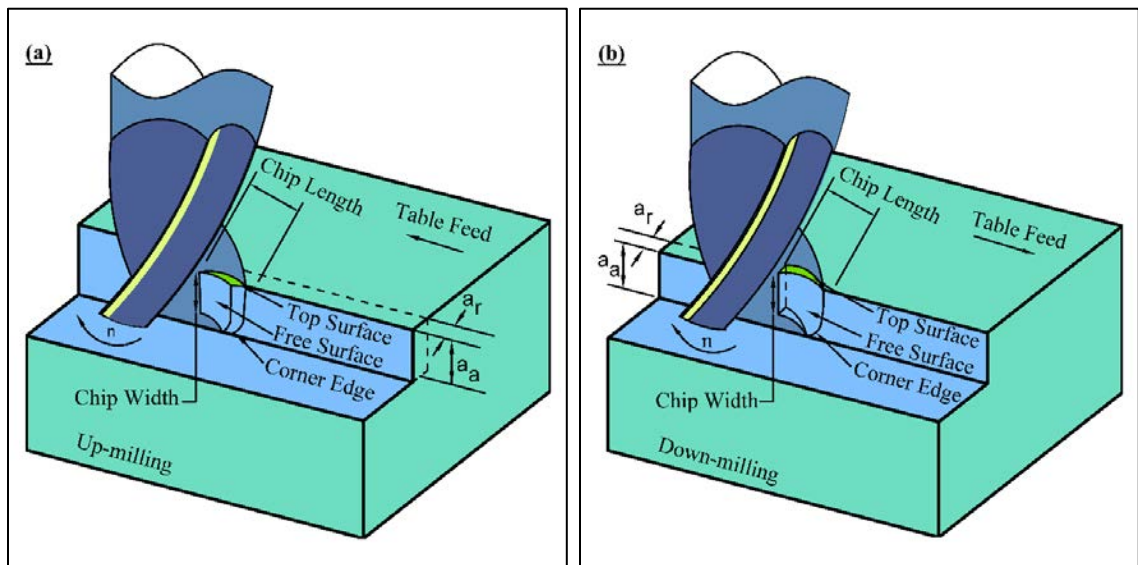


Figure 10: 3-D Chip formation during up-milling and down-milling operations. (a) Up-milling and (b) down-milling operation

In the case of down-milling operation, the chip thickness in the beginning of entry of tooth into workpiece is highest and decreases gradually till the tooth comes out of the workpiece. Although, the mechanical impact in down-milling is higher in the beginning as compared to up-milling, there is no rubbing of the tool with the workpiece. As a result, the tool wear in down-milling is lower than up-milling.

3.1.2. Chip Morphology. The free and back surfaces of chip are shown in Figure 11. As seen, the back surface of the chip is smooth and shiny. The back surface encounters high contact and shear stresses while sliding on the tool rake face, which also constrains the deformation of back surface (Sun and Guo, 2008). The free surfaces of chips for emulsion up and down-milling at passes 1, 5 and 8 are shown in Figure 12. Figure 13 shows images of chips collected after the 1st, 5th and 8th pass for emulsion up and down-milling. It has been reported that the chips formed in end-milling are serrated in nature (Patwari et al., 2010).

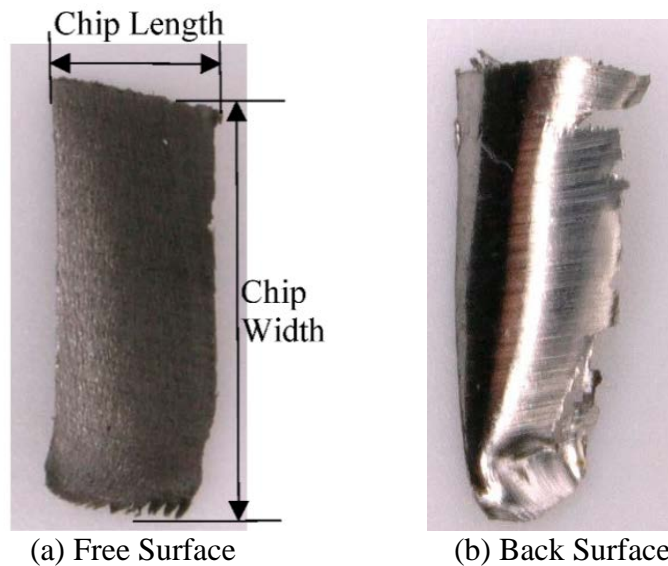


Figure 11: Free and Back surfaces of the chip. (a) Free Surface and (b) back surface

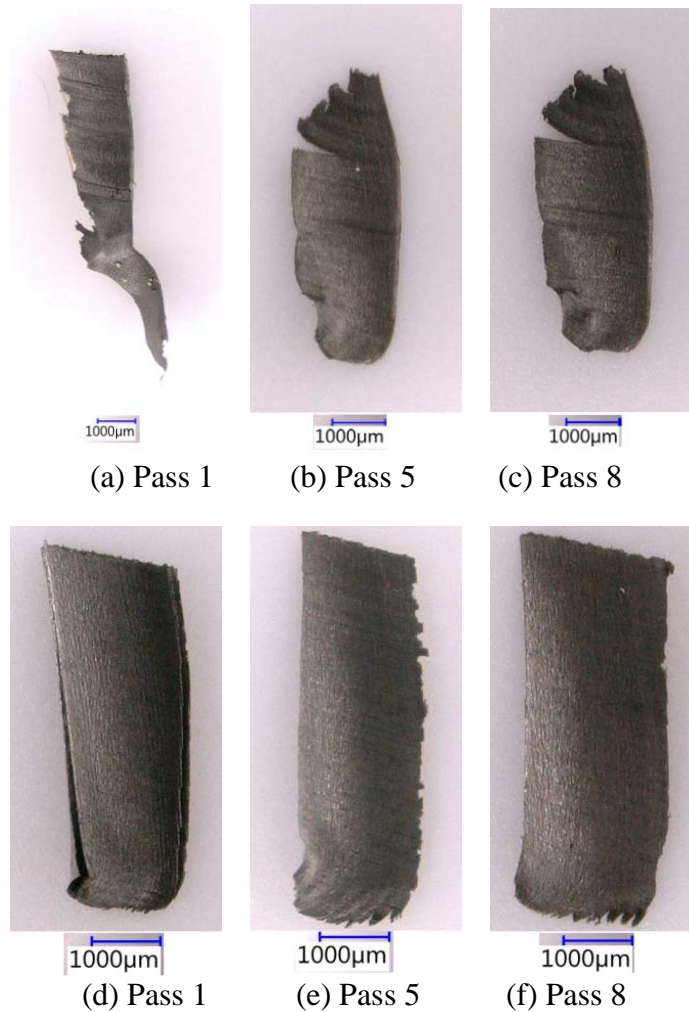


Figure 12: Free surface of chips for up and down-milling under emulsion cooling strategy. Emulsion up-milling at (a) pass 1, (b) pass 5 and (c) pass 8 and, emulsion down-milling at (d) pass 1, (e) pass 5 and (f) pass 8

Also, the free surface possess lamella structures and the major section of the lamella in the free surface was formed by side cutting edge and the corner section was formed by the corner cutting edge (Sun and Guo, 2008). This major section of lamella formed by side cutting edge was saw teeth in nature which was produced due to phase compression and adiabatic shear, resulting in fluctuation of the force exerted on tool (Patwari et al., 2010).

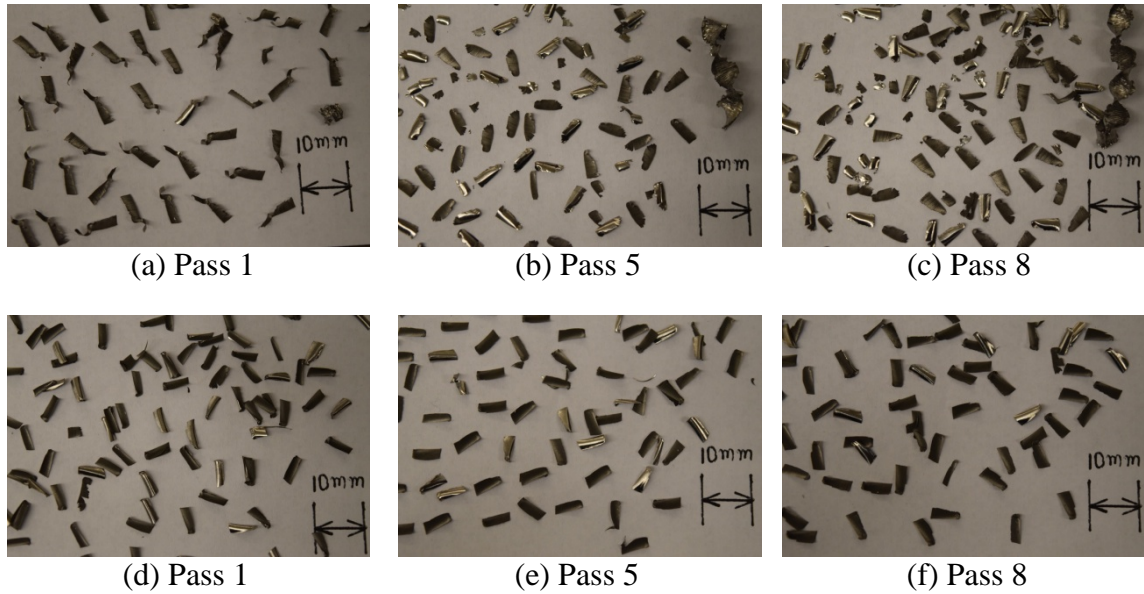


Figure 13: Images of chips for up and down-milling under emulsion cooling strategy. Emulsion up-milling at (a) pass 1, (b) pass 5 and (c) pass 8 and, emulsion down-milling at (d) pass 1, (e) pass 5 and (f) pass 8

There was a long tail obtained in 1st pass of emulsion up-milling experiment which is formed by tool nose radius as seen in Figure 12 (a). As can be seen from the Figures 12 and 13, emulsion down milling produces the chips with sharp and straight edges with minimum tear at the end edges of the chip as compared to the chips from emulsion up-milling in which the edges of the chips are irregular and torn. The 3D chip morphologies during up and down-milling operations is shown in Figure 14. During up-milling operation, some tearing can be seen at the thin edge of the chip created during tool entry parallel to the direction of chip length. During the rotation of the tool, the tip of the tool flute penetrates first into the workpiece due to its helical profile and started creating the chip. Due to high contact and shearing stresses as discussed above, the partial chip created by tool tip gets strained. As the tool further penetrates into the workpiece during its rotation, the bottom portion of the thin edge formed in the

beginning, further strained as compared to the upper portion of the thin edge. Due to this difference in the strains on the thin edge of the chip, tearing parallel to the chip length starts propagating. The tearing further exacerbated with the progression of tool wear (number of passes) as the edge of the tool became irregular and dull. During down-milling, the chip thickness was maximum in the beginning when the tool entered the workpiece. Due to maximum thickness of the chip at the beginning of tool penetration into workpiece, tearing does not initiate at all.

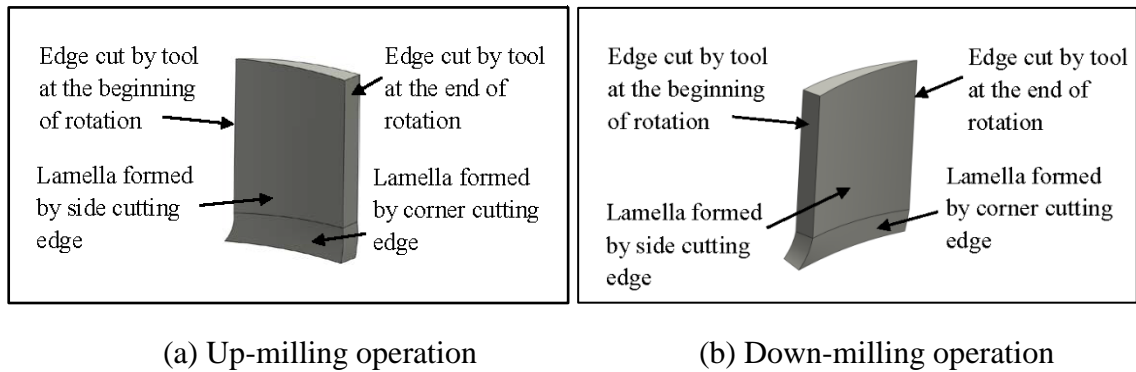


Figure 14: 3-D chip morphology during up and down-milling operations. (a) Up-milling and (b) down-milling operation

A continuous strip of chip called segmented chip with a typical saw-tooth shape (Hadi et al., 2013) was obtained in emulsion up-milling after each pass as shown in Figure 15 for passes 1, 5 and 8. The vertical cross-sections shown in Figure 15 (a) of the lamella are due to saw tooth shape of the chip. The strength of these segmented chips kept on increasing after each pass due to increased tool wear after each pass. This segmented chip was difficult to be removed by cooling strategy and interfered in the machining process and kept entangling with the tool which further increased the tool wear.

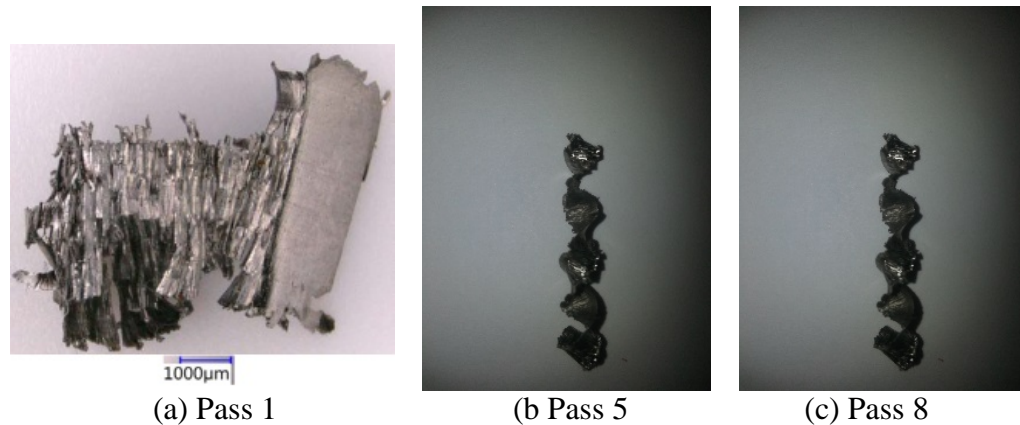


Figure 15: Segmented chips with typical saw-tooth obtained in emulsion up-milling. (a) pass 1 (b) pass 5 and (c) pass 8

Figure 16 shows the calculated chip length and measured lengths of chips for both emulsion up and down-milling methods. As can be seen, the calculated chip length was very large as compared to measured ones. The length kept on increasing with the progression of tool wear in both up and down-milling. Also, it has been seen that up-milling produce longer chips compared to down-milling method during each pass. As the chip thickness is highest when the tool comes out of workpiece, it becomes difficult for the tool to shear the thick chip from the workpiece. Also, as explained by Hadi et al. (2013), the generation of typical saw-tooth shape shows that the thermal softening overwhelms the effect of strain hardening as the local rate of heat build-up is large enough. Thus, it gets pulled while being sheared from the workpiece, which increases the chip length. During down-milling, the chip thickness starts from highest at the beginning to lowest at the end. Thus, it becomes easy to shear off the chips by the tool from workpiece. Thus, the length of chips do not increase much while shearing.

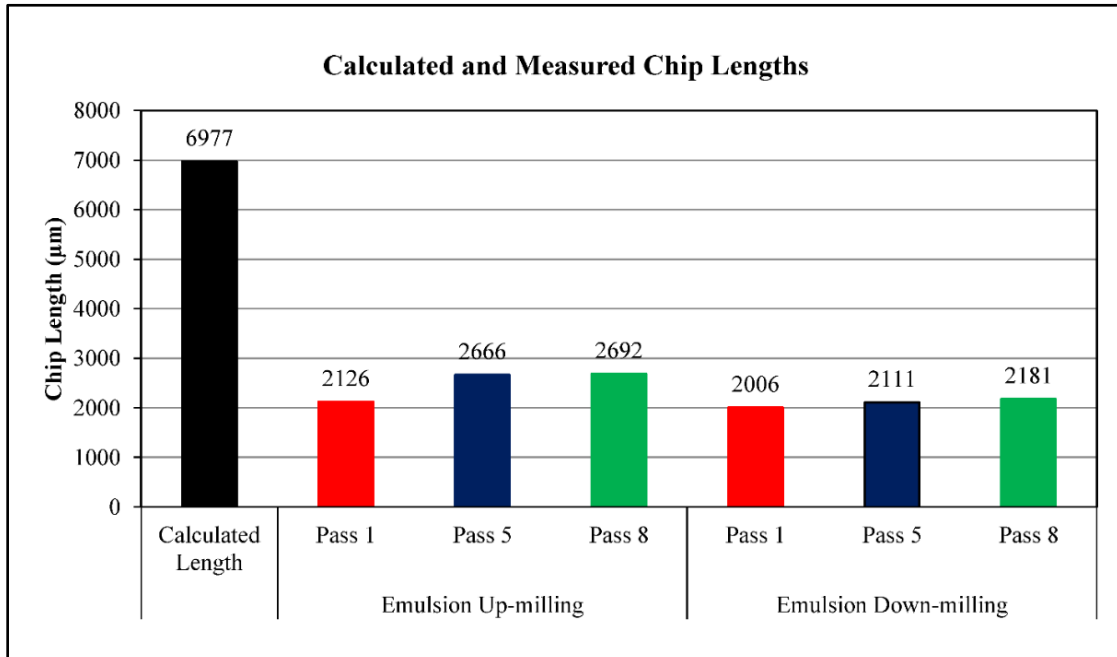


Figure 16: Calculated and measured chip lengths vs number of passes (machined length) and milling methods under emulsion cooling strategy

3.2. MAXIMUM FLANK WEAR AND CHIP MORPHOLOGY FOR UP-MILLING AND DOWN-MILLING METHOD UNDER MQL COOLING STRATEGY

3.2.1. Maximum Flank Wear. Figure 17 shows the plot for maximum flank wear vs number of passes for up and down-milling methods under MQL cooling strategy. The plot shows that maximum flank wear is least in MQL down-milling method throughout the machining length. The initial tool flank land and maximum flank wear under MQL for up and down-milling method is shown in Figure 18. As can be seen from Figures 17 and 18, the tool wear in MQL up-milling increased drastically and the tool worn out completely during 4th pass. As can be seen from the Figure 18 (b), there was excessive tool chipping from 1st pass due to high cutting forces in MQL up-milling operation.

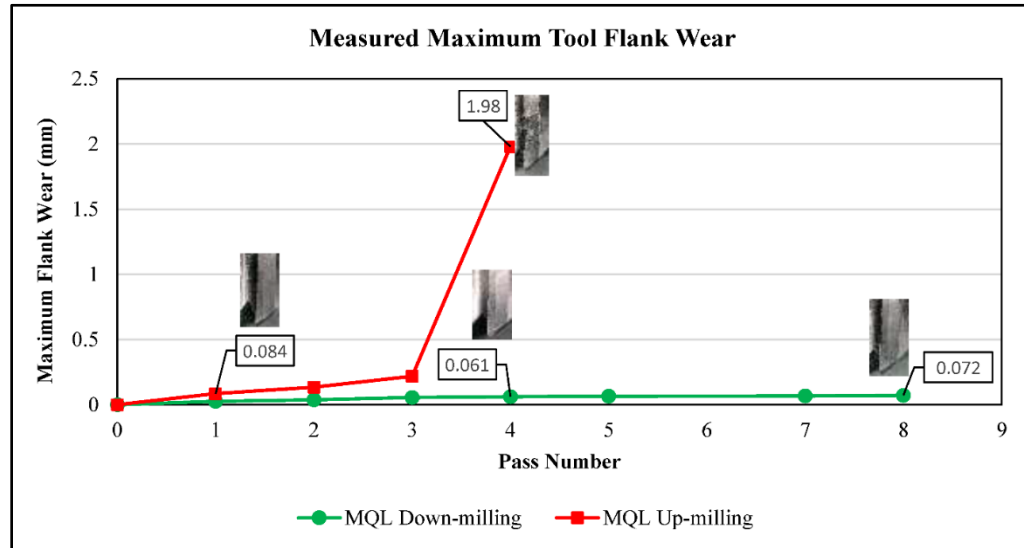


Figure 17: Maximum flank wear vs number of passes (machined length) for up and down-milling under MQL cooling strategy

This initial chipping further exacerbated the rate to tool wear. The segmented chip, formed in all passes when machining using up-milling operation, kept entangling with the cutting tool, which increased tool wear. Also, the strength of this segmented chip kept on increasing with progression of time (number of passes), which further increased the cutting forces and cutting zone temperature. By the time the tool machined 4th pass, the cutting zone temperature was increased so much that the flutes had undergone plastic deformation and were burnt completely. Thus, it was decided to terminate the machining as the tool had exceeded its life. In the case of MQL down-milling operation, tool wear after 8th pass, primarily caused by abrasion, was less than the wear at 4th pass of MQL up-milling. MQL cooling strategy was very effective in down-milling operation where the chip removal was very smooth and chips formed were discontinuous serrated in nature, which were easy to be removed. Also, MQL cooling provided the benefit of lubrication of cutting zone which in turn, decreased the tool wear.

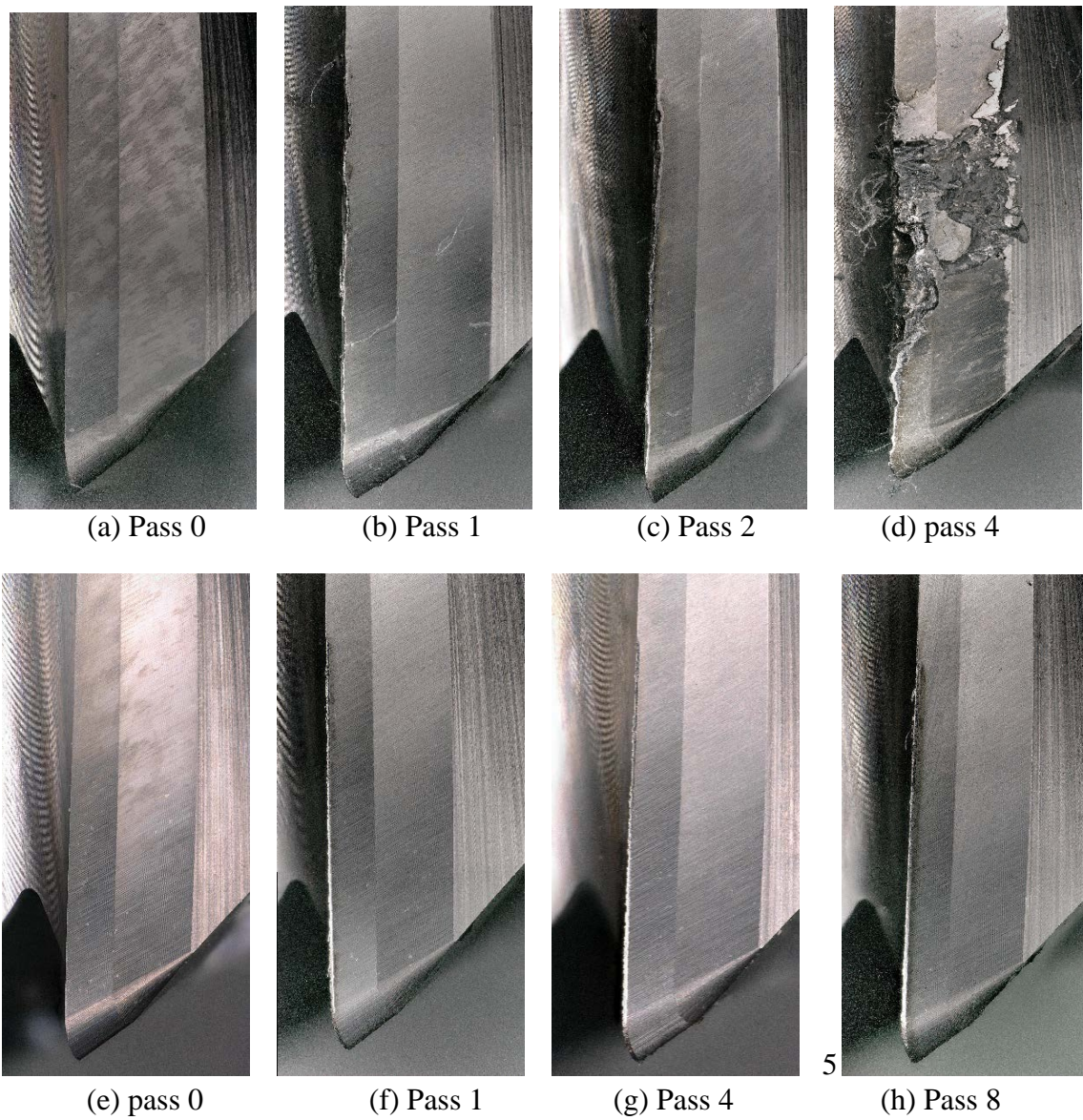


Figure 18: Measured maximum flank wear for up and down-milling under MQL cooling strategy. MQL up-milling at (a) pass 0, (b) pass 1, (c) pass 2 and (c) pass 4 and, MQL down-milling at (e) pass 0, (f) pass 1, (g) pass 4 and (h) pass 8

3.2.2. Chip Morphology. Figure 19 shows images of chips after 1st, 2nd and 4th pass for MQL up-milling and after 1st, 4th and 8th pass for MQL down-milling and Figure 20 shows the free surface of chips for MQL up and down-milling operations.

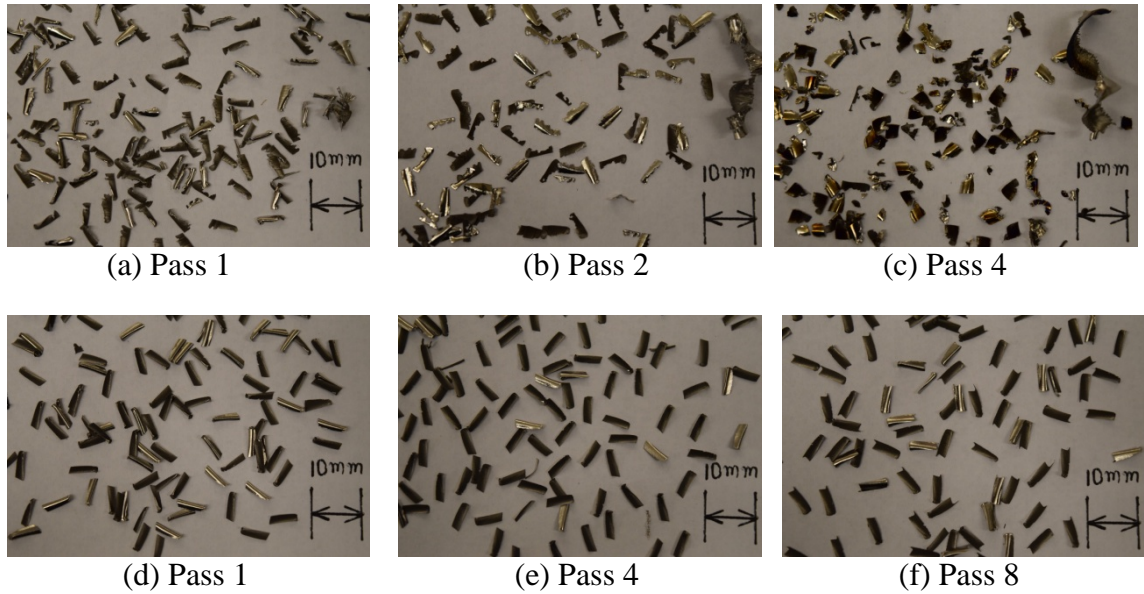


Figure 19: Images of chips for up and down-milling under MQL cooling strategy. MQL up-milling at (a) pass 1, (b) pass 2 and (c) pass 4 and, MQL down-milling at (d) pass 1, (e) pass 4 and (f) pass 8

As can be seen from Figure, tears occurred on the end-edges of the chips in MQL up-milling parallel to the direction of chip length, whereas in case of MQL down-milling, the end-edges were straight and sharp. The tearing of chips during up-milling operation became severe with progression of time (number of passes). In the 4th pass of MQL up-milling, signs of burnt chips can be seen as red hot cutting zone was observed, due to increase in cutting forces and friction between tool and workpiece. This happened because the cutting tool in MQL up-milling was not able to dissipate the heat from cutting zone effectively, which increased the cutting zone temperature. Also, the lower rate of heat dissipation than rate of heat generation at the cutting zone due to low thermal conductivity of Inconel 718 caused the cutting zone temperature to increase drastically during machining. This led the tool to plastically deform during 4th pass only and the tool could not machine more than 4 passes in case of MQL up-milling.

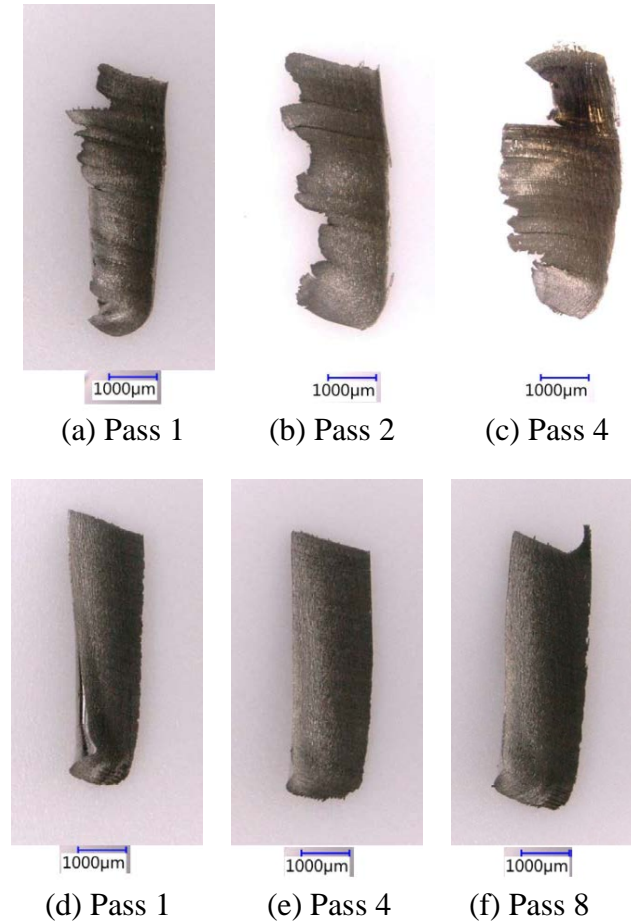


Figure 20: Free surface of chips for up and down-milling under MQL cooling strategy. MQL up-milling at (a) pass 1, (b) pass 2 and (c) pass 4 and MQL down-milling at (d) pass 1, (e) pass 4 and (f) pass 8

A segmented chip was again obtained in MQL up-milling after each pass as shown in Figure 19 (b) and (c). In the case of MQL down-milling operation, most of the heat was carried away by chips, which helped lowering the cutting zone temperature. Also, the chips were uniform in shape throughout the machining. The chip thickness increased with progression of cutting passes due to increase in tool wear.

Figure 21 shows the chip length for MQL up and down-milling. As already discussed, there were a lot of tears on the end-edges of the chips during MQL up-milling, which made the length of chips shorter in pass 2 as compared to pass 1. Pass 4 of MQL

up-milling produced chips of longer length as compared to previous passes. The chip length in MQL down-milling was quite shorter as compared to up-milling in each pass. Also, with the progression of tool wear, the chip length kept on increasing. MQL down-milling produced the shortest chips during 8th pass. The MQL cooling strategy provided lubrication to the cutting zone, which helped the chips to come out easily and were not pulled much during the shearing process.

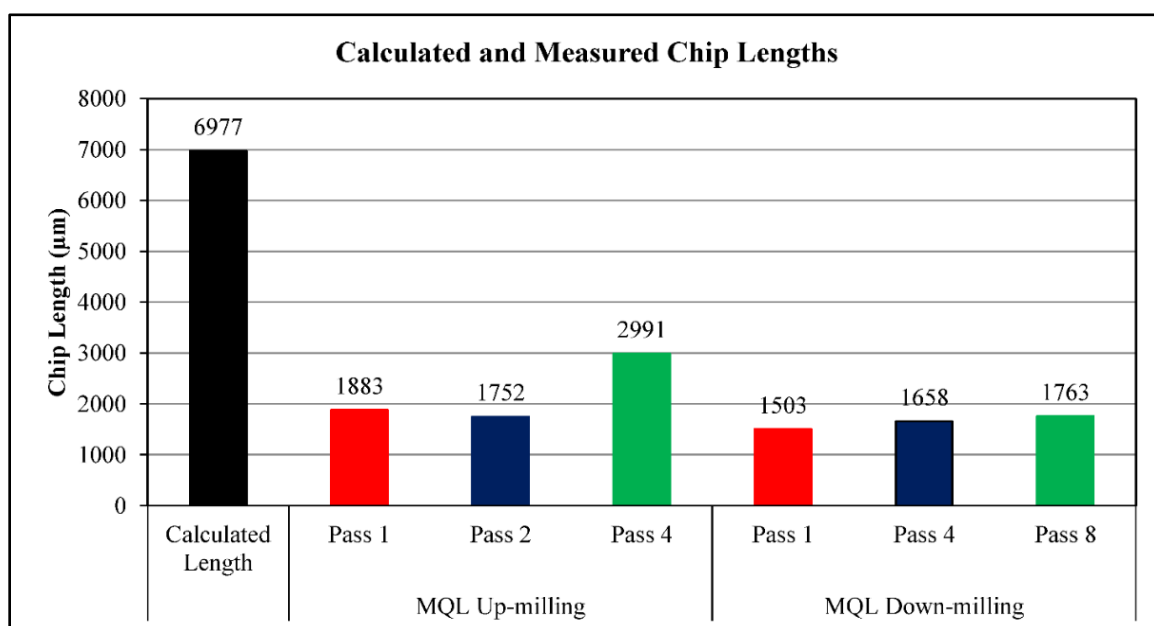


Figure 21: Calculated and measured chip lengths vs number of passes (machined length) and milling methods under MQL cooling strategy

3.3. MAXIMUM FLANK WEAR AND CHIP MORPHOLOGY FOR UP-MILLING AND DOWN-MILLING METHOD USING LN₂ COOLING STRATEGY

3.3.1. Maximum Flank Wear. Figure 22 shows the plot for maximum flank wear vs number of passes (machined length) for up and down-milling methods under LN₂ cooling strategy.

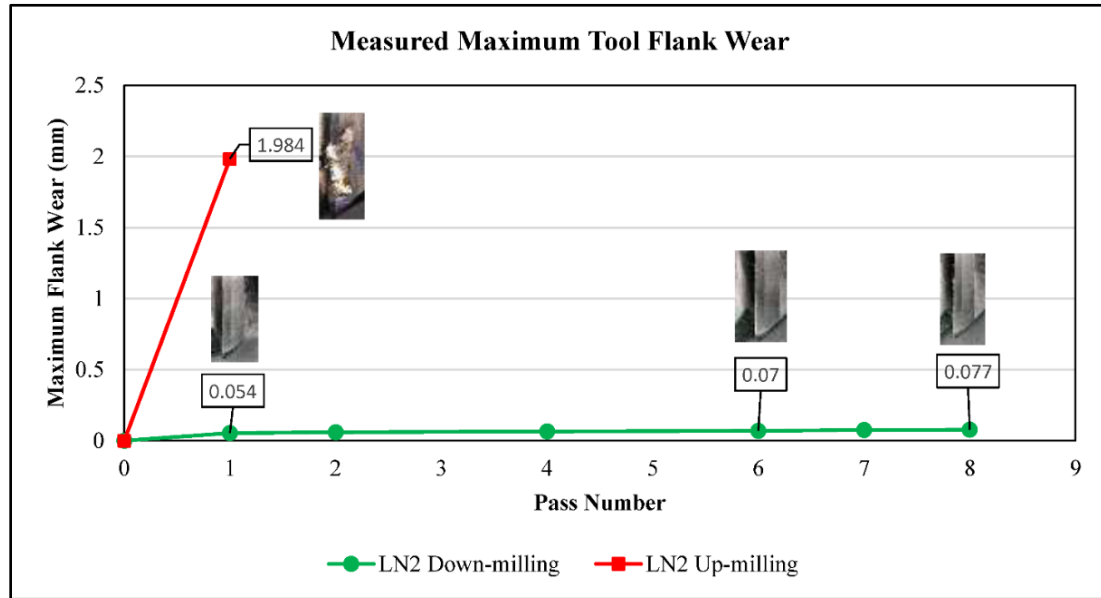


Figure 22: Maximum flank wear vs number of passes (machined length) for up and down-milling under LN₂ cooling strategy

The plot shows that the tool worn out during the 1st pass only using LN₂ up-milling method. Although, LN₂ cooling helps in reducing the temperature of the cutting zone, the combination of LN₂ with up-milling method yielded the highest tool wear among all combinations of milling methods and cooling strategies. The initial tool flank face and maximum flank wear for MQL up and down-milling method is shown in Figure 23. Although liquid nitrogen cooled down the work-piece and cutting zone temperature, the application of liquid nitrogen increased the hardness of the workpiece and did not provide any lubrication to the cutting zone at all. Also, liquid nitrogen was not very much effective in carrying the hot chips away from the cutting zone which further increased the cutting zone temperature. Thus, built-up edge started forming on the tool flutes at extremely high temperature. This led to drastic increase of tool wear and tool edges burnt completely. The tool started rubbing the workpiece instead of cutting as the

tool had undergone complete plastic deformation. Thus, the machining was terminated after 1st pass only.

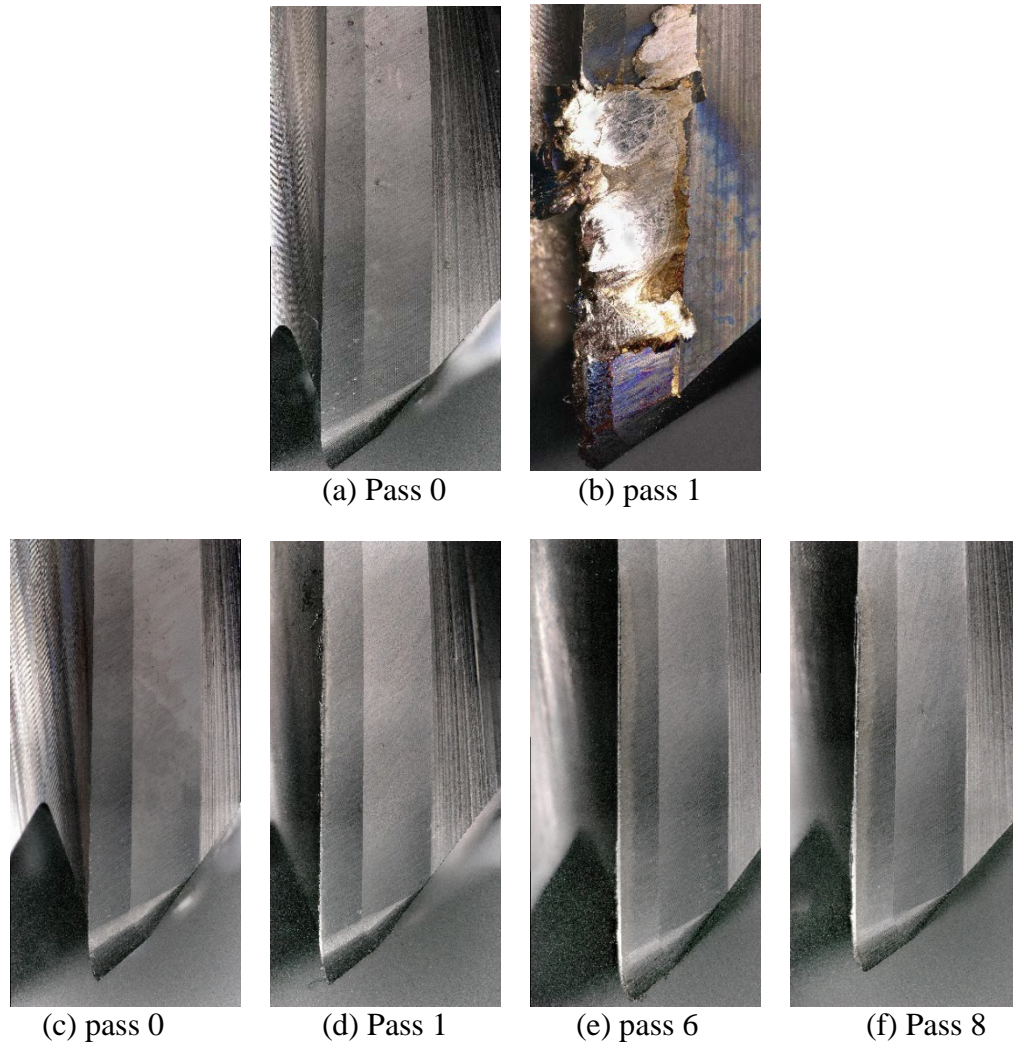


Figure 23: Maximum flank wear for up and down-milling under LN₂ cooling strategy. LN₂ up-milling at (a) pass 0 and (b) pass 1 and, LN₂ down-milling at (c) pass 0, (d) pass 1, (e) pass 6 and (f) pass 8

In case of LN₂ down-milling, the tool wear caused by abrasion, was very gradual. LN₂ cooling effectively lowered the temperature of the cutting zone and due to down-milling operation, discontinuous chips were produced which were easier to be removed by LN₂ cooling.

3.3.2. Chip Morphology. Figure 24 shows images of chips after 1st pass for LN₂ up-milling and free surface of chips after 1st, 6th and 8th pass for LN₂ down-milling

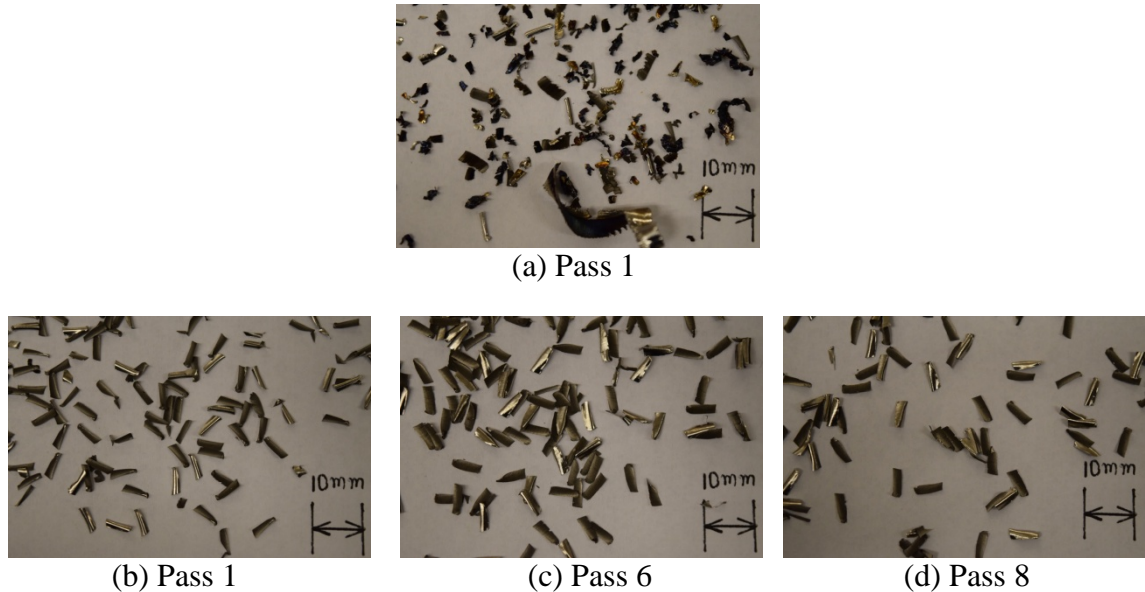


Figure 24: Images of chips for up and down-milling under LN₂ cooling strategy. LN₂ up-milling at (a) pass 1 and LN₂ down-milling at (d) pass 1, (e) pass 6 and (f) pass 8

Figure 25 shows the free and back surfaces of chips after 1st pass for LN₂ up-milling and free surface of chips after 1st, 6th and 8th pass for LN₂ down-milling. The cutting forces and vibrations in 1st pass of LN₂ were very high and the chips were highly irregular with reddish brown and dark in color as seen from Figure 24 (a) and 25 (a). Due to the nature of chips formed in machining Inconel 718 using down-milling, liquid nitrogen was very effective till 8 passes. During down-milling, abrasion of the tool adjacent to the cutting edge can be seen from Figure 23 (d – f), which further increased with number of passes. To check the effect of abrasion on tool life due to its growth around the cutting edge, two more passes were machined under LN₂ down-milling. The tool deformed plastically during the 10th pass while machining under LN₂. As the

comparison was made for 8 passes, the 9th and 10th pass were not shown here in the comparison. Some tear occurred on the end edge of the chip in down-milling. Also, width of chip increased with progression of time due to increase in wear.

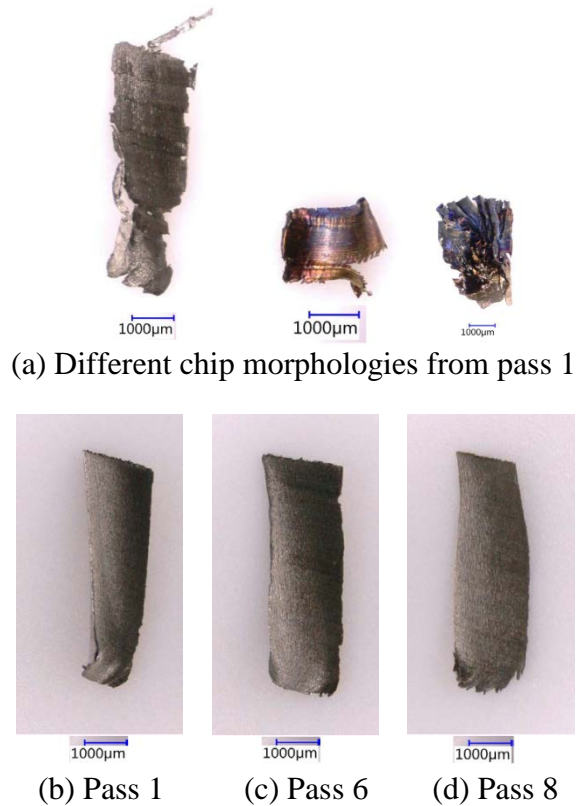


Figure 25: Free and back surface of chips for up-milling and free surface of chips for down-milling under LN₂ cooling strategy. (a) Free and back surface of chips for LN₂ up-milling at pass 1 and, free surface of chips for LN₂ down-milling at (d) pass 1, (e) pass 6 and (f) pass 8

Figure 26 shows the chip lengths from LN₂ up-milling and down-milling along with calculated chip length. The chip length from the only single pass of LN₂ up-milling was higher as compared to all passes of down-milling. The chip length in down-milling did not increase much during machining. This may be due to the fact that under LN₂ down-milling, chip breakability was better than in up-milling.

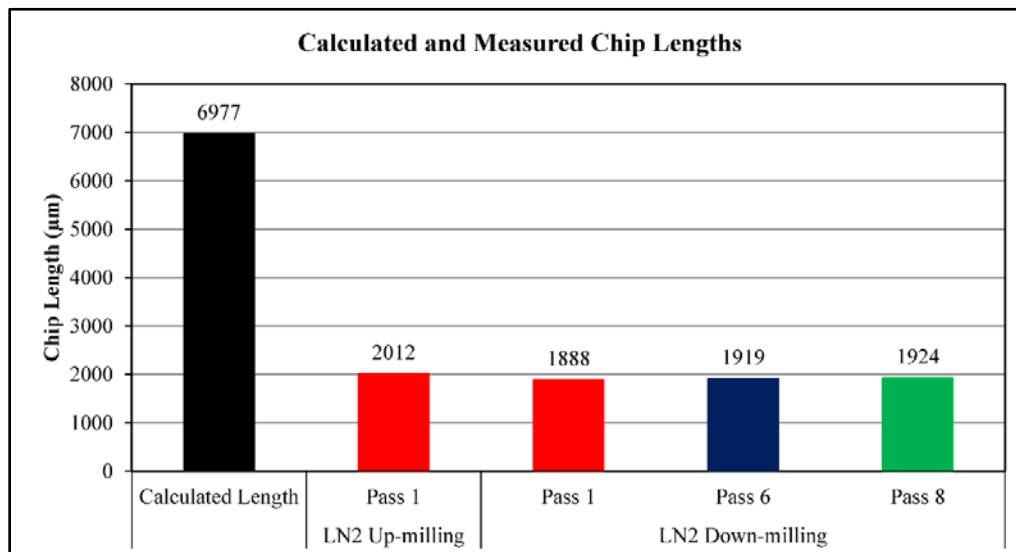


Figure 26: Calculated and measured chip lengths vs number of passes (machined length) and milling methods under LN₂ cooling strategy

3.4. MAXIMUM FLANK WEAR AND CHIP MORPHOLOGY FOR UP AND DOWN-MILLING METHOD USING COMBINED (MQL + LN₂) STRATEGY

3.4.1. Maximum Flank Wear. Figure 27 shows the plot for maximum flank wear vs number of passes for up and down-milling methods under (MQL + LN₂) cooling.

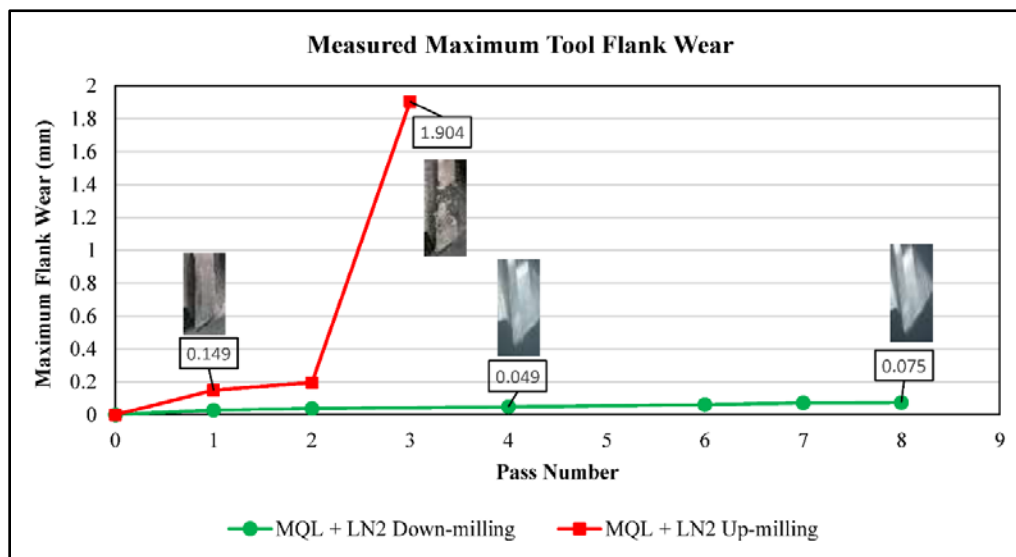


Figure 27: Maximum flank wear vs number of passes (machined length) for up and down-milling under combined (MQL + LN₂) cooling strategy

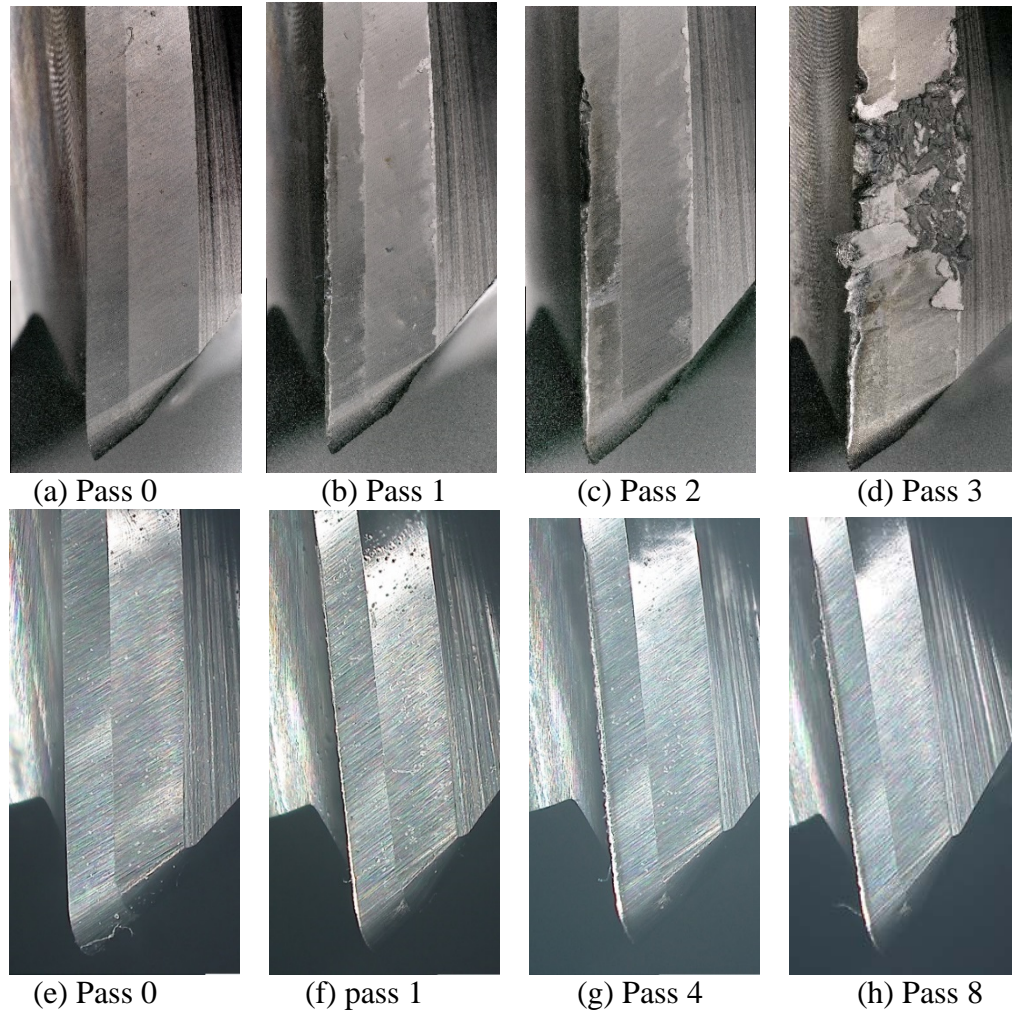


Figure 28: Measured maximum flank wear for up and down-milling under MQL + LN₂ cooling strategy. MQL + LN₂ up-milling at (a) pass 0, (b) pass 1, (c) pass 2 and (c) pass 3 and, MQL + LN₂ down-milling at (e) pass 0, (f) pass 1, (g) pass 4 and (h) pass 8

The plot shows that the maximum flank wear was less in (MQL + LN₂) down-milling method throughout the machining length. The initial tool flank land and maximum flank wear for combined (MQL + LN₂) up and down-milling method is shown in Figure 28. As can be seen from Figures 27 and 28, the tool worn out completely in 3rd pass in up-milling when machined using combined (MQL + LN₂) cooling. Moreover, a severe chipping and flanking can be seen at the tool edge from the 1st pass during up-milling, which kept on increasing and eventually the tool plastically deformed during 3rd

pass as can be seen from Figure 28 (d). Further machining was terminated as the tool had exceeded its life. Due to addition of lubrication by MQL in up-milling operation, the tool survived 3 passes as compared to LN₂ alone where the tool worn out completely in its 1st pass only. In the case of down-milling, a uniform tool wear was seen throughout the machining. Some signs of tool edge burning can also be seen from the 4th pass onwards. This might have happened due to increase in temperature due to increase in hardness of the tool because of use of LN₂, which in turn, increased the impact forces at the entry of the flute into the workpiece in down-milling operation.

3.4.2. Chip Morphology. Figure 29 shows images of chips and Figure 30 shows the free surface of chips after 1st, 2nd and 3rd pass for (MQL + LN₂) up-milling and after 1st, 4th and 8th pass for combined (MQL + LN₂) down-milling.

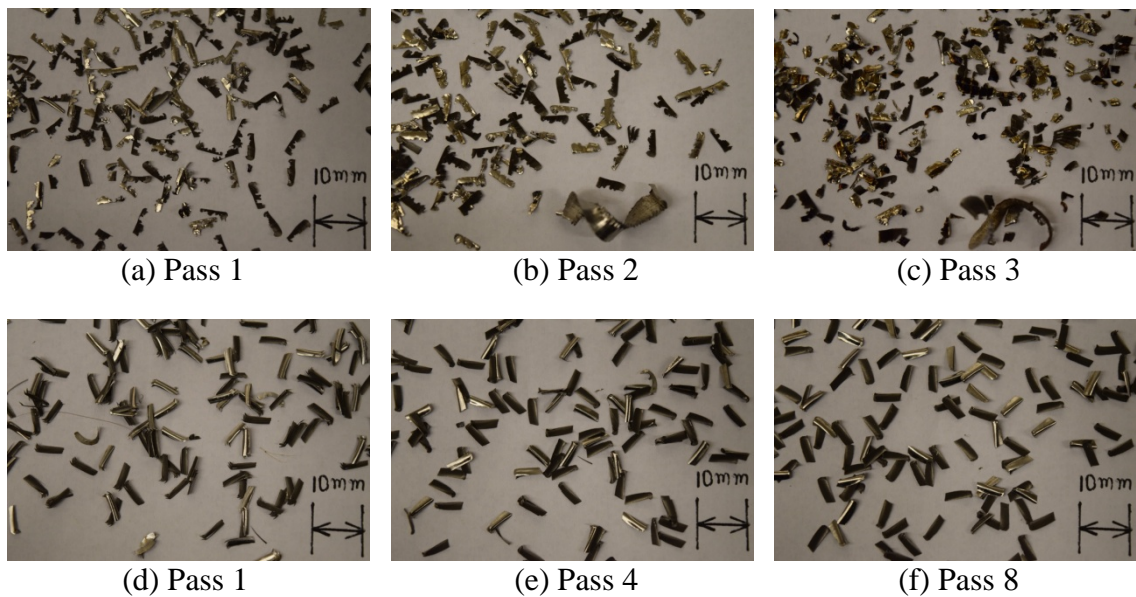


Figure 29: Images of chips for up and down-milling under MQL + LN₂ cooling strategy. MQL + LN₂ up-milling at (a) pass 1, (b) pass 2 and (c) pass 3 and MQL + LN₂ down-milling at (d) pass 1, (e) pass 3 and (f) pass 8

The chips in combined (MQL + LN₂) up-milling were very irregular and torn along the end edge. Due to high cutting forces and vibrations, the chips generated were highly irregular in shape as can be seen from Figures 29 (a - c) and 30 (a - c). The down-milling operation yielded chips with regular shapes and of almost uniform width.

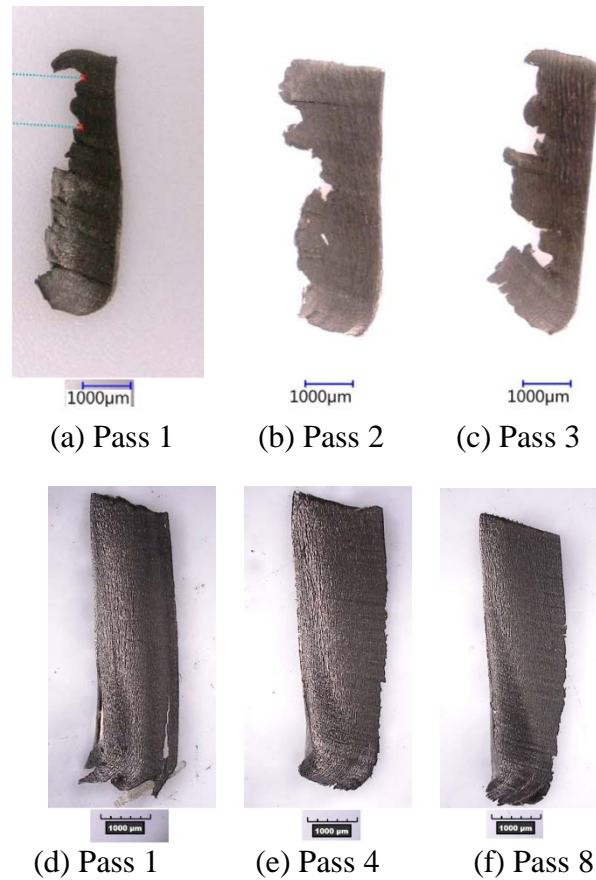


Figure 30: Free surface of chips for up and down-milling under combined (MQL + LN₂) cooling strategy. Combined (MQL + LN₂) up-milling at (a) pass 1, (b) pass 2 and (c) pass 3 and, (MQL + LN₂) down-milling at (d) pass 1, (e) pass 3 and (f) pass 8

Figure 31 shows the calculated chip length and measured lengths of chips for up and down-milling using combined (MQL + LN₂) cooling strategy. Again, up-milling provided longer chip as compared to down-milling during each passes and chip length increased with the progression of tool wear (machined passes).

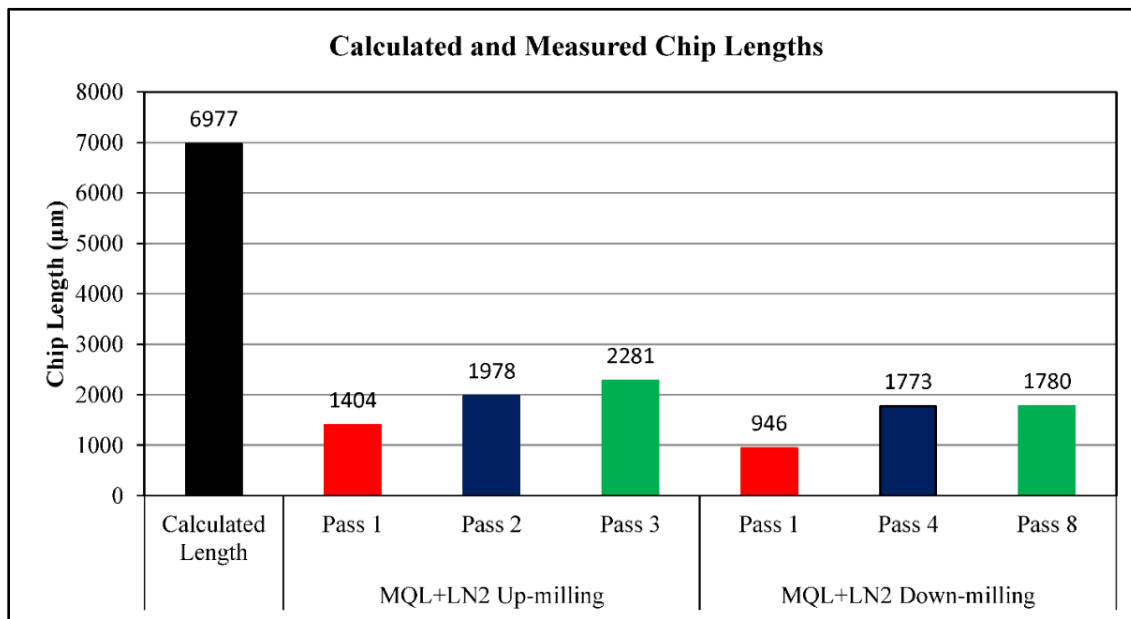


Figure 31: Calculated and measured chip lengths vs number of passes (machined length) and milling methods under MQL + LN₂ cooling strategy

Pass 1 of down-milling provided the shortest chip length in all cooling strategies and milling methods. This may be due to fact that the combination of down-milling method and combined (MQL + LN₂) cooling strategy was better in chip breakability and lubricated the cutting zone effectively.

3.5. COMPARITIVE EVALUATION OF AVERAGE SURFACE ROUGHNESS UNDER FOUR COOLING STRATEGIES FOR UP AND DOWN-MILLING METHODS

Figure 32 shows the average surface roughness under all four cooling strategies for up and down-milling operations. The lowest average surface roughness was generated under emulsion cooling with up-milling operation among all cooling strategies and milling methods. During up-milling operation, other cooling strategies were not as effective in chip removal and lowering the temperature of the cutting zone as emulsion cooling, thus, they were not able to create as smoother surface as emulsion cooling.

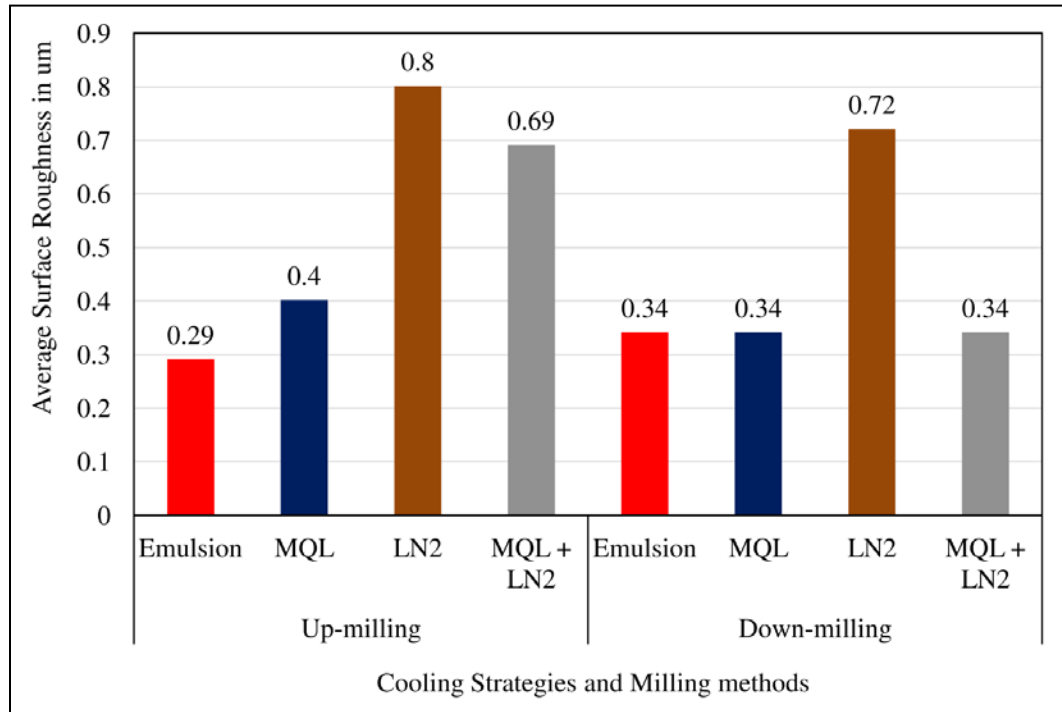


Figure 32: Surface roughness vs cooling strategies and milling methods

The application of cryogenic cooling increases the hardness of workpiece material and end-mill, exacerbating surface roughness due to increase in cutting forces and generated the highest surface roughness in both up-milling and down-milling operations. Emulsion cooling, MQL and combined (MQL + LN₂) cooling strategies generated the second lowest surface roughness as the chips were very easy to be removed from the cutting zone which made the machining smoother and hence, surface roughness was less.

3.6. COMPARATIVE INVESTIGATION OF MAXIMUM FLANK WEAR UNDER FOUR COOLING STRATEGIES FOR UP AND DOWN METHODS

Figure 33 shows the plot for maximum flank wear versus machining pass (machined length) for up-milling method under all four cooling strategies at a cutting speed of 45 m/min (1127 rpm) and 114.5 mm/min (4.510 ipm) feed-rate. As can be seen

in Figure 33, only emulsion cooling was able to machine all 8 passes using up-milling method. Although, even emulsion cooling was also not able to remove the segmented chip from the cutting zone because it was not completely detached from the material, the application of emulsion lowered the temperature of the continuous chip along at the cutting zone. Also, chips other than continuous chip were removed quickly using emulsion flood cooling. The continuous serrated chip obtained during each pass caused the chipping of the tool flutes under emulsion cooling also. On the other hand, LN₂ cooling increased the hardness of the workpiece and tool and, also was least efficient in chip removal. Due to that, the tool deformed plastically during first pass only. MQL provided better lubrication to the cutting zone but, due to presence of continuous chip and high rate of chipping, tool could not last more than 4 passes. Combined (MQL+LN₂) cooling increased tool life from 1 pass in LN₂ to 3 passes. The main causes of tool wear in up-milling operation were abrasion, chipping, and plastic deformation.

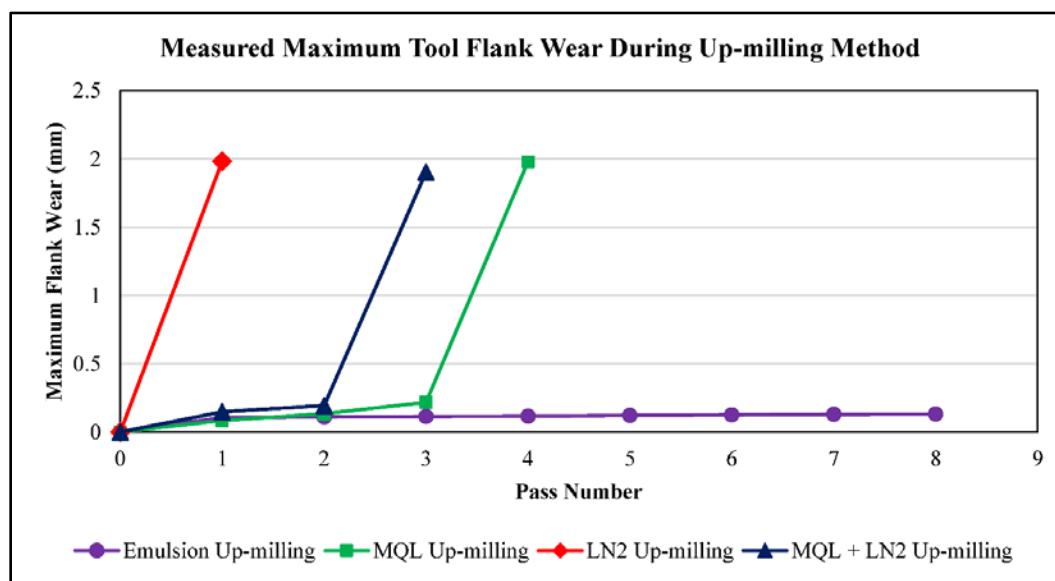


Figure 33: Maximum flank wear vs machining passes (machined length) for up-milling method under four cooling strategies

Figure 34 shows the plot for maximum flank wear versus machining pass (machined length) for down-milling method under four cooling strategies.

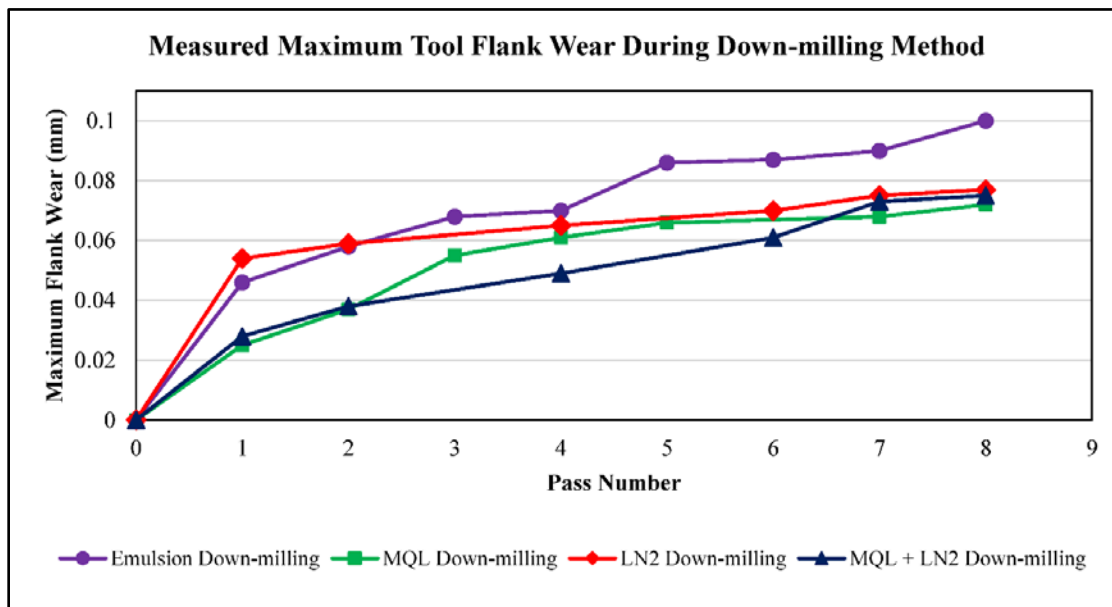


Figure 34: Maximum flank wear vs machining passes (machined length) for down-milling method under four cooling strategies

From the Figure, it can be seen that the emulsion cooling generated the highest flank wear. During the first pass, LN₂ cooling generated the highest flank wear but the trend changed and flank wear under emulsion cooling exceeded the flank wear under all other cooling strategies. Until 6th pass, combined (MQL + LN₂) cooling provided the least value of maximum flank wear, after which MQL cooling generated the least maximum flank wear at 7th and 8th passes. In the case of LN₂ cooling, maximum flank wear remained second highest when machining under down-milling method. The MQL cooling strategy generated the least value of maximum flank wear followed by combined (MQL+LN₂) among all cooling strategies and milling methods. Tool wear in down-milling operation was mainly due to abrasion.

3.7. COMPARATIVE INVESTIGATION OF CALCULATED AND MEASURED CHIP LENGTHS FOR LAST PASS UNDER FOUR COOLING STRATEGIES FOR UP-MILLING AND DOWN-MILLING METHODS

Figure 35 shows the plot for calculated and measured chip lengths from their respective last passes under four cooling strategies using up-milling and down-milling methods.

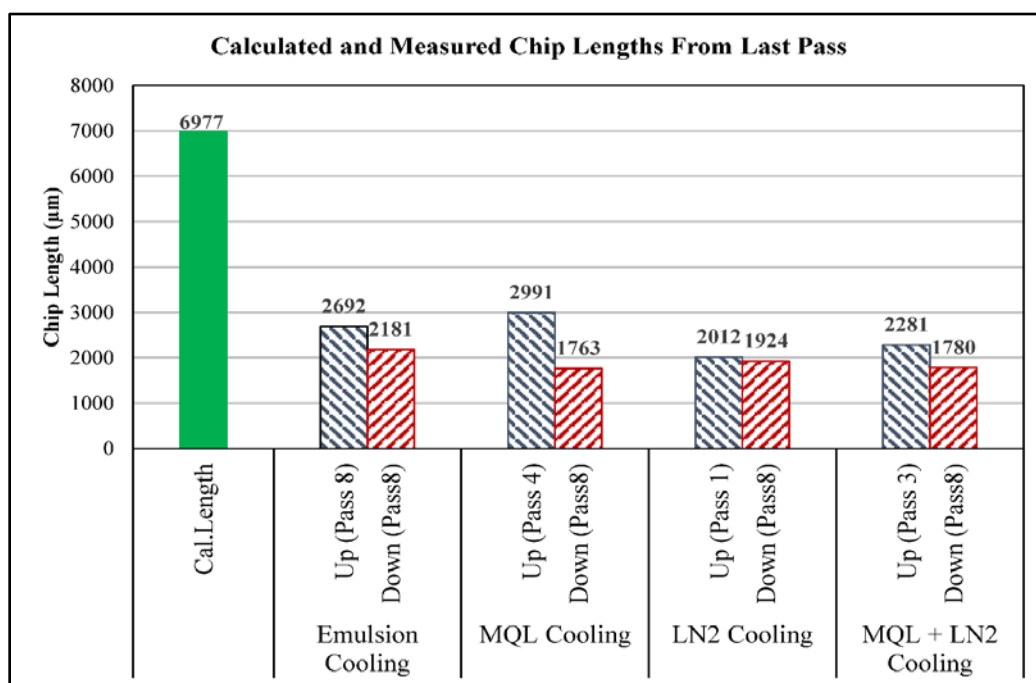


Figure 35: Calculated chip length and measured chip lengths vs milling methods and cooling strategies for for last passes

In up-milling operation, MQL cooling generated the highest chip length whereas, LN₂ cooling generated the lowest chip length during their respective last passes while machining Inconel-718. In MQL up-milling, the cutting zone temperature increased drastically during the last pass. The increase in temperature led the chips to elongate before they got sheared off. During LN₂ up-milling, the tool deformed plastically during its 1st pass due to very high temperature of the cutting zone. LN₂ cooling immediately

cooled down the red hot chips which broke the chips into parts. During down-milling, MQL cooling generated the lowest chip length followed by combined (MQL + LN₂) cooling. The combined cooling provided sufficient lubrication as well as cooling to the cutting zone. Thus, the chips were not pulled by the tool flutes before they got removed from the workpiece by cutting flutes and remained shorter. The shorter chips are easy to be removed by the cooling strategies from the cutting zone than longer chips which otherwise increase the cutting zone temperature and hence, tool wear.

4. CONCLUSIONS

This research investigated the effects of milling methods (Up-milling and Down-milling) and four cooling strategies (Conventional emulsion flood cooling, MQL, LN₂ and combined (MQL+LN₂)) on tool wear, chip morphology and surface roughness during peripheral end-milling of Inconel-718 alloy using 4-flutes uncoated solid carbide bull-nose helical end mills. From the results obtained, the following conclusions can be made:

1. Down-milling generates lower levels of flank wear than up-milling, hence improves machinability of Inconel 718.
2. Tool wear mechanism in up-milling was adhesion and failure modes were chipping and plastic deformation, causing high tool wear, while abrasion was the mechanism of tool wear in down-milling causing progressive tool wear.
3. Up-milling operation generates irregular and longer chips with mostly torn edges, whereas down-milling generates shorter chips with sharp and uniform edges.
4. Up-milling generates a segmented chip, with saw-tooth shape for each machining pass along with other chips under all cooling strategies, whereas down-milling operation generates discontinuous serrated chips under all cooling strategies.

5. Emulsion up-milling generated lowest surface roughness, whereas emulsion, MQL and combined (MQL+LN₂) generated equal and second lowest surface roughness.
6. Down-milling with MQL cooling generated lowest flank wear among all combinations of cooling strategies and milling methods and is recommended for machining Inconel-718 alloys.

ACKNOWLEDGEMENTS

The financial support from the Intelligent System Centre (ISC) of the Missouri University of Science and Technology is greatly acknowledged. The financial assistance provided in the form of Graduate Teaching Assistantship by the Department of Mechanical and Aerospace Engineering at Missouri University of Science and Technology is also greatly acknowledged

REFERENCES

- Ahmad Yasir, M. S. et al. (2009) 'Machinability of Ti-6Al-4V Under Dry and Near Dry Condition Using Carbide Tools', *The Open Industrial and Manufacturing Engineering Journal*, 2(April), pp. 1–9. doi: 10.2174/1874152500902010001.
- Aramcharoen, A. and Chuan, S. K. (2014) 'An experimental investigation on cryogenic milling of inconel 718 and its sustainability assessment', in *Procedia CIRP*, pp. 529–534. doi: 10.1016/j.procir.2014.03.076.
- Bouzakis, K. D. et al. (2008) 'Increasing tool life by adjusting the milling cutting conditions according to PVD films' properties', *CIRP Annals - Manufacturing Technology*, 57(1), pp. 105–108. doi: 10.1016/j.cirp.2008.03.070.
- Cui, X. et al. (2016) 'Chip formation and its effects on cutting force, tool temperature, tool stress, and cutting edge wear in high- and ultra-high-speed milling', *International Journal of Advanced Manufacturing Technology*, 83(1–4), pp. 55–65. doi: 10.1007/s00170-015-7539-7.
- Dhananchezian, M. and Pradeep Kumar, M. (2011) 'Cryogenic turning of the Ti-6Al-4V alloy with modified cutting tool inserts', *Cryogenics*, 51(1), pp. 34–40. doi: 10.1016/j.cryogenics.2010.10.011.

- Dhar, N. R., Ahmed, M. T. and Islam, S. (2007) 'An experimental investigation on effect of minimum quantity lubrication in machining AISI 1040 steel', *International Journal of Machine Tools and Manufacture*, 47(5 SPEC. ISS.), pp. 748–753. doi: 10.1016/j.ijmachtools.2006.09.017.
- Ezugwu, E. O. and Wang, Z. M. (1997) 'Titanium alloys and their machinability—a review', *Journal of Materials Processing Technology*, 68(3), pp. 262–274. doi: 10.1016/S0924-0136(96)00030-1.
- Fallböhmer, P. et al. (2000) 'High-speed machining of cast iron and alloy steels for die and mold manufacturing', *Journal of Materials Processing Technology*, 98(1), pp. 104–115. doi: 10.1016/S0924-0136(99)00311-8.
- Fang, N. and Wu, Q. (2009) 'A comparative study of the cutting forces in high speed machining of Ti-6Al-4V and Inconel 718 with a round cutting edge tool', *Journal of Materials Processing Technology*, 209(9), pp. 4385–4389. doi: 10.1016/j.jmatprotec.2008.10.013.
- Hadi, M. A. et al. (2013) 'Comparison between up-milling and down-milling operations on tool wear in milling Inconel 718', *Procedia Engineering*. Elsevier B.V., 68, pp. 647–653. doi: 10.1016/j.proeng.2013.12.234.
- Kim, S. W. et al. (2001) 'Evaluation of machinability by cutting environments in high-speed milling of difficult-to-cut materials', *Journal of Materials Processing Technology*, 111(1–3), pp. 256–260. doi: 10.1016/S0924-0136(01)00529-5.
- Krain, H. R., Sharman, A. R. C. and Ridgway, K. (2007) 'Optimisation of tool life and productivity when end milling Inconel 718TM', *Journal of Materials Processing Technology*, 189(1–3), pp. 153–161. doi: 10.1016/j.jmatprotec.2007.01.017.
- Li, H. Z., Zeng, H. and Chen, X. Q. (2006) 'An experimental study of tool wear and cutting force variation in the end milling of Inconel 718 with coated carbide inserts', *Journal of Materials Processing Technology*, 180(1–3), pp. 296–304. doi: 10.1016/j.jmatprotec.2006.07.009.
- Liao, Y. S., Lin, H. M. and Wang, J. H. (2008) 'Behaviors of end milling Inconel 718 superalloy by cemented carbide tools', *Journal of Materials Processing Technology*, 201(1–3), pp. 460–465. doi: <http://dx.doi.org/10.1016/j.jmatprotec.2007.11.176>.
- Musfirah, A. H., Ghani, J. A., & Haron, C. H. C. (2017). Tool wear and surface integrity of inconel 718 in dry and cryogenic coolant at high cutting speed. *Wear*, 376–377, 125–133. <https://doi.org/10.1016/j.wear.2017.01.031>
- Obikawa, T. et al. (2008) 'Micro-liter lubrication machining of Inconel 718', *International Journal of Machine Tools and Manufacture*, 48(15), pp. 1605–1612. doi: 10.1016/j.ijmachtools.2008.07.011.

- Özel, T. et al. (2010) 'Investigations on the effects of multi-layered coated inserts in machining Ti-6Al-4V alloy with experiments and finite element simulations', *CIRP Annals - Manufacturing Technology*, 59(1), pp. 77–82. doi: 10.1016/j.cirp.2010.03.055.
- Patwari, M. A. U., Amin, A. K. M. N. and Faris, W. (2010) 'Identification of Instabilities of the Chip Formation and It's Prediction Model During End Milling of Medium Carbon Steel (S45C)', *American Journal of Engineering and Applied Sciences*, 3(1), pp. 193–200. doi: 10.3844/ajeassp.2010.193.200.
- Ravi, S. and Pradeep Kumar, M. (2011) 'Experimental investigations on cryogenic cooling by liquid nitrogen in the end milling of hardened steel', *Cryogenics*, 51(9), pp. 509–515. doi: 10.1016/j.cryogenics.2011.06.006.
- Shokrani, A., Dhokia, V., & Newman, S. T. (2016). Investigation of the effects of cryogenic machining on surface integrity in CNC end milling of Ti-6Al-4V titanium alloy. *Journal of Manufacturing Processes*, 21, 172–179. <https://doi.org/10.1016/j.jmapro.2015.12.002>
- Shokrani, A., Dhokia, V., & Newman, S. T. (2017). Hybrid Cooling and Lubricating Technology for CNC Milling of Inconel 718 Nickel Alloy. *Procedia Manufacturing*, 11, 625–632. <https://doi.org/10.1016/j.promfg.2017.07.160>
- Su, Y. et al. (2006) 'An experimental investigation of effects of cooling/lubrication conditions on tool wear in high-speed end milling of Ti-6Al-4V', *Wear*, 261(7–8), pp. 760–766. doi: 10.1016/j.wear.2006.01.013.
- Su, Y. et al. (2007) 'Refrigerated cooling air cutting of difficult-to-cut materials', *International Journal of Machine Tools and Manufacture*, 47(6), pp. 927–933. doi: 10.1016/j.ijmachtools.2006.07.005.
- Su, Y., He, N. and Li, L. (2010) 'Effect of Cryogenic Minimum Quantity Lubrication (CMQL) on Cutting Temperature and Tool Wear in High-Speed End Milling of Titanium Alloys', *Applied Mechanics and Materials*, 34–35, pp. 1816–1821. doi: 10.4028/www.scientific.net/AMM.34-35.1816.
- Sun, J. and Guo, Y. B. (2008) 'A new multi-view approach to characterize 3D chip morphology and properties in end milling titanium Ti-6Al-4V', *International Journal of Machine Tools and Manufacture*, 48(12–13), pp. 1486–1494. doi: <http://dx.doi.org/10.1016/j.ijmachtools.2008.04.002>.
- Tian, X. et al. (2013) 'Effect of cutting speed on cutting forces and wear mechanisms in high-speed face milling of Inconel 718 with Sialon ceramic tools', *International Journal of Advanced Manufacturing Technology*, 69(9–12), pp. 2669–2678. doi: 10.1007/s00170-013-5206-4.

- Ulutan, D. et al. (2015) 'Comparison and Cost Optimization of Solid Tool Life in End Milling Nickel-Based Superalloy', *Procedia Manufacturing*, 1, pp. 522–533. doi: 10.1016/j.promfg.2015.09.024.
- Wang, X., Huang, C., Zou, B., Liu, G., Zhu, H., & Wang, J. (2017). Experimental study of surface integrity and fatigue life in the face milling of inconel 718. *Frontiers of Mechanical Engineering*, 13(2), 1–8. <https://doi.org/10.1007/s11465-018-0479-9>
- Yuan, S. M. et al. (2011) 'Effects of cooling air temperature on cryogenic machining of Ti-6Al-4V alloy', *Journal of Materials Processing Technology*. Elsevier B.V., 211(3), pp. 356–362. doi: 10.1016/j.jmatprotec.2010.10.009.
- Zhang, S., Li, J. F. and Wang, Y. W. (2012) 'Tool life and cutting forces in end milling Inconel 718 under dry and minimum quantity cooling lubrication cutting conditions', *Journal of Cleaner Production*, 32, pp. 81–87. doi: 10.1016/j.jclepro.2012.03.014.
- Zhao, W., He, N. and Li, L. (2007) 'High Speed Milling of Ti6Al4V Alloy with Minimal Quantity Lubrication', *Key Engineering Materials*, 375–376, pp. 435–439. doi: 10.4028/www.scientific.net/KEM.329.663.
- Zhu, Z. et al. (2016) 'Investigation on the influence of tool wear upon chip morphology in end milling titanium alloy Ti6Al4V', *International Journal of Advanced Manufacturing Technology*, 83(9–12), pp. 1477–1485. doi: 10.1007/s00170-015-7690-1.

IV. EFFECTS OF TOOL COATINGS AND COOLING STRATEGIES ON TOOL WEAR, CHIP MORPHOLOGY AND SURFACE ROUGHNESS IN HIGH SPEED DOWN-MILLING OF INCONEL 718

A. Chukwujekwu Okafor*, Paras Mohan Jasra
Computer Numeric Control and Virtual Manufacturing Laboratory
Department of Mechanical and Aerospace Engineering
Missouri University of Science and Technology
327 Toomey Hall, Rolla, MO-65409-0050, USA
Email: okafor@mst.edu

ABSTRACT

This paper presents the results of experimental investigation of the effects of tool coatings (AlTiN and GMS^2) and three cooling strategies [Minimum Quantity Lubrication (MQL), Liquid Nitrogen (LN_2) and Combined (MQL+ LN_2)] on tool wear, chip morphology and surface roughness in down-milling of Inconel-718 under high-speed machining using carbide end-mills to improve machinability and reduce cost. Tool wear mechanism under MQL and combined (MQL+ LN_2) strategies is abrasion, and adhesion under LN_2 cooling. Using LN_2 cooling alone is not recommended for machining Inconel-718 as it generates rapid tool wear. Results show that GMS^2 coated end-mills under MQL cooling strategy generated lowest tool wear, followed by AlTiN coated end-mills under (MQL+ LN_2) cooling strategy and are recommended for machining Inconel-718. AlTiN coated end-mills under MQL cooling generated lowest surface roughness. GMS^2 coated end-mills generate shorter chips under LN_2 and combined (MQL+ LN_2) cooling, whereas AlTiN coated end-mills generate chips with shorter length under MQL cooling.

Keywords: High speed machining; Inconel 718; Tool wear; Cooling strategy; Surface roughness; Chip Morphology

1. INTRODUCTION

Inconel 718 superalloy is used extensively in aerospace and nuclear industries for components such as turbine blades, low and high-pressure disc compressors used in high temperature, high load and corrosion resistance compartments of jet and gas turbine engines, due to its excellent properties such as: high strength-to-weight ratio, ability to retain its properties at high temperatures, high corrosion and creep resistance (Ezugwu and Wang, 1997). However, Inconel 718 is characterized as a very “difficult-to-cut” material, because it poses severe problems during machining. Enormous amount of heat is generated in the cutting zone due to high friction between the tool-chip interface and tool-workpiece interface and is not removed as quickly as it is generated due to its low thermal conductivity. Therefore the heat is mostly concentrated on the tool cutting edges, causing severe tool wear. Also, due to high temperature and pressure at the cutting zone, and its high chemical affinity with many cutting tool materials, some chip fragments from the workpiece get welded on the cutting edges of the tool to form built-up edge (BUE), which further exacerbates tool wear. Its good mechanical strength and ability to work harden at elevated temperatures leads to high cutting forces which further leads to high tool wear. End-milling is a widely used machining operation due to its versatility. Its applications may range from aerospace and automotive industries to small tool and die shops, as it can be used for milling many features like peripheral, slot or face milling. Some problems encountered while machining using end-milling operations are high

cutting forces, high cutting temperature, rapid tool wear, tool breakage, and chatter.

These problems associated with end-milling are further exacerbated while machining difficult-to-cut metals such as Inconel 718 because the desired properties of this difficult-to-cut metal become disadvantage while machining them.

Application of coolants and lubricants play an important role in addressing these problems, as they reduce cutting temperature, friction and tool wear, cutting force/power consumed, improve surface roughness, and hence, improve machinability. Mineral-based conventional cutting fluids commonly used in most industries are expensive, environmentally unfriendly and difficult to dispose and, cause health hazards. Due to the problems mentioned above, care must be taken to select appropriate machining parameters when machining difficult-to-cut metals. Tool wear is an important factor affecting machinability of Inconel 718, as it cannot be avoided during machining, improvement in tool wear helps to reduce the cutting zone temperature, cutting forces and improving surface roughness. Zhang et al. (2012) reported 1.57 times improvement in tool life under Minimum Quantity Cooling Lubrication (MQCL) strategy than dry cutting due to significant reduction in tool wear in end-milling of Inconel 718. Ravi and Kumar (2011) reported improvement in flank wear with cryogenic cooling by 29-34 % and 10-12 % and improvement in surface roughness by 33-40% and 25-29% over dry and wet cooling respectively in end-milling of hardened steel using carbide insert. Also, they reported decrease in cutting forces and cutting temperature using cryogenic cooling over dry and wet cooling. Kim et al. (2001) reported improvement in flank wear and tool life using compressed chilly-air coolant over dry and flood cooling in machining difficult-to-cut materials of different hardness using coated tools. Özel et al. (2010) investigated the

effects of uncoated, cBN coated, TiAlN coated and cBN+ TiAlN coated single layer and multi-layer coated tungsten carbide inserts in terms of tool wear and cutting forces in turning of Ti-6Al-4V. They reported that tool wear contours and temperature distribution showed some advantage of using coated inserts over uncoated. They concluded that cBN coated tungsten carbide inserts generated lowest tool wear. Dhananchezian and Kumar (2011) reported improvement in tool wear, cutting temperature, cutting force and surface roughness with cryogenic cooling over wet cooling in turning of Ti-6Al-4V using coated carbide inserts. Su et al. (2006) investigated the effects of various cooling/lubrication conditions (dry, flood, nitrogen gas and oil mist cooling, compressed cold nitrogen gas (CCNG) cooling at 0 and -10°C and, compressed cold nitrogen gas and oil mist (CCNGOM) cooling at -10°C) on tool life in high-speed end-milling of Ti-6Al-4V. They reported the longest tool life using CCNGOM at -10°C. Su et al. (2010) further investigated the effects of dry milling, refrigerated air cutting at two temperatures (-10°C and -20°C) and Cryogenic Minimum Quantity Lubrication (CMQL) at two temperatures (-10°C and -20°C) on tool wear and cutting temperature in high speed machining of Ti-6Al-4V. They reported the reduction in cutting zone temperature and tool wear using CMQL at -20°C.

End-mill coatings provide additional strength to the end-mill which helps in machining of difficult-to-cut metals. Jawaid et al (2000) while investigating the performance of PVD-TiN coated and CVD-TiCN + Al₂O₃ coated tools, reported improvement in performance using CVD coated tools than PVD coated tools in terms of volume of material removed and tool lives. They also reported the dominant wear pattern, failure modes and wear mechanism for both coated tools. Jawaid et al. (2001)

also compared the PVD TiN coated tools with uncoated tools and reported that at low speeds, uncoated tools performed better in face milling of Inconel 718 but TiN coated tools performed slightly better than uncoated tools at high speed. Kamata and Obikawa (2007) compared the performance of three coated carbide tools (TiCN/Al₂O₃/TiN (CVD), TiN/AlN super lattice (PVD) and TiAlN (PVD)) and three cooling strategies (dry, wet, MQL cooling) in terms of tool life and surface finish in finish turning of Inconel 718 at two cutting speeds of 1.0 m/s and 1.5 m/s. They reported that at a cutting speed of 1.0 m/s, TiCN/Al₂O₃/TiN (CVD) coated tools with MQL cooling yielded best performance (second longest tool life and second best surface finish), followed by TiN/AlN super lattice (PVD) with MQL cooling (third longest tool life and best surface finish). Wang et al. (2015) reported that carbide tools coated with TiSiN coating yielded higher life than carbide tools coated with TiAlN coating when compared the performance of TiSiN and TiAlN carbide tools coated using PVD method in high speed machining of hardened steel (SKD11/ HRC 62, S136/ HRC 51).

It has been seen that using different combinations of machining parameters, cooling strategies and milling methods produce different chip morphologies. Thus, it becomes pertinent to analyze chip morphology while investigating tool wear, to understand the effects of specific cutting conditions on machinability of Inconel 718. These chips if not removed quickly, can increase the cutting zone temperature drastically and also interrupt the machining process, which may increase tool wear and hence, lead to tool failure and breakage. Liao et al. (2008) reported that cutting temperature and chip disposal as major problems encountered in high speed end-milling of Inconel 718. Researchers have put a lot of efforts to remove the chips quickly from the cutting zone

and to decrease the cutting zone temperature by improving the chip breakability and tool profiles, and by using different cooling strategies. Dhar et al. (2007) reported improvement in tool-chip interface temperature, average principle and auxiliary flank wear and, other machinability parameters using MQL machining over dry in turning of AISI-1040 steel. Aramcharoen and Chuan (2014) reported improvement in chip breakability, tool wear, machined surface quality and the contact friction between tool-chip interface using cryogenic cooling over dry and conventional oil based coolants in milling of Inconel 718. Yuan et al. (2011) reported improvement in cutting forces, tool wear, surface roughness and chip morphology with MQL with a cooling air at -15°C in milling of Ti-6Al-4V using uncoated cemented carbide inserts. They further reported that MQL with cooling air produced the shorter chips generated fewer chips curls. Obikawa et al. (2008) used a small specially designed nozzle to spray the small amount of lubrication called micro-liter lubrication, on the cutting zone and compared it to the ordinary MQL spraying in machining of Inconel 718. They reported that tool life increased using micro-liter lubrication as compared to ordinary lubrication. Cui et al. (2016) investigated the chip formation and its effects on output parameters in high speed and ultra-high speed machining of AISI H13 hardened steel at cutting speed range between 200 – 2000 m/min. They reported that with increase in cutting speed, the frequency of saw tooth, tool-chip contact length, average value of tool temperature and amplitude of tool stresses increased. The main tool wear pattern at higher speeds was flank wear and no wear appeared at rake face due to shorter tool-chip contact at higher speed of 2000 m/min. With an increased in cutting speed from 1550 m/min to 2000 m/min, chipping started occurring at tool edge. Sun and Guo (2008) provided a new

approach to characterize the chip morphology which included four surfaces (Top, Back, Free and Cross-section Surface) of the chips. Different characteristics were shown in each 3-D chip view in end-milling of Ti-6Al-4V using flood cooling. Zhu et al. (2016) investigated the relationship under which the chip segmentation degree became more serious with progression of tool wear and cutting vibrations. Patwari et al. (2010) presented the findings from experiment on instabilities in chip during its formation in machining medium carbon steel (S45C). Hadi et al. (2013) reported improvement in tool wear under down-milling method in ball nose end-milling of Inconel 718 using MQL cooling with PVD coated carbide inserts. They also mentioned predominant failure mode affecting the tool performance. Segmented chips with typical saw-tooth shape and discontinuous serrated chips were produced under up-milling and down-milling methods respectively. High speed machining (HSM) further helps increasing productivity, improving product quality and reducing manufacturing costs and is considered most efficient manufacturing technology (Fang and Wu, 2009). Abele and Fröhlich (2008) mentioned that high speed milling of Ti-6Al-4V increases the material removal rate. Due to that, the overall performance increases with high speed as compared to conventional machining. Safari et al. (2014) investigated the 3 cutting speeds (200, 250, 300 mm/min) in cryogenic high speed end-milling of Ti-6Al-4V. They reported least cutting force at 300 mm/min using coated and uncoated tools. Krain et al. (2007) while investigating the effect of various cutting parameters, tool materials and geometries on tool life, tool wear and productivity, concluded that no single material or geometry provided the best performance.

From above literature, it can be seen that there is no comprehensive study to investigate combined effects of cooling strategies (MQL, LN₂ and combined MQL + LN₂) and end-mill coatings (AlTiN coated and GMS² coated) on tool wear, chip morphology and surface roughness in high-speed cutting range of Inconel 718 alloy. The potential of combining two different cooling strategies using carbide end-mills at machining speed higher than current industry standards (Ulutan et al., 2015) for milling nickel-based superalloy using uncoated carbide end-mills has not been investigated. Although, limited literature is available to understand wear mechanism, failure modes and chip morphology of some of the difficult-to-cut metals having high cutting speed ranges titanium alloys as shown in Figure 1, but as mentioned by Fang and Wu (2009), that research findings of one material cannot be implemented on others in high speed machining as different materials involve different machining setups. The current work focuses on investigation of different cooling strategies and end-mill coatings to improve machinability of Inconel 718.

2. EXPERIMENTAL PLAN AND PROCEDURE

Peripheral high-speed end-milling tests were conducted on Cincinnati Milacron Sabre 750 Vertical Machining Centre (VMC), equipped with Acramatic 2100 CNC controller, using 4-flutes AlTiN coated and 7-flutes GMS² coated solid carbide end-mills of diameter 12.7 mm (0.5 inches). The detailed experimental plan for the investigation of the effects of cooling strategies, tool coatings and machining parameters using coated carbide helical bull-nose solid carbide end-mills is summarized in Table 1. All the experiments were performed at constant cutting speed of 1127 rpm (45 m/min), feed-rate

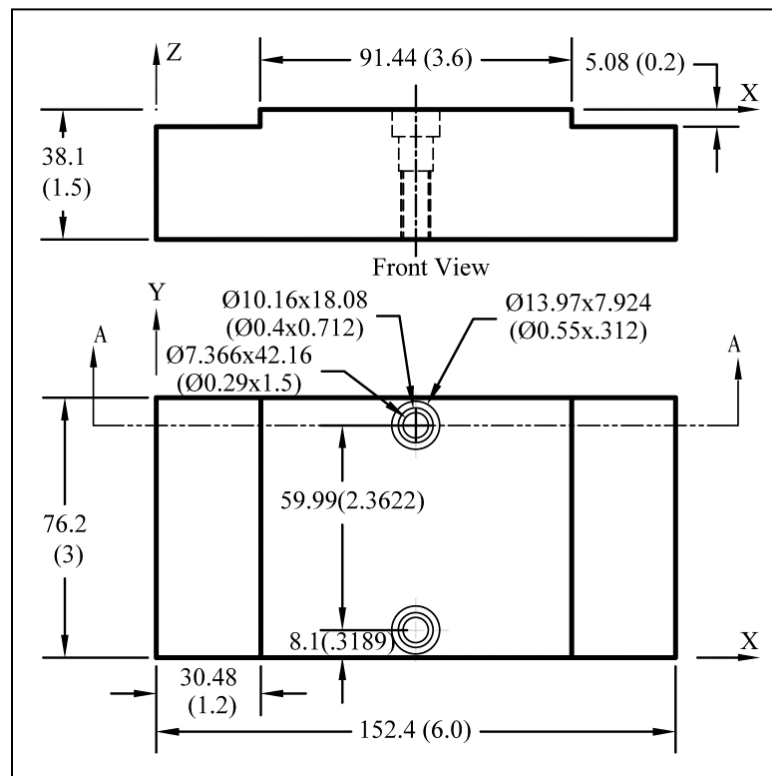
of 114.5 mm/min (4.510 ipm), axial depth of cut (a_a) of 5.08 mm (0.2 in) and radial depth of cut (a_r) of 3.81 mm (0.15 in) and were selected based on literature review and preliminary research investigation. Axial depth of cut (a_a), radial depth of cut (a_r) and feed per revolution (f_r) were kept constant and were selected to improve productivity without adversely sacrificing tool life (performance).

Table 1: Experiment plan for investigation of cooling strategies, tool coatings and machining parameters under down-milling operation using helical bull-nose solid carbide end-mills

Ex No.	Block No.	Tool Coating	Cooling Strategy	Cutting Speed m/min	Feed per revolution mm/rev	Depths of cut		MRR mm ³ /min
						Axial (a_a) mm	Radial (a_r) mm	
1	2	AlTiN	MQL	45	0.1016	5.08	3.81	2216.2
2			LN ₂ (-15°C)	45	0.1016	5.08	3.81	2216.2
3			MQL + LN ₂ (-15°C)	45	0.1016	5.08	3.81	2216.2
4	3	GMS ²	MQL	45	0.1016	5.08	3.81	2216.2
5			LN ₂ (-15°C)	45	0.1016	5.08	3.81	2216.2
6			MQL + LN ₂ (-15°C)	45	0.1016	5.08	3.81	2216.2

Each experiment consisted of 8 passes, each pass of 76.2 mm (3 inches) cutting length. Three (3) cooling strategies (MQL, LN₂ and combined (MQL+LN₂)) were investigated for each of AlTiN coated and GMS₂ coated end-mills under down-milling operation. For each set of experiments, the total number of tools used was six (6) carbide end-mills (three for each of AlTiN and GMS₂ coated end-mills) and Inconel 718 workpieces used were three (2), one for each end-mill coating. Each experiment was replicated once, thus the total number of experiments was twenty (12). The initial shape of workpiece is given in Figure 1. The initial shape of the workpiece was machined from

rectangular blocks of Inconel 718 of dimensions 152.4 mm x 76.2 mm x 38.1 mm (6 in x 3 in x 1.5 in) on Cincinnati Milacron Sabre 750 vertical machining center (VMC). Two steps were made on both sides of the workpiece, each having a width of 30.48 mm (1.2 in) and height 5.08 mm (0.2”). Each step was used to perform one experiment and thus, four experiments could be performed on one workpiece. Two counter-bored holes of diameter 7.366 (0.29 in.), 38.1 mm (1.5 in.) deep and 60 mm (2.3622 in.) apart were drilled and tapped for clamping the workpiece on a dynamometer.



All dimensions in mm (inches)

Figure 1: Initial shape of prepared work-piece, with drilled, counter-bored and tapped holes for clamping

Peripheral high-speed end-milling tests were conducted on three (3) workpiece blocks, each having two steps on each of the two sides, using 12.7 mm (0.5 in) diameter,

4-flute uncoated, 4-flute AlTiN coated and 7-flute GMS² coated carbide end-mills using down-milling operation. The workpieces with the sequence of experiments performed using three cooling strategies with each of coated end-mills is given in Figure 2.

Machining experiment under emulsion and MQL cooling strategies were conducted before machining experiment under LN₂ cooling or combined MQL + LN₂ cooling because if LN₂ or MQL + LN₂ cooling strategy was applied first, it would have affected the hardness of the workpiece steps and hence, the results of experiments following that machining experiment. Also, neither of the two cooling strategies, LN₂ or combined MQL + LN₂ was applied on the same side because they might affect the results of the subsequent cooling experiment by increasing the hardness of workpiece. A new tool was used for each cooling strategy to eliminate the effect of tool wear. The results of the six (6) experiments were analyzed to find the best cooling strategy among MQL, LN₂ and combined MQL + LN₂ cooling and better tool coating among AlTiN coated and GMS² coated end-mills. Each of the cooling strategies investigated (MQL, LN₂ and the combined (MQL+LN₂)) was set independently for each set of experiment. The Accu-Lube LB-2000 biodegradable mineral oil, used as a lubricant for these experiments, is investigated as a possible environmentally friendly coolant. To remove the enormous amount of heat from the cutting zone generated during machining of Inconel 718, cryogenic liquid nitrogen (LN₂) was applied at -15°C temperature to the cutting zone. The liquid nitrogen temperature was stepped down to a temperature from -196°C to -15°C by mixing the shop air with liquid nitrogen. This temperature of liquid nitrogen was chosen for machining Inconel 178 based on published literature (Yuan et al. 2011).

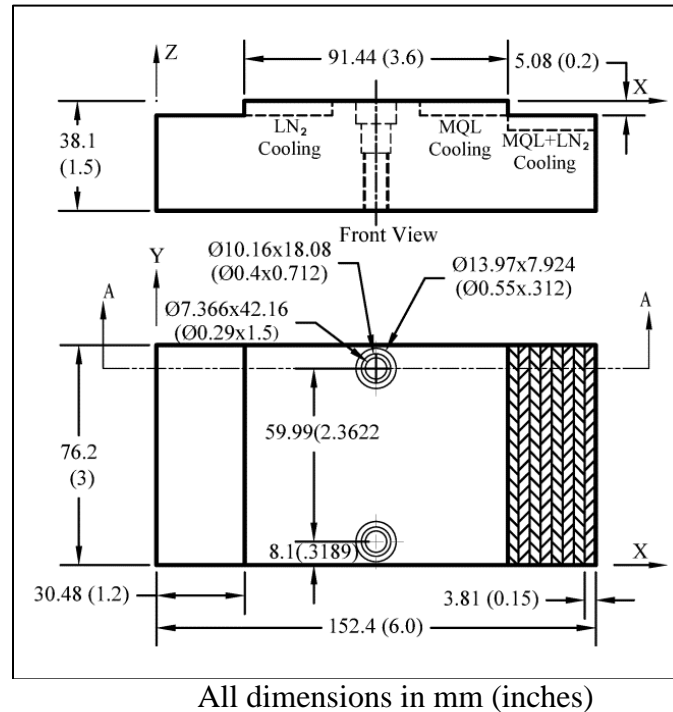


Figure 2: Schematic of experiments performed on workpiece

The prepared workpiece was clamped on Cincinnati Milacron Sabre 750 Vertical Machining Centre (VMC) and 8 machining passes were made for each experimental condition shown in Table 1 using CNC program written for each experiment. The operation was stopped after each pass, chip samples were collected for analysis, and tool was taken out from the CNC machine to measure the maximum flank wear. The maximum flank wear was measured using Keyence VHX – 5000 digital microscope. To measure the maximum flank wear, a reference line along the tool cutting edge above the axial depth of cut was drawn, from which the measurements of flank wear land were made in the beginning and after each cutting pass. This procedure was repeated after each pass. Also, the chip lengths were measured using VHX – 5000 digital microscope. The arithmetic average surface roughness (R_a) of machined surfaces were measured using a portable Brown and Sharpe pocket surf profilometer after the end of each experiment.

For each experiment, the arithmetic average surface roughness (R_a) of the machined workpiece was measured at three different locations which were 25.4 mm (1 in.) apart from each other. Measurements were made using a traverse length of 5 mm (0.195 in.) at a speed of 5.08 mm/sec. The cut-off of tracing length was 0.8 mm (0.03 in.) and the number of cut-offs used was 5 which made a total evaluation length of 4.0 mm (0.15 in.). Figure 3 shows the arithmetic average surface roughness measurement locations on the workpiece.

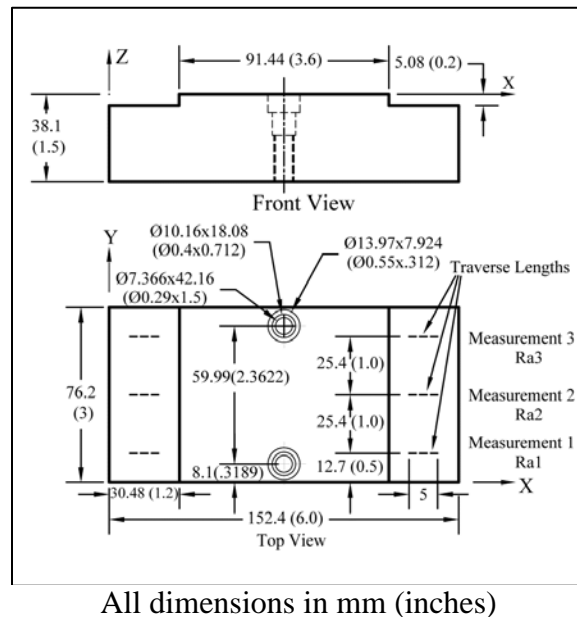


Figure 3: Workpiece with surface roughness measurement locations

After taking three measurements, the average values were calculated using the formula:

$$R_{avg} = \frac{R_{a1} + R_{a2} + R_{a3}}{3} \quad (1)$$

Where R_{a1} , R_{a2} , R_{a3} are the 1st, 2nd and 3rd arithmetic average surface roughness measurements respectively. Figure 4 shows the cutter entry angle of the tooth during down-milling operation and blown-up image showing chip length.

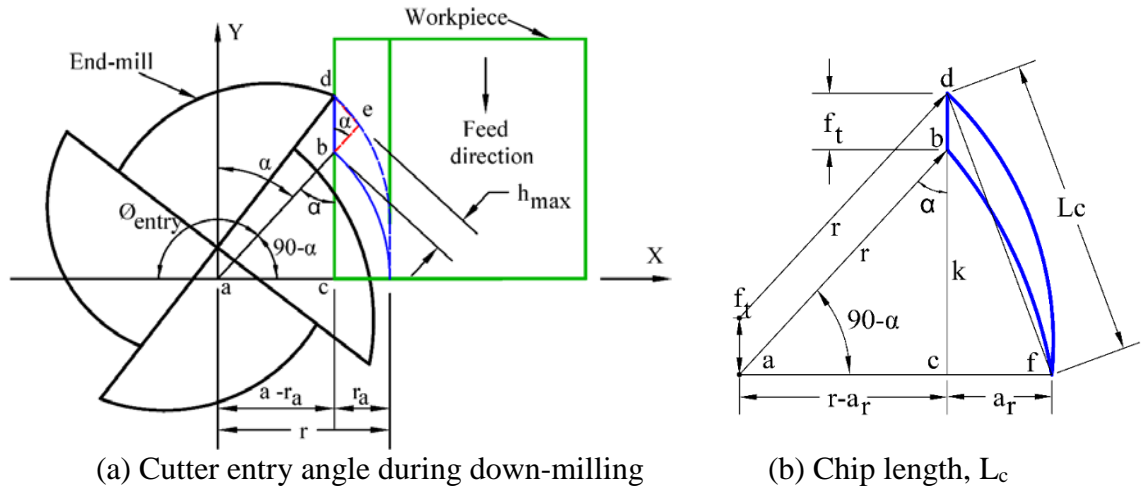


Figure 4: Cutter entry angle during down-milling operation and blown-up image showing chip length and maximum chip thickness. (a) Cutter entry angle during down-milling and (b) Chip length, L_c

The entry and exit angles for down-milling are calculated below:

The tool always comes out of the workpiece at an angle of 180° with negative x-axis.

Thus,

$$\phi_{\text{exit}} = 180^\circ \quad (2)$$

The entry angle is calculated using Figure 4a as follows:

$$\phi_{\text{entry}} = 180 - (90 - \alpha) \quad (3a)$$

From Δabc

$$\text{Cos}(90 - \alpha) = \frac{ac}{ab} = \frac{r - a_r}{r} \quad (3b)$$

where, r is the radius of tool and a_r is the radial depth of cut.

$$90 - \alpha = \arccos\left(\frac{r - a_r}{r}\right) \quad (3c)$$

$$90 - \alpha = \arccos\left(\frac{6.35 - 3.81}{6.35}\right) = \arccos(0.4) = 66.42^\circ$$

Substituting the value of $90 - \alpha$ in (3a)

$$\phi_{\text{entry}} = 180 - \arccos\left(\frac{r - a_r}{r}\right) \quad (3d)$$

$$\phi_{\text{entry}} = 180 - 66.42 = 113.58^\circ$$

The shear action of the tool while machining creates the chips of specific length and thickness depending upon the feed per tooth and radial depth of cut as shown in Figure 4b. The chip length and maximum chip thickness are calculated as follows:

Chip Length

The chip length is calculated from Figure 4b as follows:

From Δ cdf:

$$L_c^2 = a_r^2 + (k + f_t)^2 \quad (4)$$

From Δ abc:

$$\cos(\alpha) \frac{k}{r} \Rightarrow k = r \cos(\alpha) \quad (5)$$

Substituting the value of k in (4)

$$L_c^2 = a_r^2 + (k + f_t)^2 = a_r^2 + (r \cos(\alpha) + f_t)^2 \quad (6)$$

$$L_c = \sqrt{a_r^2 + (r \cos(\alpha) + f_t)^2} \quad (7)$$

From Δ abc:

$$k^2 + (r - a_r)^2 = r^2 \quad (8a)$$

$$k^2 = r^2 - (r - a_r)^2 = [r + (r - a_r)] [r - (r - a_r)] = [2r - a_r] [a_r] \quad (8b)$$

$$k = \sqrt{2r a_r - a_r^2} \quad (8c)$$

$$\text{As we know, } \cos(\alpha) = \frac{k}{r} = \frac{\sqrt{2r a_r - a_r^2}}{r} \quad [\text{From (5) and (8c)}] \quad (9)$$

Substituting the value of $\text{Cos}(\alpha)$ in (7)

$$L_c = \sqrt{a_r^2 + (r \text{Cos}(\alpha) + f_t)^2} = \sqrt{a_r^2 + \left(r \frac{\sqrt{2 r a_r - a_r^2}}{r} + f_t\right)^2} = \sqrt{a_r^2 + (\sqrt{2 r a_r - a_r^2} + f_t)^2} \quad (10)$$

Expanding (10), we get

$$L_c = \sqrt{2 r a_r + 2 f_t \sqrt{2 r a_r - a_r^2} + f_t^2} \quad (11)$$

For AlTiN coated end-mills:

$$\text{Feed per tooth: } f_t = 0.0254 \text{ mm}$$

$$L_c = \sqrt{2 \times 6.35 \times 3.81 + 2 \times 0.0254 \sqrt{2 \times 6.35 \times 3.81 - 3.81^2} + 0.0254^2} = 6.977 \text{ mm}$$

For GMS² coated end-mills:

$$\text{Feed per tooth: } f_t = 0.0145 \text{ mm}$$

$$L_c = \sqrt{2 \times 6.35 \times 3.81 + 2 \times 0.0145 \sqrt{2 \times 6.35 \times 3.81 - 3.81^2} + 0.0145^2} = 6.968 \text{ mm}$$

Chip length after each pass was also measured using digital microscope. The measured chip length was compared with calculated chip length under all cooling strategies and end-mill coatings. The tool starts cutting the workpiece during down-milling when the center of the tool is at a distance of L_1 (approach distance) from the workpiece edge perpendicular to feed direction as shown in Figure 5. The L_1 distance is given as follows.

$$L_1 = \sqrt{r^2 - (r - a_r)^2} \quad (12)$$

$$L_1 = \sqrt{6.35^2 - (6.35 - 3.81)^2} = 5.82 \text{ mm}$$

As the workpiece machined length (L) along the feed direction was 76.2 mm (3 inches), the total machined length for each machining pass becomes:

$$\text{ML (Machined Length of single pass)} = L + L_1 = 76.2 + 5.82 = 82.02 \text{ mm} \quad (13)$$

All the 8 passes resulted to a total length of cut of 656.16 mm (25.83 in). Each experiment consisted of eight (8) radial passes resulted to a total machined width of 30.48 mm (1.2 in). The corresponding machined lengths for 8 passes after adding additional approach length L_1 length to each pass, is 82.02 mm, 164.04 mm, 246.06 mm, 328.08 mm, 410.1 mm, 492.12 mm, 574.14 mm and 656.16 mm respectively.

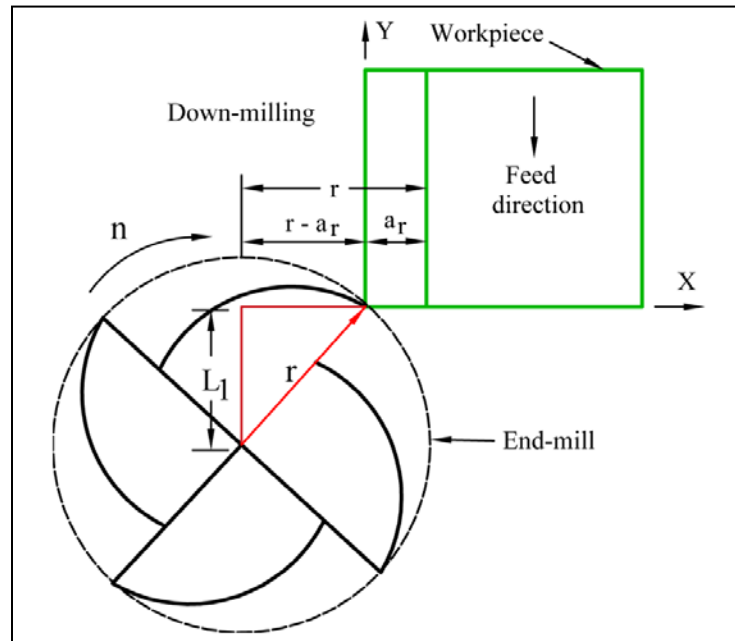


Figure 5: Approach distance during down-milling operation

3. RESULTS AND DISCUSSIONS

3.1. MAXIMUM FLANK WEAR AND CHIP MORPHOLOGY FOR ALTiN COATED END-MILLS

3.1.1. Maximum Flank Wear. Figure 6 shows the plot for maximum flank wear vs number of passes (Machined length) under three cooling strategies for AlTiN coated end-mills during down-milling operation at a cutting speed of 45 m/min (1127 rpm) and 114.5 mm/min (4.510 ipm) feed-rate.

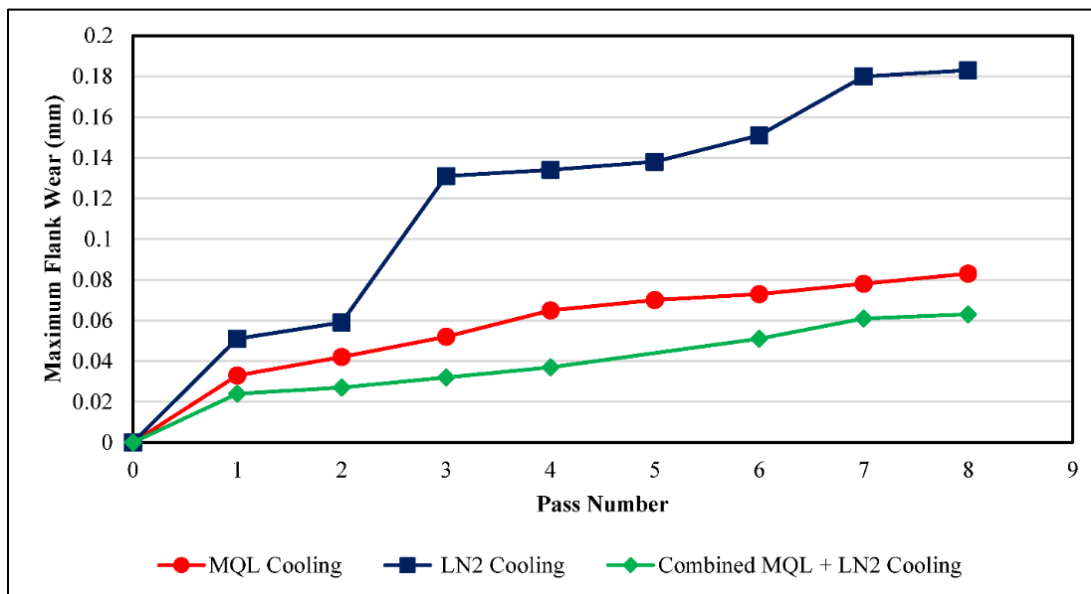


Figure 6: Maximum flank wear vs number of passes (Machined length) for AiTiN coated end-mills using four cooling strategies

The flank wear in down-milling can be explained with help of chip formation during down-milling operation as shown in Figure 7. During down-milling operation, the chip thickness at the entry of tool flute into workpiece is highest and decreases gradually until the flute comes out of the workpiece. The highest thickness of the chip at the entry of the tool into workpiece causes an impact on the tool flutes. This impact on the tool flutes causes rapid tool flank wear. Also, most of the rubbing between tool flank and workpiece occurs in the beginning of tool penetration into workpiece, which causes an abrasion on the tool flank, and decreases with rotation of tool as chip thickness decreases. Tool wear mechanism during down-milling operation was abrasive wear under all cooling strategies. As can be seen, the combined (MQL + LN₂) cooling strategy generated least value of maximum flank wear throughout the machining, followed by MQL and LN₂ cooling respectively.

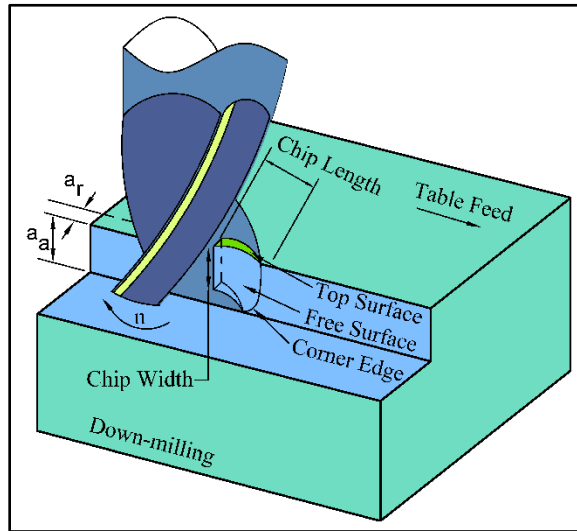


Figure 7: 3-D Chip formation during down-milling operation

The maximum flank wear using LN₂ cooling strategy increased very rapidly after 2nd pass. In case of MQL and combined (MQL + LN₂), the increase in was more uniform with progression of machining than LN₂ cooling. Although, application of LN₂ cooling strategy on the cutting zone helps reducing the cutting zone temperature, LN₂ increases the hardness of the workpiece. Also LN₂ did not provide lubrication to the cutting zone. This increased the friction between tool-workpiece and tool-chip interfaces, which further increases the tool wear and cutting forces. AlTiN coating increased the flank wear under MQL and LN₂ strategies than uncoated end-mills, but it improved wear under combined (MQL + LN₂) cooling strategy. In case of MQL cooling, the rate of increase of maximum flank wear was quite higher than combined (MQL + LN₂). After last machining pass, the combined (MQL + LN₂) cooling using AlTiN coated end-mills generated the least flank wear among all cooling strategies and was equal to flank wear generated under MQL cooling strategy using GMS² end-mills. Initial flank land and progressive flank wear after 1st, 4th and 8th passes of AlTiN coated end-mills is shown in Figure 8. Abrasion was

main tool wear mechanism while machining under MQL and combined (MQL + LN₂) cooling strategies. Under LN₂ cooling strategy, built-up edge due to adhesion of chip fragments was seen during earlier machining passes, which led to chipping of the tool edge in 4th pass. This chipping became more severe with progressing of machining passes due to adhesion of chip fragments on tool edges, which exaggerated the tool wear.

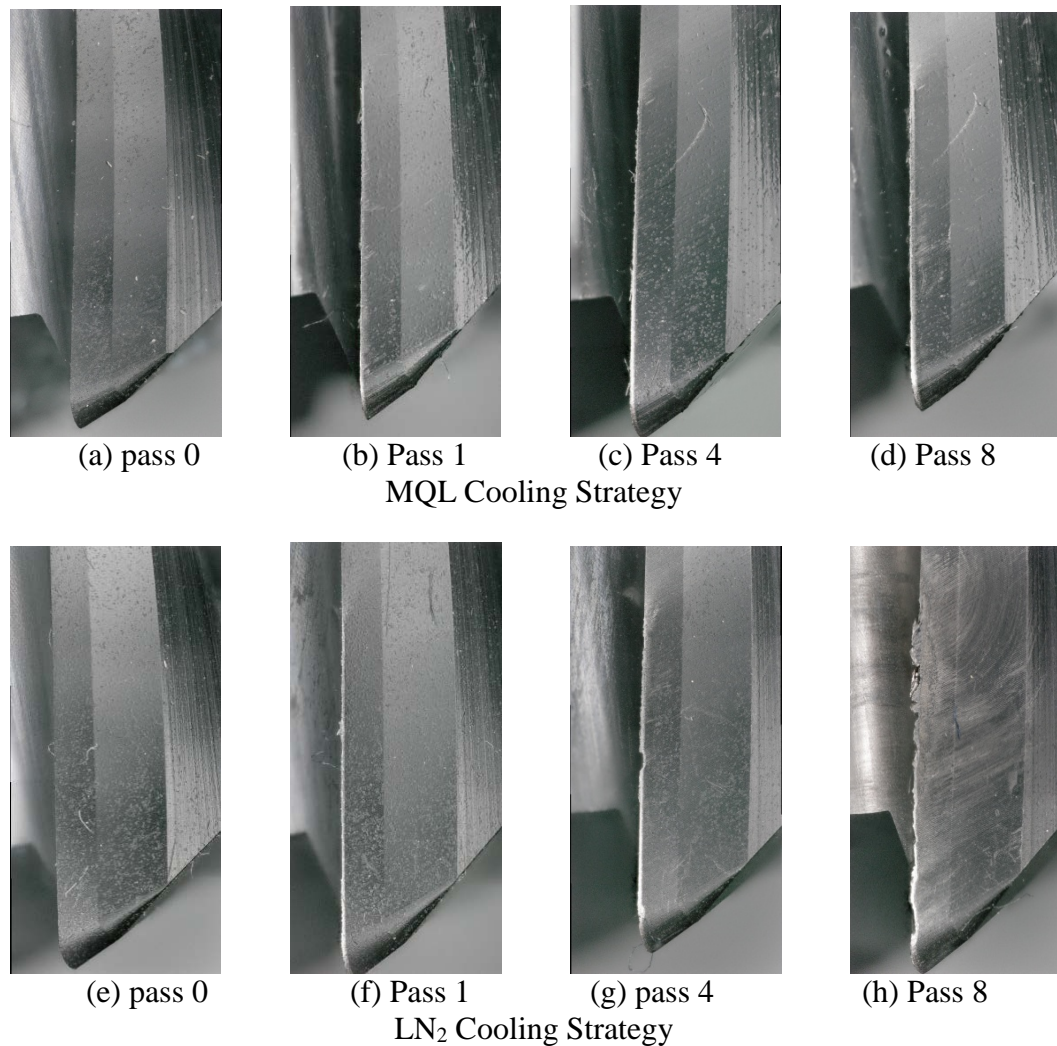


Figure 8: Initial flank land and progressive flank wear for AlTiN coated end-mills under four cooling strategies. MQL cooling (a) Pass 0, (b) Pass 1, (c) Pass 4 and (d) Pass 8, LN₂ cooling (e) Pass 0, (f) Pass 1, (g) Pass 4 and (h) Pass 8 and, Combined (MQL + LN₂) cooling (i) Pass 0, (j) Pass 1, (k) Pass 4 and (l) Pass 8

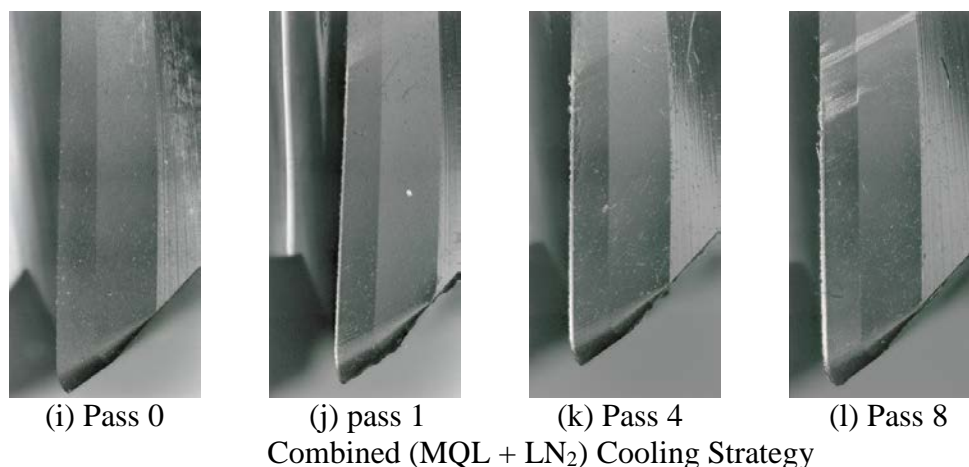


Figure 8: Initial flank land and progressive flank wear for AlTiN coated end-mills under four cooling strategies. MQL cooling (a) Pass 0, (b) Pass 1, (c) Pass 4 and (d) Pass 8, LN₂ cooling (e) Pass 0, (f) Pass 1, (g) Pass 4 and (h) Pass 8 and, Combined (MQL + LN₂) cooling (i) Pass 0, (j) Pass 1, (k) Pass 4 and (l) Pass 8 (Contd.)

Also, increase in the hardness of workpiece and tool by application of cryogenic cooling further led the tool wear to increase rapidly as compared to MQL and combined (MQL + LN₂) cooling strategies.

3.1.2. Chip Morphology. The free and back surfaces of chip are shown in Figure 9. As can be seen the back surface of the chip is smooth and shiny.

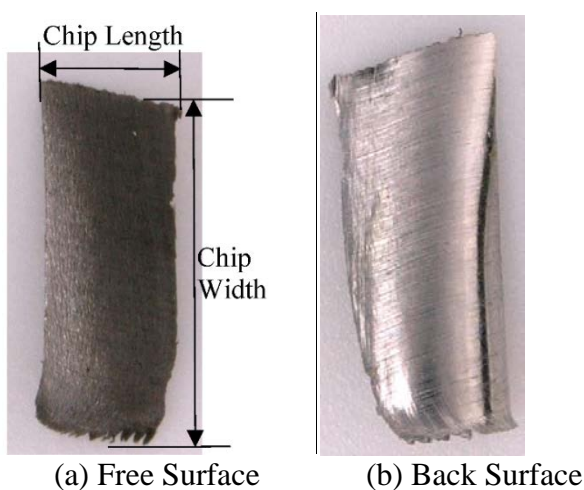


Figure 9: Free and Back surfaces of the chip. (a) Free surface and (b) Back surface

The back surface of the chip encounters high contact and shear stresses as it slides on the rake face of the workpiece, which constrains the deformation of the back surface (Cui et al. 2016). During down-milling operation, most of the heat generated during machining is carried away by chips from the cutting zone. Thus, the temperature of the cutting zone remains lower as compare to up-milling.

The free surface of chips contains lamella structures and the major section of the lamella in the free surface of the chip was formed by side cutting edge and the corner section was formed by the corner cutting edge (Sun and Guo 2008). The schematic and actual chip morphology showing lamella structure during down-milling operation is shown in Figure 10.

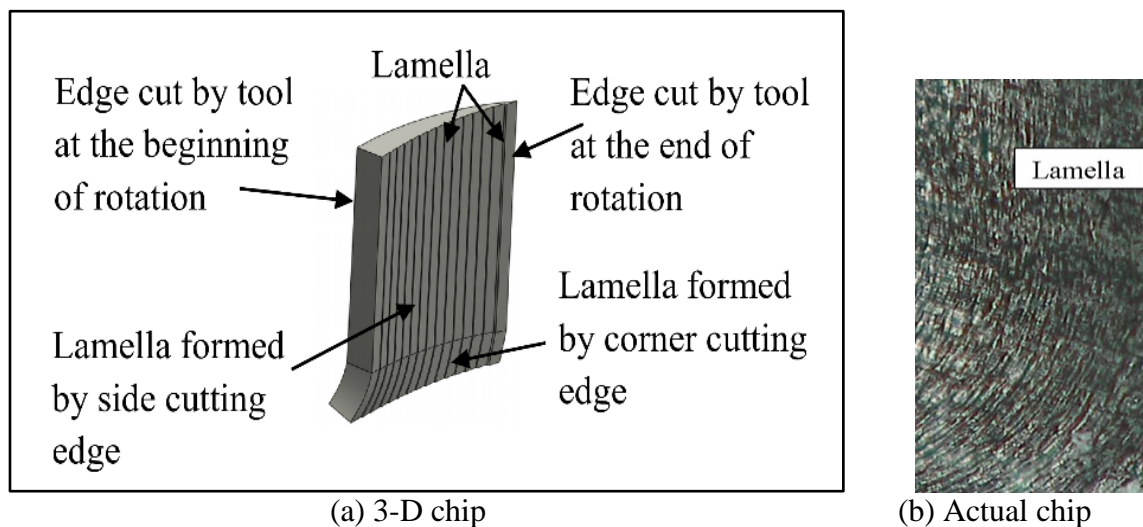


Figure 10: Schematic and actual chip morphology showing lamella structure during down-milling operation. (a) Schematic of 3-D chip and (b) Actual chip showing lamella structure

Figure 11 shows the free surface of chips after 1st, 4th and 8th passes using MQL, LN₂ and combined (MQL + LN₂) cooling strategies using AlTiN coated end-mills.

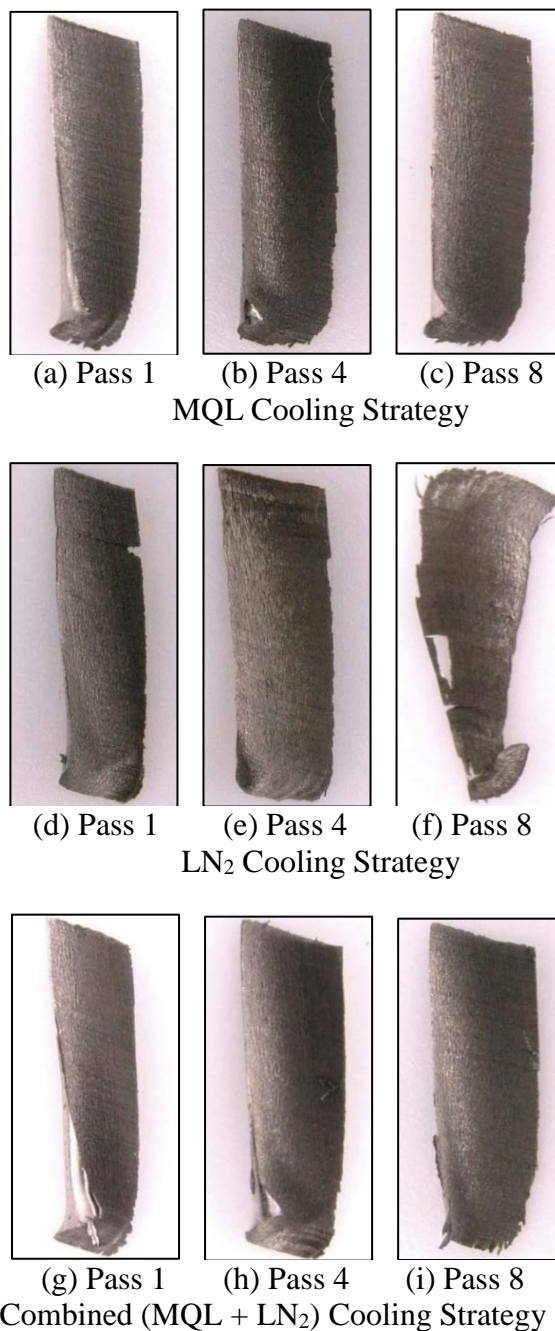


Figure 11: Free surface of chips for AlTiN coated end-mills under four cooling strategies. MQL cooling (a) Pass 1, (b) Pass 4 and (c) Pass 8, LN₂ cooling (d) Pass 1, (e) Pass 4 and (f) Pass 8 and, Combined (MQL + LN₂) cooling (g) Pass 1, (h) Pass 4 and (i) Pass 8

As can be seen, LN₂ cooling yielded chips with irregular edges. The chipping of tool edges using LN₂ cooling yielded irregular chips as compared to MQL and combined

(MQL + LN₂) cooling strategies where chips are more uniform. Figure 12 shows the images of chips collected after 1st, 4th and 8th passes AlTiN coated end-mills.

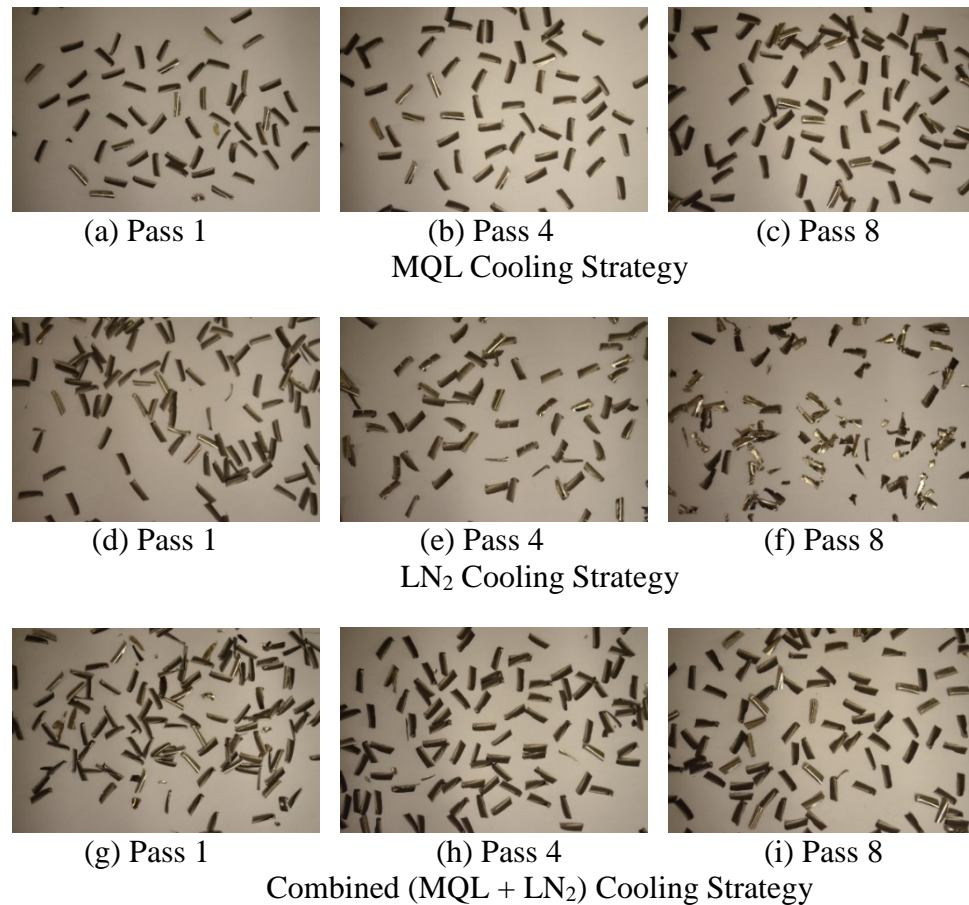


Figure 12: Images of chips for AlTiN coated end-mills under four cooling strategies. MQL cooling (a) Pass 1, (b) Pass 4 and (c) Pass 8, LN₂ cooling (d) Pass 1, (e) Pass 4 and (f) Pass 8 and, Combined (MQL + LN₂) cooling (g) Pass 1, (h) Pass 4 and (i) Pass 8

Figure 13 shows the calculated chip length and measured lengths of chips using all cooling strategies with AlTiN coated end-mills under down-milling method. As can be seen, the calculated chip length was very large as compared to measured chip lengths using all cooling strategies. During 1st pass, combined (MQL + LN₂) yielded highest chip length, followed by LN₂ and MQL respectively. During 4th and 8th passes, LN₂

cooling strategy generated longest chips among three, followed by combined (MQL + LN₂) and MQL cooling. Under all three cooling strategies, the chip length increased with progression of time.

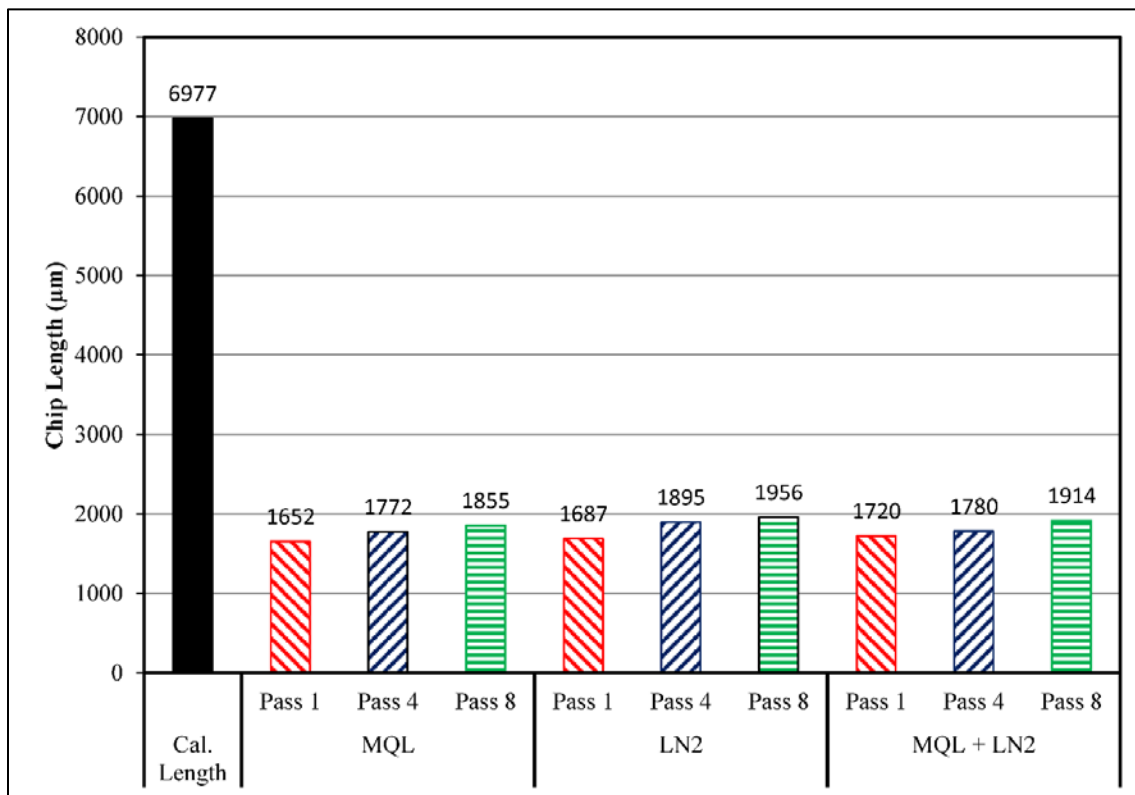


Figure 13: Calculated and measured chip lengths vs number of passes (Machined length) and cooling strategies for for AlTiN coated end-mills

3.2. MAXIMUM FLANK WEAR AND CHIP MORPHOLOGY FOR GMS² COATED END-MILLS

3.2.1. Maximum Flank Wear. Figure 14 shows the plot for maximum flank wear vs number of passes (Machined length) under three cooling strategies for GMS² Coated end-mills during down-milling operation at a cutting speed of 45 m/min (1127 rpm) and 114.5 mm/min (4.510 ipm) feed-rate.

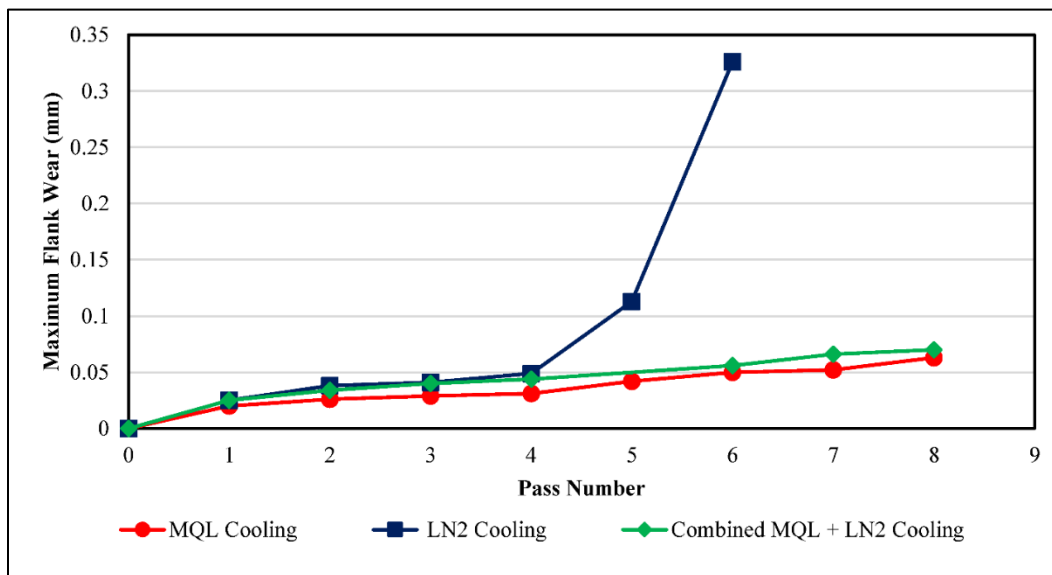


Figure 14: Maximum flank wear vs number of passes (Machined length) for GMS^2 Coated end-mills under four cooling strategies

The plot shows that MQL cooling strategy generated the least value of maximum flank wear throughout the machining, where LN_2 cooling strategy yielded the highest flank wear. During 8th pass, maximum flank wear under MQL was equal to that of $AlTiN$ coated under combined ($MQL + LN_2$) cooling strategy and was least among all cooling strategies and tool coatings. Under LN_2 cooling, the tool wear increased drastically after 4th pass. This happened because of application of LN_2 on cutting zone increased the hardness of the workpiece which increased the cutting forces and hence, tool wear. Due to more number of flutes of GMS^2 coated end-mills, all the chips were not able to escape from the cutting zone and got entangled in the flutes. This increased the cutting temperature, which increased the cutting forces so drastically that the tool failed plastically during 7th pass and broke. As the tool broke during 7th pass, it was not possible to measure the tool wear after 7th pass under LN_2 . Initial flank land and progressive flank wear after 1st, 4th and 8th passes GMS^2 Coated end-mills using MQL,

LN₂ and (MQL + LN₂) strategies is shown in Figure 15. As can be seen, the wear on the flank faces of tools under MQL and (MQL + LN₂) strategies is uniform. Under LN₂, built-up edge had started to form on the worn edge of tool during 4th pass, which gave rise to chipping and notching of the tool edge in successive passes. Severe notching of the tool edge increased the tool wear rapidly, due to which the tool eventually broke during 7th pass. Wear caused due to abrasion under MQL and (MQL + LN₂) cooling.

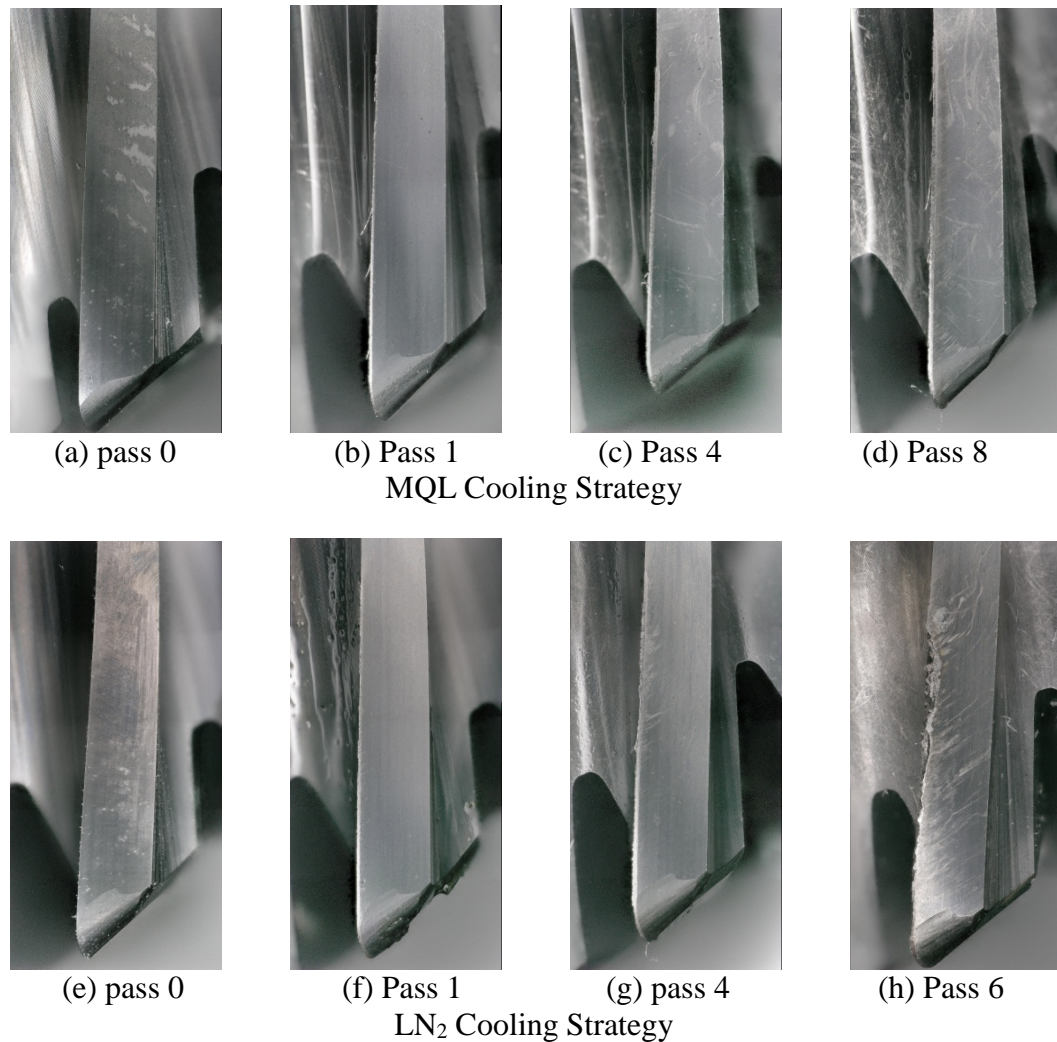


Figure 15: Initial flank land and progressive flank wear for GMS²coated end-mills under four cooling strategies. MQL cooling (a) Pass 0, (b) Pass 1, (c) Pass 4 and (d) Pass 8, LN₂ cooling (e) Pass 0, (f) Pass 1, (g) Pass 4 and (h) Pass 8 and, Combined (MQL + LN₂) cooling (i) Pass 0, (j) Pass 1, (k) Pass 4 and (l) Pass 8

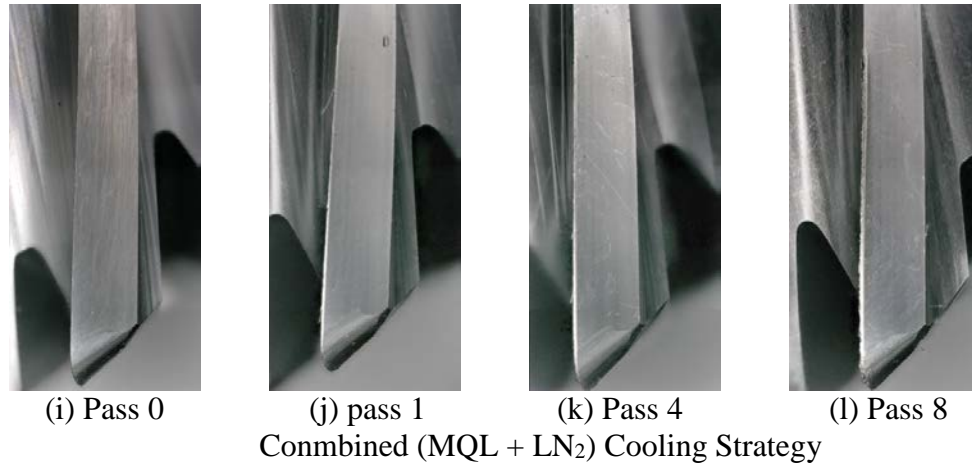


Figure 15: Initial flank land and progressive flank wear for GMS²coated end-mills under four cooling strategies. MQL cooling (a) Pass 0, (b) Pass 1, (c) Pass 4 and (d) Pass 8, LN₂ cooling (e) Pass 0, (f) Pass 1, (g) Pass 4 and (h) Pass 8 and, Combined (MQL + LN₂) cooling (i) Pass 0, (j) Pass 1, (k) Pass 4 and (l) Pass 8 (Contd.)

3.2.2. Chip Morphology. Figure 16 shows the free surface of chips after 1st, 4th and 8th passes under MQL and combined (MQL + LN₂) cooling strategies and after 1st, 4th and 7th passes under LN₂ cooling using GMS² coated end-mills.

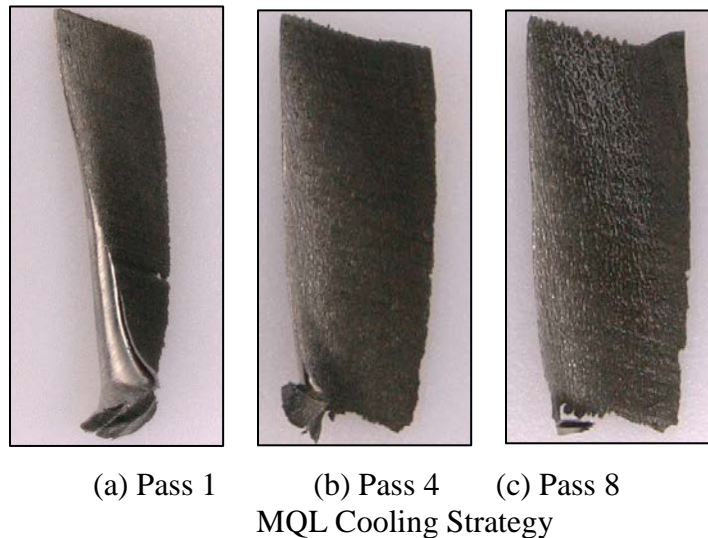


Figure 16: Free surface of chips for GMS² coated end-mills under four cooling strategies. MQL cooling (a) Pass 1, (b) Pass 4 and (c) Pass 8, LN₂ cooling (d) Pass 1, (e) Pass 4 and (f) Pass 7 and, Combined (MQL + LN₂) cooling (g) Pass 1, (h) Pass 4 and (i) Pass 8

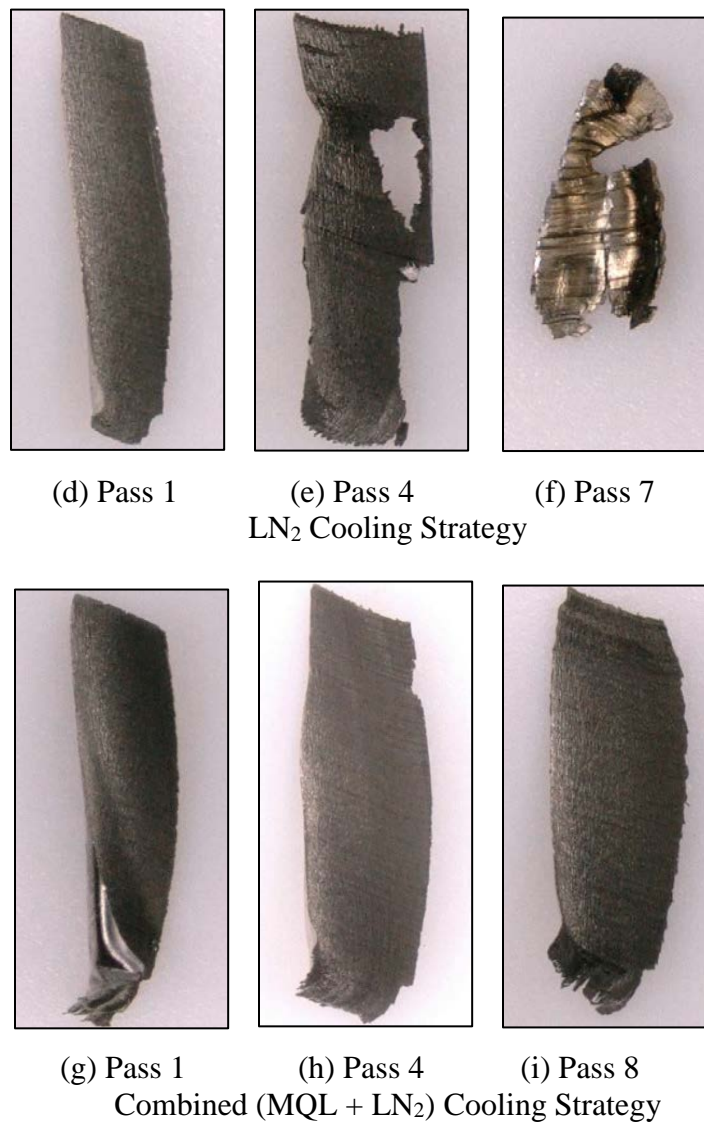


Figure 16: Free surface of chips for GMS² coated end-mills under four cooling strategies. MQL cooling (a) Pass 1, (b) Pass 4 and (c) Pass 8, LN₂ cooling (d) Pass 1, (e) Pass 4 and (f) Pass 7 and, Combined (MQL + LN₂) cooling (g) Pass 1, (h) Pass 4 and (i) Pass 8 (Contd.)

The chip edge during MQL cooling and combined (MQL + LN₂) cooling are very uniform as compared to chips produced during application of LN₂ cooling strategy. A lot of tear and chip burns can be seen after 6th pass when using LN₂ cooling due to high temperature of the cutting zone. Figure 17 shows the images of chips collected after 1st,

4th and 8th passes under MQL and combined (MQL + LN₂) cooling strategies and after 1st, 4th and 7th passes under LN₂ cooling using GMS² coated end-mills.

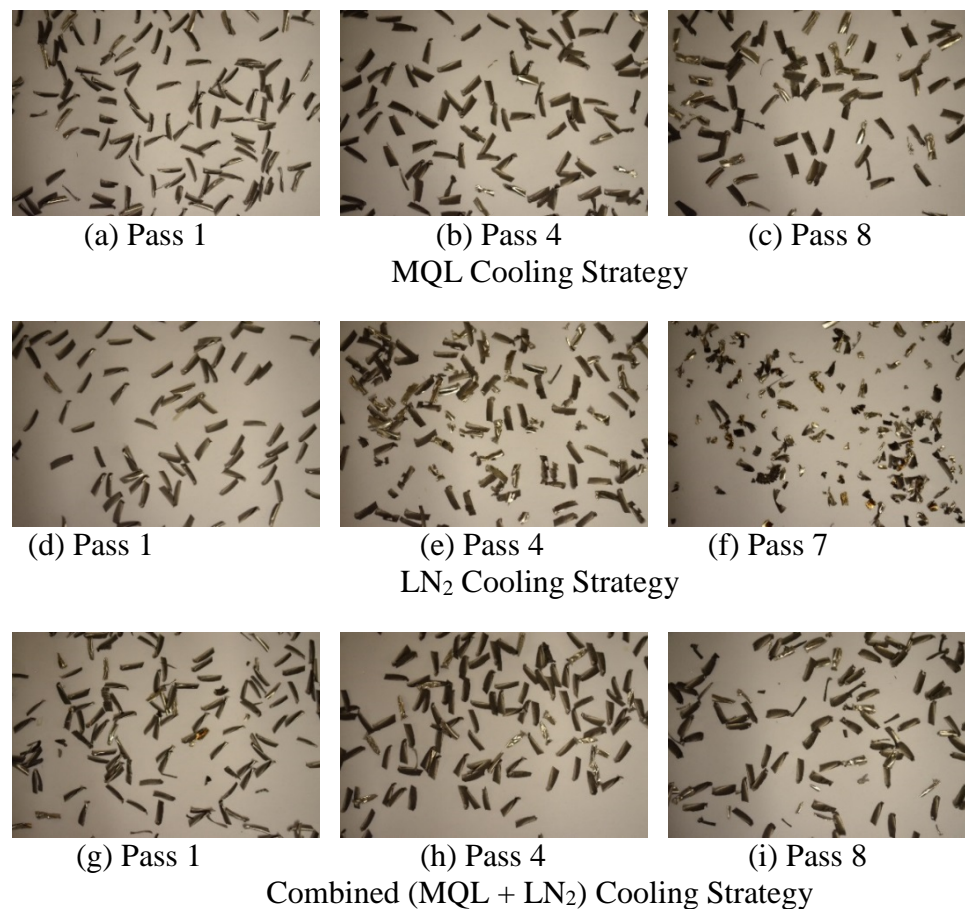


Figure 17: Images of chips for GMS² coated end-mills under four cooling strategies. MQL cooling (a) Pass 1, (b) Pass 4 and (c) Pass 8, LN₂ cooling (d) Pass 1, (e) Pass 4 and (f) Pass 7 and, Combined (MQL + LN₂) cooling (g) Pass 1, (h) Pass 4 and (i) Pass 8

Figure 18 shows the calculated chip length and measured lengths of chips using all cooling strategies with GMS² coated end-mills under down-milling method. Again, calculated chip length was very large as compared to calculated ones in all cases. Until 4th pass, LN₂ cooling strategy produced longest chips among three through the machining followed by MQL and combined (MQL + LN₂) respectively. As can be seen from the Figure, the chips produced during 6th pass in LN₂ cooling were even longer than chips

proceed during 8th pass in combined (MQL + LN₂) cooling. MQL cooling generated longer chip length than combined (MQL + LN₂) cooling which is the opposite to their respective flank wear values.

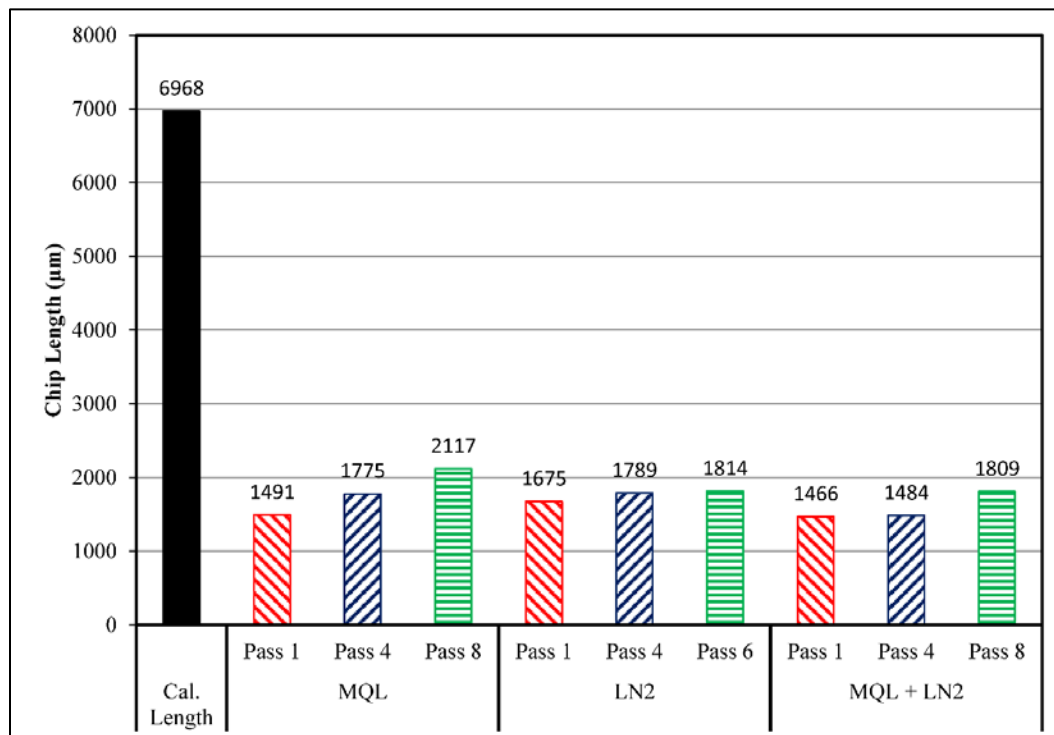


Figure 18: Calculated and measured chip lengths vs number of passes (Machined length) and cooling strategies for GMS² coated end-mills

3.3. COMPARITIVE INVESTIGATION OF MAXIMUM FLANK WEAR UNDER ALL COOLING STRATEGIES AND TOOL COATINGS

Figure 19 shows the maximum flank wear after 1st pass under different cooling strategies and end-mill coatings. As can be seen from the plot, the LN₂ cooling strategy generated highest value of maximum flank wear with all three end-mill coatings during 1st pass than other cooling strategies. For uncoated end-mills, MQL cooling yielded least value of maximum flank wear followed by combined (MQL + LN₂), emulsion and LN₂

respectively. MQL also performed better than LN₂ and combined (MQL + LN₂) when used with GMS² coated end-mills after pass 1.

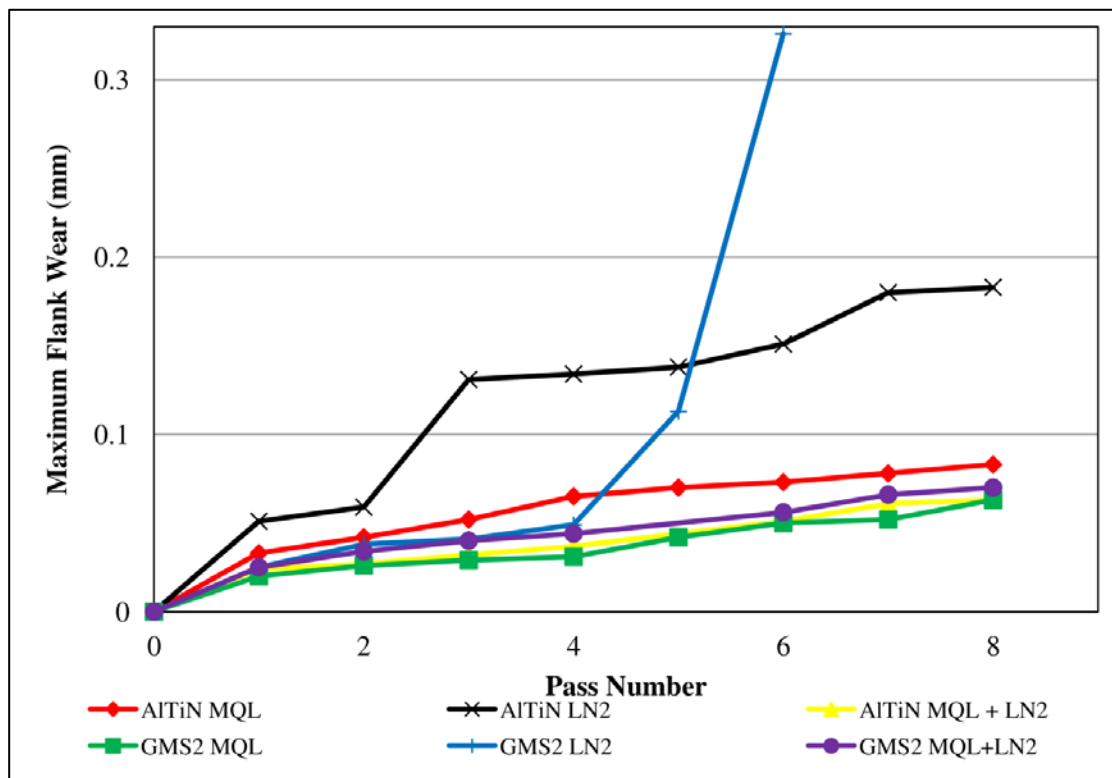


Figure 19: Maximum flank wear vs end-mill coatings and cooling strategies after 1st pass

When used with GMS² coated end-mills, LN₂ and combined (MQL + LN₂) cooling performed equally after 1st pass. Combined (MQL + LN₂) cooling performed better using AITiN coated end-mills followed by MQL and combined (MQL + LN₂) cooling strategies. GMS² coated end-mills performed better than uncoated and AITiN coated end-mills after pass 1. Also, GMS² coated end-mills using MQL cooling strategy performed the best among all others followed by AITiN coated end-mills using combined (MQL + LN₂) cooling strategy. Uncoated end-mills using MQL cooling strategy and

GMS² coated end-mills using both LN₂ and, combined (MQL + LN₂) cooling strategies yielded same magnitude of maximum flank wear after pass 1.

3.4. COMPARITIVE EVALUATION OF END-MILL COATINGS AND COOLING STRATEGIES ON AVERAGE SURFACE ROUGHNESS

Figure 20 shows the average surface roughness under all cooling strategies and end-mill coatings.

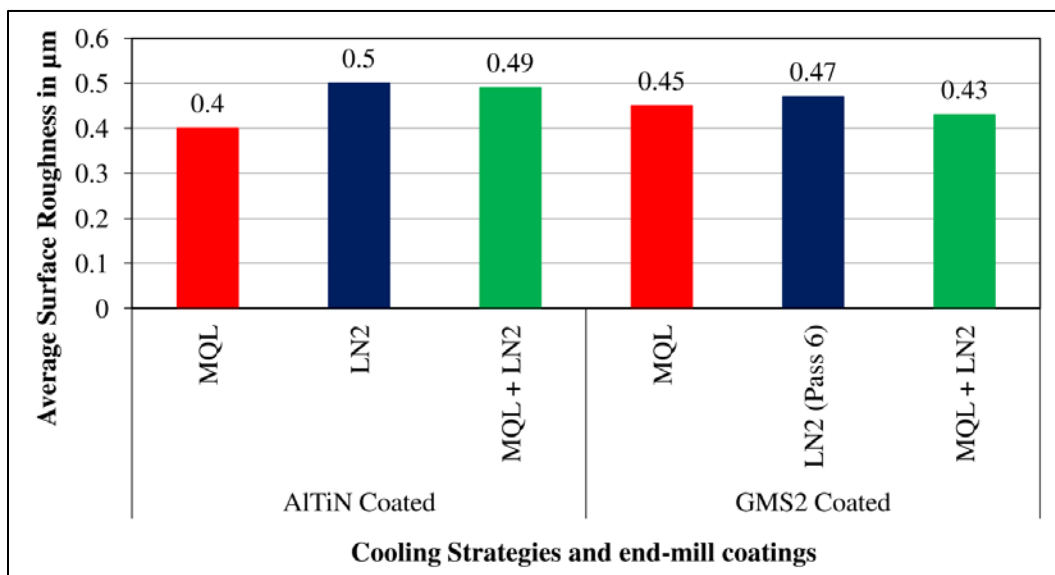


Figure 20: Average surface roughness vs cooling strategies and end-mill coatings

As can be seen, AlTiN coated end-mills under MQL cooling strategy generated lowest surface roughness, followed by GMS² coated end-mills under combined (MQL+LN₂) cooling strategy. The application of LN₂ adversely affected the roughness with all end-mills. This might have happened as application of cryogenic cooling increases the hardness of workpiece and end-mills, and does not provide sufficient lubrication to the cutting zone as well. This increases the surface roughness due to

increase in cutting forces and tool wear. Although, no specific trend was seen as no specific cooling was seen in terms of cooling which lowers the surface roughness, both MQL and combined (MQL + LN₂) cooling strategies improved the surface roughness with both end-mill coatings than LN₂ cooling.

4. CONCLUSIONS

This research investigated the effects of four cooling strategies (MQL, LN₂ and combined (MQL+LN₂)) and three tool coatings (AlTiN coated and GMS² coated) on flank wear, chip morphology and surface roughness during peripheral down-milling of Inconel-718 alloy using solid carbide bull-nose helical end-mills. From the results obtained, the following conclusions can be made:

1. For AlTiN coated end-mills, (MQL + LN₂) cooling strategy generated lowest flank wear, followed by MQL, while LN₂ cooling generated highest flank wear.
2. For GMS² coated end-mills, MQL cooling strategy generated lowest flank wear, followed by combined (MQL + LN₂), while LN₂ cooling generated highest flank wear.
3. GMS² coated end-mills under MQL cooling strategy generated lowest flank wear followed by AlTiN coated end-mills under combined (MQL + LN₂) cooling strategy, while GMS² coated end-mills under LN₂ cooling strategy generated highest flank wear among all combinations of cooling strategies and end-mill coatings.
4. Using LN₂ cooling strategy alone is not recommended for machining Inconel 718 due to rapid tool wear.

5. MQL and combined (MQL + LN2) cooling strategy generated chips with sharp and uniform edges due to less tool wear, while LN2 cooling strategy generated chips with irregular and torn edges due to high tool wear
6. Chip length increased with progression of machining time (tool wear) under all cooling strategies and end-mill coatings
7. Tool wear mechanism under MQL and combined (MQL + LN2) cooling strategies is abrasion causing progressive wear, while under LN2 cooling it is adhesion causing chipping and notching due to formation of built-up edge
8. ALTiN coated end-mills under MQL cooling strategy generated lowest surface roughness, followed by GMS2 coated end-mills under combined (MQL+LN2) cooling strategy, whereas ALTiN coated end-mills under LN2 cooling generated highest surface roughness
9. GMS2 coated end-mills under MQL cooling strategy and by ALTiN coated end-mills under are recommended for machining Inconel-718.

ACKNOWLEDGEMENTS

The financial support from the Intelligent System Centre (ISC) of the Missouri University of Science and Technology is greatly acknowledged. The financial assistance provided in the form of Graduate Teaching Assistantship by the Department of Mechanical and Aerospace Engineering at Missouri University of Science and Technology is also greatly acknowledged.

REFERENCES

- Abele, E., and B. Fröhlich. 2008. "High Speed Milling of Titanium Alloys." *Journal of Advances in Production Engineering & Management* 3, 131–40.
- Aramcharoen, Ampara, and Shaw Kah Chuan. 2014. "An Experimental Investigation on Cryogenic Milling of Inconel 718 and Its Sustainability Assessment." In *Procedia CIRP*, 14:529–34. <https://doi.org/10.1016/j.procir.2014.03.076>.
- Cui, Xiaobin, Bo Zhao, Feng Jiao, and Jianxin Zheng. 2016. "Chip Formation and Its Effects on Cutting Force, Tool Temperature, Tool Stress, and Cutting Edge Wear in High- and Ultra-High-Speed Milling." *International Journal of Advanced Manufacturing Technology* 83 (1–4):55–65. <https://doi.org/10.1007/s00170-015-7539-7>.
- Dhananchezian, M., and M. Pradeep Kumar. 2011. "Cryogenic Turning of the Ti-6Al-4V Alloy with Modified Cutting Tool Inserts." *Cryogenics* 51 (1):34–40. <https://doi.org/10.1016/j.cryogenics.2010.10.011>.
- Dhar, N. R., M. T. Ahmed, and S. Islam. 2007. "An Experimental Investigation on Effect of Minimum Quantity Lubrication in Machining AISI 1040 Steel." *International Journal of Machine Tools and Manufacture* 47 (5 SPEC. ISS.):748–53. <https://doi.org/10.1016/j.ijmachtools.2006.09.017>.
- Ezugwu, E.O., and Z.M. Wang. 1997. "Titanium Alloys and Their Machinability—a Review." *Journal of Materials Processing Technology* 68 (3):262–74. [https://doi.org/10.1016/S0924-0136\(96\)00030-1](https://doi.org/10.1016/S0924-0136(96)00030-1).
- Fallböhmer, P., C. A. Rodríguez, T. Özel, and T. Altan. 2000. "High-Speed Machining of Cast Iron and Alloy Steels for Die and Mold Manufacturing." *Journal of Materials Processing Technology* 98 (1):104–15. [https://doi.org/10.1016/S0924-0136\(99\)00311-8](https://doi.org/10.1016/S0924-0136(99)00311-8).
- Fang, N., and Q. Wu. 2009. "A Comparative Study of the Cutting Forces in High Speed Machining of Ti-6Al-4V and Inconel 718 with a Round Cutting Edge Tool." *Journal of Materials Processing Technology* 209 (9):4385–89. <https://doi.org/10.1016/j.jmatprotec.2008.10.013>.
- Hadi, M. A., J. A. Ghani, C. H. Che Haron, and M. S. Kasim. 2013. "Comparison between up-Milling and down-Milling Operations on Tool Wear in Milling Inconel 718." *Procedia Engineering* 68. Elsevier B.V.:647–53. <https://doi.org/10.1016/j.proeng.2013.12.234>.

- Jawaid, A, S Koksai, and S Sharif. 2001. "Cutting Performance and Wear Characteristics of {PVD} Coated and Uncoated Carbide Tools in Face Milling Inconel 718 Aerospace Alloy." *Journal of Materials Processing Technology* 116 (1):2–9. [https://doi.org/http://dx.doi.org/10.1016/S0924-0136\(01\)00850-0](https://doi.org/http://dx.doi.org/10.1016/S0924-0136(01)00850-0).
- Jawaid, A, S Sharif, and S Koksai. 2000. "Evaluation of Wear Mechanisms of Coated Carbide Tools When Face Milling Titanium Alloy." *Journal of Materials Processing Technology* 99 (1–3):266–74. [https://doi.org/http://dx.doi.org/10.1016/S0924-0136\(99\)00438-0](https://doi.org/http://dx.doi.org/10.1016/S0924-0136(99)00438-0).
- Kamata, Y., and T. Obikawa. 2007. "High Speed MQL Finish-Turning of Inconel 718 with Different Coated Tools." *Journal of Materials Processing Technology* 192–193:281–86. <https://doi.org/10.1016/j.jmatprotec.2007.04.052>.
- Kim, S. W., D. W. Lee, M. C. Kang, and J. S. Kim. 2001. "Evaluation of Machinability by Cutting Environments in High-Speed Milling of Difficult-to-Cut Materials." *Journal of Materials Processing Technology* 111 (1–3):256–60. [https://doi.org/10.1016/S0924-0136\(01\)00529-5](https://doi.org/10.1016/S0924-0136(01)00529-5).
- Krain, H. R., A. R C Sharman, and K. Ridgway. 2007. "Optimisation of Tool Life and Productivity When End Milling Inconel 718TM." *Journal of Materials Processing Technology* 189 (1–3):153–61. <https://doi.org/10.1016/j.jmatprotec.2007.01.017>.
- Liao, Y S, H M Lin, and J H Wang. 2008. "Behaviors of End Milling Inconel 718 Superalloy by Cemented Carbide Tools." *Journal of Materials Processing Technology* 201 (1–3):460–65. <https://doi.org/http://dx.doi.org/10.1016/j.jmatprotec.2007.11.176>.
- Obikawa, Toshiyuki, Yasuhiro Kamata, Yuki Asano, Kousuke Nakayama, and Andrew W. Otieno. 2008. "Micro-Liter Lubrication Machining of Inconel 718." *International Journal of Machine Tools and Manufacture* 48 (15):1605–12. <https://doi.org/10.1016/j.ijmachtools.2008.07.011>.
- Özel, T., M. Sima, A. K. Srivastava, and B. Kaftanoglu. 2010. "Investigations on the Effects of Multi-Layered Coated Inserts in Machining Ti-6Al-4V Alloy with Experiments and Finite Element Simulations." *CIRP Annals - Manufacturing Technology* 59 (1):77–82. <https://doi.org/10.1016/j.cirp.2010.03.055>.
- Patwari, Md. Anayet U., A. K.M. Nurul Amin, and Waleed Faris. 2010. "Identification of Instabilities of the Chip Formation and It's Prediction Model During End Milling of Medium Carbon Steel (S45C)." *American Journal of Engineering and Applied Sciences* 3 (1):193–200. <https://doi.org/10.3844/ajeassp.2010.193.200>.
- Ravi, S., and M. Pradeep Kumar. 2011. "Experimental Investigations on Cryogenic Cooling by Liquid Nitrogen in the End Milling of Hardened Steel." *Cryogenics* 51 (9):509–15. <https://doi.org/10.1016/j.cryogenics.2011.06.006>.

- Safari, H., S. Sharif, S. Izman, H. Jafari, and D. Kurniawan. 2014. "Cutting Force and Surface Roughness Characterization in Cryogenic High-Speed End Milling of Ti-6Al-4V ELI." *Materials and Manufacturing Processes* 29 (3):350–56. <https://doi.org/10.1080/10426914.2013.872257>.
- Su, Y., N. He, L. Li, and X. L. Li. 2006. "An Experimental Investigation of Effects of Cooling/lubrication Conditions on Tool Wear in High-Speed End Milling of Ti-6Al-4V." *Wear* 261 (7–8):760–66. <https://doi.org/10.1016/j.wear.2006.01.013>.
- Su, Yu, Ning He, and Liang Li. 2010. "Effect of Cryogenic Minimum Quantity Lubrication (CMQL) on Cutting Temperature and Tool Wear in High-Speed End Milling of Titanium Alloys." *Applied Mechanics and Materials* 34–35:1816–21. <https://doi.org/10.4028/www.scientific.net/AMM.34-35.1816>.
- Sun, J, and Y B Guo. 2008. "A New Multi-View Approach to Characterize 3D Chip Morphology and Properties in End Milling Titanium Ti-6Al-4V." *International Journal of Machine Tools and Manufacture* 48 (12–13):1486–94. <https://doi.org/http://dx.doi.org/10.1016/j.ijmachtools.2008.04.002>.
- Ulutan, Durul, Abram Pleta, Andy Henderson, and Laine Mears. 2015. "Comparison and Cost Optimization of Solid Tool Life in End Milling Nickel-Based Superalloy." *Procedia Manufacturing* 1:522–33. <https://doi.org/10.1016/j.promfg.2015.09.024>.
- Wang, C Y, Y X Xie, Z Qin, H S Lin, Y H Yuan, and Q M Wang. 2015. "Wear and Breakage of TiAlN- and TiSiN-Coated Carbide Tools during High-Speed Milling of Hardened Steel." *Wear* 336–337:29–42. <https://doi.org/http://dx.doi.org/10.1016/j.wear.2015.04.018>.
- Yuan, S. M., L. T. Yan, W. D. Liu, and Q. Liu. 2011. "Effects of Cooling Air Temperature on Cryogenic Machining of Ti-6Al-4V Alloy." *Journal of Materials Processing Technology* 211 (3). Elsevier B.V.:356–62. <https://doi.org/10.1016/j.jmatprotec.2010.10.009>.
- Zhang, S., J. F. Li, and Y. W. Wang. 2012. "Tool Life and Cutting Forces in End Milling Inconel 718 under Dry and Minimum Quantity Cooling Lubrication Cutting Conditions." *Journal of Cleaner Production* 32:81–87. <https://doi.org/10.1016/j.jclepro.2012.03.014>.
- Zhu, Zhaoju, Jie Sun, Jianfeng Li, and Panling Huang. 2016. "Investigation on the Influence of Tool Wear upon Chip Morphology in End Milling Titanium Alloy Ti6Al4V." *International Journal of Advanced Manufacturing Technology* 83 (9–12):1477–85. <https://doi.org/10.1007/s00170-015-7690-1>.

SECTION

2. CONCLUSIONS

2.1. CONCLUSIONS FROM EFFECTS OF UP-MILLING AND DOWN-MILLING METHODS, AND COOLING STRATEGIES ON CUTTING FORCES AND TOOTH FREQUENCY IN HIGH SPEED END-MILLING OF INCONEL 718 USING UNCOATED SOLID CARBIDE END-MILLS

1. Cutting force component F_y (along the feed direction) is the highest as compared to F_x and F_z in up-milling and increases rapidly with machining passes (tool wear).
2. Cutting force component F_x (perpendicular to the feed direction) is highest as compared to F_y and F_z in down-milling and increases with machining passes (tool wear).
3. Down-milling generates lower cutting force than up-milling and thus improves machinability.
4. The resultant cutting force follows the similar trend and magnitude as the feed force in up-milling or perpendicular to feed force in down-milling.
5. The resultant cutting force F_r is highest in up-milling as compare to down-milling.
6. The amplitude of FFT of cutting force in the x, y and z directions at 75.13 Hz tooth frequency follows almost the same trend as cutting force components.
7. The amplitudes of FFT for all cutting force components versus machining length under down-milling operation are almost flat with machined length (Number of passes) which indicates the lower vibrations and smoother operation in down-milling as compared to up-milling, while in up-milling the amplitude of FFT increases

- rapidly which indicates higher vibrations and tendency for rapid tool wear and breakage.
8. A comparative evaluation of four cooling strategies using up-milling method shows that emulsion cooling strategy generates the least resultant cutting force with LN₂ cooling strategy generating the highest resultant cutting force.
 9. A comparative evaluation of four cooling strategies using down-milling method shows that MQL cooling strategy generates the least resultant cutting force, followed by combined MQL+LN₂ with emulsion generating the highest resultant cutting force.
 10. Using LN₂ cooling strategy alone is not recommended for machining Inconel-718 due to high cutting forces and vibrations.
 11. Down-milling with MQL cooling strategy is recommended for improving the machinability of Inconel 718 alloy at given machining parameters.

2.2. CONCLUSIONS FROM EFFECTS OF COOLING STRATEGIES AND TOOL COATINGS ON CUTTING FORCES AND TOOTH FREQUENCY IN HIGH SPEED DOWN-MILLING OF INCONEL-718 USING HELICAL BULL-NOSE SOLID CARBIDE END-MILLS

1. Cutting force component F_x , perpendicular to the feed direction, is always dominant among all three cutting force components and increases with number of passes (machined length).
2. Resultant cutting force always follows similar trend and magnitude as the dominant cutting force component F_x , perpendicular to the feed direction.
3. Amplitudes of FFT of cutting forces in the x, y and z directions at tooth frequency almost follow similar trend as their respective cutting force components.

4. The amplitudes of FFT for all cutting force components versus machining length for MQL and combined (MQL + LN₂) cooling strategies are almost flat, which indicates the lower vibrations and smoother operation as compared LN₂ cooling strategy, where the amplitude of FFT increases rapidly which indicates higher vibrations and hence, cutting forces.
5. Due to increase in number of teeth, GMS² coated end-mills generates the least amplitude of FFT of cutting force components which indicates the lower vibrations, as GMS² coated end-mills scoop less material than uncoated and AlTiN coated end-mills.
6. Comparative evaluation of resultant cutting forces shows that uncoated end-mills generate lowest resultant cutting forces, followed by AlTiN coated end-mills, whereas GMS² coated end-mills generate highest resultant cutting forces under all cooling strategies.
7. Comparative evaluation of resultant cutting forces shows that the MQL cooling strategy generates lowest resultant cutting forces, followed by combined (MQL + LN₂) cooling, whereas LN₂ cooling strategy generates highest resultant cutting forces with all end-mill coatings.
8. Using LN₂ cooling strategy alone is not recommended for machining Inconel-718 due to high cutting forces and vibrations.
9. Uncoated end-mills under MQL cooling strategy are recommended for machining Inconel-718 based on cutting forces.

2.3. CONCLUSIONS FROM EFFECTS OF UP AND DOWN-MILLING METHODS, AND COOLING STRATEGIES ON TOOL WEAR, CHIP MORPHOLOGY AND SURFACE ROUGHNESS IN HIGH SPEED END-MILLING OF INCONEL-718

1. Down-milling generates lower levels of flank wear than up-milling under emulsion, MQL, LN₂ and combined (MQL+LN₂) cooling strategies investigated and thus, improves machinability of Inconel 718
2. Tool wear mechanism in up-milling was adhesion and failure modes were chipping and plastic deformation, while abrasion was the mechanism of tool wear in down-milling
3. Up-milling operation generates irregular and longer chips with mostly torn edges, whereas down-milling generates uniform and shorter chips.
4. Up-milling generates a segmented chip, with saw-tooth shape for each machining pass along with other chips under all cooling strategies
5. Down-milling operation generates discontinuous serrated chips under all cooling strategies, which were easily removed from the cutting zone by each of the cooling strategy, while segmented chips are generated in up-milling operation
6. In up-milling, emulsion cooling generated lowest surface roughness, while LN₂ generated highest surface roughness
7. In down-milling, emulsion, MQL and combined (MQL + LN₂) cooling strategies generated equal surface roughness, whereas LN₂ generated highest surface roughness
8. Emulsion up-milling generated lowest surface roughness, whereas LN₂ up-milling generated highest surface roughness among all cooling strategies and milling methods

9. A comparative evaluation of the four cooling strategies using up-milling method shows that the emulsion cooling strategy yields the lowest level of flank wear
10. A comparative evaluation of the four cooling strategies using down-milling method shows that the MQL cooling strategy generated lowest level of flank wear, followed by combined (MQL+LN₂) cooling strategy
11. MQL can successfully replace conventional emulsion cooling leading to significant cost savings and sustainable machining.
12. Down-milling with MQL cooling strategy is recommended for machining Inconel 718 alloys

2.4. CONCLUSIONS FROM EFFECTS OF TOOL COATINGS AND COOLING STRATEGIES ON TOOL WEAR, CHIP MORPHOLOGY AND SURFACE ROUGHNESS IN HIGH SPEED DOWN-MILLING OF INCONEL-718

1. For AlTiN coated end-mills, (MQL + LN₂) cooling strategy generated lowest flank wear, followed by MQL, while LN₂ cooling generated highest flank wear.
2. For GMS2 coated end-mills, MQL cooling strategy generated lowest flank wear, followed by combined (MQL + LN₂), while LN₂ cooling generated highest flank wear.
3. GMS2 coated end-mills under MQL cooling strategy generated lowest flank wear followed by AlTiN coated end-mills under combined (MQL + LN₂) cooling strategy, while GMS2 coated end-mills under LN₂ cooling strategy generated highest flank wear among all combinations of cooling strategies and end-mill coatings.
4. Using LN₂ cooling strategy alone is not recommended for machining Inconel 718 due to rapid tool wear.

5. MQL and combined (MQL + LN2) cooling strategy generated chips with sharp and uniform edges due to less tool wear, while LN2 cooling strategy generated chips with irregular and torn edges due to high tool wear
6. Chip length increased with progression of machining time (tool wear) under all cooling strategies and end-mill coatings
7. Tool wear mechanism under MQL and combined (MQL + LN2) cooling strategies is abrasion causing progressive wear, while under LN2 cooling it is adhesion causing chipping and notching due to formation of built-up edge
8. AlTiN coated end-mills under MQL cooling strategy generated lowest surface roughness, followed by GMS2 coated end-mills under combined (MQL+LN2) cooling strategy, whereas AlTiN coated end-mills under LN2 cooling generated highest surface roughness
9. GMS2 coated end-mills under MQL cooling strategy and by AlTiN coated end-mills under are recommended for machining Inconel-718.

VITA

Paras Mohan Jasra was born in Ahiyapur Tanda, Punjab, India. He earned his Bachelors of Technology degree in Mechanical Engineering from DAV Institute of Engineering and Technology, Jalandhar, India in 2007 and Master of Engineering degree in CAD/CAM & Robotics Engineering from Thapar University, Patiala, India in 2009. He was awarded a scholarship from the Ministry of Human Resource Development (MHRD) during his Masters. He has been enrolled as a PhD. Student in Mechanical and Aerospace Engineering Department at Missouri University of Science and Technology since August 2014. In May 2018, he received his Ph.D. in Mechanical Engineering from Missouri University of Science and Technology.